

# Gas, dust, and star formation in distant radio galaxies



# Gas, dust, and star formation in distant radio galaxies

Proefschrift

ter verkrijging van  
de graad van Doctor aan de Universiteit Leiden,  
op gezag van de Rector Magnificus Dr. D.D. Breimer,  
hoogleraar in de faculteit der Wiskunde en  
Natuurwetenschappen en die der Geneeskunde,  
volgens besluit van het College voor Promoties  
te verdedigen op donderdag 24 februari 2005  
te klokke 16.15 uur

door

Michiel Armijn Reuland

geboren te Groningen  
in 1972

Promotiecommissie

Promotor: Prof. dr. G.K. Miley

Co-promotores: Prof. dr. W.J.M. van Breugel (IGPP/LLNL & UC Merced, USA)  
Dr. H.J.A. Röttgering

Referent: Prof. dr. M.A. Dopita (RSAA/ANU, Australia)

Overige leden: Prof. dr. P.T. de Zeeuw  
Prof. dr. M. Franx  
Dr. G. Mellema  
Dr. P.P. van der Werf

voor mijn ouders

*But risks must be taken because the greatest hazard in life is to risk nothing. The person who risks nothing, does nothing, has nothing, is nothing. He may avoid suffering and sorrow, but he cannot learn, feel, change, grow or live. Chained by his servitude he is a slave who has forfeited all freedom. Only a person who risks is free. The pessimist complains about the wind; the optimist expects it to change; and the realist adjusts the sails.*

William Arthur Ward. (1921 - 1997)

# Table of contents

|   | Page      |
|---|-----------|
| <b>Chapter 1. Introduction</b>  | <b>1</b>  |
| 1 Theories of galaxy formation . . . . .  | 1         |
| 2 Radio galaxies . . . . .  | 3         |
| 3 Outline of this thesis . . . . .  | 5         |
| 4 Future prospects . . . . .  | 10        |
| <br>  |           |
| <b>Chapter 2. Dust and star formation in distant radio galaxies</b>                   | <b>13</b> |
| 1 Introduction . . . . .  | 13        |
| 2 Sample Selection and Observations . . . . .   | 16        |
| 2.1 SCUBA photometry . . . . .  | 17        |
| 2.2 Potential contamination of the thermal submillimetre flux . . . . .               | 18        |
| 2.3 Dust template . . . . .   | 19        |
| 3 Observational Results . . . . .   | 20        |
| 4 Analysis . . . . .  | 21        |
| 4.1 Statistical analysis . . . . .  | 22        |
| 5 Correlations between parameters . . . . .   | 24        |
| 5.1 Redshift dependent submillimetre properties . . . . .                             | 24        |
| 5.1.1 Flux density and relative detection fraction . . . . .                          | 24        |
| 5.1.2 Investigation of the difference between detections and non-detections . . . . . | 25        |
| 5.1.3 The increase of submm luminosity with redshift . . . . .                        | 26        |
| 5.2 The connection between submm and radio luminosity . . . . .                       | 27        |
| 5.3 An anti-correlation between submm flux and UV polarisation . . . . .              | 29        |
| 5.4 Submillimetre and Ly $\alpha$ flux . . . . .                                      | 29        |
| 5.5 $L_{850}$ and linear size . . . . .   | 30        |
| 5.6 Submillimetre and near-IR emission . . . . .                                      | 31        |
| 5.7 Summary . . . . .   | 32        |
| 6 A comparison of radio galaxies with QSOs . . . . .                                  | 33        |
| 7 Summary . . . . .   | 34        |
| <br>  |           |
| <b>Chapter 3. An obscured radio galaxy at high redshift</b>                           | <b>39</b> |
| 1 Introduction . . . . .  | 39        |
| 2 Observations and Results . . . . .  | 41        |
| 2.1 Selection and Keck Imaging . . . . .  | 41        |
| 2.2 JCMT and IRAM Observations . . . . .  | 42        |
| 2.3 Keck Spectroscopy . . . . .   | 42        |
| 3 Discussion . . . . .  | 43        |
| 3.1 Identification and Redshift Estimate . . . . .                                    | 43        |

|                   |  |           |
|-------------------|--|-----------|
| 3.2               | Implications . . . . .   | 44        |
| <b>Chapter 4.</b> | <b>Obscured compact ultra steep spectrum radio galaxies</b>  | <b>47</b> |
| 1                 | Introduction . . . . .   | 47        |
| 2                 | Observations and Results . . . . .   | 50        |
| 2.1               | SCUBA photometry . . . . .   | 50        |
| 2.2               | IRAM Photometry . . . . .  | 51        |
| 2.3               | Chandra . . . . .  | 51        |
| 3                 | Discussion . . . . .   | 52        |
| 3.1               | Redshift estimates . . . . .   | 52        |
| 3.2               | X-ray properties . . . . .   | 53        |
| 3.2.1             | Radio–X-ray relation . . . . .   | 53        |
| 3.2.2             | Submm–X-ray relation . . . . .   | 54        |
| 3.2.3             | Obscured nucleus . . . . .   | 55        |
| 3.3               | Young starbursting radio galaxies . . . . .  | 56        |
| 3.4               | Implications for Type II AGN and XRB . . . . .   | 57        |
| 4                 | Summary . . . . .  | 58        |
| <b>Chapter 5.</b> | <b>The influence of ISM characteristics and AGN activity on the far infrared spectral energy distributions of starburst galaxies</b> | <b>63</b> |
| 1                 | Introduction . . . . .   | 63        |
| 2                 | The Samples . . . . .  | 65        |
| 2.1               | ULIRGs . . . . .   | 65        |
| 2.2               | High redshift sources . . . . .  | 66        |
| 3                 | Infrared emission models and fitting procedures . . . . .  | 67        |
| 3.1               | Starburst Models . . . . .   | 67        |
| 3.1.1             | General . . . . .  | 67        |
| 3.1.2             | Dust and PAH implementation . . . . .  | 67        |
| 3.1.3             | ISM pressure and molecular cloud dissipation timescale . . . . .   | 68        |
| 3.1.4             | Visual extinction . . . . .  | 69        |
| 3.2               | AGN torus models . . . . .   | 69        |
| 3.3               | The fitting procedures . . . . .   | 70        |
| 4                 | Results . . . . .  | 71        |
| 4.1               | General Results . . . . .  | 71        |
| 4.2               | Comparison with literature . . . . .   | 72        |
| 5                 | Discussion . . . . .   | 73        |
| 5.1               | Limitations of the models . . . . .  | 73        |
| 5.2               | Pressure . . . . .   | 74        |
| 5.3               | Molecular cloud dissipation time scale . . . . .   | 75        |
| 5.4               | AGN contribution to MIR and FIR wavelengths and its influence on the inferred star formation rates . . . . .                         | 75        |
| 5.5               | Star formation at high redshift . . . . .  | 77        |
| 6                 | Conclusion . . . . .   | 78        |
| <b>Chapter 6.</b> | <b>Giant Ly<math>\alpha</math> nebulae associated with high redshift radio galaxies</b>  | <b>87</b> |



|  |   |            |
|--|---|------------|
| 1  | Introduction . . . . .                                      | 87         |
| 2  | Sample Selection and Observations . . . . .                 | 89         |
| 2.1  | Sample Selection . . . . .                                  | 90         |
| 2.2  | Keck Imaging . . . . .                                      | 91         |
| 2.2.1  | Ly $\alpha$ imaging . . . . .                               | 91         |
| 2.2.2  | Broad-band imaging . . . . .                                | 92         |
| 2.3  | HST Imaging . . . . .                                       | 92         |
| 2.4  | Relative Astrometry . . . . .                               | 93         |
| 2.5  | Continuum subtraction . . . . .                             | 93         |
| 3  | Results . . . . .   | 94         |
| 3.1  | 4C 41.17 . . . . .  | 94         |
| 3.2  | 4C 60.07 . . . . .  | 98         |
| 3.3  | B2 0902+34 . . . . .  | 101        |
| 4  | Discussion . . . . .  | 101        |
| 4.1  | Cooling flows and radio lobes . . . . .                     | 103        |
| 4.2  | Starburst superwinds . . . . .                              | 103        |
| 4.3  | Radiation pressure driven outflows . . . . .                | 104        |
| 4.4  | Obscured AGN . . . . .                                      | 105        |
| 5  | Conclusions . . . . .                                       | 105        |
| <br><b>Chapter 7. Metal enriched gaseous halos around distant radio galaxies</b> |   | <b>111</b> |
| 1  | Introduction . . . . .                                      | 111        |
| 2  | Observations and data analysis . . . . .                    | 113        |
| 2.1  | Sample Selection . . . . .                                  | 113        |
| 2.2  | Optical and Near-Infrared Spectroscopy . . . . .            | 114        |
| 2.2.1  | LRIS . . . . .  | 114        |
| 2.2.2  | ESI . . . . .   | 115        |
| 2.2.3  | NIRSPEC . . . . .   | 115        |
| 2.3  | Data analysis . . . . .                                     | 116        |
| 3  | Results . . . . .   | 116        |
| 3.1  | Notes on individual objects . . . . .                       | 118        |
| 3.1.1  | 4C 41.17 . . . . .  | 118        |
| 3.1.2  | 4C 60.07 . . . . .  | 122        |
| 3.1.3  | B2 0902+34 . . . . .  | 127        |
| 4  | Discussion . . . . .  | 130        |
| 4.1  | Ionizing source . . . . .                                   | 130        |
| 4.1.1  | Central region . . . . .                                    | 131        |
| 4.1.2  | Extended region along the radio axis . . . . .              | 131        |
| 4.2  | Radiative transport: to scatter or not to scatter . . . . . | 132        |
| 4.3  | Kinematics . . . . .  | 133        |
| 4.3.1  | General kinematic structures . . . . .                      | 133        |
| 4.3.2  | Outflows . . . . .  | 133        |
| 4.4  | A comparison with CO observations . . . . .                 | 135        |
| 4.5  | Metallicity . . . . .                                       | 135        |
| 4.6  | Mass estimates . . . . .                                    | 136        |

|   |                                     |            |
|---|-------------------------------------|------------|
| 4.6.1   | Luminosity based masses . . . . .   | 136        |
| 4.6.2   | Dynamical mass estimates . . . . .  | 136        |
| 4.7   | Cosmological Implications . . . . . | 137        |
| 5   | Conclusion . . . . .                | 138        |
| <b>Nederlandse samenvatting (Dutch summary)</b> |                                     | <b>143</b> |
| <b>Publications not included in this thesis</b> |                                     | <b>151</b> |
| <b>Curriculum vitae</b>                         |                                     | <b>153</b> |
| <b>Nawoord / Acknowledgments</b>                |                                     | <b>155</b> |

---

# Chapter 1

---

## Introduction and summary

**R**ADIO galaxies are some of the most energetic and largest galaxies in the Universe. They are presumed to be powered by accretion of material onto super massive black holes at their nuclei and in the early universe they are embedded in spectacular gaseous emission line nebulae. This makes them interesting objects in their own right. Further, they provide unique insights into the formation and evolution of galaxies.

The aim of this thesis is to obtain a better understanding of galaxy formation and evolution, by studying the connection between star formation and nuclear activity in radio galaxies. To achieve this, we have undertaken a large observational program to collect data for these galaxies, to obtain information on gas, dust, and star formation over a large range of the electromagnetic spectrum, from X-ray to radio waves.

The galaxies in this program provide data about their evolutionary state at a time when the Universe was approximately 10–20% of its current age (13.7 billion years according to current estimates). The next sections summarize current ideas about galaxy formation, describe key properties of radio galaxies, show why radio galaxies are uniquely suited for studying the process of galaxy formation, and set the scene for presenting the results of this thesis.

### 1 Theories of galaxy formation

Galaxies are usually classified into three main classes: the beautiful spiral galaxies, and the visually less appealing (but no less interesting) lenticulars and ellipticals. If galaxies cannot be classified in one of these classes, they are called irregulars. The spatial distribution of galaxies appears bimodal. Many galaxies are isolated, the so-called field galaxies. Others are gathered in groups or clusters. Regardless of their specific distribution, they are separated by large distances with little material in between. The tiny (of order 1:100,000) fluctuations in the cosmic micro wave background, that is thought to be the afterglow of the Big Bang, indicate that the early universe must have been very smooth. This is in stark contrast to the present clumpy distribution of matter. A fundamental question that now arises is: How and when did the initial density fluctuations amplify and form the galaxies, groups, and clusters observed in the local universe?

There are two main scenarios that attempt to answer this question. The build-up of galaxies could occur through *monolithic collapse* or through *hierarchical merging*. In the monolithic collapse scenario cooling of a single gas cloud is envisaged to result in an entire galaxy (e.g., Eggen et al. 1962). One feature of this scenario is that it can explain

the presence of massive galaxies already in the early stages of the Universe. In contrast, the hierarchical Cold Dark Matter (CDM) theory of structure formation predicts that the formation of galaxies is a gradual and biased process (e.g., Toomre & Toomre 1972; White & Rees 1978). In this scenario larger objects grow from the peaks in the initial mass fluctuations through the merging of smaller, younger objects. The most massive objects are expected to form at the centers of over-dense regions which will eventually evolve into the clusters of galaxies seen today. Initially, all objects would be very gas rich with relatively few stars and their dynamics would be dominated by the CDM halos. The merging process may strongly affect these early galaxies. It would enhance starburst activity in interacting systems and accretion onto a growing galaxy at the center may fuel central massive black holes.

The scenario of hierarchical structure formation is supported by observations of both local and distant galaxies. Locally, nearly all ultraluminous far infrared galaxies ( $L_{\text{FIR}} > 10^{12} L_{\odot}$ ; for a review see Sanders & Mirabel 1996) appear to be mergers. It is thought that their large far infrared luminosities are due to dust heated by radiation from vigorous starbursts and black holes that are being fed efficiently.

In the distant universe, *Hubble Space Telescope* observations of radio galaxies show that they have clumpy morphologies (Pentericci et al. 1999). The individual clumps are reminiscent of smaller but still massive galaxies (Lyman break galaxies; Steidel et al. 1996) that are expected to merge with the central galaxy on dynamical timescales of  $10^8$  years (Pentericci et al. 1998). Near-infrared studies also suggest that radio galaxies evolve from “fuzzy” structures with large-scale diffuse emission at early epochs into more compact objects by  $z \sim 2$  (van Breugel et al. 1998).

A fundamental prediction of CDM theories is that massive galaxies form at the centers of clusters. Recent observations of radio galaxies support this prediction (Venemans et al. 2002; Miley et al. 2004)

There appears to be a tight correlation between the masses of the stellar bulges of galaxies and their central black holes (Magorrian et al. 1998; Gebhardt et al. 2000; Ferrarese & Merritt 2000). This is an issue that a theory of galaxy formation should explain.

Furthermore, while models of galaxy formation seem to produce the observed number of intermediate-mass galaxies, they overpredict both the numbers of very massive and low-mass galaxies. Because stars can form only from cold gas, the temperature of gas is a crucial parameter. Gas is easily heated by radiative and mechanical feedback processes (e.g., UV radiation from stars, supernovae, mergers or radiation and outflows from massive black holes). Feedback, therefore, could possibly resolve the mismatches between observations and theory, but its precise role and the main agents need to be established.

In light of the big question “**When and how did galaxies form?**”, the following unsolved questions are important:

- **What is the origin of the relation between bulge mass and black hole mass?**
- **Which physical processes control the observed shape of the galaxy luminosity function?**
- **Do all massive galaxies reside in (forming) clusters ?**

Studies of radio galaxies can help to answer these.

## 2 Radio galaxies

The research presented in this thesis addresses different aspects of galaxy formation through studying some of the most extreme objects in the Universe: radio galaxies. In the nearby universe, radio galaxies are hosted by very massive ( $M \sim 10^{12-13} M_{\odot}$ ) ellipticals. Below, their properties and role in the formation of *massive* galaxies are summarized.

Radio galaxies form a subclass of active galactic nuclei (AGN). Other AGN are the optically luminous quasi stellar objects (QSOs), Seyferts 1 and 2, and Blazars. The current understanding is that AGN are powered by massive black holes ( $10^{6-9} M_{\odot}$ ) that accrete matter through an accretion disk. Because the conversion into energy of matter that falls into a black hole can happen very efficiently ( $\sim 10\%$  of the rest mass can be radiated away before it crosses the Schwarzschild radius; more in spinning black holes), this results in prodigious amounts of radiation being emitted from a small central region. Hence the name “active galactic nuclei”. In certain cases (e.g., QSOs) these small inner regions can outshine the approximately 100 billion stars that make up a typical galaxy. Consequently, the term AGN is used somewhat loosely to designate both the central regions and the galaxies hosting AGN.

The defining characteristic of radio galaxies is that they emit strongly at radio wavelengths ( $P_{178\text{MHz}} > 10^{26} \text{ WHz}^{-1}$ ). This is over two orders of magnitude more than radio-quiet AGN, and there seems to be a dichotomy between the two classes. The power-law spectrum and high polarization indicate that the process responsible for the radio emission is synchrotron radiation. Although the exact mechanism producing the synchrotron radiation in radio galaxies is not fully understood, it likely involves efficient accretion of matter onto a *spinning super massive* ( $\sim 10^9 M_{\odot}$ ) black hole (Rees 1978; Blandford & Payne 1982).

Not only the mechanism responsible for producing powerful radio structures, but also the evolution of these structures is subject to debate. The typical life time of radio-source activity is short, 10–100 Myr. The observed range in sizes of  $z \sim 0.5$  powerful radio sources, from subgalactic ( $< 1 \text{ kpc}$ ) to cluster scales ( $> 1 \text{ Mpc}$ ) has been interpreted as evidence for evolution of radio source size with age. Presumably, radio sources begin in the very compact Gigahertz Peaked Spectrum (GPS;  $< 1 \text{ kpc}$ ) phase, pass through the Compact Steep Spectrum (CSS; 1–20 kpc) stage, and ultimately evolve into the classical edge brightened Fanaroff & Riley class II (FR II; Fanaroff & Riley 1974) radio sources.

Historically, interest in AGN has been their use as cosmological probes. Because they are extremely luminous they previously were the only objects that could be seen out to large distances. With the availability of 10-m class telescopes thousands of “normal” galaxies at redshifts  $z > 2$  have been discovered (Steidel et al. 1996; Steidel et al. 1999; Labbé et al. 2003). AGN are extreme sources and very rare in the local universe. It has therefore been argued that they are interesting, but statistically not significant. However, there are at least two reasons why radio galaxies are not “freaks” but instead signify an important phase in the evolution of massive galaxies. First, the discovery of the tight correlation, mentioned earlier, between black hole mass and stellar mass indicates the importance of (feedback from) massive black holes. Secondly, the observation

that the space density of AGN was much larger in the past (the population peaks at redshifts of  $z = 2-3$ ) and behaves in a similar way as the estimated star formation rate density, suggests that AGN and star formation are closely linked. It is therefore well possible that every massive galaxy once was a powerful radio source, albeit for a short period.

At low redshifts ( $z < 1$ ), powerful radio sources are uniquely identified with massive elliptical galaxies. There is a tight correlation between the near-infrared  $K$ -band magnitude of radio galaxies and their redshift (the “Hubble”  $K - z$  relation; De Breuck et al. 2002). It seems to trace the most massive systems at any epoch and suggests that radio galaxies are tracers of possible over-dense regions and the sites of forming massive galaxies. In scenarios of biased galaxy formation these would mark the peaks in the early density field, and are expected to be at the centers of forming clusters of galaxies. Studies of high redshift ( $z > 2$ ) clusters of galaxies are important to constrain galaxy evolution and cosmological models (Bahcall & Fan 1998), and the radio galaxies themselves are important for constraining the upper mass end of models of galaxy formation, where current models fail.

Although both radio galaxies and QSOs host massive black holes, emit energy over large wavelength ranges, and can be found at high redshift, radio galaxies are preferred for studies of galaxy formation. This is because QSOs outshine their host galaxies completely, whereas for radio galaxies the bright central region is thought to be blocked by an optically thick torus. Therefore, in radio galaxies the extended host galaxy can be studied in detail. Because star formation mostly occurs in dust obscured regions, optical surveys for star formation give a biased view and large correction factors are required. The long wavelength selection of radio galaxies is not sensitive to such obscuration and can therefore help to constrain the relative fractions of unobscured and obscured star formation. Furthermore, radio galaxies are often embedded in large  $> 100$  kpc gaseous halos (Chapter 6, 7; van Ojik et al. 1996; Villar-Martín et al. 2003) from which they could be forming. Because of their large spatial extents these gaseous reservoirs are excellent laboratories for studying feedback processes at high redshift in detail.

Consequently, many searches for distant radio galaxies ( $z > 2$ ) have been conducted (e.g., Röttgering et al. 1997; De Breuck et al. 2001). Because radio galaxies are rare, large numbers of foreground galaxies have to be filtered out to find high redshift candidates. The most efficient selection technique is based on spectroscopic follow-up of sources with ultra steep radio spectra ( $USS$ ;  $\alpha_{325\text{MHz}}^{1400\text{MHz}} \lesssim -1.30$ ;  $S_\nu \propto \nu^\alpha$ ), which is analogous to a “red radio color” (e.g., Blumenthal & Miley 1979). De Breuck et al. (2000) constructed a large sample of 669 ultra steep spectrum radio sources for this specific purpose. The galaxies were selected from a radio sample with flux densities  $10 < S_{1.4\text{GHz}} < 100$  mJy, fainter than most previous surveys. This recipe for finding distant sources has proved highly successful with spectroscopic followup of these sources with faint near-infrared counterparts showing emission line based redshifts  $z > 3$  in  $\sim 35\%$  of the cases (for details see De Breuck et al. 2001). Presently, of order 150 radio galaxies are known at redshifts  $z > 2$ . They constitute an unique sample to study the formation of massive galaxies and the role of feedback processes therein.

### 3 Outline of this thesis

This thesis aims to study the evolution of massive galaxies by focusing on three inter-related ingredients of radio galaxies: gas, dust, and star formation. The work is based on a large amount of observations with ground- and space-based telescopes, from the radio through X-ray wavelength range.

#### *Gas*

Spectroscopic observations of distant radio galaxies have shown that they are embedded in large gaseous halos. The role of these halos in galaxy formation is not yet fully understood. Answers to the following questions could provide a better understanding: What is the extent of the halos? Which processes provide the energy that ionizes these halos? Is the gas infalling in a cooling flow or is the gas the result of outflows and radiation from starburst and AGN? How does this affect the galaxy formation process? Are active, massive forming galaxies capable of enriching the intra-cluster media with metals and thus affect cluster evolution? Only few high-quality images of these halos existed prior to the work in this thesis. Higher quality images are of great interest because of the potential diagnostics they may provide about the very early stages of galaxy formation, and about starburst/AGN feedback and chemical enrichment during this process. Chapter 6 presents the deepest of such images ever obtained. Follow-up optical and near-infrared spectroscopy is presented in Chapter 7.

#### *Star formation*

In the case of the radio galaxy 4C 41.17 there is direct evidence for massive star formation (up to  $\sim 1500 M_{\odot} \text{ yr}^{-1}$  after correction for extinction) based on stellar absorption lines (Dey et al. 1997). Recent mm-interferometry studies of CO line and continuum emission for three  $z > 3$  distant radio galaxies have shown that the star formation occurs galaxy wide over distances up to 30 kpc (Papadopoulos et al. 2000; De Breuck et al. 2003). Together this suggests that we are observing not merely scaled up versions of local ultraluminous infrared galaxies (ULIRGs) where the bursts are confined to the inner few kpc, but wide-spread starbursts within which the galaxies are forming the bulk of their eventual stellar populations. Chapter 5 presents a theoretical investigation of the physical parameters controlling the spectral energy distributions of such extended starbursts.

#### *Dust*

Dust is expected to play an important role in star forming regions. It absorbs UV/optical radiation from the starburst and reradiates it at far-infrared wavelengths. Optical searches for distant galaxies (e.g., using the Lyman-break technique; Steidel et al. 1996; Steidel et al. 1999) are thus likely to be biased against dusty objects. Finding distant star forming galaxies through submillimeter (rest-frame FIR) emission selects only the most obscured sources. So far there has been little overlap between the opti-

cal and submillimeter selected star forming sources. It remains unclear whether they are members of a continuous population (e.g., Adelberger & Steidel 2000; Webb et al. 2003) and arguments have been made that either one of them could dominate the star formation density at high redshift. Since selection at radio wavelengths circumvents the aforementioned selection biases it could help determine the relative contributions of obscured and unobscured star formation to the star formation history of the universe. Until recently, many searches for dust in distant radio galaxies proved largely unsuccessful. Chapter 2 is a study of the change of dust obscured star formation rate in radio galaxies over a large range in redshift. Chapters 3 and 4 investigate the role of dust in young distant radio sources.

A brief outline of each chapter is given below.

## Chapter 2

Multi-wavelength observations of distant radio galaxies have provided considerable information about how the formation and evolution of present day brightest cluster galaxies must have taken place. One of the great uncertainties is the role of dust. Dust is produced by starbursts. This dust absorbs most of the ultraviolet/optical light from the young hot stars in the starbursts and re-emits it in the infrared waveband. Therefore far-infrared emission is often used as a measure of the star formation rate. Emission from cool ( $\sim 30\text{--}50\text{ K}$ ) dust has a spectrum with maximum intensity at far-infrared ( $\sim 60\text{--}100\ \mu\text{m}$ ) wavelengths. For very distant ( $z > 1$ ) galaxies this peak is redshifted to submillimeter ( $200\text{--}1000\ \mu\text{m}$ ) wavelengths. At observed wavelengths of  $850\ \mu\text{m}$  the dimming of galaxies due to increasing distance is compensated for as the far-infrared peak shifts into the bandpass. Instruments that observe this wavelength are (almost) equally sensitive to star formation in galaxies up to redshifts of  $z \sim 10$ , as they are to galaxies at  $z \sim 1$  and are well-suited for studying star formation over large cosmological timescales.

We therefore initiated an observing program with the Submillimetre Common User Bolometer Array (SCUBA) to measure the dust continuum emission from 24  $z > 1$  radio galaxies. We detected submillimeter emission in 12 galaxies, including 9 detections at  $z > 3$ . When added to previous published results the data almost triple the number of radio galaxies with  $z > 3$  detected in the submillimeter and yield a sample of 69 observed radio galaxies over the redshift range  $z = 1\text{--}5$ . We find that the galaxies are luminous at submillimeter wavelengths. We confirm and strengthen the result from previous submillimeter observations of radio galaxies that the detection rate is a strong function of redshift. We compare the redshift dependence of the submillimeter properties of radio galaxies with those of quasars and find that for both classes of objects the observed submillimeter flux density increases with redshift to  $z \approx 4$ , beyond which, for the galaxies, we find tentative evidence for a decline.

If this change in submillimeter flux is due to a change in the intrinsic star formation rate, it is consistent with a scenario in which the bulk of the stellar population of radio galaxies forms rapidly around redshifts of  $z = 3\text{--}5$  after which they are more passively evolving (c.f. Best, Longair, & Röttgering 1998). However, dust can be heated



by UV/optical radiation not only from starbursts but also from AGN. This complicates the use of submillimeter fluxes as a measure of star formation rate. We have therefore searched for evidence of possible contamination by AGN. The lack of evidence for a correlation between radio-power and submillimeter emission and an anti-correlation between submillimeter luminosity and fractional polarization of the UV continuum (AGN light is expected to be highly polarized) indicate that starbursts are the dominant source of heating for dust in radio galaxies. We conclude that distant radio galaxies are massive forming galaxies, forming stars at rates up to a few thousand  $M_{\odot} \text{ yr}^{-1}$ .

### Chapters 3 and 4

As described above, ultra steep radio spectrum (USS;  $\alpha_{325\text{MHz}}^{1400\text{MHz}} \lesssim -1.30$ ;  $S_{\nu} \propto \nu^{\alpha}$ ) selection is an efficient criterion for finding distant radio galaxies. However, a large fraction ( $\sim 30\%$ ) of selected high redshift radio galaxy *candidates* fails to show emission lines in deep spectroscopic exposures at Keck, even though some galaxies are detected in the continuum. Generally, they are characterized by compact ( $\theta \lesssim 2''$ ) radio morphologies. The compact radio structures could indicate that we observe them shortly after the onset of the radio activity and that they are possibly very young. The observation that their parent objects are only detected in the near-infrared suggests that they are heavily obscured and/or at very high redshift. This is of interest because a population of high redshift heavily obscured AGN seems the best candidate to account for a substantial fraction (30–40%) of the 5–10 keV cosmic X-ray background (XRB). In both scenarios their host galaxies could be expected to be forming stars at large rates. Therefore, these sources are of interest for studying radio source evolution and particularly for studying possible connections between star formation and the onset of radio source activity. To search for signatures of dust and help constrain the nature and redshifts of these “no- $z$ ” radio galaxies, we have conducted a program of submillimeter and millimeter observations.

In Chapter 3, we report the results of a detailed study of one of these objects, WN J0305+3525. It appears associated with a small group of faint near-infrared ( $K \sim 21$ – $22$ ) objects and it is a strong detection at both 850  $\mu\text{m}$  and 1.25 mm. On the basis of its faint  $K$ -band magnitude, spectral energy distribution and other evidence we estimate that the radio galaxy is probably at a redshift  $z \simeq 3 \pm 1$ . This would make WN J0305+3525 a radio-loud hyper luminous infrared galaxy ( $L_{\text{FIR}} \sim 10^{13} L_{\odot}$ ) similar to, but more obscured than, other dusty radio galaxies in this redshift range.

Chapter 4 describes the results of a submillimeter survey for ten such “no- $z$ ” compact USS sources (including WN J0305+3525) and includes *Chandra* X-ray observations for the three strongest submillimeter detections. In total four galaxies were detected in the submillimeter with  $S/N > 4$ . This submillimeter detection fraction is close to the one for  $z > 2.5$  radio galaxies in surveys of comparable sensitivity (Chapter 2; Archibald et al. 2001). Also, a relatively strong statistical signal  $\langle S_{850, < 3\sigma}^{\text{CSS}} \rangle = 2.48 \pm 0.48 \text{ mJy}$  was found in the stacked non-detections. Together, this indicates that an obscured phase and the triggering of radio sources are connected, and that this compact obscured phase may be a common ingredient in AGN evolution.

None of the galaxies was detected with *Chandra*. Assuming redshifts  $z \sim 3$  and

based on the empirical radio to X-ray relation for AGN, intrinsic X-ray luminosities of  $L_{2-10\text{keV}} \sim 10^{44-46} \text{ erg s}^{-1}$  and column densities of a few  $10^{23} \text{ cm}^{-2}$  are inferred. This shows that if many AGN go through such a compact obscured stage, they could maybe contribute to the hard X-ray background.

## Chapter 5

As mentioned above, both AGN and starbursts can heat dust in galaxies. Many previous studies have reported that the fraction of far infrared luminosity ( $L_{\text{FIR}}$ ) that is contributed by an AGN increases with  $L_{\text{FIR}}$ . In order to infer reliable star formation rates, quantification of the respective contributions is essential. We have therefore examined the far-infrared spectral energy distributions (SEDs) of 41 local ultra luminous infrared galaxies (ULIRGs) using data from the literature. These observed SEDs are fitted with SEDs that were constructed by coadding the output from ionization models for dynamically evolving H II regions with a sophisticated treatment of embedded dust. The theoretical SEDs include a contribution from a dusty narrow line region in order to model enshrouded AGN.

From these models it is found that almost all ULIRGs are best fitted with high ( $P/k > 10^6 \text{ cm}^{-3} \text{ K}$ ) pressures of the interstellar medium, similar to the pressures inferred from emission line ratios. These high pressures are likely related to the pressure above which blowout occurs in a galactic superwind.

We have investigated the implications of our findings for high redshift sources. It seems that the physical mechanisms controlling their SEDs may be similar to those for local ULIRGs, and that the models are applicable also in the distant universe. Fitting of three high redshift radio galaxies with good far-infrared observations indicates that to fit their SEDs may require even higher pressures than found for ULIRGs. Such high pressures could be related to the presence of the radio source and possibly jet induced star formation. They would increase the effective temperature of these highly luminous sources and agree with the recently reported far infrared luminosity-temperature relation (Blain et al. 2004).

We find that the relative contribution of an embedded AGN can vary significantly. Taking this AGN related component into account can decrease star formation rates as inferred from  $L_{\text{FIR}}$  by factors of 2–3. For the high redshift radio galaxies, the high dust temperatures together with hidden AGN activity would decrease the star formation rates to values lower than is commonly inferred.

## Chapter 6

In the previous chapters we focused on the star formation rates in connection with radio source evolution. Here we discuss the gaseous environments of the radio galaxies. Ly $\alpha$  nebulae may be the first evidence for accretion in large dark matter halos. They may signal the formation of massive galaxies through merging of smaller starburst systems or cooling flows.

We report deep Keck narrow-band Ly $\alpha$  images of the luminous  $z > 3$  radio galaxies 4C 41.17, 4C 60.07, and B2 0902+34. The images show giant, 100–200 kpc scale emis-

sion line nebulae, centered on these galaxies, which exhibit a wealth of morphological structure, including extended low surface brightness emission in the outer regions, radially directed filaments, cone-shaped structures and (indirect) evidence for extended Ly $\alpha$  absorption. We discuss these features within a general scenario where the nebular gas cools gravitationally in large CDM halos, forming stars and multiple stellar systems. Merging of these “building blocks” triggers large scale starbursts, forming the stellar bulges of massive radio galaxy hosts, and feeds super-massive black holes which produce the powerful radio jets and lobes. The radio sources, starburst superwinds and AGN radiation may disrupt the accretion process, limiting galaxy and black hole growth, and imprint the observed filamentary and cone-shaped structures of the Ly $\alpha$  nebulae.

## Chapter 7

In this final chapter, we present deep optical and near-infrared spectroscopic data of the giant nebular emission line halos described in Chapter 6. Previous optical studies found that the inner high surface-brightness regions exhibit disturbed kinematics with velocity dispersions  $>1000 \text{ km s}^{-1}$  that seem to be closely related to the radio source. The outer regions of the halos exhibit kinematics with typical velocity dispersions of a few hundred  $\text{km s}^{-1}$ , and velocity characteristics consistent with rotation.

To investigate this further we obtained additional optical spectroscopic data at position angles perpendicular to the radio axes. Since Ly $\alpha$  is subject to resonance scattering, interpretation of the inferred kinematics is difficult. We therefore performed near-infrared spectroscopy for these emission line halos, targeting [O II] and [O III]. Evidence for the presence of enriched material (oxygen) throughout the nebula of 4C 41.17 (up to a distance of  $\sim 60 \text{ kpc}$  along the radio-axis) is found. The oxygen emission has a similar spatial and kinematic distribution as the Ly $\alpha$  emission. We argue that this implies that the Ly $\alpha$  cannot be purely scattered light, and that the halo had already been enriched by a previous generation of stars. It is possible that the extended oxygen has been transported from the central starburst region aided by the radio source. We discuss various feedback processes and their implications for galaxy formation in the context of the nature and origin of these halos. The evidence presented here could help cast observational light on the good correlation found in galaxies between the stellar velocity dispersion and the black hole mass. Silk & Rees (1998) and Sazonov et al. (2004) have speculated that this results from outflows which are driven by radiation pressure provided by the black hole. In the case of 4C 41.17 we have good evidence that the radio lobes are driving this outflow, assisted by radiation pressure and starburst winds. Together these data help us to better understand the formation of cluster ellipticals. It seems that the radio sources, starburst superwinds and AGN radiation may disrupt the accretion process limiting galaxy and black hole growth, and possibly help enrich the inter cluster medium. These processes may help shape the high-mass end of the galaxy luminosity function.

## 4 Future prospects

The cosmological parameters have recently been constrained with unprecedented precision and the basic concepts of galaxy formation and evolution seem to be understood. This leads to a situation in which we can hope to start answering outstanding questions in the formation of massive galaxies with some confidence.

Using the data presented in this thesis we have shown that the evolution of radio-loud AGN couples strongly with the evolution of their host galaxies. However, many more observations and better modeling are required to investigate this in a quantitative way and to obtain a continuous sampling from the present to earlier cosmic epochs.

The giant emission line nebulae around radio galaxies provide important laboratories for studies of feedback from central regions of radio galaxies. Deep spectroscopy targeting non-resonant emission lines are important to constrain various feedback scenarios, and determine the gas kinematics, metallicities and sources of ionization. To fully exploit narrow-band emission-line images as a tool for studies of galaxy formation requires the use of optical and near-infrared integral field units (2-D spatial + 1-D spectral, imaging devices) on 8-10 m (and 30-100 m?) telescopes with advanced adaptive optics systems (e.g., van Breugel & Bland-Hawthorn 2000).

We are now at a time where unprecedented quality observations are driving models forward. The high quality data will allow better constraints on the physical processes that are important for galaxy formation. Models will be able to move away from semi-analytical approaches and include more of the real physics. Models for galaxy evolution depend heavily on the full coverage of the spectral energy distributions. *Spitzer* and the future *ALMA* and *Herschel* will be crucial for this in the mid-infrared to millimeter regime and therefore for studies of the star formation rates over large cosmological times. Furthermore, these instruments will provide means of estimating the masses of distant galaxies through observing the dynamics of molecular line emission and observations of their stellar populations in the rest-frame near-infrared.

Cosmology is an observationally driven science. The greatest leaps forward came with the arrival of new instruments opening up new wavelength regimes or providing data of order of magnitude better sensitivity and resolution. In the coming years it is almost guaranteed that instruments such as LOFAR and XEUS will once again revolutionize our view of the universe. XEUS will provide information on the first massive black holes at redshifts up to  $z \sim 10$ . LOFAR will provide extreme sensitivity in presently poorly explored frequency regimes. It is likely to discover many new exciting astrophysical objects. Further, LOFAR is expected to detect radio galaxies at redshifts  $z \sim 8$ . This will allow us to study the coevolution of massive galaxies and their central black holes to even earlier cosmic epochs than is presently possible.

## References

- Adelberger K. L., Steidel C. C., 2000, *ApJ*, 544, 218  
Archibald E. N., Dunlop J. S., Hughes D. H., Rawlings S., Eales S. A., Ivison R. J., 2001, *MNRAS*, 323, 417  
Bahcall N. A., Fan X., 1998, *ApJ*, 504, 1  
Best P. N., Longair M. S., Röttgering H. J. A., 1998, *MNRAS*, 295, 549  
Blain, A. W., Chapman, S. C., Smail, I., & Ivison, R. 2004, *ApJ*, 611, 52  
Blandford, R. D. & Payne, D. G. 1982, *MNRAS*, 199, 883

- Blumenthal, G., & Miley, G. 1979, *A&A*, 80, 13
- De Breuck C., van Breugel W., Röttgering H. J. A., Miley G., 2000, *A&AS*, 143, 303
- De Breuck C., van Breugel W., Röttgering H., Stern D., Miley G., de Vries W., Stanford S. A., Kurk J., Overzier R., 2001, *AJ*, 121, 1241
- De Breuck C., van Breugel W., Stanford S. A., Röttgering H., Miley G., Stern D., 2002, *AJ*, 123, 637
- De Breuck C., Neri R., Morganti R., Omont A., Rocca-Volmerange B., Stern D., Reuland M., van Breugel W., Röttgering H., Stanford S. A., Spinrad H., Vigotti M., Wright M., 2003, *A&A*, 401, 911
- Dey A., van Breugel W., Vacca W. D., Antonucci R., 1997, *ApJ*, 490, 698
- Eggen, O. J., Lynden-Bell, D., & Sandage, A. R. 1962, *ApJ*, 136, 748
- Fanaroff B. L., Riley J. M., 1974, *MNRAS*, 167, 31P
- Ferrarese, L. & Merritt, D. 2000, *ApJ*, 539, L9
- Gebhardt, K., Bender, R., Bower, G., et al. 2000, *ApJ*, 539, L13
- Labbé, I., et al. 2003, *AJ*, 125, 1107
- Magorrian, J., Tremaine, S., Richstone, D., et al. 1998, *AJ*, 115, 2285
- Miley, G. K., et al. 2004, *Nature*, 427, 47
- Papadopoulos P. P., Röttgering H. J. A., van der Werf P. P., Guilloteau S., Omont A., van Breugel W. J. M., Tilanus R. P. J., 2000, *ApJ*, 528, 626
- Pentericci L., Röttgering H. J. A., Miley G. K., Spinrad H., McCarthy P. J., van Breugel W. J. M., Macchetto F., 1998, *ApJ*, 504, 139
- Pentericci L., Röttgering H. J. A., Miley G. K., McCarthy P., Spinrad H., van Breugel W. J. M., Macchetto F., 1999, *A&A*, 341, 329
- Rees, M. J. 1978, *Nature*, 275, 516
- Röttgering, H. J. A., van Ojik, R., Miley, G. K., et al. 1997, *A&A*, 326, 505
- Sanders D. B., Mirabel I. F., 1996, *ARA&A*, 34, 749
- Sazonov, S. Y., Ostriker, J. P., Ciotti, L., & Sunyaev, R. A. 2004, *ArXiv Astrophysics e-prints*
- Silk, J. & Rees, M. J. 1998, *A&A*, 331, L1
- Steidel, C.C., Giavalisco, M., Pettini, M., Dickinson, M. & Adelberger, K.L. 1996, *ApJ*, 462, L17
- Steidel, C. C., Adelberger, K. L., Giavalisco, M., Dickinson, M., & Pettini, M. 1999, *ApJ*, 519, 1
- Toomre, A., & Toomre, J. 1972, *ApJ*, 178, 623
- van Breugel, W.J.M., Stanford, S.A., Spinrad, H., Stern, D. & Graham, J.R., 1998, *ApJ*, 502, 614
- van Breugel, W. & Bland-Hawthorn, J. 2000, *PASP*, 112, 579
- van Ojik, R., Röttgering, H. J. A., Carilli, C. L., et al. 1996, *A&A*, 313, 25
- Venemans, B. P. et al. 2002, *ApJ*, 569, L11
- Villar-Martín, M., Vernet, J., di Serego Alighieri, S., et al. 2003, *MNRAS*, 346, 273
- Webb T. M., Eales S., Foucaud S., Lilly S. J., McCracken H., Adelberger K., Steidel C., Shapley A., Clements D. L., Dunne L., Le Fèvre O., Brodwin M., Gear W., 2003, *ApJ*, 582, 6
- White, S. D. M., & Rees, M. J. 1978, *MNRAS*, 183, 341



---

## Chapter 2

---

# Dust and star formation in distant radio galaxies

Michiel Reuland, Huub Röttgering, Wil van Breugel, and Carlos De Breuck, *Monthly Notices of the Royal Astronomical Society*, Vol. 353, p. 377, 2004

We present the results of an observing program with the SCUBA bolometer array to measure the submillimetre (submm) dust continuum emission of 24 distant ( $z > 1$ ) radio galaxies. We detected submm emission in 12 galaxies with  $S/N > 3$ , including 9 detections at  $z > 3$ . When added to previous published results these data almost triple the number of radio galaxies with  $z > 3$  detected in the submm and yield a sample of 69 observed radio galaxies over the redshift range  $z = 1-5$ . We find that the range in rest-frame far-infrared luminosities is about a factor of 10. We have investigated the origin of this dispersion, correlating the luminosities with radio source power, size, spectral index,  $K$ -band magnitude and  $\text{Ly}\alpha$  luminosity. No strong correlations are apparent in the combined data set. We confirm and strengthen the result from previous submm observations of radio galaxies that the detection rate is a strong function of redshift. We compare the redshift dependence of the submm properties of radio galaxies with those of quasars and find that for both classes of objects the observed submm flux density increases with redshift to  $z \approx 4$ , beyond which, for the galaxies, we find tentative evidence for a decline. We find evidence for an anti-correlation between submm luminosity and UV polarisation fraction, for a subsample of 13 radio galaxies, indicating that starbursts are the dominant source of heating for dust in radio galaxies.

## 1 Introduction

**T**HERE is strong evidence that powerful high redshift radio galaxies (HzRGs;  $z > 2$ ) are the progenitors of the brightest cluster ellipticals seen today. HzRGs are the infrared brightest and presumably the most massive galaxies at any epoch (De Breuck et al. 2002) and host actively-accreting super massive black holes with masses of order  $10^9 M_{\odot}$  (Lacy et al. 2001; Dunlop et al. 2003). Therefore, they are key objects for studying the formation and evolution of massive galaxies and super-massive black holes.

HzRGs are likely to be in an important phase of their formation process for several reasons: They have large reservoirs of gas from which they could be forming, as shown by spectacular ( $> 100$  kpc) luminous  $\text{Ly}\alpha$  haloes (e.g., McCarthy 1993; van Ojik et al.

1996; Reuland et al. 2003) and widespread HI absorption features in the Ly $\alpha$  profiles (van Ojik et al. 1997). Their rest-frame UV morphologies are characterized by clumpy structures, similar to the Lyman-break galaxies at  $z \sim 3$ , that will merge with the central galaxy on dynamical time-scales of  $10^8$  yrs (Pentericci et al. 1998; Pentericci et al. 1999). In the case of 4C 41.17 there is direct evidence for massive star formation (up to  $\sim 1500 M_{\odot} \text{ yr}^{-1}$  after correction for extinction) based on stellar absorption-lines (Dey et al. 1997). Finally, mm-interferometry studies of CO line and continuum emission for three  $z > 3$  HzRGs have shown that the star formation occurs galaxy wide over distances up to 30 kpc (Papadopoulos et al. 2000; De Breuck et al. 2003) and there is even evidence for star formation on scales of 250 kpc (Stevens et al. 2003). Together this suggests that we are observing not merely scaled up versions of local ultraluminous infrared galaxies (ULIRGs) where the bursts are confined to the inner few kpc, but wide-spread starbursts within which the galaxies are forming the bulk of their eventual stellar populations.

HzRGs are an important sample for studying the star formation history of the universe because their selection is based on long wavelength radio emission whose propagation is not affected by the presence of dust. Dust is expected to play a significant role in star forming regions, absorbing UV/optical radiation from the starburst and reradiating it at far-infrared (FIR) wavelengths (Sanders & Mirabel 1996). Optical searches for distant galaxies (e.g., using the Lyman-break technique; Steidel et al. 1996; Steidel et al. 1999; Ouchi et al. 2001) are thus likely to be biased against dusty objects. Finding distant star forming galaxies through submillimetre (submm; rest-frame FIR) emission (e.g., Hughes et al. 1998; Bertoldi et al. 2002; Chapman et al. 2002a; Cowie et al. 2002; Scott et al. 2002; Smail et al. 2002; Webb et al. 2003a; Eales et al. 2003) selects only the most obscured sources. So far there has been little overlap between the optical and submm selected star forming sources (selection on very red near-IR colours may prove more fruitful; e.g., Frayer et al. 2004). It remains unclear whether they are members of a continuous population (e.g., Adelberger & Steidel 2000; Webb et al. 2003b) and arguments have been made that either one of them could dominate the star formation density at high redshift (Blain et al. 1999; Adelberger & Steidel 2000). Since selection at radio wavelengths circumvents the aforementioned selection biases it could help determine the relative contributions of obscured and unobscured star formation to the star formation history of the universe.

Archibald et al. (2001, hereafter A01) have conducted the first systematic submm survey to study the star formation history of radio galaxies over a redshift interval of  $0.7 < z < 4.4$ . In their sample of 47 galaxies, they found evidence for a considerable range in FIR luminosities, a substantial increase in 850  $\mu\text{m}$  detection rate with redshift and that the average 850  $\mu\text{m}$  luminosity rises at a rate  $(1+z)^{3-4}$  out to  $z \simeq 4$ . These results prompt the following questions: Is the dispersion in FIR luminosities due to differences in their star formation rates or dust contents? Does the strong increase with redshift reflect an increase in star formation rates or could it be related to changing dust properties? Does the FIR luminosity keep on rising with redshift or does it level off and is there a redshift cut-off? Are the inferred star formation rates comparable to those derived from the optical/UV? Do the submm properties of quasars (QSOs) and radio galaxies show similar trends or do the two classes of objects evolve differently?



| Source       | $z$   | RA(J2000) |    |       | DEC (J2000) |    |      | LAS<br>" | $F_{Ly\alpha}$<br>cgs | $K$<br>mag | References          |
|--------------|-------|-----------|----|-------|-------------|----|------|----------|-----------------------|------------|---------------------|
|              |       | h         | m  | s     | °           | '  | "    |          |                       |            |                     |
| WNJ0528+6549 | 1.210 | 5         | 28 | 46.07 | +65         | 49 | 57.3 | 1.9      | —                     | 18.2       | DB00a, dV03         |
| MRC1138–262  | 2.156 | 11        | 40 | 48.25 | –26         | 29 | 10.1 | 15.8     | 13.9                  | 16.1       | Röt97, Pen97, DB00b |
| WNJ1115+5016 | 2.550 | 11        | 15 | 6.87  | +50         | 16 | 23.9 | 0.2      | 2.0                   | 19.2       | DB00a, DB01, DB02   |
| WNJ0747+3654 | 2.992 | 7         | 47 | 29.38 | +36         | 54 | 38.1 | 2.1      | 0.8                   | 20.0       | DB00a, DB01, DB02   |
| WNJ0231+3600 | 3.079 | 2         | 31 | 11.48 | +36         | 0  | 26.6 | 14.8     | 1.1                   | —          | DB00a, DB01, DB02   |
| B3J2330+3927 | 3.086 | 23        | 30 | 24.91 | +39         | 27 | 11.2 | 1.9      | 4.4                   | 18.8       | DB03a               |
| TNJ1112–2948 | 3.090 | 11        | 12 | 23.86 | –29         | 48 | 6.2  | 9.1      | 2.9                   | —          | DB00a, DB01         |
| MRC0316–257  | 3.130 | 3         | 18 | 12.06 | –25         | 35 | 9.7  | 7.6      | 2.4                   | —          | McC90, ER96, DB00b  |
| PKS1354–17   | 3.150 | 13        | 47 | 96.03 | –17         | 44 | 02.2 | —        | —                     | —          | Dri97               |
| WNJ0617+5012 | 3.153 | 6         | 17 | 39.37 | +50         | 12 | 54.7 | 3.4      | 0.8                   | 19.7       | DB00b, DB01, DB02   |
| MRC0251–273  | 3.160 | 2         | 53 | 16.70 | –27         | 9  | 9.6  | 3.9      | —                     | —          | McC96, Kap98        |
| WNJ1123+3141 | 3.217 | 11        | 23 | 55.85 | +31         | 41 | 26.1 | 25.8     | 6.2                   | 17.5       | DB00a, DB01, DB02   |
| WNH1702+6042 | 3.223 | 17        | 3  | 36.23 | +60         | 38 | 52.2 | 11.5     | —                     | —          | Ren98               |
| TNJ0205+2242 | 3.506 | 2         | 5  | 10.69 | +22         | 42 | 50.3 | 2.7      | —                     | 18.8       | DB00a, DB01, DB02   |
| TNJ0121+1320 | 3.516 | 1         | 21 | 42.74 | +13         | 20 | 58.3 | 0.3      | —                     | 18.8       | DB00a, DB01, DB02   |
| 6C1908+722   | 3.532 | 19        | 8  | 23.70 | +72         | 20 | 11.8 | 14.4     | 32.0                  | 16.5       | Dey99, Pap00, DB01  |
| WNJ1911+6342 | 3.590 | 19        | 11 | 49.54 | +63         | 42 | 9.6  | 1.8      | 1.4                   | 18.6       | DB00a, DB01, DB02   |
| MG2141+192   | 3.592 | 21        | 44 | 7.50  | +19         | 29 | 15.0 | 8.5      | 6.2                   | 19.3       | S99                 |
| WNJ0346+3039 | 3.720 | 3         | 46 | 42.68 | +30         | 39 | 49.3 | 0.4      | —                     | 17.8       | DB00a, DB02, dV03   |
| 4C60.07      | 3.791 | 5         | 12 | 55.15 | +60         | 30 | 51.0 | 16.0     | 10.1                  | 19.3       | Röt97, Pap00, DB00b |
| TNJ2007–1316 | 3.830 | 20        | 7  | 53.23 | –13         | 16 | 43.6 | 7.2      | 2.5                   | 17.9       | DB00a, DB02, DB03b  |
| TNJ1338–1942 | 4.100 | 13        | 38 | 26.06 | –19         | 42 | 30.1 | 5.5      | 10.1                  | 19.7       | DB99                |
| TNJ1123–2154 | 4.109 | 11        | 23 | 10.15 | –21         | 54 | 5.3  | 0.8      | 0.2                   | 20.4       | DB00a, DB01, DB02   |
| TNJ0924–2201 | 5.190 | 9         | 24 | 19.92 | –22         | 1  | 41.5 | 1.2      | 0.4                   | 19.9       | vB99                |

**Table 1** — Redshifts, radio positions, largest angular sizes,  $Ly\alpha$  fluxes,  $K$ -band magnitudes and references to papers from which these data were taken for all objects that were observed in our submm program. The  $Ly\alpha$  fluxes are in units of  $10^{-16}$  ergs  $s^{-1}$  cm  $^{-2}$ , and the  $K$ -band magnitudes were measured in a 64 kpc diameter aperture where possible. References: DB99, DB00a, DB00b, DB01, DB02, DB03a, DB03b = De Breuck et al. (1999, 2000); De Breuck et al. (2000); De Breuck et al. (2001); De Breuck et al. (2002, 2003, De Breuck et al. in preparation), dV03 = de Vries et al. in preparation, Dey99 = Dey (1999), Dri97 = Drinkwater et al. (1997), ER96 = Eales & Rawlings (1996), McC90 = McCarthy et al. (1990), McC96 = McCarthy et al. (1996), Kap98 = Kapahi et al. (1998), Pap00 = Papadopoulos et al. (2000), Pen97 = Pentericci et al. (1997), Ren98 = Rengelink (1998), Röt97 = Röttgering et al. (1997), S99 = Stern et al. (1999), vB99 = van Breugel et al. (1999).

The submm findings from A01 were based on a limited number of detections at high redshift ( $z > 3$ ). To put these results on a statistically firmer footing and search for possible correlations with other galaxy parameters more submm observations were required. Here we present such observations of all  $z > 3$  HzRGs known at the beginning of 2001 (e.g., De Breuck et al. 2001) which had not been observed in the submm. Adding these to the survey of A01 almost triples the number of detections at high redshift, creating a sample which is statistically significant over the full redshift range  $z = 1 - 5$ .

The structure of this paper is as follows: the sample selection, observations and data analysis are described in Section 2. Results and notes on some individual sources are presented in Section 3. Various correlations with submm properties of HzRGs are investigated in Section 4 and described in detail in Section 5. Section 6 presents a comparison between HzRGs and QSOs. We discuss and summarize our conclusions in Section 7. Throughout this paper, we adopt a flat universe with  $\Omega_M = 0.3$ ,  $\Omega_\Lambda = 0.7$ , and  $H_0 = 65$  km  $s^{-1}$  Mpc  $^{-1}$ . Using this cosmology the look-back time at  $z \sim 2.5$  (the median redshift of our sample) is  $11.7 h_{65}^{-1}$  Gyr and a galaxy at such a redshift must be less than  $2.8 h_{65}^{-1}$  Gyr old.

| Source       | $z$   | $N_{\text{int}} \times 50$ | $S_{850}^a$<br>mJy     | S/N  | Quality | $3\sigma$ lim.<br>mJy | $S_{450}$<br>mJy | $L_{850}$<br>W Hz $^{-1}$ sr $^{-1}$ | $L_{\text{FIR}}$<br>$L_{\odot}$ | $L_{3\text{GHz}}$<br>W Hz $^{-1}$ sr $^{-1}$ |
|--------------|-------|----------------------------|------------------------|------|---------|-----------------------|------------------|--------------------------------------|---------------------------------|--|
| WNJ0528+6549 | 1.210 | 4+4                        | $-1.9 \pm 1.3$         | -1.4 | A       | <3.9                  | $2 \pm 29$       | <23.05                               | <12.63                          | 24.59  |
| MRC1138-262  | 2.156 | 2                          | $12.8 \pm 3.3^b$       | 3.9  | B       |                       | $-65 \pm 134$    | 23.26 <sup>b</sup>                   | 12.83 <sup>b</sup>              | 27.15  |
| WNJ1115+5016 | 2.550 | 4                          | $3.0 \pm 1.3$          | 2.3  | A       | <6.9                  | $-20 \pm 11$     | <23.31                               | <12.90                          | 25.95  |
| WNJ0747+3654 | 2.990 | 6                          | $4.8 \pm 1.1$          | 4.5  | A       |                       | $18 \pm 15$      | 23.15                                | 12.73                           | 26.22  |
| WNJ0231+3600 | 3.080 | 7                          | $5.9 \pm 1.6$          | 3.7  | B       |                       | $-29 \pm 22$     | 23.23                                | 12.81                           | 26.27  |
| B3J2330+3927 | 3.086 | 3                          | $14.1 \pm 1.7^c$       | 8.5  | A       |                       | $49 \pm 18$      | 23.61                                | 13.19                           | 26.56  |
| TNJ1112-2948 | 3.090 | 5                          | $5.8 \pm 1.1$          | 5.1  | A       |                       | $15 \pm 9$       | 23.23                                | 12.81                           | 26.66  |
| MRC0316-257  | 3.130 | 2                          | $0.6 \pm 2.7$          | 0.2  | B       | <8.8                  | $5 \pm 48$       | <23.41                               | <12.99                          | 27.22  |
| PKS1354-17   | 3.150 | 2                          | $20.5 \pm 2.6^d$       | 8.0  | B       |                       | $-47 \pm 77$     | 23.77                                | -                               | 27.71  |
| WNJ0617+5012 | 3.153 | 6+6                        | $1.0 \pm 0.7$          | 1.3  | B       | <3.2                  | $3 \pm 16$       | <22.96                               | <12.55                          | 26.10  |
| MRC0251-273  | 3.160 | 2                          | $0.6 \pm 2.8$          | 0.2  | A       | <8.9                  | $-54 \pm 91$     | <23.41                               | <12.99                          | 27.00  |
| WNJ1123+3141 | 3.220 | 8                          | $4.9 \pm 1.2$          | 4.1  | A       |                       | $4 \pm 14$       | 23.15                                | 12.73                           | 26.60  |
| WNH1702+6042 | 3.223 | 1                          | $-0.4 \pm 3.6$         | -0.1 | B       | <10.8                 | $-73 \pm 91$     | <23.49                               | <13.07                          | 26.40  |
| TNJ0205+2242 | 3.506 | 6                          | $1.3 \pm 1.3$          | 1.0  | A       | <5.2                  | $27 \pm 23$      | <23.17                               | <12.75                          | 26.58  |
| TNJ0121+1320 | 3.517 | 7+4                        | $7.5 \pm 1.0$          | 7.6  | A       |                       | $4 \pm 16$       | 23.33                                | 12.91                           | 26.55  |
| 6CJ1908+722  | 3.532 | 6                          | $10.8 \pm 1.2^c$       | 9.0  | A       |                       | $33 \pm 17$      | 23.49                                | 13.07                           | 27.25  |
| WNJ1911+6342 | 3.590 | 2                          | $1.3 \pm 3.6$          | 0.4  | B       | <11.9                 | $-38 \pm 50$     | <23.53                               | <13.11                          | 26.26  |
| MG2141+192   | 3.592 | 7+5                        | $2.3 \pm 0.9^{b,e}$    | 2.6  | A       | <5.0                  | $12 \pm 13$      | 22.96 <sup>b</sup>                   | <12.55 <sup>b</sup>             | 27.30  |
| WNJ0346+3039 | 3.720 | 4                          | $-0.5 \pm 1.3$         | -0.4 | A       | <3.8                  | $-5 \pm 12$      | <23.02                               | <12.61                          | 26.43  |
| 4C60.07      | 3.791 | 5                          | $11.5 \pm 1.5^{b,c,e}$ | 7.6  | A       |                       | $10 \pm 13$      | 23.61 <sup>b</sup>                   | 13.19 <sup>b</sup>              | 27.15  |
| TNJ2007-1316 | 3.830 | 5                          | $5.8 \pm 1.5$          | 4.0  | A       |                       | $4 \pm 45$       | 23.21                                | 12.79                           | 26.98  |
| TNJ1338-1942 | 4.100 | 4+7                        | $6.9 \pm 1.1$          | 6.2  | A       |                       | $-36 \pm 32$     | 23.29                                | 12.87                           | 27.05  |
| TNJ1123-2154 | 4.109 | 2                          | $1.5 \pm 1.7$          | 0.9  | A       | <6.7                  | $-7 \pm 11$      | <23.27                               | <12.85                          | 26.76  |
| TNJ0924-2201 | 5.190 | 8+4                        | $-0.7 \pm 1.1$         | -0.7 | A       | <3.2                  | $-0 \pm 26$      | <22.94                               | <12.53                          | 27.24  |

**Table 2** — Observed 850  $\mu\text{m}$  and 450  $\mu\text{m}$  submm flux densities  $S_{850 \mu\text{m}}$  and  $S_{450 \mu\text{m}}$  with their standard errors for the radio sources in the program. The total duration of the observations,  $N_{\text{int}}$  is given in sets of 50 integrations.  $3\sigma$  upper limits to the 850  $\mu\text{m}$  flux are shown for sources whose S/N is below 3. Only B3 J2330+3927 may have been detected at  $2\sigma$  at 450  $\mu\text{m}$ . Logarithms of inferred rest-frame 850  $\mu\text{m}$  luminosities  $L_{850}$ , far-IR luminosities,  $L_{\text{FIR}}$  and radio luminosities  $L_{3\text{GHz}}$  are shown for the dust template with  $\beta = 1.5$ ,  $T_d = 40$  K and a flat universe with  $\Omega_M = 0.3$ ,  $\Omega_\Lambda = 0.7$ , and  $H_0 = 65$  km s $^{-1}$  Mpc $^{-1}$ .

<sup>a</sup>This does not include the 10–15 per cent uncertainty in absolute photometric calibration.

<sup>b</sup>For the statistical analysis we use  $S_{850} = 5.9 \pm 1.1$  mJy,  $S_{850} = 3.3 \pm 0.7$  mJy and  $S_{850} = 14.4 \pm 1.0$  mJy for MRC 1138-262, MG 2141+192 and 4C 60.07, respectively.  $L_{850}$  and  $L_{\text{FIR}}$  were inferred using those values. See Section 4 for details.

<sup>c</sup>Data published in CO imaging studies by Papadopoulos et al. (2000) and De Breuck et al. (2003).

<sup>d</sup>PKS 1354-17 is likely to be dominated by non-thermal emission (c.f. Section 2.2).

<sup>e</sup>Also part of the survey by A01.

## 2 Sample Selection and Observations

The observations presented here include submm observations of distant radio galaxies. The targets were selected from an increasing sample of HzRGs that is the result of an ongoing effort by our group and others (De Breuck et al. 2000, 2001, de Vries et al. in preparation; Spinrad private communication) to find distant radio galaxies based on Ultra Steep Radio Spectrum (USS; i.e. red radio color) and near-IR identification selection criteria (for details see De Breuck et al. 2001).

We selected all HzRGs known at the beginning of 2001 with redshifts  $z \gtrsim 3$  and declination  $\delta > -30^\circ$  that did not have prior submm observations. Our aim was to observe a significant sample of HzRGs to complement the observations of A01 and, in particular, to obtain better statistics at the highest redshifts. MG 2141+192 and 4C 60.07 were observed in both programs, because, at the time of observation, their inclusion in the A01 sample was unknown to us. The 850  $\mu\text{m}$  results for B3 J2330+3927, 6C J1908+722,

and 4C 60.07 have been published previously as part of their CO imaging studies (Papadopoulos et al. 2000; De Breuck et al. 2003). MRC 1138–262 was included in the program because of its wealth of supporting data (e.g., Pentericci et al. 1997; Carilli et al. 2002) and WN J1115+5016 because it is one of only two radio galaxies showing a broad absorption line (BAL) system (De Breuck et al. 2001), the other BAL radio galaxy, 6C J1908+722, being a strong CO emitter (Papadopoulos et al. 2000). WN J0528+6549 at  $z = 1.210$  was observed because it was first thought to be at redshift  $z = 3.120$  (actually belonging to another galaxy on the slit).

The coordinates, redshifts, largest angular sizes of the radio sources,  $\text{Ly}\alpha$  fluxes,  $K$ -band magnitudes, and references for the full sample observed in the submm are listed in Table 1.

## 2.1 SCUBA photometry

The observations were carried out between October 1997 and January 2002 with the Submillimetre Common–User Bolometer Array (SCUBA; Holland et al. 1999) at the 15 m James Clerk Maxwell Telescope (JCMT). We observed at  $450\ \mu\text{m}$  and  $850\ \mu\text{m}$  wavelengths resulting in beam sizes of  $7.5''$  and  $14.7''$  respectively. We employed the 9-point jiggle photometry mode, which samples a  $3 \times 3$  grid with  $2''$  spacing between grid points, while chopping  $45''$  in azimuth at 7.8 Hz. Frequent pointing checks were performed to ensure pointings better than  $2''$  and reach optimal sensitivity.

Our original goal was to observe all sources down to 1 mJy rms at  $850\ \mu\text{m}$ . This is a sensible limit, since at  $850\ \mu\text{m}$  confusion becomes a problem for sources weaker than 2 mJy (Hughes et al. 1998; Hogg 2001), it is obtainable in 3 hrs per source, and it is matched to the survey by A01. However, because of scheduling constraints, and because our priority was to obtain a large sample of HzRGs with  $850\ \mu\text{m}$  detections, this limit was not always reached. Rather, the next target was observed as soon as an apparent  $5\sigma$  detection had been obtained at  $850\ \mu\text{m}$ .

The atmospheric optical depths  $\tau_{850}$ ,  $\tau_{450}$  were calculated using the empirical CSO–tau correlations given by Archibald et al. (2002), unless the values obtained through skydips disagreed strongly, in which case those were used instead. The optical depth  $\tau_{850}$  varied between 0.14 and 0.38 with an average value of 0.26. The data were clipped at the  $4\sigma$  level to ensure accurate determination of the sky level, flat–fielded, corrected for extinction, sky noise was removed after which they were co–added and clipped at the  $2.5\sigma$  level using the Scuba User Reduction Facility software package (SURF; Jenness & Lightfoot 1998), following standard procedures outlined in the SCUBA Photometry Cookbook<sup>1</sup>. The concatenated data were checked for internal consistency using a Kolmogorov–Smirnov (K–S) test and severely deviating measurements (if any) were removed. Finally, flux calibration was performed using HLTAU, OH231.8 and CRL618 as photometric calibrators. The typical photometric uncertainty for our program is of order 10–15 per cent, as estimated from our results on three sources (TN J0121+1320, TN J1338–1942, and MG 2141+192) that were observed at two separate instances each. This photometric accuracy is consistent with an estimated 10 per cent systematic uncertainty in the  $850\ \mu\text{m}$  flux density scale (see e.g., Papadopoulos et al. 2000; Jenness

<sup>1</sup>The SCUBA Photometry Cookbook is available at <http://www.starlink.rl.ac.uk/star/docs/sc10.htx/sc10.html>

et al. 2001). Given that HzRGs appear to be located in submm overdense regions (e.g., Stevens et al. 2003) flux may have been lost due to chopping onto a nearby galaxy. However this very unlikely to have affected more than a few sources.

Following Omont et al. (2001), Table 2 includes a column indicating the quality of the observation. Good quality data is indicated by an ‘A’, whereas poor quality is indicated by a ‘B’. Poor quality reflects bad atmospheric conditions (e.g. large seeing), short integration time ( $< 2$  sets of 50 integrations each), or poor internal consistency as shown by the K–S test (i.e. the measurements were not consistent, but it was impossible to determine which were the outliers. In such cases the average of all measurements was used).

## 2.2 Potential contamination of the thermal submillimetre flux

Because all our objects are powerful radio galaxies, it is important to estimate any synchrotron contribution to the observed submm band. We used flux densities from the WENSS (325 MHz Rengelink et al. 1997), Texas (365 MHz; Douglas et al. 1996) and NVSS (1.4 GHz; Condon et al. 1998) surveys to extrapolate to 350 GHz (850  $\mu\text{m}$ ) frequencies using a power law. For 53W069, we extrapolated from the 600 MHz and 1.4 GHz values in Waddington et al. (2000). We find that the synchrotron contribution at 850  $\mu\text{m}$  is negligible for most galaxies in our sample. Only for some objects from A01 (and PKS 1354–17) would this require corrections larger than the  $1\sigma$  uncertainties in the 850  $\mu\text{m}$  measurements.

Synchrotron spectra often steepen at high frequencies (e.g., A01; Athreya et al. 1997; Andreani et al. 2002; Sohn et al. 2003), and linear extrapolation should be considered an upper limit to the synchrotron contribution. A01 performed parabolic fits to account for the curvature of the radio spectrum. Using the midpoint between linear and parabolic fits they find corrections larger than 1.5 mJy to the 850  $\mu\text{m}$  flux densities in only 6 cases. One could argue that parabolic fits are more appropriate, in which case all corrections would be negligible.

Note that the radio measurements reflect the spatially integrated flux densities of the sources. The radio cores have flatter spectra than the lobes and could dominate at higher frequencies. However, they are usually faint and for USS sources even the radio cores tend to have steep spectra (e.g., A01; Athreya et al. 1997) indicating that contamination by the core is likely to be negligible as well.

Given these uncertainties, extrapolation from the radio regime to submm wavelengths is uncertain and is likely to result in an overestimate of the non-thermal contribution due to steepening of the radio spectrum. This is demonstrated for the case of B3 J2330+3927, for which De Breuck et al. (2003) estimate a non-thermal contribution of  $\sim 1.3$  mJy at 113 GHz but measured a flux density  $< 0.3$  mJy that seems to be of thermal origin. Therefore we do not correct for a contribution to the submm continuum from the non-thermal radio emission, except for a few sources discussed below. For these reasons (and following Willott et al. 2002) we have chosen also to use uncorrected fluxes from A01 in the remainder of this paper.

There are two exceptions that we exclude from our final sample. Following A01, we reject B2 0902+34, as this source has a bright flat-spectrum radio core which could dominate the submm emission. We also reject the flat spectrum radio source PKS 1354–17.

It is significantly brighter than any of the other sources at 850  $\mu\text{m}$  ( $S_{850} = 20.5 \pm 2.6$  mJy), but linear extrapolation from the radio regime shows that the non-thermal contribution at 850  $\mu\text{m}$  could be as large as 40 mJy and could easily account for all of the submm signal.

Gravitational lensing may be important in some cases (Lacy 1999), resulting in enhanced submm fluxes. However, recent estimates (e.g., Chapman et al. 2002b; Dunlop 2002) show that this is limited to a small but significant fraction (3–5 per cent of sources with  $S_{850} > 10$  mJy may have been boosted by a factor  $\gtrsim 2$ ) and that for most objects there is no evidence for strong gravitational lensing. Corrections for lensing must be made on a case-to-case basis and are strongly model dependent. Since these corrections are likely to be small, they have not been attempted for the present sample.

### 2.3 Dust template

As has been noted by many authors (e.g., A01; Hughes et al. 1997), choosing the dust template is an important step in inferring the bolometric far infra-red luminosities ( $L_{\text{FIR}}$ ), star formation rates (SFR) and dust masses ( $M_{\text{d}}$ ). A complication is that the appropriate dust template may change over redshift due to changing dust properties with the evolutionary states of the galaxies.

Throughout this paper we adopt single temperature, optically thin greybody emission for two sets of emissivity index  $\beta$  and temperature  $T_{\text{d}}$  (see Dunne & Eales 2001; Dupac et al. 2003, for possible concerns) as the functional parametrization for thermal dust emission from high redshift sources. We choose  $\beta = 1.5$  and  $T_{\text{d}} = 40$  K for comparison with other papers (e.g., A01; and see Dunne et al. 2000; Eales et al. 2003), and also briefly investigate the effects of assuming  $\beta = 2.0$  and  $T_{\text{d}} = 40$  K as seems reasonable for some hyperluminous IR galaxies ( $T_{\text{d}} = 35$  K; HyLIRGs Farrah et al. 2002) and  $z > 4$  quasars ( $T_{\text{d}} = 40$ –50 K; Priddey & McMahan 2001; Willott et al. 2002). Measuring the value of  $\beta$  for HzRGs directly would require observations at many more rest-frame FIR wavelengths than presented here. Increasing  $\beta$  or the dust temperature decreases the inferred  $L_{\text{FIR}}$  of high redshift sources relative to lower redshift sources for a given flux density.

The fraction of absorbed UV/optical light,  $\delta_{\text{SB}}$ , and possible departures from the prototype Salpeter initial mass function, parametrized with  $\delta_{\text{IMF}}$ , are other uncertain factors. Generally accepted approximations (see e.g., Papadopoulos et al. 2000; Omont et al. 2001; De Breuck et al. 2003) for the dust mass, inferred FIR luminosity and star formation rate are respectively:

$$M_{\text{d}} = \frac{S_{\text{obs}} D_{\text{L}}^2}{(1+z) \kappa_{\text{d}}(\nu_{\text{rest}}) B(\nu_{\text{rest}}, T_{\text{d}})},$$

$$L_{\text{FIR}} = 4\pi M_{\text{d}} \int_0^{\infty} \kappa_{\text{d}}(\nu) B(\nu, T_{\text{d}}) d\nu =$$

$$\frac{8\pi h}{c^2} \frac{\kappa_{\text{d}}(\nu)}{\nu^{\beta}} \left( \frac{kT}{h} \right)^{\beta+4} \Gamma(\beta+4) \zeta(\beta+4) M_{\text{d}},$$

and

$$\text{SFR} = \delta_{\text{IMF}} \delta_{\text{SB}} (L_{\text{FIR}} / 10^{10} L_{\odot}) M_{\odot} \text{ yr}^{-1},$$

with  $\kappa_d(\nu) \propto \nu^\beta$  the frequency dependent mass absorption coefficient which modifies the Planck function,  $B(\nu, T_d)$ , to describe the isothermal greybody emission from dust grains,  $\Gamma$  the Gamma function,  $\zeta$  the Riemann Zeta function,  $D_L$  the luminosity distance and  $S_{\text{obs}}$  the observed flux density. The mass absorption coefficient is poorly constrained (e.g., Chini et al. 1986; Downes et al. 1992; De Breuck et al. 2003; James et al. 2002) and we conform to the intermediate value of  $\kappa_d(375\text{GHz}) = 0.15 \text{ m}^2 \text{ kg}^{-1}$  chosen by A01.

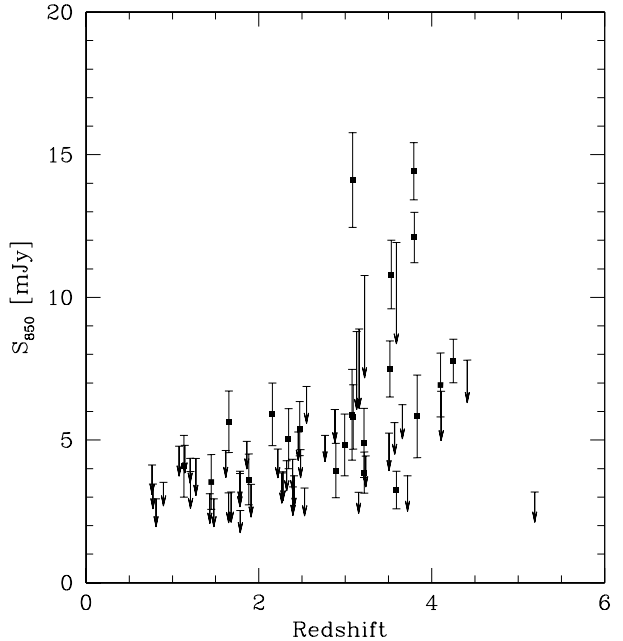
### 3 Observational Results

24 radio sources were observed. The results of the observations, the inferred rest-frame 850  $\mu\text{m}$  luminosities  $L_{850}$ , total far-IR luminosities  $L_{\text{FIR}}$ , and radio luminosities  $L_{3\text{GHz}}$  are summarized in Table 2. 12 of the HzRGs are detected at  $>3\sigma$  significance at 850  $\mu\text{m}$ . The median rms flux density of the observations is  $\sigma_{850} = 1.5 \text{ mJy}$  with an interquartile range of 0.8 mJy. Only B3 J2330+3927 may have been detected at 450  $\mu\text{m}$  at a  $2\sigma$  level ( $S_{450} = 49.1 \pm 17.7 \text{ mJy}$ ).

Particularly noteworthy is MG 2141+192. This source was detected by A01 at the  $4.8\sigma$ -level at  $S_{850} = 4.61 \pm 0.96 \text{ mJy}$ , using the narrow filterset whereas we observed  $S_{850} = 2.16 \pm 1.10 \text{ mJy}$  and  $S_{850} = 2.45 \pm 1.58 \text{ mJy}$  at two separate instances with the wide filter set and did not detect the source. Similarly 4C 60.07 has been detected in photometry mode at  $S_{850} = 11.5 \pm 1.5$ ,  $17.1 \pm 1.3$  and in a jiggle map at  $21.6 \pm 1.3$  (A01; Papadopoulos et al. 2000; Stevens et al. 2003). These measurements are consistent to within 2–3 $\sigma$  from the mean. However, naively, they could also be interpreted as signs of submm variability. A01 and Willott et al. (2002) also found tentative evidence for variability in the submm, but ascribed it to problems with sky subtraction for data obtained with the single-element bolometer UKT14 versus SCUBA. It is hard to see how widespread star formation could result in submm variability on the time-scale of years. Significant changes in  $L_{\text{FIR}}$  might be easier to envisage as the result of UV variability often seen in AGN and if the submm emission results from quasar heated dust. However, even in this scenario changes in the UV are expected to average over time in the observed submm regime, unless the FIR emitting region is compact. While the typical scale sizes for UV emission from the AGN are on parsec scales, the minimum extent of the FIR emitting region must be about 1 kpc to match the observed luminosity and dust temperature (e.g., Carilli et al. 2001). Submm variability, if real, is therefore hard to explain if reprocessing by dust is the dominant mechanism for the FIR emission. If, alternatively, the FIR emission would be non-thermal emission from the AGN, then the emission should be unresolved in contrast to the observed extents of a few tens of kpc. Moreover, observations indicate that AGN contribute at most 30 per cent of the FIR luminosity at wavelengths longer than 50  $\mu\text{m}$ , at least for HyLIRGs (Rowan-Robinson 2000; Farrah et al. 2002).

Possible explanations therefore may be that (i) for different chopping angles and distances sometimes flux is accidentally lost due to companion galaxies in the off-beam since the fields are overdense (Stevens et al. 2003), or (ii) that sometimes the AGN do in fact contribute close to the maximum amount expected (note that the submm flux for 4C 60.07 is centrally concentrated; Fig. 2 in Stevens et al. 2003), even though the

**Figure 1** — Observed 850  $\mu\text{m}$  flux density and  $3\sigma$  upper limits versus redshift of all 67 radio galaxies discussed in this paper. The size of the arrows and error bars correspond to  $1\sigma$  rms.



starbursts still dominate. (iii) Finally of course there is still the possibility of pointing errors, uncertainties in absolute flux calibration, and differences in atmospheric transparency that could shift the effective bandpass by a few GHz, which could make a difference due to the very steep slope of the spectrum.

## 4 Analysis

In the following we discuss a sample of 67 radio galaxies (46/47 from A01, 23/24 from this paper, two sources were observed in both samples). This excludes the flat-spectrum sources B2 0902+34 and PKS 1354–17 (see Section 2.2). For the statistical analysis we use the inverse variance weighted averages of the measurements of MG 2141+192 ( $\langle S_{850} \rangle = 3.3 \pm 0.7$  mJy) and 4C 60.07 ( $\langle S_{850} \rangle = 14.4 \pm 1.0$  mJy) and for MRC 1138–262 we prefer the value of  $S_{850} = 5.9 \pm 1.1$  mJy obtained by Stevens et al. (2003) over our observation under adverse conditions. The median rms flux density for this entire sample is  $\sigma_{850} = 1.1$  mJy with a 0.24 mJy interquartile range.

Figure 1 shows that the observed submm flux densities and therefore the inferred luminosities (see Table 2) at  $z > 3$  vary significantly from object to object. For the assumed dust template we find a range from  $L_{\text{FIR}} < 4 \times 10^{12} L_{\odot}$  for undetected targets to  $L_{\text{FIR}} \sim 2 \times 10^{13} L_{\odot}$  for detected sources. There are several viable scenarios to explain this. First, if all the warm dust is heated solely by young stars, then  $L_{\text{FIR}}$  is linked to the SFR, implying that the SFR differs significantly between objects. Alternatively, there may be a range in produced dust masses as substantial dust production may take more than a billion years if low-mass stars are the principal contributors (e.g., Edmunds 2001). In this case the range in  $L_{\text{FIR}}$  may reflect a range in starburst ages. The recent detection of significant amounts of dust in the local supernova remnant Cassiopeia A (Dunne et al. 2003), indicates that much faster evolving massive stars

| Variable<br>Dependent | Independent       | Percentage of |           | Significance ( $P$ ) |           |               | Correlation<br>Present? |
|-----------------------|-------------------|---------------|-----------|----------------------|-----------|---------------|-------------------------|
|                       |                   | Data Censored | Cox       | Kendall              | Spearman  |               |                         |
| $S_{850\mu\text{m}}$  | $z$               | 67% (52)%     | 0% (0%)   | 0% (0%)              | 0% (0%)   | YES (YES)     |                         |
| $D_{\text{lin}}$      | $L_{3\text{GHz}}$ | 0%            | 17%       | 34%                  | 32%       | NO            |                         |
| $L_{3\text{GHz}}$     | $z$               | 0%            | 1%        | 2%                   | 2%        | YES           |                         |
| $L_{850\mu\text{m}}$  | $L_{3\text{GHz}}$ | 67% (52)%     | 1% (1%)   | 7% (8%)              | 10% (8%)  | MAYBE (MAYBE) |                         |
| $L_{850\mu\text{m}}$  | $z$               | 67% (52)%     | 0% (0%)   | 0% (0%)              | 0% (0%)   | YES (YES)     |                         |
| $L_{850\mu\text{m}}$  | $\alpha$          | 67% (52)%     | 1% (1%)   | 1% (0%)              | 1% (0%)   | YES (YES)     |                         |
| $L_{850\mu\text{m}}$  | $D_{\text{lin}}$  | 67% (52)%     | 56% (22%) | 79% (89%)            | 96% (78%) | NO (NO)       |                         |
| $\alpha$              | $L_{3\text{GHz}}$ | 0%            | 36%       | 20%                  | 19%       | NO            |                         |
| $\alpha$              | $z$               | 0%            | 0%        | 0%                   | 0%        | YES           |                         |

**Table 3** — Results of survival analysis for all 67 sources. The significance  $P$  is the probability of the variables not being correlated according to each test. If all three tests yield  $P \lesssim 5$  per cent, then the variables are taken to be correlated. If only some yield  $P \lesssim 5$  per cent then a correlation is regarded as possible, but uncertain. Results are shown for both a  $3\sigma$  and  $2\sigma$  (between brackets) detection limit.

may be at least as important in producing dust. A considerable contribution from high-redshift supernovae would significantly lower the required time-scales for dust production and would favor a range in SFRs to explain the range in  $L_{\text{FIR}}$ .

Despite the various uncertainties, the result that the far infrared luminosities are high is robust. This has important implications for the starburst nature of these galaxies: inserting the values for  $L_{\text{FIR}}$  that we find using either dust template confirms that HzRGs are vigorously forming stars up to rates of a few  $1000 M_{\odot} \text{ yr}^{-1}$  and have dust masses of a few times  $10^8 M_{\odot}$ . This is consistent with the notion that they are in a critical phase of their formation, forming the bulk of their stellar masses.

#### 4.1 Statistical analysis

We have performed statistical tests to search for possible correlations of the submm with other properties of the radio galaxies. Specifically, we investigated whether there are correlations with redshift (as reported by A01), radio luminosity (as indicator of AGN contribution), largest angular size of the radio source (as indicator of age),  $K$ -band magnitude (as indicator of stellar mass or star formation rate),  $\text{Ly}\alpha$  flux (as a possible indicator of starburst “fuel”), and UV polarisation (as indicator of the relative contributions of starburst and AGN to the UV continuum). Below, we discuss these in more detail.

Since the sample contains a large fraction (of order 50 per cent) of non-detections (i.e. upper limits) we have conducted survival analysis tests similar to A01. Survival analysis allows the mixing of detections and upper limits (“censored data points”) in a statistically meaningful way thereby preserving as much information as possible. The results of the survival tests are summarized in Tables 3 and 4. Table 3 represents the results for the entire sample, whereas Table 4 only considers the 32 galaxies with redshifts  $z > 2.5$ .

We have defined the subsample with redshift  $z > 2.5$  to test for selection effects and remove them from our sample. The well known and strong (see A01) radio power-redshift relation in flux limited samples is likely to be the origin of many apparent correlations with redshift (see Table 3). Another example of selection effects is the correlation found between  $L_{850}$  and radio spectral index  $\alpha$  (Table 3). It reflects the tight correlations between spectral index and redshift (part of our search criteria for



| Variable<br>Dependent | Independent           | Percentage of<br>Data Censored | Significance (P) |           |           | Correlation<br>Present? |
|-----------------------|-----------------------|--------------------------------|------------------|-----------|-----------|-------------------------|
|                       |                       |                                | Cox <sup>a</sup> | Kendall   | Spearman  |                         |
| $S_{850\mu\text{m}}$  | $z$                   | 53% (34%)                      | 95% (81%)        | 17% (25%) | 34% (38%) | NO (NO)                 |
| $D_{\text{lin}}$      | $L_{3\text{GHz}}$     | 0%                             | 66%              | 8%        | 9%        | NO                      |
| $L_{3\text{GHz}}$     | $z$                   | 0%                             | 7%               | 4%        | 4%        | MAYBE                   |
| $L_{850\mu\text{m}}$  | $L_{3\text{GHz}}$     | 53% (34%)                      | 21% (33%)        | 33% (48%) | 46% (58%) | NO (NO)                 |
| $L_{850\mu\text{m}}$  | $z$                   | 53% (34%)                      | 88% (75%)        | 20% (34%) | 35% (52%) | NO (NO)                 |
| $L_{850\mu\text{m}}$  | $\alpha$              | 53% (34%)                      | 88% (99%)        | 81% (69%) | 99% (71%) | NO (NO)                 |
| $L_{850\mu\text{m}}$  | $D_{\text{lin}}$      | 53% (34%)                      | 13% (6%)         | 16% (7%)  | 13% (6%)  | NO (NO)                 |
| $L_{850\mu\text{m}}$  | $L_{\text{Ly}\alpha}$ | 59% (41%)                      | —                | 86% (91%) | 4% (4%)   | MAYBE (MAYBE)           |
| $L_{850\mu\text{m}}$  | $K_{\text{mag}}$      | 59% (44%)                      | —                | 47% (33%) | 88% (72%) | NO (NO)                 |
| $\alpha$              | $L_{3\text{GHz}}$     | 0%                             | 56%              | 21%       | 11%       | NO                      |
| $\alpha$              | $z$                   | 0%                             | 2%               | 10%       | 8%        | MAYBE                   |

**Table 4** — Similar to Table 3. Results of survival analysis for 32 sources at redshifts  $z > 2.5$ .

<sup>a</sup> Cox’s proportional hazard model only allows censoring in the dependent variable, therefore this test could not be applied with the  $\text{Ly}\alpha$  and  $K$ -band data.

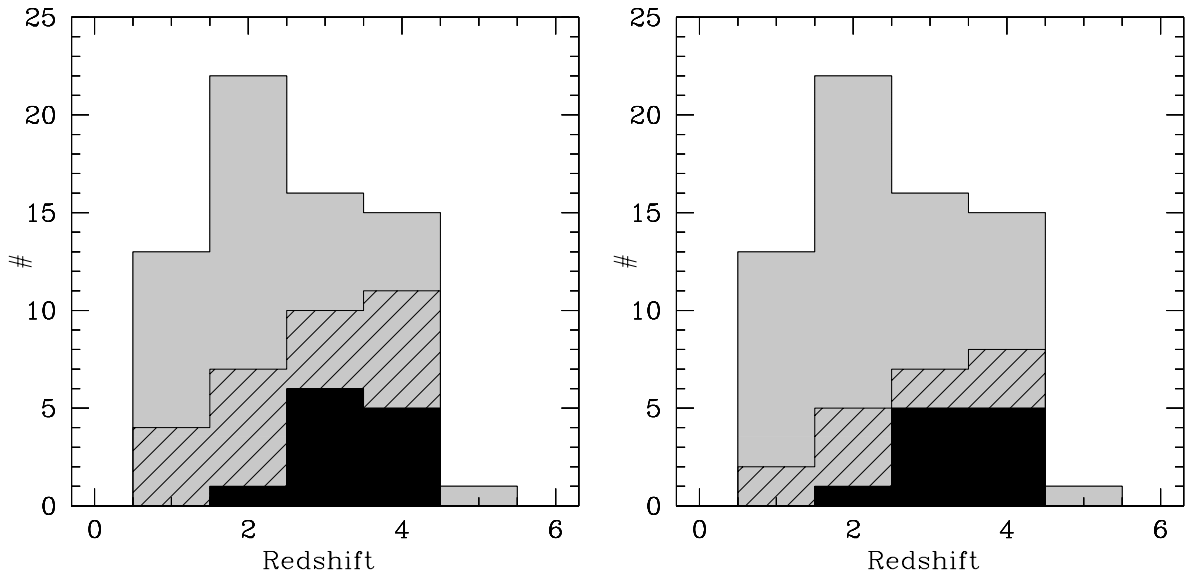


**Figure 2** — Histograms of  $850\mu\text{m}$  SCUBA detections with  $S/N > 2$  (left) and  $S/N > 3$  (right) versus the total number of observed radio galaxies (grey) as a function of redshift. The detections from Archibald et al. (2001) are shown as dashed, the detections from our program are shown in black. At  $z > 2.5 \sim 50\text{--}67$  per cent of the galaxies are detected, as opposed to  $\sim 15$  per cent at  $z < 2.5$ . The bins have a width of unit redshift and are centered at  $z = 1, 2, 3, 4, 5$ .

HzRGs) and between  $L_{850}$  and redshift. In the  $z > 2.5$  sample this correlation almost disappears even though there is a large range in both  $L_{850}$  and  $\alpha$ , confirming that it was spurious. An additional advantage of this subsample is the homogeneity of the supporting data (Ly $\alpha$  fluxes and  $K$ -band magnitudes are understandably sparse for lower redshift sources).

Below, we describe the details of the survival analysis and the criteria used to determine whether a correlation is present. In Section 5, we discuss the correlations individually.

### *Survival analysis*

The application of survival analysis methods to astronomical data has been described in detail by Feigelson & Nelson (1985) and Isobe et al. (1986). We have made use of the routines in the STSDAS package of IRAF<sup>2</sup> (Tody 1993), which were modelled after the ASURV package (Lavalley et al. 1992). Cox's proportional hazard model, the generalized Spearman's rank order correlation coefficient, and the generalized Kendall's tau correlation coefficient test the null hypothesis that no correlation is present in the sample. We adopt the convention that two variables are correlated if the chance  $P$  of the null hypothesis being true is smaller than 5 per cent. While these tests should give similar results they have different specific limitations and strong points. Therefore, a correlation is considered to be reliable if all tests yield  $P \lesssim 5$  per cent, and possible but unconfirmed if only some indicate  $P \lesssim 5$  per cent. Note that the Cox test only allows censoring in the dependent variable and that the generalized Spearman's Rho routine is not reliable for small data sets ( $N < 30$ ). SCUBA occasionally yields negative flux densities. We defined the  $n\sigma$  upperlimit for those cases to be  $n \times$  the rms flux density. Similarly, the  $n\sigma$  upperlimit for a positive signal is defined as  $S + n \times$  the rms flux density, with  $S$  the observed signal.

## 5 Correlations between parameters

Tables 3 and 4 represent the results of the survival analysis as described above. We will now discuss the motivation for each test and the implications of the correlations (or lack thereof) found in order of importance.

### 5.1 Redshift dependent submillimetre properties

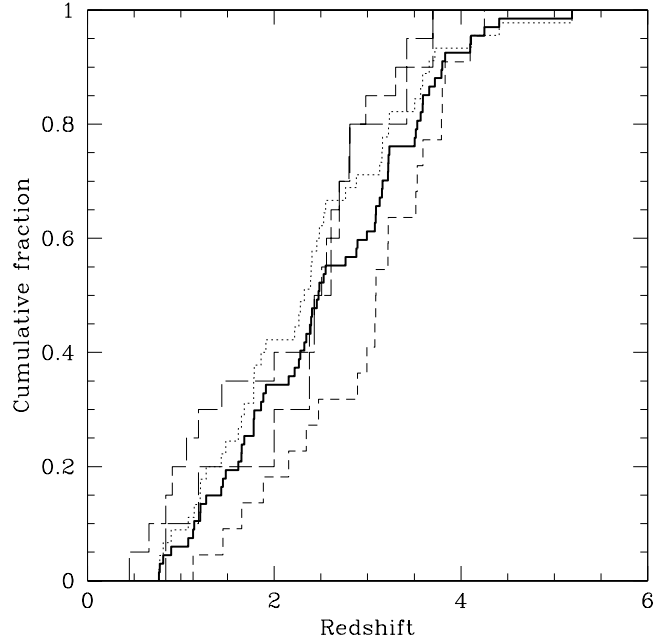
#### 5.1.1 Flux density and relative detection fraction

Table 3 shows that the observed submm flux densities  $S_{850}$  are strongly correlated with redshift. This is reflected in Figure 1 and 2. Figure 1 shows the observed 850  $\mu\text{m}$  flux densities against redshift. Figure 2 shows the number of radio galaxies that have been observed in a particular redshift bin and the number of those which have been detected given a  $2\sigma$  or  $3\sigma$  detection criterion. The success rate of our  $z > 3$  program is

---

<sup>2</sup>IRAF is distributed by the National Optical Astronomy Observatories, which are operated by the Association of Universities for Research in Astronomy, Inc., under cooperative agreement with the National Science Foundation.

**Figure 3** — Cumulative histograms  $\Sigma N(z)$  for redshifts of submm sources from the literature and the 67 radio galaxies (solid line) discussed in this paper. The short-dashed and the dotted line indicate submm detections of radio galaxies versus non-detections given a  $3\sigma$  detection criterion, respectively. The detections have a higher median redshift ( $z = 3.1$ ) than the parent sample ( $z = 2.5$ ). The two long-dashed lines represent  $\Sigma N(z)$  of the 10 submm sources with spectroscopic redshifts found by Chapman et al. (2003a) and using 9 additional spectroscopic redshifts (Ivison et al. 1998; Ivison et al. 2000; Dey et al. 1999; Soucail et al. 1999; Eales et al. 2000; Ledlow et al. 2002; Chapman et al. 2002b,c; Aretxaga et al. 2003; Frayer et al. 2003).



truly remarkable, and corroborates the conclusion of A01 that the detection fraction of  $\sim 50$ – $67$  per cent at  $z > 2.5$  is significantly different from the detection fraction of  $\sim 15$  per cent at  $z < 2.5$ . Removing the 4 brightest sources from the sample does not destroy this relation.

### 5.1.2 Investigation of the difference between detections and non-detections

Given a  $3\sigma$  detection criterion the average submm flux density of the 22 detected radio sources and 45 non-detections are  $\langle S_{850, \geq 3\sigma} \rangle = 6.60 \pm 0.71$  mJy and  $\langle S_{850, < 3\sigma} \rangle = 0.81 \pm 0.20$  mJy respectively, while the average for the entire sample is  $\langle S_{850, \text{sample}} \rangle = 2.71 \pm 0.43$  mJy. For a  $2\sigma$  detection criterion the average submm flux density of the 32 detected galaxies and 35 non-detections are  $\langle S_{850, \geq 2\sigma} \rangle = 5.29 \pm 0.60$  mJy and  $\langle S_{850, < 2\sigma} \rangle = 0.34 \pm 0.19$  mJy respectively.

Figure 3 shows cumulative redshift distributions  $\Sigma(z)$  for various subsets of the radio galaxy sample together with spectroscopic redshifts for other submm samples from the literature. As was suspected from Figure 2, the radio galaxies detected in the submm follow a distribution that differs significantly from both the undetected sources and the parent sample. The K–S test shows with  $P > 99$  per cent confidence that using a  $2\sigma$  or  $3\sigma$  detection criterion picks out the same population (both for the detections and for the non-detections), whereas the chance that the detections and non-detections are distributed similarly is  $P < 1$  per cent.

Does the high median redshift ( $z = 3.1$ ) of the detected sources (the parent sample has  $z = 2.5$ ) purely reflect the strong negative  $K$ -correction or does it reflect a change in  $L_{\text{FIR}}$ ? Figure 3 shows that the median redshift of the detections is higher than the median redshift ( $z = 2.4$ ) for SCUBA sources (Chapman et al. 2003a), while the redshift distribution of the parent sample follows the SCUBA population closely. This argues in favor of a different  $L_{\text{FIR}}$  for detections and non-detections. What then causes the dif-

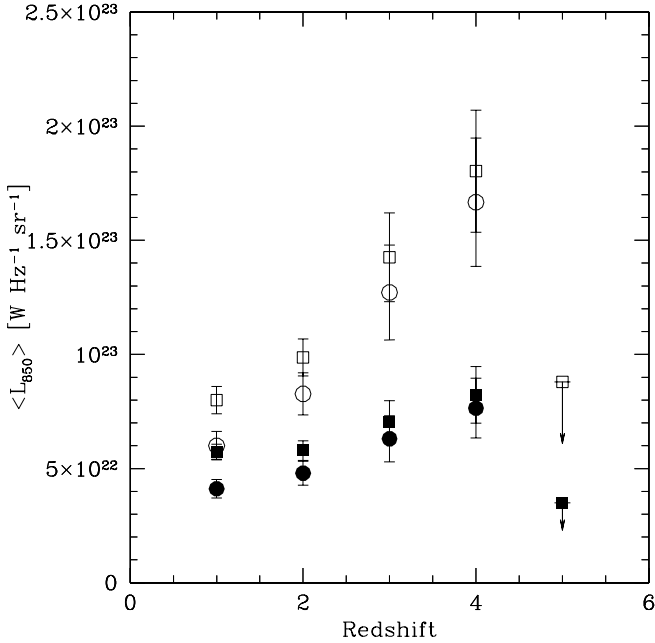


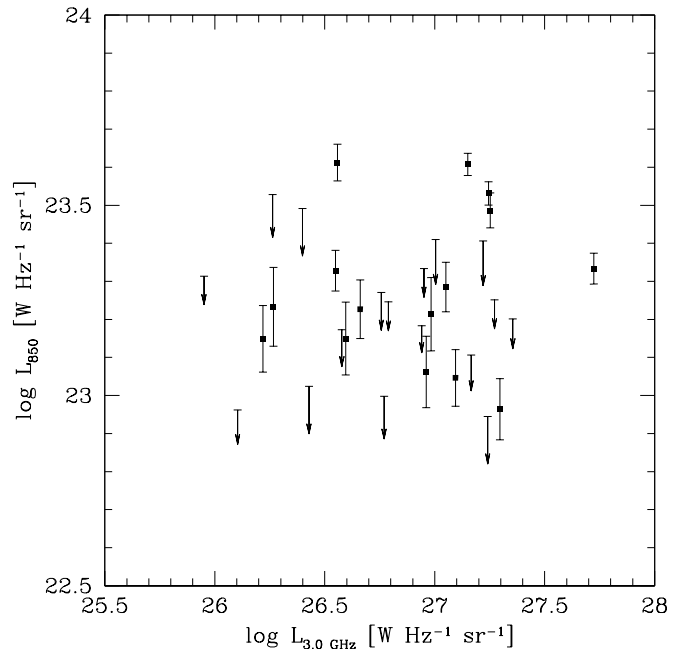
**Figure 4** — The average rest-frame 850  $\mu\text{m}$  luminosity versus redshift for 67 radio galaxies as estimated using the Kaplan–Maier estimator for each redshift bin. The data points indicated with open squares and circles were calculated assuming the same dust template as A01 ( $\beta = 1.5$ ,  $T_d = 40\text{K}$ ) for  $3\sigma$  and  $2\sigma$  detection criteria respectively. The solid symbols are similar but assume  $\beta = 2.0$  instead. The data points at  $z = 5$  are  $3\sigma$  upperlimits based on the non-detection of TN J0924–2201.

ference in redshift distribution between detected HzRGs and the submm population? There are at least two possible explanations. It may indicate that HzRGs are more massive, at the centers of protoclusters (Venemans et al. 2003), and therefore undergo a faster evolution than ‘normal’ submm sources and finish the bulk of their formation process early. Alternatively, it may reflect a selection effect as the requirement of a faint radio counterpart prior to spectroscopic follow-up for the submm sample selects against high redshift galaxies (Chapman et al. 2003a).

### 5.1.3 The increase of submm luminosity with redshift

Figure 4 shows the inferred 850  $\mu\text{m}$  luminosity  $L_{850}$  as a function of redshift. For each redshift bin  $L_{850}$  has been estimated using the Kaplan–Maier estimator, a survival analysis technique which tries to estimate the true distribution of the underlying population by incorporating both upperlimits and detections. We have computed the luminosities both using a dust template with  $\beta = 1.5$  and  $\beta = 2.0$ . Adding our data to the sample of A01 confirms that HzRGs have higher submm luminosities than lower redshift sources. However, there are significant differences with the findings from A01: (i)  $L_{850}$  at low redshifts is higher than inferred by A01. This is because we have chosen, not to correct for possible synchrotron contamination (see Section 2.3) (ii) There is weak evidence for a turnover or leveling off at  $z > 4$  (based on the lower flux densities of the five galaxies with  $z > 4$  compared to redshifts  $3 < z < 4$ ; see Fig. 1). This explains why there is no strong correlation between  $L_{850}$  and  $z$  in the high redshift subsample (see Table 4). (iii) A01 remarked that the increase in  $L_{850}$  becomes less pronounced if one assumes a dust template with  $\beta = 2$ . Because  $L_{850}$  at low redshifts is higher than in A01, this effect is even stronger in our sample and we find that  $L_{850}$  may be rather constant. The sources would still be highly submm luminous, implying huge dust masses and star formation rates.

**Figure 5** — Submillimetre luminosity against radio power  $L_{3\text{GHz}}$  for 32 radio galaxies with  $z > 2.5$ . No strong correlation is apparent, indicating that heating of the dust by AGN is not a dominant process for radio galaxies. Symbols as in Figure 1.



## 5.2 The connection between submm and radio luminosity

Radio galaxies host luminous AGNs and for favorable geometries (e.g., dusty warped disks) heating of dust by only a small fraction ( $\leq 20$  per cent) of their UV radiation could easily explain typical far-IR luminosities (e.g., Sanders et al. 1989). Therefore, an important question is: do the AGN heat the large-scale dust significantly, i.e. are  $L_{\text{radio}}$  and  $L_{\text{FIR}}$  correlated?

To answer this question we have estimated the rest-frame radio power at 3 GHz,  $L_{3\text{GHz}}$ . We have chosen this frequency because for the redshift range  $1.1 < z < 7.2$  this requires only interpolation between between 365 MHz and 1.4 GHz. Of course this assumes that the UV emission of the central source relates to its radio output (e.g., Willott et al. 1999; De Breuck et al. 2000).

While Table 3 shows that there is a possible correlation between  $L_{850}$  and  $L_{3\text{GHz}}$  over the entire redshift range of our sample, this is probably an effect of the strong redshift dependence of both  $L_{850}$  and  $L_{3\text{GHz}}$ . The tests represented in Table 4 only take radio galaxies with  $z > 2.5$  into account and even though this subsample contains almost all submm detections the correlation disappears. The scatterplot in Figure 5 is a graphical representation of the same result. We don't find evidence for dust heating by AGN, in accordance with earlier findings (e.g., A01; Willott et al. 2002; Andreani et al. 2002) but see Haas et al. (2003) for a contrasting view based on ISO observations of local (most have  $0.1 < z < 1.0$ ) hyperluminous quasars. This analysis is likely to be an oversimplification because the typical time-scales for starburst and radio activity differ by an order of magnitude.

| Source       | $z$   | P(%)  | $S_{850}$ (mJy) |
|--------------|-------|-------|-----------------|
| 3C356        | 1.079 | 14    | < 4.8           |
| 3C368        | 1.132 | < 1   | 4.1             |
| 3C324        | 1.206 | 12    | < 4.4           |
| 4C40.36      | 2.265 | 7.3   | < 3.9           |
| 4C48.48      | 2.343 | 8.4   | 5.1             |
| 4C23.56      | 2.483 | 15.3  | < 4.7           |
| MRC0316–257  | 3.130 | < 4   | < 8.9           |
| TNJ0121+1320 | 3.516 | 7     | 7.5             |
| TX1243+036   | 3.570 | 11.3  | < 5.6           |
| 6C1908+722   | 3.532 | < 5   | 10.8            |
| 4C41.17      | 3.798 | < 2.4 | 12.1            |
| TNJ2007–1316 | 3.830 | < 3   | 5.8             |
| TNJ1338–1942 | 4.100 | 5     | 6.9             |

**Table 5** — UV/optical polarisation fractions and submm fluxes for all radio galaxies for which both have been observed. UV/optical polarisation data are taken from Dey et al. (1997), Vernet et al. (2001), and De Breuck et al. in preparation, the submm data are from A01 and this paper.

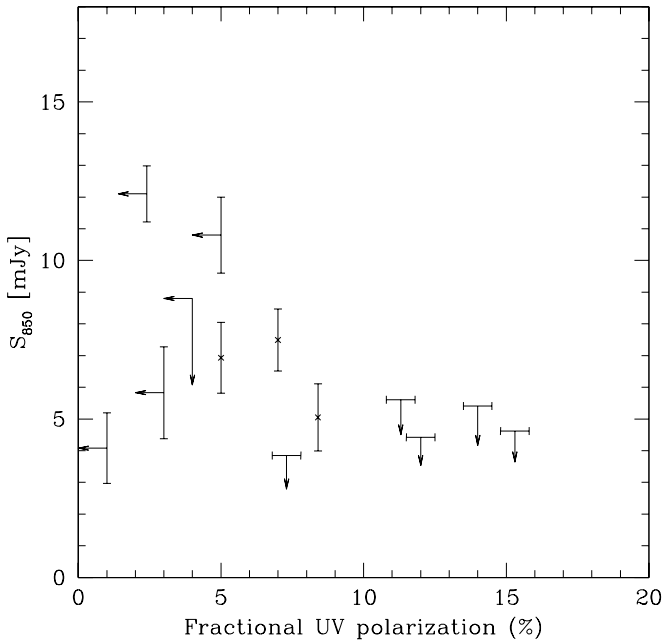


**Figure 6** — 850  $\mu\text{m}$  flux  $S_{850}$  against observed UV continuum polarisation fraction. None of the highly polarized sources are detected in the submm, indicating that low polarisation (indicative of a starburst) and high  $L_{\text{FIR}}$  both trace star formation.

### 5.3 An anti-correlation between submm flux and UV polarisation

Optical polarimetry studies can be used to search for direct signs of starburst activity and determine the relative contributions of AGN and starburst to the UV continuum (e.g., Dey et al. 1997; Vernet et al. 2001). If the starburst dominates the UV/optical light, then the scattered (i.e. polarized) AGN light is diluted and one expects a low polarisation fraction of the UV continuum and perhaps a correlation with the observed submm flux densities.

Polarimetry results exist for 13 of the galaxies in our sample (Dey et al. 1997; Vernet et al. 2001, De Breuck et al. in preparation). A summary of the polarisation fractions and corresponding 850  $\mu\text{m}$  flux densities is given in Table 5. We have plotted the observed submm flux density against UV continuum polarisation fraction in Figure 6. No sources with high UV polarisation are detected in the submm. This is supported formally by survival analysis: Kendall Tau gives a probability  $P = 3$  per cent that there is no correlation.

This result is consistent with the view that for HzRGs star formation and submm emission are closely linked while any AGN contribution to the FIR is negligible. Tadhunter et al. (2002) also found some evidence for this. Two out of the three objects which are starburst dominated in their sample of 2-Jy radio galaxies are also extremely FIR luminous. Further support for low polarisation in starbursting systems comes from the luminous submm source SMM J02399–0136 (Vernet & Cimatti 2001) which shows only moderate ( $P \sim 5$  per cent) polarisation.

The weakness of the submm luminosity in highly polarized sources together with the tentative correlation between  $\text{Ly}\alpha$  and submm flux (see next section) is consistent with the anti-correlation between  $\text{Ly}\alpha$  luminosity and UV polarisation reported by Vernet et al. (2001). They argue that  $\text{Ly}\alpha$  photons are resonantly destructed by dust and that scattering by the same dust results in a higher fractional polarisation. This explanation, however, seems at odds with the lower submm flux densities in highly polarized sources unless there would be significant amounts of dust that is too hot to be detected in the submm.

### 5.4 Submillimetre and $\text{Ly}\alpha$ flux

Since many HzRGs are embedded in giant  $\text{Ly}\alpha$  haloes (e.g., McCarthy 1993; van Ojik et al. 1996; Reuland et al. 2003) it would be interesting to see if one can relate the amount of available star formation ‘fuel’, as estimated roughly by the spatial size, or luminosity, of these emission line haloes and the amount of HI as probed by  $\text{Ly}\alpha$  absorption to the observed rest-frame FIR luminosities. Alternatively, one might expect a strong anti-correlation due to destruction of  $\text{Ly}\alpha$  emission by dust.

Many HzRGs are identified based on their  $\text{Ly}\alpha$  line and good data on the observed  $\text{Ly}\alpha$  fluxes is available in most cases. There is a strong selection effect, however, since sources with low  $\text{Ly}\alpha$  flux densities are less likely to be recognized as HzRGs. Interestingly, Table 4 and Figure 7 indicate that a correlation may be present. While this relation is tentative only, it offers perspectives for future programs. Better data should make it possible to investigate whether there is a possible relationship between the dust content and  $\text{Ly}\alpha$  to CIV or NV emission line ratio, as indicators of metallicity

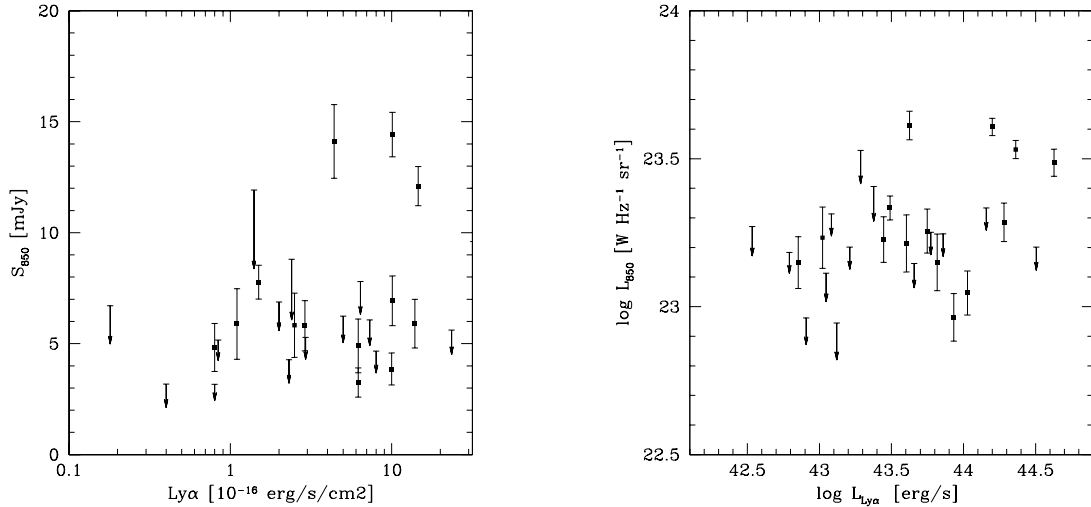


**Figure 7** —  $S_{850 \mu m}$  against observed  $Ly\alpha$  line flux (left) and inferred luminosities  $L_{850}$  against  $L_{Ly\alpha}$  (right). Tentative evidence for a correlation is apparent. The galaxies brightest in  $Ly\alpha$  seem to have higher submm flux densities, possibly indicating that galaxies with richer gaseous environments (as traced by  $Ly\alpha$ ) also host more massive starbursts. Symbols as in Figure 1.

(c.f. Vernet et al. 2001). This would be especially interesting in the light of findings by Hamann & Ferland (1999) and Fan et al. (2001) that QSOs show (super)solar abundances out to the highest redshifts and must already have undergone significant star formation. A comparison with the more readily studied HzRG host galaxies would be crucial to better understand this result.

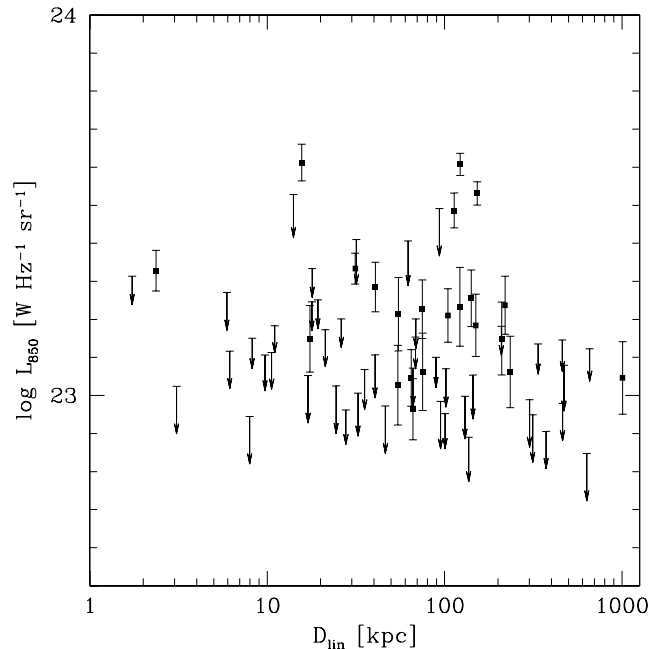
The detection of both  $Ly\alpha$  and dust in many HzRGs is intriguing because already a small amount of dust can extinguish  $Ly\alpha$  radiation efficiently. The detection of  $Ly\alpha$  in the submm sources of Chapman et al. (2003a) is equally surprising. One explanation may be that  $Ly\alpha$  emission and dust are located predominantly in different locations (e.g., a merger between one dusty and one less dusty component). Some evidence for this comes from 4C 60.07 at  $z = 3.8$  in which the spatially resolved dust continuum emission (Papadopoulos et al. 2000) is anti-correlated with the  $Ly\alpha$  emission (Fig. 5 in Reuland et al. 2003). Smail et al. (2003) also report evidence for an offset between far-IR and UV emitting regions in the  $z = 2.38$  starburst galaxy N2 850.4.

## 5.5 $L_{850}$ and linear size

Willott et al. (2002) found an anti-correlation between linear size and  $850 \mu m$  luminosity for their sample of  $z \sim 1.5$  radio loud quasars. This effect was attributed to a possible relation between the jet-triggering event and a short-lived starburst or quasar-heated dust in QSOs. No such correlation was found for a matched subset of the A01 sample centered at the same redshift. We have briefly investigated whether such a correlation exists in the present sample. Figure 8 shows the observed submm flux plotted against the projected linear size. No correction for possible differences in inclination angle was made because such corrections are expected to be relatively small among radio galaxies (even when comparing radio galaxies with quasars projection effects re-



**Figure 8** — 850  $\mu\text{m}$  luminosity  $L_{850}$  against the radio source projected linear size  $D_{\text{lin}}$ . There is no evidence for a strong anti-correlation as was found for radio loud quasars by Willott et al. (2002). Symbols as in Figure 1.



sult in only a factor  $\approx 1.6$  difference in projected linear size for  $\theta_{\text{trans}} = 53^\circ$ ; Willott et al. 2000, 2002). Our analysis does not support such a strong relation and if one interprets linear size as an estimate of the age of the radio source (reasonable if one assumes that the environments and jet powers do not change significantly; see e.g., Blundell, Rawlings & Willott 1999), then this would be consistent with the scenario sketched by Willott et al. that the correlation found for QSOs is indicative of short starbursts while the starbursts in HzRGs have longer time-scales and could be forming the bulk of the stellar populations. Despite the absence of a clear correlation, some relation between age of radio source and starburst might have been expected if the black-hole and stellar bulge grow in a symbiotic fashion (e.g., Williams et al. 1999). However, in realistic scenarios many complicating factors can be envisaged such as the significantly different time-scales involved. Growth of the radio source may first induce star formation by compressing molecular clouds (Begelman & Cioffi 1989; Bicknell et al. 2000) and may then actually signal the end of the starburst by clearing out all the cool gas from the central region (Rawlings 2003).

### 5.6 Submillimetre and near-IR emission

As discussed by Isaak et al. (2002), for QSOs one might naively expect a correlation between the submm and optical flux densities. This correlation might arise regardless of whether stars or a buried AGN are responsible for heating of the dust since black hole mass scales with stellar bulge mass. Priddey et al. (2003) note that the picture is likely to be more complex and that any correlation might be smeared out due to differences in relative timing between AGN fueling and starburst, or varying dust-torus geometries. Radio galaxies might be better suited for such studies, since according to orientation based unification schemes (e.g., Barthel 1989) the AGN are obscured by a natural coronagraph and rest-frame  $B$ -band luminosity therefore is a fairly reliable

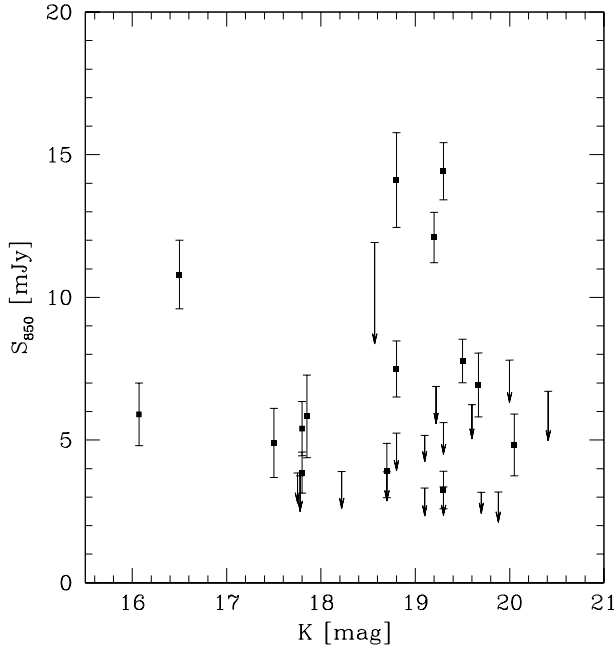


**Figure 9** —  $S_{850 \mu\text{m}}$  against observed  $K$ -band magnitude. No correlation is apparent, and no relation between  $L_{\text{FIR}}$  and stellar mass/optical star formation rate of the host galaxy can be established. Symbols as in Figure 1.

measure of the mass of the stellar population or starburst activity. For this reason we have correlated the  $K$ -band magnitudes (samples rest-frame  $B, V$  for  $z > 3$ ) with the submm flux densities. As can be seen from Table 4 and Figure 9 no such correlation is apparent. This remains true, if we apply a  $K$ -correction to the near-IR magnitudes. However, the dataset is rather inhomogeneous and more sensitive data in both the submm and near-IR are required to truly rule out any correlation. Sensitive multi-band observations could be used to (i) construct a redshift independent estimate of the line-free rest-frame optical continuum for comparison with  $L_{\text{FIR}}$  ( $[\text{O III}]$  and  $\text{H}\alpha$  can sometimes dominate the  $K$ -band e.g., 4C 30.36, 4C 39.37; Egami et al. 2003), and (ii) check whether FIR emission is stronger for sources with higher intrinsic reddening (following e.g., Calzetti 1997; Adelberger & Steidel 2000; Seibert et al. 2002).

## 5.7 Summary

From our analysis we consider the following results the most interesting:

1.  $S_{850}$  and  $z$  are strongly correlated. Whether this is true also for  $L_{\text{FIR}}$  and  $z$  depends on the assumed dust template.
2.  $L_{850}$  and radio power  $L_{3\text{GHz}}$  do not correlate strongly, indicating that AGN do not dominate the submm emission (either through synchrotron contamination or dust heating by the UV continuum).
3.  $S_{850}$  and  $\text{Ly}\alpha$  appear weakly correlated. While this is not very convincing, the interesting result is the absence of a strong anti-correlation as expected naively from the destruction of  $\text{Ly}\alpha$  emission by dust.
4.  $S_{850}$  and UV polarisation fraction appear anti-correlated. This is expected if the UV continuum of the buried AGN does not contribute significantly to the dust heating.

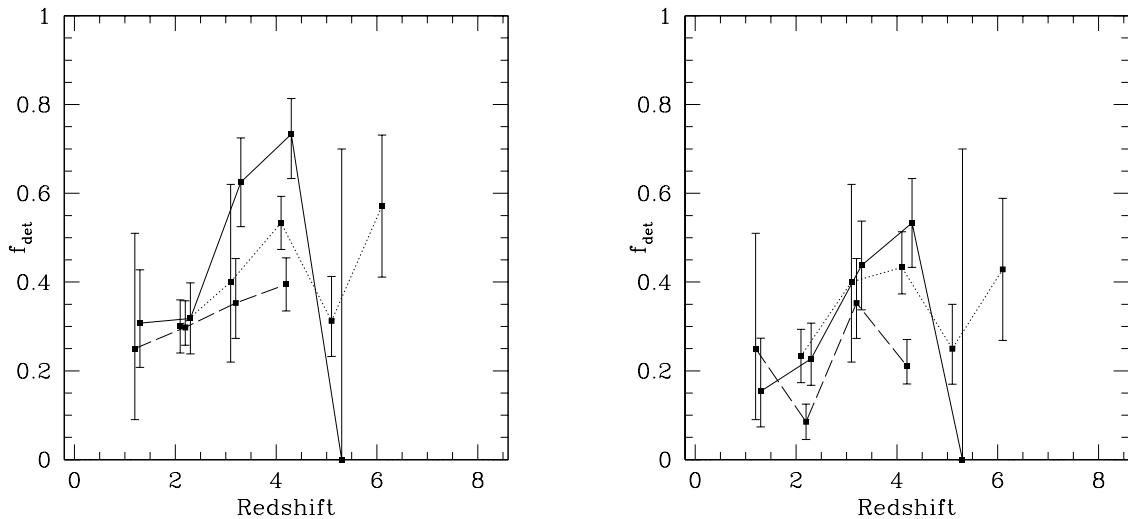


**Figure 10** — The 850  $\mu\text{m}$  detection (left  $S/N > 2$ ; right  $S/N > 3$ ) fractions of radio galaxies as function of redshift (solid line). The fractions rise up to a redshift of  $z = 4$ . For comparison we also plot the detection fraction for observations of radio quiet QSOs at  $z = 1 - 5$ , and radio loud quasars at  $z \sim 1.5$  (after matching the sensitivity to 3 mJy rms) at 850  $\mu\text{m}$  (dashed line; Priddey et al. 2003; Isaak et al. 2002; Willott et al. 2002) and 1.25 mm (dotted line; Omont et al. 2001, 2003; Carilli et al. 2001; Petric et al. 2003; Bertoldi et al. 2003). The detection rates for the QSOs appear to follow the same trend as for the radio galaxies, but the QSO datapoint at  $z = 5$  seems indicative of a turnover (the  $z = 5$  point for the HzRGs is based on only 1 galaxy, but taking all  $z > 4$  HzRGs yields a similar result). The datapoint at  $z = 6$  could indicate a detection fraction larger even than what is observed for  $z = 4$ . This might reflect, the extreme properties of those sources.

## 6 A comparison of radio galaxies with QSOs

The optically thin (sub-)mm emission of starbursts should be largely independent of viewing angle. Orientation based unification schemes for AGN (e.g., Barthel 1989) therefore suggest that we can combine observations of radio galaxies with those of QSOs, allowing us to study the evolution of star formation in their host galaxies over a larger redshift range. Extensive surveys of high-redshift (mostly radio-quiet) QSOs have been published recently (Carilli et al. 2001; Omont et al. 2001, 2003; Isaak et al. 2002; Priddey et al. 2003; Petric et al. 2003; Bertoldi et al. 2003). We have combined their results and compare those with our sample.

Figure 10 shows the detection fraction as a function of redshift for the QSO and radio galaxy samples. In many redshift bins only a small number of detections and non-detections is responsible for estimating the success rates for the present effective flux limits. We have estimated the range over which the ‘true success rate’ could vary such that there would be a 68 per cent chance of measuring the observed detection fraction. This range is indicated by the errorbars. Figure 11 shows the average (sub-)mm flux density for the various samples as a function of redshift.

Reassuringly, the trends for the QSOs and radio galaxies shown in these figures mimic each other. The average observed (sub-)mm flux density rises to redshifts of  $z \sim 4$ . For higher redshifts there is some evidence for a decline (see the discussion in Section 5.1.3 and the  $z = 5$  data point of the MAMBO QSO observations). However, the

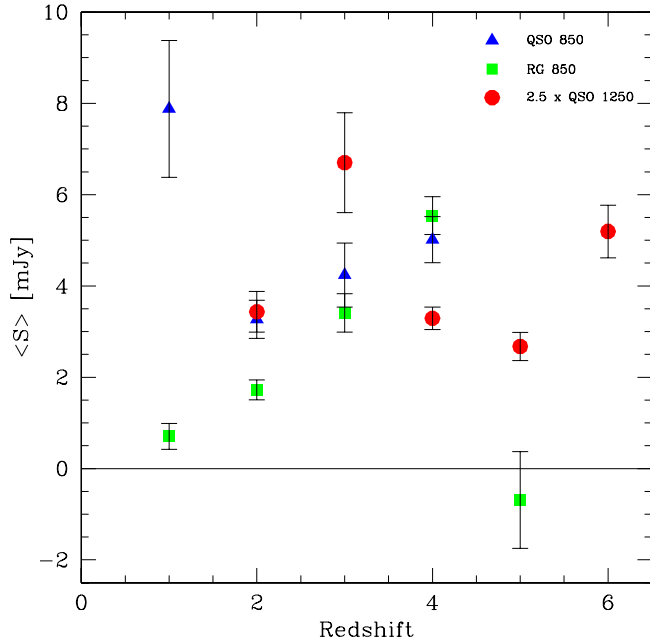


**Figure 11** — The average measured (sub-)mm flux density binned in redshift has been plotted for QSOs and radio galaxies. The squares represent observations of radio galaxies at  $850 \mu\text{m}$ , the triangles QSOs at  $850 \mu\text{m}$ , while the circles represent observations of QSOs at  $1250 \mu\text{m}$  multiplied by a factor of 2.5 for easier comparison. The data-point at  $z \approx 1.5$  represents the radio loud quasars from Willott et al. (2002). The trends with redshift are similar to what is seen in Figure 10 and confirm the steady rise from  $z = 1$  to  $z = 4$  for the galaxies.

observations of  $z > 4$  QSOs would also be consistent with a fairly constant or even a rise in the detection fraction and average FIR luminosity out to the highest redshifts. This depends rather critically on the  $z \sim 6$  QSOs, which are likely to be atypical even for QSOs.

The average flux density and detection rate of the QSOs is comparable to that of the HzRGs, even though the HzRG surveys are more sensitive than the QSO surveys by a factor of approximately 3. This, coupled with the assumption that quasars are on average more luminous than radio galaxies in AGN unification schemes based on receding torus models (e.g., Simpson 2003), may be viewed as further support for an AGN related component in QSOs, similar to what was found for radio quasars (Andreani et al. 2002; Willott et al. 2002). Note that the quasars discussed by Willott et al. (2002) are exceptionally bright compared to the mostly radio quiet QSOs represented in Figs. 10,11.

Due to a lack of carefully matched surveys fundamental differences between type I and type II AGN and radio-loud versus radio-quiet targets cannot be properly investigated yet, although slowly progress is being made.

## 7 Summary

We have presented SCUBA observations of 24 radio galaxies and compared those with earlier results of 47 radio galaxies from the survey by A01. We confirm that HzRGs are massive forming galaxies, forming stars up to rates of a few thousand  $M_{\odot} \text{yr}^{-1}$  and that there is no strong evidence for a correlation with radio power. Further evidence for a predominantly starburst nature of the far-IR emission comes from the striking anti-correlation between submm flux density and UV polarisation (Fig. 6).

In agreement with A01 we find that submm detection rate appears to be primarily

a function of redshift. If this is interpreted as being due to a change in the intrinsic far-IR luminosity, it would be consistent with a scenario in which the bulk of the stellar population of radio galaxies forms rapidly around redshifts of  $z = 3 - 5$  after which they are more passively evolving (c.f. Best, Longair, & Röttgering 1998). We also find that the median redshift of the HzRGs with SCUBA detections ( $z = 3.1$ ) is higher than the median redshift of the submm population ( $z = 2.4$ ; Chapman et al. 2003a). In the current picture of hierarchical galaxy formation, this could be interpreted as that HzRGs are more massive galaxies, which are then thought to begin their collapse at earlier cosmic times and evolve faster and finish the bulk of their formation process earlier. Alternatively, it could indicate that higher redshift submm sources are being missed due to the requirement of a radio counterpart prior to spectroscopic follow-up.

HzRGs have accurately determined redshifts and host identifications and are thought to be the most massive galaxies at any epoch (De Breuck et al. 2002). Therefore, HzRGs are a key population for studies of galaxy formation in the early universe, allowing detailed follow-up mm-interferometry observations to study their dust and gas content. Currently, they offer the best way to obtain reliable dynamic masses for a significant number of massive high redshift galaxies. These HzRGs would be especially suited to constrain any evolution in galaxy mass with redshift, study changes in evolutionary status, gas mass, and the starburst-AGN connection. If all of these turn out to have masses larger than  $10^{11} M_{\odot}$ , then this could have important consequences (depending on rather uncertain correction factors for the fraction of similar galaxies for which the black hole is dormant) for our understanding of galaxy formation, because only few such massive galaxies are expected at such high redshifts (Genzel et al. 2003).

## Acknowledgments

We thank Chris Willott and Steve Rawlings for useful discussions and the anonymous referee for helpful suggestions to improve the paper. We gratefully acknowledge the excellent help of the JCMT staff and ‘flexible’ observers who collected data for our program. In particular the help of Remo Tilanus was indispensable. The authors wish to extend special thanks to those of Hawaiian ancestry on whose sacred mountain we are privileged to be guests. The JCMT is operated by JAC, Hilo, on behalf of the parent organizations of the Particle Physics and Astronomy Research Council in the UK, the National Research Council in Canada and the Scientific Research Organization of the Netherlands. The work of M.R. and W.v.B. was performed under the auspices of the U.S. Department of Energy, National Nuclear Security Administration by the University of California, Lawrence Livermore National Laboratory under contract No. W-7405-Eng-48.

## References

- Adelberger K. L., Steidel C. C., 2000, *ApJ*, 544, 218
- Andreani P., Fosbury R. A. E., van Bemmell I., Freudling W., 2002, *A&A*, 381, 389
- Archibald E. N., Dunlop J. S., Hughes D. H., Rawlings S., Eales S. A., Ivison R. J., 2001, *MNRAS*, 323, 417
- Archibald E. N., Jenness T., Holland W. S., Coulson I. M., Jessop N. E., Stevens J. A., Robson E. I., Tilanus R. P. J., Duncan W. D., Lightfoot J. F., 2002, *MNRAS*, 336, 1
- Aretxaga I., Hughes D. H., Chapin E. L., Gaztañaga E., Dunlop J. S., Ivison R. J., 2003, *MNRAS*, 342, 759

- Athreya R. M., Kapahi V. K., McCarthy P. J., van Breugel W., 1997, *MNRAS*, 289, 525
- Barthel P. D., 1989, *ApJ*, 336, 606
- Begelman M. C., Cioffi D. F., 1989, *ApJ*, 345, L21
- Bertoldi F., Carilli C. L., Cox P., Fan X., Strauss M. A., Beelen A., Omont A., Zylka R., 2003, *A&A*, 406, L55
- Bertoldi F., Menten K. M., Kreysa E., Carilli C. L., Owen F., 2002, *Highlights in Astronomy*, 12, 473
- Best P. N., Longair M. S., Röttgering H. J. A., 1998, *MNRAS*, 295, 549
- Bicknell G. V., Sutherland R. S., van Breugel W. J. M., Dopita M. A., Dey A., Miley G. K., 2000, *ApJ*, 540, 678
- Blain A. W., Smail I., Ivison R. J., Kneib J.-P., 1999, *MNRAS*, 302, 632
- Blundell K. M., Rawlings S., Willott C. J., 1999, *AJ*, 117, 677
- Calzetti D., 1997, *AJ*, 113, 162
- Carilli C. L., Bertoldi F., Rupen M. P., Fan X., Strauss M. A., Menten K. M., Kreysa E., Schneider D. P., Bertarini A., Yun M. S., Zylka R., 2001, *ApJ*, 555, 625
- Carilli C. L., Harris D. E., Pentericci L., Röttgering H. J. A., Miley G. K., Kurk J. D., van Breugel W., 2002, *ApJ*, 567, 781
- Chapman S. C., Blain A. W., Ivison R. J., Smail I. R., 2003, *Nature*, 422, 695
- Chapman S. C., Scott D., Borys C., Fahlman G. G., 2002a, *MNRAS*, 330, 92
- Chapman S. C., Shapley A., Steidel C., Windhorst R., 2002c, *ApJ*, 572, L1
- Chapman S. C., Smail I., Ivison R. J., Blain A. W., 2002b, *MNRAS*, 335, L17
- Chini R., Kruegel E., Kreysa E., 1986, *A&A*, 167, 315
- Condon J. J., Cotton W. D., Greisen E. W., Yin Q. F., Perley R. A., Taylor G. B., Broderick J. J., 1998, *AJ*, 115, 1693
- Cowie L. L., Barger A. J., Kneib J.-P., 2002, *AJ*, 123, 2197
- De Breuck C., Neri R., Morganti R., Omont A., Rocca-Volmerange B., Stern D., Reuland M., van Breugel W., Röttgering H., Stanford S. A., Spinrad H., Vigotti M., Wright M., 2003, *A&A*, 401, 911
- De Breuck C., Röttgering H., Miley G., van Breugel W., Best P., 2000b, *A&A*, 362, 519
- De Breuck C., van Breugel W., Minniti D., Miley G., Röttgering H., Stanford S. A., Carilli C., 1999, *A&A*, 352, L51
- De Breuck C., van Breugel W., Röttgering H., Stern D., Miley G., de Vries W., Stanford S. A., Kurk J., Overzier R., 2001, *AJ*, 121, 1241
- De Breuck C., van Breugel W., Röttgering H. J. A., Miley G., 2000a, *A&AS*, 143, 303
- De Breuck C., van Breugel W., Stanford S. A., Röttgering H., Miley G., Stern D., 2002, *AJ*, 123, 637
- Dey A., 1999, in *The Most Distant Radio Galaxies The Early History of Powerful Radio Galaxies*. pp 19–+
- Dey A., Graham J. R., Ivison R. J., Smail I., Wright G. S., Liu M. C., 1999, *ApJ*, 519, 610
- Dey A., van Breugel W., Vacca W. D., Antonucci R., 1997, *ApJ*, 490, 698
- Douglas J. N., Bash F. N., Bozyan F. A., Torrence G. W., Wolfe C., 1996, *AJ*, 111, 1945
- Downes D., Radford J. E., Greve A., Thum C., Solomon P. M., Wink J. E., 1992, *ApJ*, 398, L25
- Drinkwater M. J., Webster R. L., Francis P. J., Condon J. J., Ellison S. L., Jauncey D. L., Lovell J., Peterson B. A., Savage A., 1997, *MNRAS*, 284, 85
- Dunlop J. S., McLure R. J., Kukula M. J., Baum S. A., O’Dea C. P., Hughes D. H., 2003, *MNRAS*, 340, 1095
- Dunlop J. S., McLure R. J., Yamada T., Kajisawa M., Peacock J. A., Mann R. G., Hughes D. H., Aretxaga I., Muxlow T. W. B., Richards A. M., Dickinson M., Ivison R. J., Smith G. P., Smail I., Serjeant S., Almaini O., Lawrence A., 2002, *ArXiv Astrophysics e-prints*
- Dunne L., Eales S., Edmunds M., Ivison R., Alexander P., Clements D. L., 2000, *MNRAS*, 315, 115
- Dunne L., Eales S., Ivison R., Morgan H., Edmunds M., 2003, *Nature*, 424, 285
- Dunne L., Eales S. A., 2001, *MNRAS*, 327, 697
- Dupac X., Bernard J.-P., Boudet N., Giard M., Lamarre J.-M., Mény C., Pajot F., Ristorcelli I., Serra G., Stepnik B., Torre J.-P., 2003, *A&A*, 404, L11
- Eales S., Bertoldi F., Ivison R., Carilli C., Dunne L., Owen F., 2003, *MNRAS*, 344, 169
- Eales S., Lilly S., Webb T., Dunne L., Gear W., Clements D., Yun M., 2000, *AJ*, 120, 2244
- Eales S. A., Rawlings S., 1996, *ApJ*, 460, 68
- Edmunds M. G., 2001, *MNRAS*, 328, 223

- Egami E., Armus L., Neugebauer G., Murphy T. W., Soifer B. T., Matthews K., Evans A. S., 2003, *AJ*, 125, 1038
- Fan X., Narayanan V. K., Lupton R. H., Strauss M. A., Knapp G. R., Becker R. H., White R. L., Pentericci L., Leggett S. K., Haiman Z., Gunn J. E., Ivezić Ž., Schneider D. P., Anderson S. F., Brinkmann J., 2001, *AJ*, 122, 2833
- Farrah D., Serjeant S., Efstathiou A., Rowan-Robinson M., Verma A., 2002, *MNRAS*, 335, 1163
- Feigelson E. D., Nelson P. I., 1985, *ApJ*, 293, 192
- Frayser D. T., Armus L., Scoville N. Z., Blain A. W., Reddy N. A., Ivison R. J., Smail I., 2003, *AJ*, 126, 73
- Frayser D. T., Reddy N. A., Armus L., Blain A. W., Scoville N. Z., Smail I., 2004, *AJ*, 127, 728
- Genzel R., Baker A. J., Tacconi L. J., Lutz D., Cox P., Guilloteau S., Omont A., 2003, *ApJ*, 584, 633
- Haas M., Klaas U., Müller S. A. H., Bertoldi F., Camenzind M., Chini R., Krause O., Lemke D., Meisenheimer K., Richards P. J., Wilkes B. J., 2003, *A&A*, 402, 87
- Hamann F., Ferland G., 1999, *ARA&A*, 37, 487
- Hogg D. W., 2001, *AJ*, 121, 1207
- Holland W. S., Robson E. I., Gear W. K., Cunningham C. R., Lightfoot J. F., Jenness T., Ivison R. J., Stevens J. A., Ade P. A. R., Griffin M. J., Duncan W. D., Murphy J. A., Naylor D. A., 1999, *MNRAS*, 303, 659
- Hughes D. H., Dunlop J. S., Rawlings S., 1997, *MNRAS*, 289, 766
- Hughes D. H., Serjeant S., Dunlop J., Rowan-Robinson M., Blain A., Mann R. G., Ivison R., Peacock J., Efstathiou A., Gear W., Oliver S., Lawrence A., Longair M., Goldschmidt P., Jenness T., 1998, *Nature*, 394, 241
- Isaak K. G., Priddey R. S., McMahan R. G., Omont A., Peroux C., Sharp R. G., Withington S., 2002, *MNRAS*, 329, 149
- Isobe T., Feigelson E. D., Nelson P. I., 1986, *ApJ*, 306, 490
- Ivison R. J., Dunlop J. S., Smail I., Dey A., Liu M. C., Graham J. R., 2000, *ApJ*, 542, 27
- Ivison R. J., Smail I., Le Borgne J.-F., Blain A. W., Kneib J.-P., Bezecourt J., Kerr T. H., Davies J. K., 1998, *MNRAS*, 298, 583
- James A., Dunne L., Eales S., Edmunds M. G., 2002, *MNRAS*, 335, 753
- Jenness T., Lightfoot J. F., 1998, in *ASP Conf. Ser. 145: Astronomical Data Analysis Software and Systems VII Reducing SCUBA Data at the James Clerk Maxwell Telescope*. pp 216–+
- Jenness T., Stevens J. A., Archibald E. N., Economou F., Jessop N., Robson E. I., Tilanus R. P. J., Holland W. S., 2001, in *ASP Conf. Ser. 238: Astronomical Data Analysis Software and Systems X Automated Reduction and Calibration of SCUBA Archive Data Using ORAC-DR*. pp 299–+
- Kapahi V. K., Athreya R. M., van Breugel W., McCarthy P. J., Subrahmanya C. R., 1998, *ApJ*, 118, 275
- Lacy M., 1999, in *The Most Distant Radio Galaxies Galaxies and clusters around and in front of radio sources at  $0.5 < z < 4.5$* . pp 437–+
- Lacy M., Laurent-Muehleisen S. A., Ridgway S. E., Becker R. H., White R. L., 2001, *ApJ*, 551, L17
- Lavalley M., Isobe T., Feigelson E., 1992, in *ASP Conf. Ser. 25: Astronomical Data Analysis Software and Systems I ASURV: Astronomy Survival Analysis Package*. pp 245–+
- Ledlow M. J., Smail I., Owen F. N., Keel W. C., Ivison R. J., Morrison G. E., 2002, *ApJ*, 577, L79
- McCarthy P. J., 1993, *ARA&A*, 31, 639
- McCarthy P. J., Kapahi V. K., van Breugel W., Persson S. E., Athreya R., Subrahmanya C. R., 1996, *ApJ*, 107, 19
- McCarthy P. J., Kapahi V. K., van Breugel W., Subrahmanya C. R., 1990, *AJ*, 100, 1014
- Omont A., Beelen A., Bertoldi F., Cox P., Carilli C. L., Priddey R. S., McMahan R. G., Isaak K. G., 2003, *A&A*, 398, 857
- Omont A., Cox P., Bertoldi F., McMahan R. G., Carilli C., Isaak K. G., 2001, *A&A*, 374, 371
- Ouchi M., Shimasaku K., Okamura S., Doi M., Furusawa H., Hamabe M., Kimura M., Komiyama Y., Miyazaki M., Miyazaki S., Nakata F., Sekiguchi M., Yagi M., Yasuda N., 2001, *ApJ*, 558, L83
- Papadopoulos P. P., Röttgering H. J. A., van der Werf P. P., Guilloteau S., Omont A., van Breugel W. J. M., Tilanus R. P. J., 2000, *ApJ*, 528, 626
- Pentericci L., Röttgering H. J. A., Miley G. K., McCarthy P., Spinrad H., van Breugel W. J. M., Macchetto F., 1999, *A&A*, 341, 329
- Pentericci L., Röttgering H. J. A., Miley G. K., Carilli C. L., McCarthy P., 1997, *A&A*, 326, 580

- Pentericci L., Röttgering H. J. A., Miley G. K., Spinrad H., McCarthy P. J., van Breugel W. J. M., Macchetto F., 1998, *ApJ*, 504, 139
- Petric A. O., Carilli C. L., Bertoldi F., Fan X., Cox P., Strauss M. A., Omont A., Schneider D. P., 2003, *AJ*, 126, 15
- Priddey R. S., Isaak K. G., McMahon R. G., Omont A., 2003, *MNRAS*, 339, 1183
- Priddey R. S., McMahon R. G., 2001, *MNRAS*, 324, L17
- Rawlings S., 2003, *New Astronomy Review*, 47, 397
- Rengelink R., 1998, Ph.D. Thesis
- Rengelink R. B., Tang Y., de Bruyn A. G., Miley G. K., Bremer M. N., Röttgering H. J. A., Bremer M. A. R., 1997, *A&AS*, 124, 259
- Reuland M., van Breugel W., Röttgering H., de Vries W., Stanford S. A., Dey A., Lacy M., Bland-Hawthorn J., Dopita M., Miley G., 2003, *ApJ*, 592, 755
- Röttgering H. J. A., van Ojik R., Miley G. K., Chambers K. C., van Breugel W. J. M., de Koff S., 1997, *A&A*, 326, 505
- Rowan-Robinson M., 2000, *MNRAS*, 316, 885
- Sanders D. B., Mirabel I. F., 1996, *ARA&A*, 34, 749
- Sanders D. B., Phinney E. S., Neugebauer G., Soifer B. T., Matthews K., 1989, *ApJ*, 347, 29
- Scott S. E., Fox M. J., Dunlop J. S., Serjeant S., Peacock J. A., Ivison R. J., Oliver S., Mann R. G., Lawrence A., Efstathiou A., Rowan-Robinson M., Hughes D. H., Archibald E. N., Blain A., Longair M., 2002, *MNRAS*, 331, 817
- Seibert M., Heckman T. M., Meurer G. R., 2002, *AJ*, 124, 46
- Simpson C., 2003, *New Astronomy Review*, 47, 211
- Smail I., Chapman S. C., Ivison R. J., Blain A. W., Takata T., Heckman T. M., Dunlop J. S., Sekiguchi K., 2003, *MNRAS*, 342, 1185
- Smail I., Ivison R. J., Blain A. W., Kneib J.-P., 2002, *MNRAS*, 331, 495
- Sohn B. W., Klein U., Mack K.-H., 2003, *A&A*, 404, 133
- Soucail G., Kneib J. P., Bézecourt J., Metcalfe L., Altieri B., Le Borgne J. F., 1999, *A&A*, 343, L70
- Steidel C. C., Adelberger K. L., Giavalisco M., Dickinson M., Pettini M., 1999, *ApJ*, 519, 1
- Steidel C. C., Giavalisco M., Pettini M., Dickinson M., Adelberger K. L., 1996, *ApJ*, 462, L17+
- Stern D., Dey A., Spinrad H., Maxfield L., Dickinson M., Schlegel D., González R. A., 1999, *AJ*, 117, 1122
- Stevens J. A., Ivison R. J., Dunlop J. S., Smail I. R., Percival W. J., Hughes D. H., Röttgering H. J. A., van Breugel W. J. M., Reuland M., 2003, *Nature*, 425, 264
- Tadhunter C., Dickson R., Morganti R., Robinson T. G., Wills K., Villar-Martin M., Hughes M., 2002, *MNRAS*, 330, 977
- Tody D., 1993, in *ASP Conf. Ser. 52: Astronomical Data Analysis Software and Systems II IRAF in the Nineties*. pp 173–+
- van Breugel W., De Breuck C., Stanford S. A., Stern D., Röttgering H., Miley G., 1999, *ApJ*, 518, L61
- van Ojik R., Röttgering H. J. A., Carilli C. L., Miley G. K., Bremer M. N., Macchetto F., 1996, *A&A*, 313, 25
- van Ojik R., Röttgering H. J. A., Miley G. K., Hunstead R. W., 1997, *A&A*, 317, 358
- Venemans B. P., Kurk J. D., Miley G. K., Röttgering H. J. A., 2003, *New Astronomy Review*, 47, 353
- Vernet J., Cimatti A., 2001, *A&A*, 380, 409
- Vernet J., Fosbury R. A. E., Villar-Martín M., Cohen M. H., Cimatti A., di Serego Alighieri S., Goodrich R. W., 2001, *A&A*, 366, 7
- Waddington I., Windhorst R. A., Dunlop J. S., Koo D. C., Peacock J. A., 2000, *MNRAS*, 317, 801
- Webb T. M., Eales S., Foucaud S., Lilly S. J., McCracken H., Adelberger K., Steidel C., Shapley A., Clements D. L., Dunne L., Le Fèvre O., Brodwin M., Gear W., 2003b, *ApJ*, 582, 6
- Webb T. M., Eales S. A., Lilly S. J., Clements D. L., Dunne L., Gear W. K., Ivison R. J., Flores H., Yun M., 2003a, *ApJ*, 587, 41
- Williams R. J. R., Baker A. C., Perry J. J., 1999, *MNRAS*, 310, 913
- Willott C. J., Rawlings S., Archibald E. N., Dunlop J. S., 2002, *MNRAS*, 331, 435
- Willott C. J., Rawlings S., Blundell K. M., Lacy M., 1999, *MNRAS*, 309, 1017
- Willott C. J., Rawlings S., Blundell K. M., Lacy M., 2000, *MNRAS*, 316, 449



---

## Chapter 3

---

# An obscured radio galaxy at high redshift

Michiel Reuland, Wil van Breugel, Huub Röttgering, Wim de Vries, Carlos De Breuck and Daniel Stern, *The Astrophysical Journal Letters*, Vol. 528, p. 71, 2003

Perhaps as many as 10% of high redshift radio galaxy (HzRG;  $z > 2$ ) candidates that are selected using an Ultra Steep radio Spectrum (USS) criterion fail to show optical emission (continuum, lines) in deep Keck exposures. Their parent objects are only detected in the near-IR and are probably heavily obscured and/or at very high redshift. To search for signatures of dust and help constrain the nature and redshifts of these “no- $z$ ” radio galaxies, we have conducted a program of submillimeter and millimeter observations. Here we report the first results of a detailed study of one of these objects, WN J0305+3525.

WN J0305+3525 appears associated with a small group of  $K \sim 21 - 22$  objects and is strongly detected at both  $850 \mu\text{m}$  and  $1.25 \text{ mm}$ . On the basis of its faint  $K$ -band magnitude, spectral energy distribution (SED) and other evidence we estimate that the radio galaxy is probably at a redshift  $z \simeq 3 \pm 1$ . This would make WN J0305+3525 a radio-loud Hyper Luminous Infrared Galaxy ( $L_{\text{FIR}} \sim 10^{13} L_{\odot}$ ) similar to, but more obscured than, other dusty radio galaxies in this redshift range. This, together with the absence of  $\text{Ly}\alpha$  emission and compact ( $\theta \lesssim 1''.9$ ) radio structure, suggests that WN J0305+3525 is embedded in a very dense, dusty medium and is probably at an early stage of its formation.

### 1 Introduction

HIGH redshift active galactic nuclei (AGNs) have gained renewed interest as cosmological probes with the findings that (i) there is a good correlation between the masses of the stellar bulges of galaxies and their central black holes suggesting a causal connection in their formation (e.g., Magorrian et al. 1998) and (ii) that a population of high redshift heavily obscured AGNs seems the best candidate to account for a substantial fraction (30–40%) of the 5–10 keV cosmic X-ray background (XRB) (e.g., Hasinger 2002; Stern et al. 2002; Willott et al. 2002).

The most vigorously star forming galaxies radiate strongly in the far-IR (Sanders & Mirabel 1996). Sub-mm observations show that as many as 50% of  $z > 3$  HzRGs are “Hyper Luminous Infrared Galaxies” (HyLIRGs,  $L_{\text{FIR}} \sim 10^{13} L_{\odot}$ ; Chapter 2; Archibald et al. 2001; Reuland et al. 2004). While some HyLIRGs are powered by an obscured AGN, there also exist many in which the starburst dominates (Rowan-Robinson 2000). The detection of strong rest-frame UV absorption features show that there are hot young stars at  $z \sim 3.8$  in at least one case (Dey et al. 1997), and CO mm-interferometry

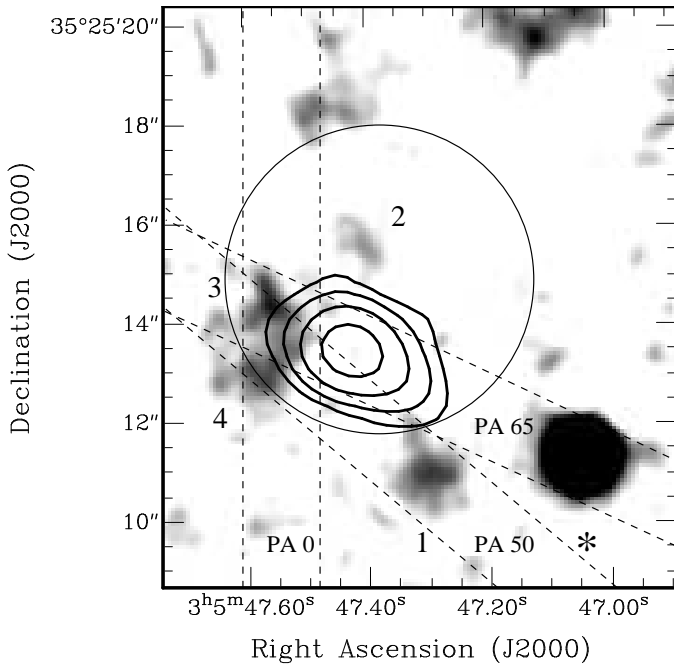


**Figure 1** — Keck/NIRC  $K$ -band image with 4.85 GHz VLA radio contours (De Breuck et al. 2000) overlaid of the HzRG candidate WN J0305+3525. The greyscale image has been smoothed to a resolution of  $0''.7$  and the contour levels are 0.25, 0.5, 1, and  $2 \text{ mJy beam}^{-1}$ . Note the multiple components. The bright object to the SW is a spectroscopically confirmed star. The circle with  $3''$  radius represents the nominal  $3\sigma$  astrometric uncertainty for the centroid of the  $850 \mu\text{m}$  emission and dashed lines indicate the LRIS slit positions.

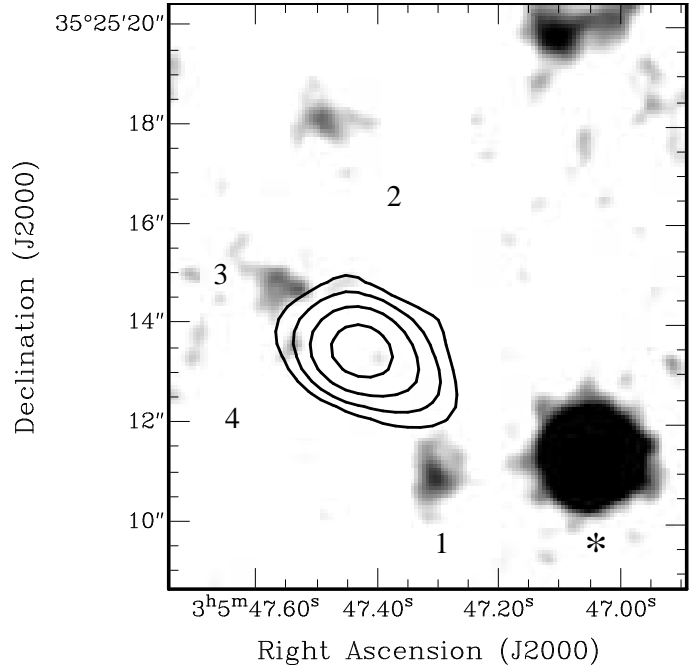
studies show that star formation occurs galaxy wide over scales of up to  $\sim 30 \text{ kpc}$  (Papadopoulos et al. 2000). These observations provide direct evidence that powerful HzRGs are massive galaxies forming stars at rates as high as  $2000 \text{ M}_{\odot} \text{ yr}^{-1}$ . From the near-IR Hubble  $K - z$  diagram HzRGs are known to be the most luminous galaxies at any redshift up to  $z \sim 5.2$  (De Breuck et al. 2002, hereafter DB02). Furthermore, actively-accreting supermassive black holes ( $M_{\text{BH}} \sim 10^9 \text{ M}_{\odot}$ ; Lacy et al. 2001) are required to power radio sources. Therefore, HzRGs are excellent targets to study the formation and coevolution of the most massive galaxies and their black holes.

De Breuck et al. (2001) found that 36% of a sample of 33 USS ( $\alpha_{325\text{MHz}}^{1400\text{MHz}} \lesssim -1.30$ ;  $S_{\nu} \propto \nu^{\alpha}$ ) selected radio sources with spectroscopic information was at redshifts  $z > 3$ . A surprisingly large fraction (24%) of these USS sources did *not* show emission lines even in moderately long exposures (1–2 hrs) at Keck. Of these latter sources, 3 (or 9% of the entire sample) did not show optical continuum emission down to a limit of  $R \sim 25$  and were detected only at near-IR ( $K$ -band) wavelengths.

The nature of these “no- $z$ ” objects is unclear. As discussed by De Breuck et al. one can think of the following possible explanations: objects which do show optical continuum (i) may be in the “redshift desert” ( $1.5 < z < 2.3$ ) where strong emission lines fall outside the observable window or (ii) may be pulsars; objects without optical continuum (iii) may be highly obscured AGNs or (iv) be at such high redshift ( $z \gtrsim 7$ ) that  $\text{Ly}\alpha$  is shifted out of the optical passband. In the latter two cases they may be young HzRGs in an exceptionally vigorous stage of their formation, and one would expect large amounts of dust associated with them. To search for this we have conducted a program of sub-mm and mm observations of these “no- $z$ ” radio galaxies. Here we report the first results of a detailed study of one such object, WN J0305+3525.

To facilitate comparison with other papers we adopt an universe with  $\Omega_{\text{M}} = 1.0$ ,  $\Omega_{\Lambda} = 0$ , and  $H_0 = 50 \text{ km s}^{-1} \text{ Mpc}^{-1}$  unless stated otherwise. The angular scale at  $z = 3$

**Figure 2** — Same as Figure 1, but for the greyscale representation of the Keck/NIRC *J*-band image of WN J0305+3525. The image has been smoothed to a resolution of  $0''.7$ . Objects 2 and 4 which were visible in *K*-band remain undetected. This image is similar to the *I*-band image (not shown).



is then  $7.3 \text{ kpc arcsec}^{-1}$  and the look-back time is 11.4 Gyr, or 88% of the age of the universe.

## 2 Observations and Results

### 2.1 Selection and Keck Imaging

VLA observations by De Breuck et al. (2000) show that WN J0305+3525 is a compact ( $\theta \lesssim 1''.9$ ) steep spectrum ( $\alpha_{325\text{MHz}}^{1.4\text{GHz}} = -1.33$ ) radio source with flux density  $S_{1.4\text{GHz}} = 15.8 \text{ mJy}$ . As part of our program aimed at finding  $z > 3$  radio galaxies among USS sources DB02 obtained a 15 min *I*-band image with  $0''.7$  seeing and a 38 min *K*-band image with  $0''.55$  seeing at Keck. We obtained a 58 min Keck *J*-band image on UT 2000 January 30 (seeing  $\sim 0''.6$ ) with the Near Infrared Camera (NIRC; Matthews & Soifer 1994), which was reduced following DB02. Formal  $5\sigma$  detection limits in  $2''$  diameter circular apertures are  $I_{\text{lim}} = 23.37$ ,  $J_{\text{lim}} = 23.15$ , and  $K_{\text{lim}} = 22.61$ . Astrometry for the *I*-band image was determined using the USNO-A2.0 catalog (Monet 1998) giving a formal uncertainty of  $0''.15$ . The absolute rms uncertainties with respect to the international celestial reference frame of the catalog and radio image are  $0''.2$  and  $0''.25$  respectively (e.g., DB02). The small near-IR images were registered to the  $6' \times 7'$  *I*-band image to better than  $0''.05$  rms, resulting in relative astrometry between the near-IR and radio images accurate to  $1\sigma \sim 0''.4$  rms.

Figure 1 shows the *K*-band image with 5 GHz radio map overlaid. It reveals fuzzy structure with multiple components within  $2''$ – $3''$  of the radio source. Note that none of the objects appears directly associated with the radio emission itself. Table 1 summarizes the observed properties of these objects. Objects 2 and 4 remain undetected in the *I* and *J*-band images (Fig. 2).

| Source                | R.A. (J2000) | DEC (J2000) | $I^a$            | $J^a$            | $K^a$            | $(I - J)^b$   | $(J - K)^b$   |
|-----------------------|--------------|-------------|------------------|------------------|------------------|---------------|---------------|
| 1                     | 3:05:47.30   | +35:25:11.0 | $22.88 \pm 0.15$ | $22.03 \pm 0.20$ | $21.16 \pm 0.19$ | 0.9           | 0.9           |
| 2                     | 3:05:47.40   | +35:25:15.6 | $> 23.37$        | $> 23.15$        | $22.18 \pm 0.33$ | –             | $\gtrsim 1.0$ |
| 3                     | 3:05:47.56   | +35:25:14.4 | $23.16 \pm 0.19$ | $22.06 \pm 0.20$ | $21.30 \pm 0.20$ | 1.1           | 0.8           |
| 4                     | 3:05:47.56   | +35:25:13.0 | $> 23.37$        | $> 23.15$        | $21.44 \pm 0.24$ | –             | $\gtrsim 1.7$ |
| Ensemble <sup>c</sup> |              |             | $23.41 \pm 0.92$ | $21.07 \pm 0.18$ | $20.71 \pm 0.24$ | $\gtrsim 2.3$ | 0.4           |
| 850 $\mu\text{m}$     | 3:05:47.38   | +35:25:15.0 |                  |                  |                  |               |               |
| 4.85 GHz <sup>d</sup> | 3:05:47.42   | +35:25:13.4 |                  |                  |                  |               |               |
| SW Stellar Object (*) | 3:05:47.05   | +35:25:11.3 | $19.61 \pm 0.01$ | $18.50 \pm 0.04$ | $18.36 \pm 0.05$ | 1.1           | 0.1           |

**Table 1** — Optical, near-IR, 850  $\mu\text{m}$  and radio parameters of WN J0305+3525.

<sup>a</sup> Magnitudes have been corrected for Galactic reddening using the Cardelli, Clayton, & Mathis (1989) extinction curve with  $A_V = 0.85$  as determined from the IRAS 100  $\mu\text{m}$  maps of Schlegel, Finkbeiner, & Davis (1998) and were measured in 2'' diameter circular apertures, unless noted otherwise.

<sup>b</sup> Calculated using formal  $5\sigma$  detection limits in the aperture ( $I_{\text{lim}} = 23.37$ ,  $J_{\text{lim}} = 23.15$ ,  $K_{\text{lim}} = 22.61$ ) if fainter than those. <sup>c</sup> Magnitudes have been measured in a 6'' diameter circular aperture centered on object 3 also encompassing objects 2 and 4.

<sup>d</sup> Position from De Breuck et al. (2000)

## 2.2 JCMT and IRAM Observations

We observed WN J0305+3525 on UT 1999 December 6 and 7 at 850  $\mu\text{m}$  and 450  $\mu\text{m}$  with the Submillimetre Common-User Bolometer Array (SCUBA; Holland et al. 1998) at the James Clerk Maxwell Telescope in stable atmospheric conditions  $\tau_{850} \sim 0.29 - 0.32$ . We performed two sets of 50 integrations each night using the 9-point jiggle photometry mode while chopping 45'' in azimuth at 7.8 Hz. Pointing was better than 2''. Flux calibration was performed on Saturn, HLTAU, and CRL618 and we adopted a gain  $C_{850} \sim 182 \text{ mJy beam}^{-1} \text{ V}^{-1}$ . The data were reduced following procedures outlined in the SCUBA Photometry Cookbook<sup>1</sup>. Combining the data from both nights yields an average 850  $\mu\text{m}$  flux density of  $12.5 \pm 1.5 \text{ mJy}$ , while at 450  $\mu\text{m}$  we measured  $21 \pm 19 \text{ mJy}$  and did not detect the object. The FWHM of the beam at 850  $\mu\text{m}$  for SCUBA is  $\theta_{\text{FWHM}} = 14''.5$ . We imaged WN J0305+3525 with SCUBA on UT 2000 February 26, 27, and 28, reaching  $\sim 1.5 \text{ mJy rms}$ , to obtain a more accurate position for the sub-mm source. The position of the 850  $\mu\text{m}$  centroid  $\alpha = 03^{\text{h}}05^{\text{m}}47^{\text{s}}.38$ ,  $\delta = +35^{\circ}25'15''.0$  (J2000) with estimated  $3\sigma$  astrometric uncertainty of  $\pm 3 \times \theta_{\text{FWHM}} / (2 \times S/N) \sim 3''$  (following Serjeant et al. 2002) is indicated in Figure 1.

WN J0305+3525 was also observed at 1.25 mm using the 37 channel MPIfR Bolometer Array (MAMBO II; Kreysa et al. 1998) at the IRAM 30 m telescope on UT 2000 July 18. We performed 11 symmetric “ON-OFFs” with a chop-nod distance of 45'', each with 20 subscans of 10 s per subscan. The atmospheric extinction  $\tau_{1.25}$  varied between 0.16 and 0.34 and pointing corrections were less than 2''. The calibration factor of 13.3 counts  $\text{mJy}^{-1}$  was estimated from on-offs on Uranus and Saturn. Using MOPSI with sky-noise filtering we detect the object at  $4.17 \pm 0.56 \text{ mJy}$ .

## 2.3 Keck Spectroscopy

We have attempted to measure the redshift of WN J0305+3525 using the Low-Resolution Imaging Spectrometer (LRIS; Oke et al. 1995) with the 150  $\ell \text{ mm}^{-1}$  grating blazed at

<sup>1</sup>The SCUBA Photometry Cookbook is available at <http://www.starlink.rl.ac.uk/star/docs/sc10.htx/sc10.html>

7500 Å and 1".5 wide slit resulting in a spectral resolution of 15 Å and wavelength coverage of 4100 – 10000 Å. Between exposures we shifted the object by 10" along the slit to facilitate fringe removal in the red parts of the CCD. The slit positions are indicated in Figure 1. A 3 × 30 min observation at PA=50° on UT 1999 December 20 through targets 1 and 3 did not show emission lines. On UT 2000 February 1 we first observed 2 × 30 min at PA=65° through target 3, the formal radio source position, and the SW stellar object (\*). No emission lines were found, but the latter object was identified as a Galactic M giant. A second set of similar exposures at PA=0° through targets 3 and 4 did not show emission lines either, but we may have detected faint continuum ( $F_{\lambda}^{\text{cont}} \approx 2 \pm 3 \times 10^{-19} \text{ erg s}^{-1} \text{ cm}^{-2} \text{ \AA}^{-1}$ ) redward of  $\lambda \approx 6300 \text{ \AA}$  from object 3. Object 2 was not observed spectroscopically, but it is unlikely that it would have been detected given its faintness. Assuming that Ly $\alpha$  would fall between 5100 Å and 8900 Å where the sky is well behaved and assuming a line width  $\sim 30 \text{ \AA}$  (e.g., Dey et al. 1997), we derive a  $3\sigma$  upper limit to the Ly $\alpha$  flux density of  $3 \times 10^{-17} \text{ erg s}^{-1} \text{ cm}^{-2}$ .

### 3 Discussion

#### 3.1 Identification and Redshift Estimate

What are the chances that the sub-mm source, the radio source and the *K*-band objects are all unrelated? Sub-mm surveys have shown that the  $S_{850 \mu\text{m}} \gtrsim 10 \text{ mJy}$  number density is less than 100 per square degree (Hughes et al. 2002). Radio surveys show that there are less than 12 radio sources with  $S_{1.4\text{GHz}} \gtrsim 15 \text{ mJy}$  per square degree (de Vries et al. 2002). Within the sub-mm error circle (3" radius; by far the largest of the three), the chance of finding a chance superposition of a  $\gtrsim 10 \text{ mJy}$  sub-mm source and a  $\gtrsim 15 \text{ mJy}$  radio source is negligible ( $< 2.3 \times 10^{-4}$ ). The chance of finding three unrelated  $K < 22 \text{ mag}$  objects within the error circle is less than 10% given a number density  $\sim 2 \times 10^5$  per square degree (Djorgovski et al. 1995). Despite the offsets between the *K*-band objects and the radio source there are good reasons to believe that they are related. Many USS selected radio galaxies consist of multiple components (van Breugel et al. 1998). Furthermore, in most HzRGs the radio AGN are obscured (Reuland et al. 2003) and there are other cases where the AGN appears to be located off center from the bulk of the parent galaxy (e.g., 3C294; Quirrenbach et al. 2001).

Without a spectroscopic redshift we can use only indirect arguments to estimate the redshift of WN J0305+3525 such as the *K* – *z* diagram, the shape of the SED and the near-IR colors. We cannot use the radio to sub-mm index as a redshift indicator (Carilli & Yun 1999) as WN J0305+3525 is radio loud. The *K* – *z* diagram as determined for HzRGs (DB02) seems to hold also for the sub-mm population (Dunlop 2002). If we take a total magnitude of  $K \sim 21$  to be representative for WN J0305+3525 (Table 1), then we estimate from the *K* – *z* diagram that WN J0305+3525 is at  $3 \lesssim z \lesssim 7$ .

Comparing the (sub)-mm ratios  $S_{1250}/S_{850} = 0.33$  and  $S_{450}/S_{850} \lesssim 6$  with redshifted models of dusty starforming galaxies (c.f. Fig. 3 in Hughes et al. 1998) results in redshift estimates of  $3 \lesssim z \lesssim 6$  and  $z > 1 - 2$  respectively. Moreover, almost all USS radio galaxies that are detected in the sub-mm are at redshifts  $z > 2.5$ . Figure 3 represents the observed SED of WN J0305+3525 and shows that the (sub)-mm emission is of thermal origin and effectively rules out that the object is a pulsar. A starburst SED with

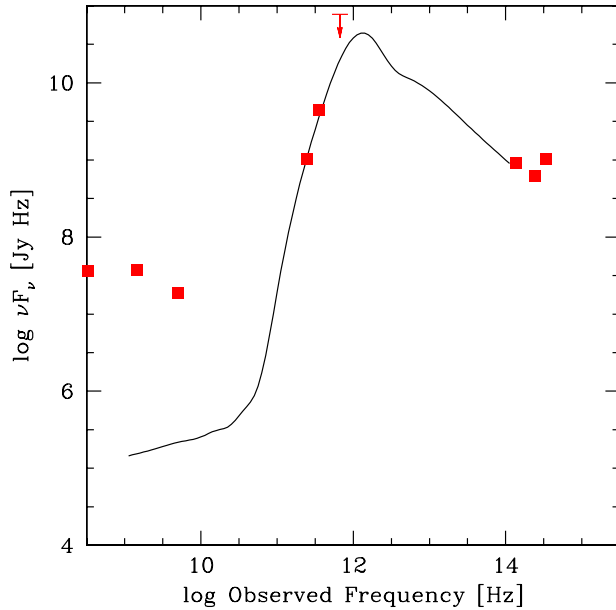


**Figure 3** — Radio to near-IR SED of WN J0305+3525 using data from the VLA (De Breuck et al. 2000), IRAM, JCMT, and Keck (squares and  $5\sigma$  upper limit for 450 micron point). Extrapolation of the steep radio spectrum shows that the contribution of the non-thermal radio emission is negligible at sub-mm wavelengths. For comparison we overplot a schematic SED representing local ultraluminous galaxies, shifted to  $z = 3$  (Lutz et al. 2001,  $H_0 = 75 \text{ km s}^{-1} \text{ Mpc}^{-1}$ ).

$1 \lesssim z \lesssim 4$  would fit the data closely at both the near-IR and (sub-)mm points.

The colors of the  $K$ -band objects are too uncertain to usefully constrain the redshifts using stellar evolution models (Stevens & Lacy 2001). The possible detection of faint continuum redward of  $\lambda \approx 6300 \text{ \AA}$  in object 3 is consistent with the object being at high redshift: it could be featureless continuum redward of a  $\text{Ly}\alpha$  forest region at  $z \sim 4.2$ .

Based on the above arguments we conclude that there is very good circumstantial evidence that WN J0305+3525 is at high redshift, probably at  $z \simeq 3 \pm 1$ .

### 3.2 Implications

If WN J0305+3525 is indeed at  $z \simeq 3$  then its restframe FIR properties are  $L_{\text{FIR}} \sim 10^{13} L_{\odot}$ , implying  $M_{\text{dust}} \sim 1.5 \times 10^8 M_{\odot}$  and star formation rate  $\sim 1500 M_{\odot} \text{ yr}^{-1}$  for standard dust models and cosmology (c.f. 4C 60.07;  $H_0 = 75 \text{ km s}^{-1} \text{ Mpc}^{-1}$ ; Papadopoulos et al. 2000). This is comparable to the radio-“quiet” sub-mm/mm source Lockman 850.1 which has been estimated to be at  $2 \lesssim z \lesssim 4$ , based on its sub-mm/mm SED (Lutz et al. 2001), as well as other, radio-“loud” galaxies in this redshift range. Compared with traditional HzRGs, the  $\text{Ly}\alpha$  emission ( $L_{\text{Ly}\alpha} \lesssim 10^{42.3} \text{ erg s}^{-1}$ ) is relatively weak given its radio power ( $P_{325\text{MHz}} \simeq 10^{35.1} \text{ erg s}^{-1} \text{ Hz}^{-1}$ ), but still within the large observed scatter (c.f. Fig. 10 in De Breuck et al. 2000). Thus WN J0305+3525 appears to be a heavily obscured radio-loud luminous sub-mm source. We consider two options that could explain the strong obscuration.

Recently, Greenberg & Shen (2000) and Todini & Ferrara (2001) suggested that dust particles in high redshift galaxies may be predominantly smaller than in local starbursting systems. The argument is based on a different origin of the dust: at high redshifts there has been little time for M giants (the primary sources of local dust) to appear, and most early dust would be produced by M supergiants and supernovae instead. The increase of the sub-mm detection rate with redshift for radio galaxies

(Chapter 2; Archibald et al. 2001; Reuland et al. 2004) might then be interpreted as being due to changing dust properties with redshift. Smaller dust particles lower the estimated dust masses and star formation rates and, because they are more efficient UV absorbers, this might explain why some of the most massive starforming galaxies are not seen in the optical at all.

Another reason that WN J0305+3525 is heavily dust enshrouded might be related to its young evolutionary stage. This is supported by the compactness of the associated radio source for WN J0305+3525 and the other “no-z” HzRG-candidates. It seems reasonable to assume that, on average, compact sources are younger than more extended ones (Blundell, Rawlings & Willott 1999). The dense circumnuclear dust configuration would then quench the Ly $\alpha$  emission.

This suggests a scenario in which massive radio galaxies form with a large starburst, perhaps simultaneously in several smaller, merging components. This starburst manifests itself as a luminous “sub-mm source”. During the next stage a massive black hole is formed and/or activated, but any rest-frame optical emission remains obscured by dust from the starburst. As the radio source evolves it grows and expels the obscuring dust envelope, becoming visible as a HzRG (c.f. Jarvis et al. 2002; Reuland et al. 2003). This is essentially the radio-loud version of scenarios where “Ultra Luminous Infrared Galaxies” evolve into quasars as envisaged by Sanders et al. (1988a).

Radio galaxies are the most massive and most extended galaxy sized systems that are known to exist at high redshift. They are therefore good targets for studying the origin of the relationship between galaxies and their central black holes. WN J0305+3525 may be at the stage where both the galaxy and the black hole are being put together. As with other sub-mm sources it is difficult to obtain spectroscopic redshifts and it is important to obtain further information about their SEDs at mid- and far-IR wavelengths. X-ray imaging could show whether or not there is a bright AGN associated with WN J0305+3525. We are actively pursuing follow-up observations to address some of these issues.

## Acknowledgments

We gratefully acknowledge the help of the Keck, and JCMT staff. We thank the IRAM staff and Albrecht Sievers in particular for carrying out observations in Director’s Discretionary Time, project Delta 00-04, and reducing the data. The work of M.R., W.v.B., and W.d.V. was performed under the auspices of the U.S. Department of Energy, National Nuclear Security Administration by the University of California, Lawrence Livermore National Laboratory under contract No. W-7405-Eng-48. The work of D.S. was carried out at the Jet Propulsion Laboratory, California Institute of Technology, under a contract with NASA.

## References

- Archibald, E., Dunlop, J., Hughes, D., Rawlings, S., Eales, S. & Ivison, R., 2001, MNRAS, 323, 417
- Blundell, K., Rawlings, S. & Willott, C. 1999, AJ, 117, 677
- Cardelli, J., Clayton, G. & Mathis, J. 1989, ApJ, 345, 245
- Carilli, C. & Yun, M., 1999, ApJ, 513, L13

- De Breuck, C., van Breugel, W., Röttgering, H. & Miley, G., 2000a, *A&AS*, 143, 303  
De Breuck, C., Röttgering, H., Miley, G., van Breugel, W. & Best, P. 2000b, *A&A*, 362, 519  
De Breuck, C., et al., 2001, *AJ*, 121, 1241  
De Breuck, C., van Breugel, W., Stanford, S., Röttgering, H., Miley, G. & Stern, D., 2002, *AJ*, 123, 637, (DB02)  
de Vries, W. H. et al. 2002, *AJ*, 123, 1784  
Dey, A., van Breugel, W., Vacca, W.D. & Antonucci, R., 1997, *ApJ*, 490, 698  
Djorgovski, S. et al. 1995, *ApJ*, 438, L13  
Dunlop, J., 2002, preprint, astro-ph/0203183  
Greenberg, M. & Shen, C., 2000, preprint, astro-ph/0006337  
Hasinger, G., 2002, preprint, astro-ph/0202430  
Holland, W. et al. 1998, *Proc. SPIE*, 3357, 305  
Hughes, D. H. et al. 1998, *Nature*, 394, 241  
Hughes, D. H. et al. 2002, *MNRAS*, 335, 871  
Jarvis, M., Wilman, R., Röttgering, H. & Binette, L., 2002, *MNRAS*, in press, astro-ph/0209159  
Kreysa, E. et al. 1998, *Proc. SPIE*, 3357, 319  
Lacy, M., Laurent-Muehleisen, S., Ridgway, S., Becker, R. & White, R., 2001, *ApJ*, 551, L17  
Lutz, D. et al. 2001, *A&A*, 378, 70  
Magorrian, J. et al. 1998, *AJ*, 115, 2285  
Matthews, K. & Soifer, B. 1994, *ASSL Vol. 190: Astronomy with Arrays, The Next Generation*, 239  
Monet, D., 1998, *American Astronomical Society Meeting*, 193, 112003  
Oke, J. et al., 1995, *PASP*, 107, 375  
Papadopoulos, P. et al. 2000, *ApJ*, 528, 626  
Quirrenbach, A., Roberts, J. E., Fidkowski, K., de Vries, W., & van Breugel, W. 2001, *ApJ*, 556, 108  
Reuland M., van Breugel W., Röttgering H., de Vries W., Stanford S. A., Dey A., Lacy M., Bland-Hawthorn J., Dopita M., Miley G., 2003, *ApJ*, 592, 755  
Reuland, M., Röttgering, H., van Breugel, W., & De Breuck, C. 2004, *MNRAS*, 353, 377  
Rowan-Robinson, M., 2000, *MNRAS*, 316, 885  
Sanders, D. et al. 1988, *ApJ*, 325, 74  
Sanders, D. & Mirabel, I., 1996, *ARA&A*, 34, 749  
Schlegel, D., Finkbeiner, D. & Davis, M., 1998, *ApJ*, 500, 525  
Serjeant, S. et al. 2002, *MNRAS*, submitted, astro-ph/0201502  
Stern, D. et al. 2002, *ApJ*, 568, 71  
Stevens, R. & Lacy, M. 2001, *MNRAS*, 325, 897  
Todini, P. & Ferrara, A. 2001, *MNRAS*, 325, 726  
van Breugel, W., Stanford, S., Spinrad, H., Stern, D. & Graham, J., 1998, *ApJ*, 502, 614  
Willott, C. J. et al. 2002, *MNRAS*, in press, astro-ph/0210248



---

# Chapter 4

---

## Dust enshrouded compact radio-loud AGN at high redshift

Michiel Reuland, Wil van Breugel, Wim de Vries, Huub Röttgering, and Carlos De Breuck,  
Monthly Notices of the Royal Astronomical Society, submitted

We present submillimetre and X-ray observations of a sample of ten radio galaxies for which no spectroscopic redshift could be determined in 1–2 hr Keck observations. Generally, these galaxies are characterised by compact ( $\theta \lesssim 2''$ ) radio morphologies and ultra-steep radio spectra ( $\alpha_{325\text{MHz}}^{1400\text{MHz}} \lesssim -1.30$ ;  $S_\nu \propto \nu^\alpha$ ). The galaxies were selected from a radio sample with flux densities  $10 < S_{1.4\text{GHz}} < 100$  mJy, fainter than most previous surveys. Four of the ten galaxies were detected in the submillimetre with  $S/N > 4$ . Circumstantial evidence suggests that they are at redshifts  $z > 3$  and then constitute up to 30% of the high redshift radio galaxy population. Their host galaxies are faint in the near-IR ( $K \gtrsim 19$ ), were generally not detected in the optical ( $R \gtrsim 24$ ) or X-ray, but appear to be as bright as  $z > 3$  radio galaxies at submillimetre wavelengths. This suggests that these galaxies are embedded in dense gaseous environments, from which they are forming. The high submillimetre detection fraction and the signal  $\langle S_{850, < 3\sigma}^{\text{CSS}} \rangle = 2.48 \pm 0.48$  mJy in the stacked non-detections indicate that this compact obscured phase may be a common ingredient in AGN evolution. Based on the empirical radio to X-ray relation for AGN, intrinsic X-ray luminosities of  $L_{2-10\text{keV}} \sim 10^{44-46}$  ergs $^{-1}$  and column densities of a few  $10^{23}$  cm $^{-2}$  are inferred, showing that they could maybe contribute to the hard X-ray background.

### 1 Introduction

**P**OWERFUL radio galaxies and quasars are among the most luminous galaxies and can be studied in great detail out to large distances (e.g., De Breuck et al. 2002, and references therein). Their radio structures, powered by actively accreting super massive black holes, interact strongly with the host galaxies and environments. Therefore, they are excellent laboratories for studies of galaxy formation and black hole growth in the early universe. The powerful radio source population comes in a wide variety of sizes and ranges from the very compact Gigahertz Peaked Spectrum (GPS;  $< 1$  kpc) and Compact Steep Spectrum (CSS; 1–20 kpc) objects to the classical edge brightened Fanaroff & Riley class II (FR II; up to  $> 1$  Mpc; Fanaroff & Riley 1974) radio sources. The consensus is that for low redshifts ( $z < 1$ ) this is best interpreted as evidence for

evolution of radio source size with age (e.g., Phillips & Mutel 1982; de Vries 2003). The situation at higher redshifts, however, is much less clear.

The average density and galaxy merger rate must have been much higher in the early universe than they are presently. This is likely to have resulted in a stronger interaction between early radio sources and their environments. Conceivably, the ISM could have been sufficiently dense to prevent a large fraction of GPS/CSS sources from expanding (the frustration scenario; e.g., van Breugel et al. 1984). A difference in evolution between low and high redshift sources is suggested also by the fact that almost all known GPS/CSS sources at redshifts  $z < 1$  are associated with galaxies, whereas for  $z > 1$  they are associated with quasars. Their X-ray properties have been found to be different as well (e.g., O’Dea et al. 2000; Siemiginowska et al. 2003). This is unexpected in the simple picture that quasars and galaxies are alike, but viewed under different angles. The GPS/CSS sources constitute approximately 30–40% of bright centimeter-frequency-selected samples (O’Dea 1998). Observations of such compact radio galaxies at high redshift could further our understanding of galaxy formation processes and jet triggering events.

Another incentive to study young active galactic nuclei (AGN) stems from deep X-ray surveys (Chandra, XMM, ROSAT) which have shown that the cosmic X-ray background (XRB) is largely due to discrete, actively accreting supermassive black holes (see Hasinger 2003, for a recent review). These consist of a mixture of unobscured (Type I) and obscured (Type II) AGN. The obscured AGN may have space densities several times larger than unobscured AGN and could contribute up to 40% of the 5–10 keV cosmic X-ray background (e.g., Mushotzky et al. 2000; Giacconi et al. 2001). Because of their obscuration, optical identifications have remained elusive and their properties and ubiquity have been poorly explored, requiring more observations.

Spectroscopic followup of sources with an ultra steep radio spectrum (USS;  $\alpha_{\frac{1400\text{MHz}}{325\text{MHz}}} \lesssim -1.30$ ;  $S_\nu \propto \nu^\alpha$ ) and faint near-IR counterpart show redshifts  $z > 3$  in  $\sim 35\%$  of the cases (for details see De Breuck et al. 2001). However, a significant fraction ( $\sim 25\%$ ) of the galaxies that fulfill all requirements of our efficient high redshift radio galaxy (HzRG;  $z > 2$ ) candidate selection criteria fail to yield emission line redshifts in 1–2 hr spectroscopic observations at the 10 m Keck telescopes. Generally, these are compact objects ( $\theta \lesssim 2\text{--}3''$ ). A possible explanation for the lack of line emission is that they are situated in extremely dense and dusty environments. One of them has been studied before in detail (WN J0305+3525; Reuland et al. 2003) and was found to be very (sub-)millimetre (submm) luminous and highly obscured.

Could it be that all these USS compact sources are heavily obscured? Does the fraction of such sources increase with redshift? Is such an obscured and compact phase a universal stage in the birth process of radio galaxies? This could hint at a radio-loud analog to the ULIRG–QSO evolutionary scheme presented by Sanders et al. (1988a) and Haas et al. (2003), where a luminous submm phase partly coincides with the emergence of a HzRG. What are the intrinsic X-ray luminosities and obscuring column depths, and could the AGN be part of the population that contributes to the hard XRB?

To help answer these questions we have obtained (sub-)mm (SCUBA/JCMT, MAMBO/IRAM) and X-ray (Chandra) observations of 10 HzRG-candidates of this intriguing class. Results of this observing campaign are reported in this paper.

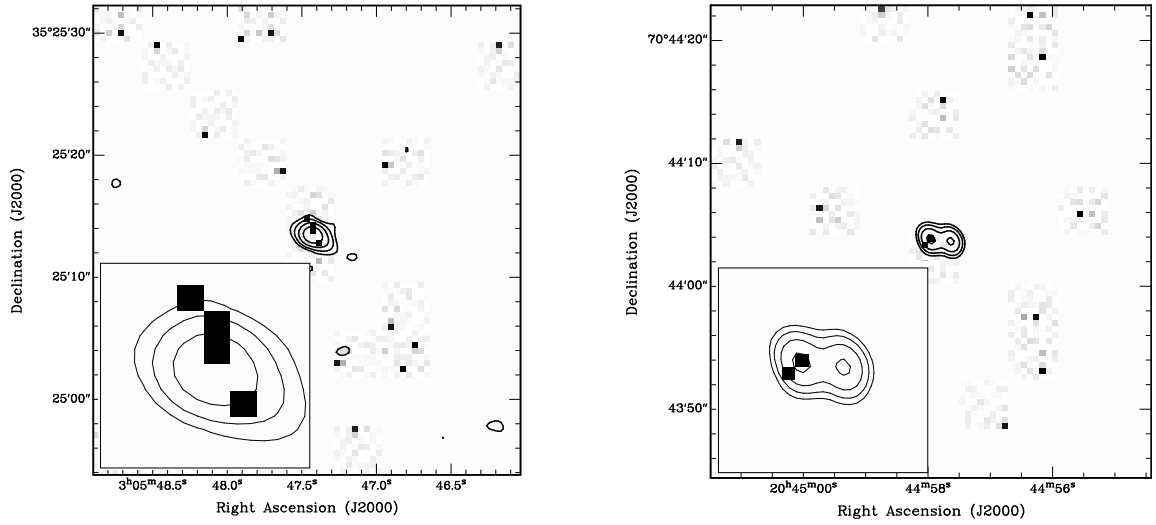


**Figure 1** — Contour overlays of 5 GHz VLA maps of WN J0305+3525 (left) and WN J2044+7044 (right) on the 0.5–7 keV images obtained with Chandra. The contour levels are 0.5, 1.0, 2.0 mJy beam<sup>-1</sup> for WN J0305+3525 and 0.5, 1.0, 2.0, 3.0 mJy beam<sup>-1</sup> for WN J2044+7044.

| Source       | RA(J2000)<br>h m s | DEC (J2000)<br>° ' " | $N_{\text{H}}$<br>cm <sup>-2</sup> | LAS<br>" | $\alpha_{325}^{1.4}$ | $S_{1.4\text{GHz}}$<br>mJy | $K$<br>mag | $R^1$<br>mag | $R - K$<br>mag | Continuum |
|--------------|--------------------|----------------------|------------------------------------|----------|----------------------|----------------------------|------------|--------------|----------------|-----------|
| WNJ0305+3525 | 03 05 47.42        | +35 25 13.4          | $1.2 \times 10^{21}$               | 1.9      | -1.33                | 15.8                       | 20.7       | 23.4*        | 2.7*           | U         |
| WNJ0310+3644 | 03 10 54.80        | +36 44 02.5          | $1.2 \times 10^{21}$               | 2.0      | -1.70                | 24.2                       | —          | 23.0*        | —              | F         |
| TNJ1026–2116 | 10 26 22.37        | -21 16 07.7          | $6.6 \times 10^{20}$               | 1.0      | -1.39                | 61.5                       | 19.8       | > 24         | > 4.2          | U         |
| WNJ1314+3649 | 13 14 17.86        | +36 49 14.6          | $1.0 \times 10^{20}$               | 1.3      | -1.41                | 36.4                       | 22.1       | > 26         | > 3.9          | F         |
| WNJ1355+3848 | 13 55 29.50        | +38 48 11.1          | $9.4 \times 10^{19}$               | 2.3      | -1.42                | 25.6                       | 19.3       | > 25         | > 5.7          | F         |
| WNJ1525+3010 | 15 25 01.21        | +30 10 30.2          | $2.0 \times 10^{20}$               | 1.2      | -1.46                | 17.2                       | 19.5       | 25.3         | 5.8            | U         |
| WNJ1836+5210 | 18 36 23.22        | +52 10 28.4          | $4.5 \times 10^{20}$               | 1.4      | -1.41                | 24.2                       | 17.7       | 21.0         | 3.3            | B         |
| WNJ1917+6635 | 19 17 35.50        | +66 35 38.5          | $6.2 \times 10^{20}$               | 1.9      | -1.30                | 11.2                       | 20.0       | 23.7         | 3.7            | F         |
| TNJ1954–1207 | 19 54 24.15        | -12 07 48.7          | $1.0 \times 10^{21}$               | < 7.0    | -1.38                | 102.8                      | 19.9       | —            | —              | F         |
| WNJ2044+7044 | 20 44 57.80        | +70 44 03.8          | $1.7 \times 10^{21}$               | 1.3      | -1.38                | 41.7                       | 19.2       | > 24         | > 4.8          | U         |

**Table 1** — Radio positions, Galactic HI column densities  $N_{\text{H}}$ , largest angular radio sizes, radio spectral indices  $\alpha_{325}^{1.4}$ , 1.4 GHz flux densities,  $K$  and  $R$ -band magnitudes,  $R - K$  colours. The near-IR and optical magnitudes were all measured within 4" diameter circular apertures, only for WN J0305+3525 a 6" diameter aperture was used due to the extended nature of the source. The spectra of some sources showed continuum emission but no identifiable features. The last column indicates whether the continuum was bright (B;  $F_{5000\text{\AA}} > 2\mu\text{Jy}$ ), faint (F;  $F_{5000\text{\AA}} < 2\mu\text{Jy}$ ) at 5000 Å (close to the blueward limit of the spectrographic observations for most sources) or whether it remained undetected (U). For the TN sources the spectral index has been estimated using observations at 365 MHz as the lower frequency instead of 325 MHz. These data were taken from the following papers: De Breuck et al. (2000, 2001); De Breuck et al. (2002) and Reuland et al. (2003).

This paper is organised as follows. In §2 the target selection, details on the observations and observational results are presented. We discuss redshift estimates, possible scenarios to explain the results and their implications in §3. These are then summarised in §4. We assume a flat universe with  $H_0 = 65 \text{ km s}^{-1} \text{ Mpc}^{-1}$ ,  $\Omega_{\text{M}} = 0.3$  and  $\Omega_{\Lambda} = 0.7$  throughout.

| Source       | $S_{850}^a$<br>mJy | S/N | $3\sigma$ limit<br>mJy | $S_{1250}$<br>mJy | S/N | $z_{\text{est}}^K$ |
|--------------|--------------------|-----|------------------------|-------------------|-----|--------------------|
| WNJ0305+3525 | $12.5 \pm 1.5$     | 8.3 |                        | $4.2 \pm 0.6$     | 7.4 | > 3                |
| WNJ0310+3644 | $7.0 \pm 1.6$      | 4.2 |                        | —                 | —   | —                  |
| TNJ1026–2116 | $0.2 \pm 1.7$      | 0.1 | < 5.14                 | —                 | —   | > 1                |
| WNJ1314+3649 | $5.3 \pm 1.2^b$    | 4.3 |                        | $2.2 \pm 0.7$     | 3.3 | > 5                |
| WNJ1355+3848 | $2.9 \pm 1.3$      | 2.3 | < 6.68                 | —                 | —   | > 2                |
| WNJ1525+3010 | $3.5 \pm 1.6$      | 2.1 | < 8.37                 | —                 | —   | > 1.5              |
| WNJ1836+5210 | $2.8 \pm 1.3$      | 2.2 | < 6.58                 | —                 | —   | > 0.5              |
| WNJ1917+6635 | $1.1 \pm 1.4$      | 0.8 | < 5.27                 | —                 | —   | > 2                |
| TNJ1954–1207 | $3.6 \pm 1.3$      | 2.8 | < 7.44                 | —                 | —   | > 1.5              |
| WNJ2044+7044 | $5.6 \pm 1.3$      | 4.3 |                        | $1.4 \pm 0.6$     | 2.3 | > 2                |

**Table 2** — Observed 850  $\mu\text{m}$  and 1250  $\mu\text{m}$  flux densities with their standard errors, and redshift estimates based on the  $K$ -band magnitudes of the radio sources in the program.  $3\sigma$  upper limits are shown for sources whose S/N ratios are below 3. The lower limits to the redshift estimates are based on the faint envelope (1.5 mag fainter than the best-fit average) of the  $K$ - $z$  relation for HzRGs (Fig. 7 in De Breuck et al. 2002).

<sup>a</sup> This does not include the 10–15 per cent uncertainty in absolute photometric calibration.

<sup>b</sup> Affected by an estimated 4'' pointing error due to problems with the tracking model for observations with elevations above 60 degrees. See [http://www.jach.hawaii.edu/JCMT/Facility\\_description/Pointing/tracking\\_fault.html](http://www.jach.hawaii.edu/JCMT/Facility_description/Pointing/tracking_fault.html) for details.

## 2 Observations and Results

The targets were selected from a sample of the 669 USS radio sources compiled by De Breuck et al. (2000). This sample has been constructed using radio flux densities that are 1–2 orders of magnitude fainter than steep spectrum samples based on previous radio catalogs such as 3C, 4C, and 6C. It forms the basis of our ongoing search for HzRGs. De Breuck et al. (2001) found that  $\sim 25\%$  of the galaxies that fulfill all requirements of our HzRG-candidate pre-selection criteria (see De Breuck et al. for details) failed to yield emission line redshifts in 1–2 hrs optical and near-IR spectrographic observations with LRIS or NIRSPEC at the Keck 10 m telescope. Some of these did not even show optical continuum ( $R \gtrsim 24$ –25) and only have faint near-IR ( $K \gtrsim 19$ ) counterparts. These “no- $z$ ” objects with a very compact ( $\theta \lesssim 2$ –3'') radio structure are the subject of the present study. The coordinates, references,  $R$  and  $K$ -band magnitudes and relevant radio properties of our targets are given in Table 1.

### 2.1 SCUBA photometry

Observations were carried out between December 2000 and February 2001 with the Submillimetre Common–User Bolometer Array (SCUBA; Holland et al. 1998) at the 15 m James Clerk Maxwell Telescope (JCMT). We observed at 850  $\mu\text{m}$  wavelengths resulting in a beam size of 15''. We employed the 9-point jiggle photometry mode, with a chop throw of 45'' in azimuth at 7.8 Hz. Frequent pointing checks were performed to ensure pointings better than 2''.

The observing conditions were generally good with optical depths  $\tau_{850}$  varying between 0.15 and 0.35. The data were reduced using the Scuba User Reduction Facility

| Source        | Date<br>JD  | $t_{\text{exp}}$<br>ks | Flux<br>counts | Backgr.<br>counts | $3\sigma$ limit<br>counts | Net count rate<br>counts s <sup>-1</sup> | $S_{0.5-10\text{keV}}$<br>erg s <sup>-1</sup> cm <sup>-2</sup> | $S_{2\text{keV}}$<br>mJy | $\alpha_{\text{SX}}$ |
|---------------|-------------|------------------------|----------------|-------------------|---------------------------|--|--|--------------------------|----------------------|
| WN J0305+3525 | Dec/01/2002 | 12.6                   | 4              | 0.14              | < 14.3                    | < $1.1 \times 10^{-3}$                   | < $1.0 \times 10^{-14}$  | < $7.1 \times 10^{-7}$   | < -1.18              |
| WN J1314+3649 | Jul/28/2003 | 9.0                    | 0              | 0.10              | < 6.5                     | < $0.7 \times 10^{-3}$                   | < $0.5 \times 10^{-14}$  | < $3.6 \times 10^{-7}$   | < -1.16              |
| WN J2044+7044 | Apr/14/2003 | 5.1                    | 2              | 0.04              | < 10.8                    | < $2.0 \times 10^{-3}$                   | < $2.0 \times 10^{-14}$  | < $14.2 \times 10^{-7}$  | < -1.08              |

**Table 3** — Summary of the Chandra observations, with  $3\sigma$  Poissonian upper limits following Gehrels (1986). The source and background count rates have been measured within  $3.5''$  diameter apertures and converted into X-ray flux densities assuming a photon index  $\Gamma = 2$  and correcting for Galactic absorption. The last column shows  $3\sigma$  upperlimits to the submm-to-X-ray spectral index  $\alpha_{\text{SX}}$  and is discussed in Section 3.2.2

software package (SURF; Jenness & Lightfoot 2000) following the procedure outlined in Reuland et al. (2004). Flux calibration was performed using HLTAU, OH231.8 and CRL618 as photometric calibrators. The typical photometric uncertainty for our program is of order 10–15 per cent (see e.g., Jenness et al. 2001).

The results of the SCUBA observations are summarised in Table 2. Of the ten sources observed at  $850 \mu\text{m}$  four were detected with flux densities  $S_{850} > 5 \text{ mJy}$  at larger than  $4\sigma$  confidence level.

## 2.2 IRAM Photometry

Following their detections with SCUBA, we observed WN J1314+3649 and WN J2044+7220 at  $1.25 \text{ mm}$  using the MPIfR bolometer arrays (MAMBO II; Kreysa et al. 1998) at the IRAM 30 m telescope in service mode. The 117-channel bolometer array was used in December 2001 and the 37-channel bolometer array during January and February 2002. The symmetric “ON-OFF” mode with wobbler throws in the range of  $32\text{--}46''$  was employed and the observations were done using on-offs with 16–20 subscans of 12 s per subscan. The atmospheric extinction  $\tau_{1.25}$  varied between 0.09 and 0.24. Pointing corrections were found to be better than  $2''$ . The on-off data was reduced with MOPSIC with sky-noise filtering<sup>2</sup>.

Including previous observations of WN J0305+3525, two out of three submm sources have been detected ( $> 3\sigma$ ) at  $1.25 \text{ mm}$  with MAMBO (Table 2), confirming the reality of the emission found with SCUBA.

## 2.3 Chandra

Three of the galaxies detected in the submm were observed with the Chandra X-ray Observatory (Weisskopf et al. 2000) between December 2002 and July 2003. The exposures were obtained using the back-illuminated ACIS-S3 chip in TE mode with 3.2 s readout and FAINT telemetry format. The data were processed using the standard tool CIAO 2.3<sup>3</sup>. The detector lightcurves showed no evidence for contamination by flares, therefore the total length of the exposures was used effectively. Following Giacconi et al. (2001) we limited the bandpass to 0.5–7 keV, because inclusion of the 7–10 keV band always decreases the signal-to-noise ratio. For comparison with other papers, fluxes are quoted in the 0.5–10 keV band, as extrapolated from the measured count

<sup>2</sup>Zylka, R. The MOPSI Cookbook

<sup>3</sup><http://xc.harvard.edu/ciao>

rate. All count rates and X-ray flux densities are calculated using PIMMS v3.4<sup>4</sup>, assuming a photon index  $\Gamma = 2$  which is appropriate for obscured AGN (Fabian et al. 2000).

Table 3 summarizes the Chandra observations. The X-ray counts were measured within 3.5'' diameter circular apertures, comparable to the extents of the radio sources. The background was estimated using a large annular region, centered on the radio position, after removal of point sources. None of the sources observed with Chandra were formally detected in the X-ray regime. Upper limits on the counts are estimated with Poisson statistics following Gehrels (1986). Figure 1 shows that, despite the low number of counts, for WN J0305+3525 and WN J2044+7044 there appears to be concentration of photons at the position of the radio emission. Especially for WN J0305+3525 it is worth noting that in the 10 arcmin<sup>2</sup> field for which we have *I*-band imaging the five other regions that contain more than three photons in a 3.5'' diameter aperture all have obvious *I*-band counterparts. Hence it seems probable that the four photons detected are indeed associated with WN J0305+3525.

### 3 Discussion

While we have detected a significant fraction of these “no-*z*” radio sources in the mm and submm regime, none of the sources was detected significantly with Chandra. These results prompt the following questions: What is the origin of the submm emission? Does the lack of X-ray photons indicate high obscuration by a dense medium favouring the frustrated radio source scenario or is it because the targets are intrinsically weak X-ray emitters? Are these nearby starbursting systems or highly obscured type II AGN possibly at high redshift? What are the HI absorbing column densities and how compare these with dust masses derived from the submm luminosities? Where do these sources fit into radio galaxy evolution and AGN unification scenarios?

#### 3.1 Redshift estimates

With the available data, it is impossible to obtain accurate redshift estimates. Still, we can address whether or not the sources are at large cosmological distances. As discussed in Reuland et al. (2003) we have several indirect means of estimating their redshifts. Circumstantial evidence that a large fraction of these objects could be at redshifts  $z \sim 3$  comes from the following: (i) They are USS selected radio sources which tend to be at high redshifts (De Breuck et al. 2001), (ii) It has been long known that powerful radio galaxies trace the bright outer envelopes in so-called *K*-*z* diagrams which relate the observed *K*-band magnitude (rest-frame UV/optical) to redshift (e.g., De Breuck et al. 2002). Recently such a relation was found to hold also for submm sources (Dunlop 2002), although a detailed comparison between the two populations by Serjeant et al. (2003) shows that the radio-quiet objects may be  $\gtrsim 2$  mag fainter with a larger dispersion. Therefore, the faint *K*-band magnitudes suggest that they are at high redshift (see column labeled  $z_{\text{est}}^K$  in Table 2). This is corroborated by their red near-IR colours of  $R - K > 4-6$  (see Table 1) typical of distant massive galaxies (McCarthy 2004), (iii)

<sup>4</sup><http://heasarc.gsfc.nasa.gov/Tools/w3pimms.html>

| Source        | $S_{325\text{MHz}}$<br>mJy | $S_{1.4\text{GHz}}$<br>mJy | $S_{4.8\text{GHz}}$<br>mJy | $\alpha_{325}^{1.4}$ | $\alpha_{1.4}^{4.8}$ |
|---------------|----------------------------|----------------------------|----------------------------|----------------------|----------------------|
| WN J0305+3525 | 110                        | 15.8                       | 3.74                       | -1.33                | -1.17                |
| WN J1314+3649 | 286                        | 36.4                       | —                          | -1.41                | —                    |
| WN J2044+7044 | 311                        | 41.7                       | 7.18                       | -1.38                | -1.43                |

**Table 4** — Summary of radio flux densities and spectral indices of the sources observed with Chandra

Their submm detection fraction of four out of ten is closer to the one for  $z > 2.5$  HzRGs in surveys of comparable sensitivity ( $\sim 50\%$ ; Archibald et al. 2001; Reuland et al. 2004) than to the fraction ( $\sim 15\%$ ) for lower redshift radio galaxies. (iv) For six objects no emission is found blueward of  $4800 \text{ \AA}$ , which corresponds to the  $\text{Ly}\alpha$  break at  $z \sim 3$ . In contrast, WN J0310+3644 and WN J1355+3848 show very faint continuum emission possibly down to  $4000 \text{ \AA}$ , and for WN J1836+5210, and TN J1954–1207 the spectra cut off at  $4800 \text{ \AA}$  where the continuum is still fairly bright. Clearly, those four sources must be at  $z < 3$  although  $z \sim 2$  is still possible.

While none of these indicators by itself can be considered compelling, for most cases they favour redshifts  $z \sim 3$ . In the following we assume a redshift  $z = 3$  to be representative for the sources and discuss possible implications.

### 3.2 X-ray properties

Since none of the objects were formally detected with Chandra, we compare the upper limits with expected count rates using various assumptions discussed below.

#### 3.2.1 Radio–X-ray relation

There is a plethora of X-ray emission processes operating in radio galaxies such as Inverse Compton scattering of cosmic microwave background photons or local far-IR radiation fields, Synchrotron Self Compton radiation, synchrotron emission from the lobes, jets or cores, and thermal emission from shocked gas. Brinkmann et al. (2000) investigated radio–X-ray ( $L_r/L_x$ ) correlations for a variety of objects (both radio-loud and radio-quiet) from a comparison between the ROSAT All-Sky Survey and the VLA 1.4 GHz FIRST catalogue. The processes responsible for radio-related non-thermal nuclear X-ray emission and the characteristic scales on which they operate are not well understood but the simplest model may be one in which the X-rays originate in the jet itself (for a discussion see Hardcastle & Worrall 1999).

The Brinkmann et al. relation for flat spectrum radio-loud AGN to estimate the expected unobscured X-ray luminosity  $L_x$  at 2 keV given a 5 GHz radio luminosity  $L_r$  is:

$$\log L_x = (11.2 \pm 1.6) + (0.48 \pm 0.05) \times \log L_r, \quad (1)$$

with  $L_r$  and  $L_x$  in  $\text{erg s}^{-1} \text{ Hz}^{-1}$ .

Table 4 lists radio properties from the literature (De Breuck et al. 2000) of the three sources observed with Chandra. The inferred rest-frame radio and X-ray luminosities are given in Table 5. We used PIMMs to convert these luminosities into count rates if

| Source        | $z_{\text{est}}$ | $\log(L_{325\text{MHz}})$<br>$\text{W Hz}^{-1}$ | $\log(L_{1.4\text{GHz}})$<br>$\text{W Hz}^{-1}$ | $\log(L_{5\text{GHz}})$<br>$\text{W Hz}^{-1}$ | $\log(L_{2\text{keV}})$<br>$\text{erg s}^{-1} \text{Hz}^{-1}$ | $\log(L_{0.5-2\text{keV}})$<br>$\text{erg s}^{-1}$ | $\log(L_{2-10\text{keV}})$<br>$\text{erg s}^{-1}$ |
|---------------|------------------|---|---|---|---|--|---|
| WN J0305+3525 | 3.0              | 28.2  | 27.3  | 26.6  | 27.45   | 45.27  | 45.34   |
| WN J1314+3649 | 3.0              | 28.7  | 27.8  | 27.0  | 27.64   | 45.46  | 45.53   |
| WN J2044+7044 | 3.0              | 28.7  | 27.8  | 27.0  | 27.64   | 45.46  | 45.53   |

**Table 5** — Inferred radio and unobscured X-ray luminosities of the sample. The X-ray luminosities are estimated from the 5 GHz radio luminosity  $L_{5\text{GHz}}$  using equation 1 and assuming a photon index  $\Gamma = 2$ .

| Source        | $z_{\text{est}}$ | $\log(L_{0.5-10\text{keV}})$<br>$\text{erg s}^{-1}$ | $S_{0.5-10\text{keV}}$<br>$\text{erg s}^{-1} \text{cm}^{-2}$ | $S_{0.5-10\text{keV}}$<br>$\text{counts s}^{-1}$ | $S_{2-10\text{keV}}$<br>$\text{counts s}^{-1}$ |
|---------------|------------------|---|--|--|--|
| WN J0305+3525 | 3.0              | 45.61   | $4.54 \times 10^{-14}$                                       | $5.0 \times 10^{-3}$                             | $1.1 \times 10^{-3}$                           |
| WN J1314+3649 | 3.0              | 45.80   | $7.03 \times 10^{-14}$                                       | $9.8 \times 10^{-3}$                             | $1.8 \times 10^{-3}$                           |
| WN J2044+7044 | 3.0              | 45.80   | $7.03 \times 10^{-14}$                                       | $7.1 \times 10^{-3}$                             | $1.8 \times 10^{-3}$                           |

**Table 6** — Predicted unobscured X-ray count rates for Chandra. These count rates are based on the X-ray luminosities as derived using equation 1 and assuming a typical photon index  $\Gamma = 2$ . The count rates are corrected for the Galactic foreground columns  $N_{\text{H}}$  given in Table 1.

they would be observed with the Chandra ACIS-S chips, as shown in Table 6. Comparison of these predicted count rates ( $\sim 1 \times 10^{-2} \text{ counts s}^{-1}$ ) with the observations show that they are an order of magnitude higher than measured ( $\lesssim 1 \times 10^{-3} \text{ counts s}^{-1}$ ; Table 3). Below we discuss possible explanations for this discrepancy.

One explanation might be that the trend described by equation (1) does not hold for our USS sources. Unfortunately, no  $L_{\text{r}}/L_{\text{X}}$  correlations exist in the literature for USS galaxies. A complication with predicting the intrinsic X-ray luminosities of the objects in the present study from their radio emission is that the compact USS sources are likely to be dominated by the lobe emission (for nearby CSS sources  $< 0.4\%$  of the radio luminosity originates from the core; Fanti et al. 1995) since they are almost unresolved and intrinsically small. However, Worrall et al. (2004) showed that the lobe-dominated ( $< 1\%$  of the 1.5 GHz flux arises from the core) CSS source 3C48 falls on the relation for flat-spectrum sources, suggesting that the relation remains applicable.

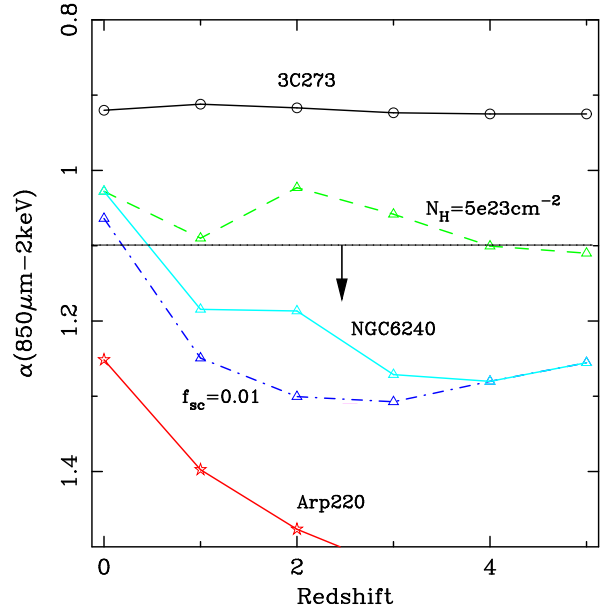
### 3.2.2 Submm–X-ray relation

One could explain the lack of X-ray emission if the radio emission were due to non-AGN related activities. Star formation seems a viable alternative as it can lead to significant radio emission ( $L_{\text{far-IR}}/L_{\text{radio}}$  relation; Condon 1992) and (as was demonstrated for WN J0305+3525) the observed submillimetre emission is likely related to vigorous starbursts. For comparison we take the ultra luminous infrared starburst galaxy Arp 220 as a template. Arp 220 has a 1.4 GHz radio luminosity of  $\log L_{1.4\text{GHz}} = 23.41$ . Assuming similar radio luminosities for our sources would imply redshifts on the order of  $z \sim 0.05-0.08$ . Such low redshifts, however, would be at odds with the  $K > 19$  magnitudes and observed submillimetre flux densities of a few mJy because Arp 220, which is at  $z = 0.02$ , is orders of magnitudes brighter with  $K = 9.852 \pm 0.036$  (Jarrett et al. 2003) and  $S_{850} = 832 \pm 86 \text{ mJy}$  (Dunne et al. 2000). This shows that almost the entire radio emission for our sources must be related to an AGN.

The submm-to-X-ray energy spectral index  $\alpha_{\text{SX}}$ , is another tool to differentiate be-



**Figure 2** — Submillimetre-to-X-ray energy spectral index,  $\alpha_{\text{SX}}$ , versus redshift. The horizontal line indicates the  $3\sigma$  upper limit to  $\alpha_{\text{SX}}$  for the three sources in the program. The expected  $\alpha_{\text{SX}}$  values for Compton thin AGN (3C 273), obscured AGN (NGC 6240; assuming  $f_{\text{sc}} = 0.05$ ), and ultraluminous starburst galaxies (Arp 220) are overplotted. Alternate curves for NGC 6240 with a smaller scattered flux fraction ( $f_{\text{sc}} = 0.01$ ) and less internal absorption ( $N_{\text{H}} = 5 \times 10^{23} \text{ cm}^{-2}$ ) are plotted also. This figure has been adapted from Fabian et al. (2000).



tween Compton-thin AGN, Compton-thick AGN, and starburst systems (see Figure 2 and Fabian et al. 2000). This index is only a weak function of redshift, and therefore especially suited to analyse the “no- $z$ ” sources. The spectral indices of order  $\lesssim -1.1$  (see Table 3), are inconsistent with Compton-thin AGN (such as 3C 273) at any redshift and confirm that the sources most likely host highly obscured AGN although pure starbursts cannot be ruled out based on this parameter alone. The double radio structure of WN J2044+7044 together with the difficulty of attributing the radio emission purely to star formation strongly favours highly obscured nuclear activity to simultaneously explain the radio emission and paucity of X-ray photons.

### 3.2.3 Obscured nucleus

That the USS sources appear underluminous in the X-rays is not all that surprising. In orientation based unification schemes of AGN (e.g., Barthel 1989) emission from the cores of radio galaxies passes through an obscuring torus. This torus is optically thick in the optical and, depending on its properties, may even strongly absorb hard X-rays (0.5–10 keV observed frame corresponds with 2–40 keV rest-frame at a redshift  $z = 3$ ). Since the relation used above was derived for flat spectrum quasars which are being observed close to the jet axis allowing a direct view of the core emission, the obscuring effects of this torus must be taken into account.

In Table 7 we list the predicted count rates for the same luminosities as in Table 6, but include an additional obscuring medium with column densities  $N_{\text{H}}$  of  $1\text{--}100 \times 10^{22} \text{ cm}^{-2}$  at the redshift of the source. From this table we infer that column densities  $N_{\text{H}}$  of a few  $\times 10^{23} \text{ cm}^{-2}$  are sufficient to explain the fact that we did not detect the sources. These values are slightly higher than but consistent with the findings by O’Dea (1998), who inferred absorbing columns of at least a few  $\times 10^{22} \text{ cm}^{-2}$  to explain why GPS/CSS galaxies are approximately two orders of magnitude fainter in the X-rays than quasars. Similar absorption columns were found also by Siemiginowska et al. (2003).

Powerful FR II radio galaxies are also known to be observed through such obscuring tori, with most observed X-ray and radio emission arising from a diverse variety of processes in the extended components. Comparison with the intrinsic X-ray luminosities of these sources could serve as an important check, however the paucity of X-ray data for HzRGs makes direct comparisons complicated. Carilli et al. (2002) report that for Cygnus A and MRC 1138–262 the ratio between unobscured nuclear X-ray emission and total radio power  $L_{2-10\text{keV}}^{\text{nucleus}}/L_{0.1-10\text{GHz}}^{\text{total}} \sim 2.5$  is constant to within a factor of two. Scaling with the 0.1-10 GHz radio power yields hard X-ray luminosities  $L_{2-10\text{keV}}$  of order  $\sim 5 \times 10^{44} \text{ erg s}^{-1}$  for our sources, similar to but slightly below the values derived using equation 1 (see Table 5). Overzier et al. (2004) also report that 3 out of 4 sources in their sample of  $z \sim 2$  radio galaxies agree well with the  $L_r/L_X$  relation if they use a photon index  $\Gamma = 1.8$  to calculate the luminosity at rest-frame 2 keV. It must be noted however, that a much lower value for the nuclear X-ray emission is found by Scharf et al. (2003) for the archetype HzRG 4C 41.17 at  $z = 3.8$ . They report an intrinsic X-ray luminosity of only  $9 \times 10^{43} \text{ erg s}^{-1}$  instead of  $1 \times 10^{45} \text{ erg s}^{-1}$  as expected based on a radio power of  $L_{0.1-10\text{GHz}}^{\text{total}} 3 \times 10^{38} \text{ W}$ . If the X-ray luminosities of the compact USS sources would fall below the  $L_r/L_X$  relation by the same amount as 4C 41.17, intrinsic column depths  $N_{\text{H}} \sim 10^{22} \text{ cm}^{-2}$  would be sufficient to explain why we did not detect their X-ray emission.

### 3.3 Young starbursting radio galaxies

Based on the circumstantial evidence discussed above, it seems likely that many of the compact USS sources in this program are indeed at large cosmological distances. Since all the submm emission must be related to dust emission (extrapolation of the USS radio spectrum according to a power law shows the synchrotron contribution at submm wavelengths to be negligible and heating of dust by AGN does usually not contribute significantly at rest-frame far-IR wavelengths; e.g., Archibald et al. 2001; Farrah et al. 2002), this implies large star formation rates  $\sim 1500 \text{ M}_{\odot} \text{ yr}^{-1}$  and dust masses  $M_{\text{d}} \sim 1.5 \times 10^8 \text{ M}_{\odot}$  (see e.g., Reuland et al. 2003).

The lack of line emission, the high obscuration inferred from the X-ray emission, and their compact sizes all point towards a scenario in which these galaxies are situated in dense gaseous environments, possibly signatures of merger-induced starbursts, that are both fueling the central engine and forming the galaxy.

Indeed, the medium that is obscuring the X-ray emission could be related to the starburst. If one assumes intrinsic column densities of  $N_{\text{H}} \sim 10^{23} \text{ cm}^{-2}$  at a radius of  $\sim 5 \text{ kpc}$  (since it must be larger than the emission line region or else we should have detected it in the optical spectroscopy) then one derives a total HI mass of order  $2 \times 10^{11} \text{ M}_{\odot}$ . For typical ratios (as appropriate for ULIRGs; Sanders et al. 1991) of  $M_{\text{HI}}/M_{\text{H}_2} \sim 2$  and  $M_{\text{H}_2}/M_{\text{d}} \sim 500$  this yields dust masses  $M_{\text{d}} \sim 2 \times 10^8 \text{ M}_{\odot}$ , consistent with the submm emission.

This would suggest that the obscuration may be related to a young evolutionary stage in a radio-loud analog to the ULIRG-QSO sequence first presented by Sanders et al. (1988a) and phase 1-2 in the more detailed scheme of Haas et al. (2003). If the submm emission would be directly related to the jet-triggering event we would have expected a submm detection fraction higher for these compact objects than for regular

| Source        | $z_{\text{est}}$ | $\log(L_{0.5-10\text{keV}})$<br>erg s $^{-1}$ | $\log(N_{\text{H}}) = 22$<br>counts s $^{-1}$ | $\log(N_{\text{H}}) = 23$<br>counts s $^{-1}$ | $\log(N_{\text{H}}) = 24$<br>counts s $^{-1}$ |
|---------------|------------------|---|---|---|---|
| WN J0305+3525 | 3.0              | 45.61   | $4.7 \times 10^{-3}$                          | $3.3 \times 10^{-3}$                          | $0.9 \times 10^{-3}$                          |
| WN J1314+3649 | 3.0              | 45.80   | $9.1 \times 10^{-3}$                          | $5.7 \times 10^{-3}$                          | $1.4 \times 10^{-3}$                          |
| WN J2044+7044 | 3.0              | 45.80   | $6.7 \times 10^{-3}$                          | $4.8 \times 10^{-3}$                          | $1.3 \times 10^{-3}$                          |

**Table 7** — Predicted 0.5–10 keV count rates for Chandra. These count rates are similar to the ones in Table 6, but assume additional intrinsic obscuring columns of  $N_{\text{H}} 1 \times 10^{22} \text{ cm}^{-2}$ ,  $N_{\text{H}} = 1 \times 10^{23} \text{ cm}^{-2}$ , and  $N_{\text{H}} = 1 \times 10^{24} \text{ cm}^{-2}$  at the redshift of the source.

HzRGs. Interestingly, this may be what we have observed, since the inverse variance weighted average of the non-detections  $\langle S_{850, < 3\sigma}^{\text{CSS}} \rangle = 2.48 \pm 0.48 \text{ mJy}$  is higher than the weighted average  $\langle S_{850, < 3\sigma}^{\text{HzRGs}} \rangle = 1.39 \pm 0.30 \text{ mJy}$  for 17 regular radio galaxies at  $z > 2.5$  (c.f. Archibald et al. 2001; Reuland et al. 2004). Such a relation between compactness and submm emission was not found for other radio galaxies, but has been reported for radio-loud quasars at  $z \sim 1.5$  (Willott et al. 2002) for which it was attributed to a small secondary nuclear starburst or quasar heated dust.

Comparison with HzRGs shows that the typical  $K$ -band magnitudes of the compact sources are  $\sim 0.5$ – $1$  mag fainter. If they are at comparable redshifts, then an explanation may be the high obscuration (some HzRGs may suffer significant line contamination in the  $K$ -band; Eales & Rawlings 1993), or that they are in an earlier stage of their evolution with a lower fraction of their stellar masses having formed.

### 3.4 Implications for Type II AGN and XRB

Since none of the galaxies was detected in the X-rays it is difficult to establish their contribution to the hard X-ray background. The upper limits on the count rates are consistent with them being quite similar to (and possibly even more luminous than) the type II QSOs detected in much deeper observations (see Table 8 and Stern et al. 2002; Norman et al. 2002). The similarity goes further, since their  $K$ -band magnitudes are rather faint for regular HzRGs but more similar to the  $z > 3$  type II QSOs, and one type II QSO at  $z = 3.7$  has now been detected in the submm with a comparable flux density ( $S_{850} = 4.8 \pm 1.1 \text{ mJy}$ ; Mainieri et al. 2004). A problem is that the space density of such CSS sources is uncertain. While traditionally it is thought that only 10% of the QSOs is radio-loud and therefore less interesting statistically, it is worth noting that recent surveys indicate that the bimodality in the radio-loud versus radio-quiet distribution may be much weaker (White et al. 2000). This is consistent with suggestions that radio loudness may increase with the mass of quasar host galaxies and their central black holes (McLure et al. 1999; Dunlop et al. 2003) or, perhaps more fundamentally, with accretion rate (Ho & Peng 2001). Furthermore, it seems possible that many high redshift CSS sources are going through a dusty submm luminous obscured optical/X-ray phase. Especially for low power sources their radio-jets could be contained by the large amounts of dust such that they do not always evolve into the large radio structures typical of HzRGs. This could imply that the ratio of obscured to unobscured AGN could have been higher at high redshift. Until recently there was little overlap (5–10%) between X-ray and submm samples. However, Smail et al. (2003)

| Source                    | Type   | $z$   | $S_{1.4\text{GHz}}$<br>mJy | $\alpha_{325}^{1.4}$ | $N$<br>counts | Count rate<br>counts ks <sup>-1</sup> | Reference                          |
|---------------------------|--------|-------|----------------------------|----------------------|---------------|---------------------------------------|------------------------------------|
| B2 0902+34                | HzRG   | 3.395 | 329                        | -0.91                | 94            | 9.7                                   | Fabian, Crawford, & Iwasawa (2002) |
| 4C 41.17 <sub>total</sub> | HzRG   | 3.798 | 264                        | -1.15                | 162           | 1.2                                   | Scharf et al. (2003)               |
| 4C 41.17 <sub>core</sub>  |        |       |                            |                      | 37            | 0.3                                   |                                    |
| MRC 1138 <sub>core</sub>  | HzRG   | 2.156 | 600                        | -1.20                | 663           | 19.4                                  | Carilli et al. (2002)              |
| CXO 52                    | QSO II | 3.288 | < 1                        |                      | 54            | 0.29                                  | Stern et al. (2002)                |
| CXOUJ 2153+1742           | QSO II | 0.7-1 |                            |                      | 86            | 9.5                                   | Fabian et al. (2000)               |
| CXOCDFS 0332-2751         | QSO II | 3.700 |                            |                      | 130           | 0.13                                  | Norman et al. (2002)               |
| WN J0305+3525             |        | 3:    | 15.8                       | -1.33                | < 14.3        | < 1.1                                 |                                    |
| WN J1314+3649             |        | 3:    | 36.4                       | -1.41                | < 6.5         | < 0.7                                 |                                    |
| WN J2044+7044             |        | 3:    | 41.7                       | -1.38                | < 10.8        | < 2.0                                 |                                    |

**Table 8** — Comparison of photon fluxes ( $N$ ) and count rates of the sources in this programs with *Chandra* observations of HzRGs and type II QSOs from the literature.

found statistical evidence for X-ray counterparts to submm sources in overdense fields around HzRGs for a similar fraction ( $\sim 40\%$ ) as found in the deep 2 Ms *Chandra* observation discussed by Alexander et al. (2003). This indicates that we do expect to find *Chandra* counterparts to our bright submm sources. No systematic searches for these objects have been conducted to date, but the implications for both AGN evolutionary scenarios and the XRB could be significant.

Bauer et al. (2004) analysed X-ray number counts in the 1–2 Ms *Chandra* Deep Fields to determine the properties of the populations contributing to the XRB. They found that the soft XRB is dominated by relatively unobscured ( $N_{\text{H}} < 10^{22} \text{ cm}^{-2}$ ) luminous  $L_{0.5-8\text{keV}} > 10^{43.5} \text{ erg s}^{-1}$  sources. The hard XRB seems dominated by intrinsically less luminous sources with  $L_{0.5-8\text{keV}} = 10^{42.5} - 10^{44.5} \text{ erg s}^{-1}$  and a broad range of absorbing column densities  $N_{\text{H}} \sim 10^{22} - 10^{24} \text{ cm}^{-2}$ . They interpreted this trend as evidence that even less intrinsically luminous, more highly obscured AGN may dominate the number counts at higher energies where the XRB intensity peaks (20–40 keV). It seems reasonable to postulate that the compact USS sources discussed in this paper and their lower luminosity counterparts could be part of these latter two populations.

## 4 Summary

We have presented SCUBA, MAMBO and *Chandra* observations of ten compact ultra steep spectrum radio sources for which no spectroscopic redshift could be determined and compared those with earlier results of HzRGs and type II QSOs.

Four of the objects were detected in the submm, very similar to the detection rate of  $z > 2.5$  radio galaxies. The strong statistical submm signal from the non-detections, their faint  $K > 19$  magnitudes, and the lack of line emission suggest that a significant fraction (30%) of USS sources may be very obscured HzRGs, possibly in an early stage of their evolution. More observations are necessary to establish whether this obscured phase is a common ingredient in AGN evolution.

As with other distant submm sources it is difficult to obtain spectroscopic redshifts for such targets. Therefore, it is important to obtain further information about their spectral energy distributions at mid- and far-infrared wavelengths with *Spitzer*. Even then continuum far-IR/submm photometric redshifts may not be very accurate, unless an estimate for the luminosity-dust temperature for radio galaxies can be determined

(Blain et al. 2003). Searching for PAH features with IRS spectroscopy seems the best strategy to determine their redshifts.

Despite the lack of X-ray photons detected, we have inferred large intrinsic X-ray luminosities and obscuring column densities based on the empirical  $L_r/L_x$  relation for AGN. If this obscured CSS radio phase is common, then these sources could contribute to the hard XRB. Much deeper observations would be required however, to obtain solid X-ray detections and measure their photon indices.

## Acknowledgments

We thank Robert Zylka and Andrew Baker for their help and suggestions on the MOP-SIC data reduction. We gratefully acknowledge the help of the staff at the JCMT and IRAM observatories. In particular the help of Remo Tilanus was indispensable. We thank Roderik Overzier, Bram Venemans and Andrew Zirm for productive discussions. The JCMT is operated by JAC, Hilo, on behalf of the parent organizations of the Particle Physics and Astronomy Research Council in the UK, the National Research Council in Canada and the Scientific Research Organization of the Netherlands. IRAM is supported by INSU/CNRS (France), MPG (Germany) and IGN (Spain). The work of M.R., W.v.B., and W.d.V. was performed under the auspices of the U.S. Department of Energy, National Nuclear Security Administration by the University of California, Lawrence Livermore National Laboratory under contract No. W-7405-Eng-48. W.v.B. also acknowledges NASA grant CXO-05700580 in support of HzRG research with *Chandra* at LLNL.

## References

- Alexander D. M., Bauer F. E., Brandt W. N., Hornschemeier A. E., Vignali C., Garmire G. P., Schneider D. P., Chartas G., Gallagher S. C., 2003, *AJ*, 125, 383
- Archibald E. N., Dunlop J. S., Hughes D. H., Rawlings S., Eales S. A., Ivison R. J., 2001, *MNRAS*, 323, 417
- Barthel P. D., 1989, *ApJ*, 336, 606
- Bauer F. E., Alexander D. M., Brandt W. N., Schneider D. P., Treister E., Hornschemeier A. E., Garmire G. P., 2004, *ArXiv Astrophysics e-prints*
- Blain A. W., Barnard V. E., Chapman S. C., 2003, *MNRAS*, 338, 733
- Brinkmann W., Laurent-Muehleisen S. A., Voges W., Siebert J., Becker R. H., Brotherton M. S., White R. L., Gregg M. D., 2000, *A&A*, 356, 445
- Carilli C. L., Harris D. E., Pentericci L., Röttgering H. J. A., Miley G. K., Kurk J. D., van Breugel W., 2002, *ApJ*, 567, 781
- Condon J. J., 1992, *ARA&A*, 30, 575
- De Breuck C., Röttgering H., Miley G., van Breugel W., Best P., 2000, *A&A*, 362, 519
- De Breuck C., van Breugel W., Röttgering H., Stern D., Miley G., de Vries W., Stanford S. A., Kurk J., Overzier R., 2001, *AJ*, 121, 1241
- De Breuck C., van Breugel W., Röttgering H. J. A., Miley G., 2000, *A&AS*, 143, 303
- De Breuck C., van Breugel W., Stanford S. A., Röttgering H., Miley G., Stern D., 2002, *AJ*, 123, 637
- de Vries W., 2003, *Publications of the Astronomical Society of Australia*, 20, 6
- Dunlop J. S., 2002, in *ASP Conf. Ser. 283: A New Era in Cosmology The Near-Infrared Hubble Diagram for sub-mm Galaxies*. pp 381–126
- Dunlop J. S., McLure R. J., Kukula M. J., Baum S. A., O’Dea C. P., Hughes D. H., 2003, *MNRAS*, 340, 1095
- Dunne L., Eales S., Edmunds M., Ivison R., Alexander P., Clements D. L., 2000, *MNRAS*, 315, 115
- Eales S. A., Rawlings S., 1993, *ApJ*, 411, 67
- Fabian A. C., Crawford C. S., Iwasawa K., 2002, *MNRAS*, 331, L57

- Fabian A. C., Smail I., Iwasawa K., Allen S. W., Blain A. W., Crawford C. S., Etori S., Ivison R. J., Johnstone R. M., Kneib J.-P., Wilman R. J., 2000, *MNRAS*, 315, L8
- Fanaroff B. L., Riley J. M., 1974, *MNRAS*, 167, 31P
- Fanti C., Fanti R., Dallacasa D., Schilizzi R. T., Spencer R. E., Stanghellini C., 1995, *A&A*, 302, 317
- Farrah D., Serjeant S., Efstathiou A., Rowan-Robinson M., Verma A., 2002, *MNRAS*, 335, 1163
- Gehrels N., 1986, *ApJ*, 303, 336
- Giacconi R., Rosati P., Tozzi P., Nonino M., Hasinger G., Norman C., Bergeron J., Borgani S., Gilli R., Gilmozzi R., Zheng W., 2001, *ApJ*, 551, 624
- Haas M., Klaas U., Müller S. A. H., Bertoldi F., Camenzind M., Chini R., Krause O., Lemke D., Meisenheimer K., Richards P. J., Wilkes B. J., 2003, *A&A*, 402, 87
- Hardcastle M. J., Worrall D. M., 1999, *MNRAS*, 309, 969
- Hasinger G., 2003, *ArXiv Astrophysics e-prints*
- Ho L. C., Peng C. Y., 2001, *ApJ*, 555, 650
- Holland W. S., Cunningham C. R., Gear W. K., Jenness T., Laidlaw K., Lightfoot J. F., Robson E. I., 1998, in *Proc. SPIE Vol. 3357*, p. 305-318, *Advanced Technology MMW, Radio, and Terahertz Telescopes*, Thomas G. Phillips; Ed. SCUBA: a submillimeter camera operating on the James Clerk Maxwell Telescope. pp 305–318
- Jarrett T. H., Chester T., Cutri R., Schneider S. E., Huchra J. P., 2003, *AJ*, 125, 525
- Jenness T., Lightfoot J. F., 2000, in *JCMT Reports SURF - SCUBA User Reduction Facility 1.6 User's manual*
- Jenness T., Stevens J. A., Archibald E. N., Economou F., Jessop N., Robson E. I., Tilanus R. P. J., Holland W. S., 2001, in *ASP Conf. Ser. 238: Astronomical Data Analysis Software and Systems X Automated Reduction and Calibration of SCUBA Archive Data Using ORAC-DR*. pp 299+
- Kreysa E., Gemuend H., Gromke J., Haslam C. G., Reichertz L., Haller E. E., Beeman J. W., Hansen V., Sievers A., Zylka R., 1998, in *Proc. SPIE Vol. 3357*, p. 319-325, *Advanced Technology MMW, Radio, and Terahertz Telescopes*, Thomas G. Phillips; Ed. Bolometer array development at the Max-Planck-Institut fuer Radioastronomie. pp 319–325
- Mainieri V., Rigopoulou D., Lehmann I., Scott S., Matute I., Almaini O., Tozzi P., Hasinger G., S. D. J., 2004, *MNRAS*, in press
- McCarthy P. J., 2004, *ARA&A*, 42, 477
- McLure R. J., Kukula M. J., Dunlop J. S., Baum S. A., O'Dea C. P., Hughes D. H., 1999, *MNRAS*, 308, 377
- Mushotzky R. F., Cowie L. L., Barger A. J., Arnaud K. A., 2000, *Nature*, 404, 459
- Norman C., Hasinger G., Giacconi R., Gilli R., Kewley L., Nonino M., Rosati P., Szokoly G., Tozzi P., Wang J., Zheng W., Zirm A., Bergeron J., Gilmozzi R., Grogin N., Koekemoer A., Schreier E., 2002, *ApJ*, 571, 218
- O'Dea C. P., 1998, *PASP*, 110, 493
- O'Dea C. P., De Vries W. H., Worrall D. M., Baum S. A., Koekemoer A., 2000, *AJ*, 119, 478
- Overzier R. A., Harris D. E., Carilli C. L., Pentericci L., Röttgering H. J. A., Miley G. K., 2004, *A&A*, submitted
- Phillips R. B., Mutel R. L., 1982, *A&A*, 106, 21
- Reuland M., Röttgering H., van Breugel W., De Breuck C., 2004, *MNRAS*, 353, 377
- Reuland M., van Breugel W., Röttgering H., de Vries W., De Breuck C., Stern D., 2003, *ApJ*, 582, L71
- Sanders D. B., Scoville N. Z., Soifer B. T., 1991, *ApJ*, 370, 158
- Sanders D. B., Soifer B. T., Elias J. H., Madore B. F., Matthews K., Neugebauer G., Scoville N. Z., 1988, *ApJ*, 325, 74
- Scharf C., Smail I., Ivison R., Bower R., van Breugel W., Reuland M., 2003, *ApJ*, 596, 105
- Serjeant S., Farrah D., Geach J., Takagi T., Verma A., Kaviani A., Fox M., 2003, *MNRAS*, 346, L51
- Siemiginowska A., Aldcroft T. L., Bechtold J., Brunetti G., Elvis M., Stanghellini C., 2003, *Publications of the Astronomical Society of Australia*, 20, 113
- Smail I., Scharf C. A., Ivison R. J., Stevens J. A., Bower R. G., Dunlop J. S., 2003, *ApJ*, 599, 86
- Stern D., Moran E. C., Coil A. L., Connolly A., Davis M., Dawson S., Dey A., Eisenhardt P., Elston R., Graham J. R., Harrison F., Helfand D. J., Holden B., Mao P., Rosati P., Spinrad H., Stanford S. A., Tozzi P., Wu K. L., 2002, *ApJ*, 568, 71
- van Breugel W., Miley G., Heckman T., 1984, *AJ*, 89, 5

- 
- Weisskopf M. C., Tananbaum H. D., Van Speybroeck L. P., O'Dell S. L., 2000, in Proc. SPIE Vol. 4012, p. 2-16, X-Ray Optics, Instruments, and Missions III, Joachim E. Truemper; Bernd Aschenbach; Eds. Chandra X-ray Observatory (CXO): overview. pp 2-16
- White R. L., Becker R. H., Gregg M. D., Laurent-Muehleisen S. A., Brotherton M. S., Impey C. D., Petry C. E., Foltz C. B., Chaffee F. H., Richards G. T., Oegerle W. R., Helfand D. J., McMahon R. G., Cabanela J. E., 2000, ApJ, 126, 133
- Willott C. J., Rawlings S., Archibald E. N., Dunlop J. S., 2002, MNRAS, 331, 435
- Worrall D. M., Hardcastle M. J., Pearson T. J., Readhead A. C. S., 2004, MNRAS, 347, 632





---

## Chapter 5

---

# The influence of ISM characteristics and AGN activity on the far infrared spectral energy distributions of starburst galaxies

We examine the far infrared spectral energy distributions (SEDs) of 41 local ultraluminous infrared galaxies (ULIRGs) using data from the literature. These SEDs are fitted with theoretical SEDs for dust enshrouded solar metallicity starbursts presented by Dopita et al. (2004) that have been expanded to include a dusty narrow line region. From these models it is found that almost all ULIRGs are best fitted with high ( $P/k > 10^6 \text{ cm}^{-3} \text{ K}$ ) pressures of the interstellar medium, similar to the pressures inferred from emission line ratios. These high pressures are likely related to the pressure above which blowout occurs in a galactic superwind. Furthermore, infrared luminosity ( $L_{\text{FIR}}$ ) and the timescale over which molecular clouds dissipate appear correlated, indicating that bigger starbursts tend to be more dust enshrouded.

We have investigated the implications of our findings for high redshift sources. It seems that the physical mechanisms may be similar to local ULIRGs, and that the models are applicable also in the distant universe. Fitting of three high redshift radio galaxies with good far-IR observations indicates that to fit their SEDs may require even higher pressures than found for ULIRGs. Such high pressures could be related to the presence of the radio source and possibly jet induced star formation. They would increase the effective temperature of these highly luminous sources and agree with the infrared luminosity-temperature relation. Many previous studies have reported that the fraction of  $L_{\text{FIR}}$  that is contributed by an active galactic nucleus (AGN) increases with  $L_{\text{FIR}}$ . We do not confirm such a correlation. Rather, we find that the relative contribution of an embedded AGN can vary significantly for any  $L_{\text{FIR}}$ . Taking this AGN related component into account can lower star formation rates inferred from  $L_{\text{FIR}}$  by a factor of 2–3. For the high redshift radio galaxies, the high dust temperatures together with hidden AGN activity would lower the star formation rates to values lower than commonly inferred.

## 1 Introduction

ONE of the primary goals of cosmology is to understand the processes controlling mass assembly in the universe. Madau et al. (1996) used the Hubble Deep Field to construct an overview of the observed star formation rate per unit comoving vol-

ume in the universe from the present to when it was less than 10% of its current age. The initial overview was predominantly based on optical data. The brightness of the cosmic infrared background (CIB) indicates that approximately half of the activity in the universe is or has been obscured by dust (e.g., Puget et al. 1996; Fixsen et al. 1998; Hauser & Dwek 2001). Therefore, large correction factors to the optically based star formation rates are required.

In luminous infrared galaxies (LIRGs;  $L_{\text{IR}} > 10^{11} L_{\odot}$ ; IR; 5–500  $\mu\text{m}$ ) most of the ultraviolet/optical light from their starbursts is absorbed by dust and re-emitted in the infrared waveband (for a review see Sanders & Mirabel 1996). These LIRGs dominate the population of extragalactic objects in the local universe ( $z < 0.3$ ). At even higher IR luminosities lie the ultraluminous (ULIRGs;  $L_{\text{IR}} > 10^{12} L_{\odot}$ ) and hyperluminous (HyLIRGs;  $L_{\text{IR}} > 10^{13} L_{\odot}$ ) infrared galaxies. Although these are rare in the local universe ( $\sim 0.1\%$  of the local galaxy population; Kim & Sanders 1998), their comoving number density shows strong evolution with redshift (e.g., Lagache et al. 2003, and references therein). It seems likely that the submillimeter galaxies (SMGs) are high redshift analogues to the local ULIRGs, with possibly  $\sim 1000$  times higher comoving space densities (e.g., Scott et al. 2002). These high number densities and IR luminosities indicate that it is essential to probe obscured sites of star formation in order to understand when and how the bulk of stars formed in the early universe.

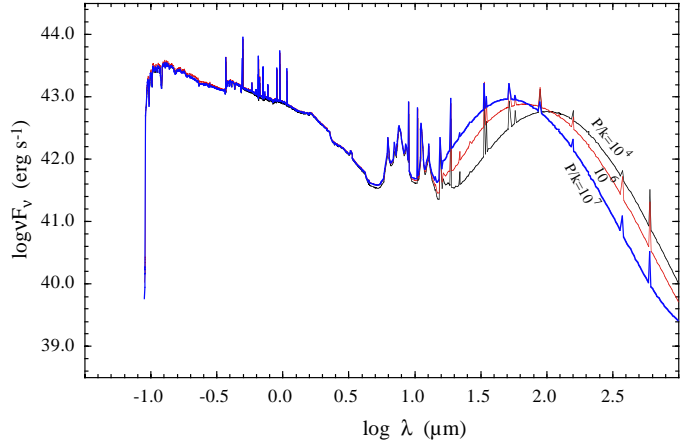
The excellent performance of the *Spitzer* space observatory (Werner et al. 2004) has spawned renewed interest in studies of the star formation history of the universe. It is delivering data of significantly better quality in the 3–180  $\mu\text{m}$  range than previous missions or ground-based facilities, providing a detailed sampling of the IR part of the spectral energy distributions (SEDs) of starburst galaxies in the local and distant universe. Therefore, it is now timely to aim for a better understanding of physical parameters controlling the SEDs of sources that are hosting massive starbursts, and estimate their star formation rates.

Presently, many properties of ULIRGs are still unknown. One of the major unanswered questions concerns the longstanding starburst-AGN controversy. Is the dominant power source of ULIRGs, and by implication of the SMG population, AGN or starburst related? Clearly, the answer to this question is crucial for our understanding of mass assembly.

Dopita et al. (2004) have developed theoretical models for obscured starbursts. The models combine state-of-the-art radiative transfer for evolving H II regions with a sophisticated treatment of embedded dust. In that paper (the first of a series) the dependence of the SEDs on the pressure of the interstellar medium and the molecular cloud dissipation time scale was investigated and a first comparison with the observed SEDs of Arp 220 and NGC 6240 was made.

In the present paper we have expanded the Dopita et al. starburst models to include a model dusty narrow line region. With these models we cannot only derive star formation rates for obscured sources, but also probe the underlying physical parameters of the ISM. Moreover, since we are modeling the entire SEDs and have included an obscured AGN we obtain a handle on the dependence of the SEDs on the power source. This allows us to estimate the fractional contribution of AGN activity to far-IR luminosities  $L_{\text{FIR}}$  commonly used to infer star formation rates for distant objects such

**Figure 1** — The starburst spectral energy distributions for ISM pressures  $P/k = 10^4, 10^6$  and  $10^7 \text{ cm}^{-3}\text{K}$ , scaled to an absolute star formation rate of  $1 M_{\odot} \text{ yr}^{-1}$  and computed for the case in which the molecular cloud covering factor decreases linearly with time. This figure is reproduced from Dopita et al. (2004) in which a detailed description of the underlying assumptions and model parameters can be found. For a linearly decreasing molecular cloud dissipation scale, pressures of  $P/k = 10^4, 10^6, 10^7 \text{ cm}^{-3}\text{K}$  correspond to single temperature modified blackbody dust temperatures of  $T_{\text{dust}} = 30, 35,$  and  $41 \text{ K}$  respectively.



as SMGs.

This study has two main goals. First, to check the applicability of the Dopita et al. models using literature data for a large sample of local ULIRGs, estimate the fractional AGN contributions to  $L_{\text{FIR}}$ , investigate the pressures in the ISM, and obtain estimates for the star formation rates. Secondly, to extend this investigation to a few high redshift sources with good far-IR observations.

The structure of this paper is as follows: The sample selection is described in §2. In §3 we present some key aspects of the models and fitting procedures used. §4 presents the results. The implications for starburst galaxies at low and high redshift are discussed in §5, and in §6 we provide a summary of our conclusions. In this paper we assume a flat universe with  $\Omega_{\text{M}} = 0.27$ ,  $\Omega_{\Lambda} = 0.73$ , and  $H_0 = 71 \text{ km s}^{-1} \text{ Mpc}^{-1}$  (Spergel et al. 2003; Tonry et al. 2003).

## 2 The Samples

For comparison with the theoretical models we have compiled data for low and high redshift starbursts from the literature. Below we first describe the sample selected and data acquisition for a detailed analysis of ULIRGs at low redshift. Then we discuss the selection of high redshift sources for which good sampling of their SEDs is available. These allow us to investigate how the methods developed in this paper apply to starbursts in the early universe.

### 2.1 ULIRGs

We have selected the 41 ULIRGs observed with ISO by Klaas et al. (2001), because their SEDs are well sampled over the wavelength regime  $1\text{--}200 \mu\text{m}$ . This sample is representative of nearby ( $z < 0.2$ ) ULIRGs, but also includes the slightly less luminous objects NGC 6240, Mrk463, and four objects with redshifts in the range  $0.2 < z < 0.4$ .

Flux densities were collected using the NASA/IPAC Extragalactic Database (NED) supplemented with a wide selection of on-line catalogues and papers. Generally, the UV/optical fluxes were taken from the third reference catalogue of bright galaxies v3.9

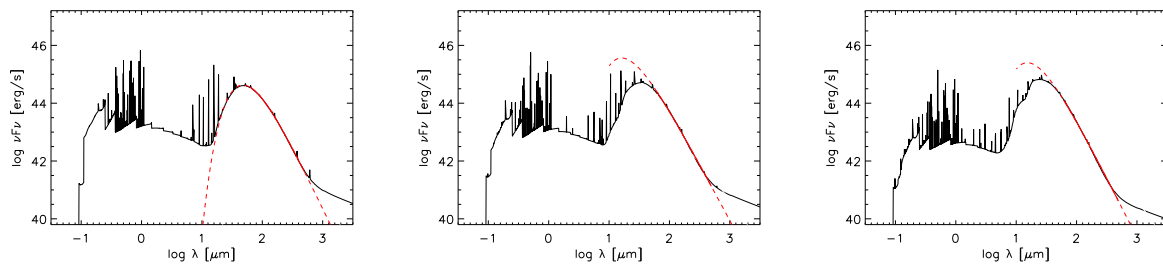


**Figure 2** — Spectral energy distributions of the obscured AGN in the models with increasing ionization parameter from left to right ( $\log U = -3.0, -2.0, -1.0$ ). The total energy output has been scaled to  $L = 10^{45} \text{ erg s}^{-1}$ . Also shown are single temperature grey body fits to the 60–500  $\mu\text{m}$  region.

(de Vaucouleurs et al. 1991). Many optical and near-IR fluxes were also taken from Spinoglio et al. (1995) and the APM and 2MASS databases. The majority of 1–1300  $\mu\text{m}$  data points are from Klaas et al. (1997, 2001). Other data points were taken from Sanders et al. (1988a), Sanders et al. (1988b), Murphy et al. (1996), Rigopoulou et al. (1996), Duc et al. (1997), Benford (1999), Rigopoulou et al. (1999), Surace & Sanders (2000), Lisenfeld et al. (2000), Dunne et al. (2000); Dunne & Eales (2001), Scoville et al. (2000), Spoon et al. (2004) and references therein.

Where available the UV/optical and near-IR (*JHK*-band) points include aperture corrections to allow a direct comparison with the larger aperture mid- and far-IR fluxes (e.g., Spinoglio et al. 1995). All UV to near-IR fluxes have been corrected for Galactic extinction using the  $E(B-V)$  values based upon IRAS 100  $\mu\text{m}$  cirrus emission maps (Schlegel, Finkbeiner, & Davis 1998) and extrapolating following Cardelli, Clayton, & Mathis (1989).

## 2.2 High redshift sources

Because of their obscured nature only few “normal” SMGs have unambiguously identified counterparts and accurately determined redshifts. While the number of SMGs with known redshifts is gradually increasing (Chapman et al. 2003a; Smail et al. 2004), they are usually too faint to have an accurate sampling of their SEDs. Therefore, most of the few high-redshift sources for which good data is available are quasars with a significant contribution of beamed radiation from the active nucleus (e.g., Priddey & McMahon 2001). Radio galaxies are similarly extreme sources, but for those the direct glare from the AGN is thought to be blocked by an optically thick torus. They are better suited for studying the galaxies themselves. Archibald et al. (2001) and Reuland et al. (2004) observed 450  $\mu\text{m}$  and 850  $\mu\text{m}$  emission for 69 sources of this latter population over a redshift range  $z=1-5$ . We selected, B3 J2330+3927, 4C 41.17, and 8C 1435+635 from amongst the combined sample, because they have the best coverage of the rest-frame far-IR and UV (observed *R-K*-band). The data were collected from Chambers et al. (1990), Ivison et al. (1998), Archibald et al. (2001), and De Breuck et al. (2003, 2004).

**Table 1** — Characteristic temperatures  $T_{\text{dust}}$  and  $\beta$ 's for the AGN models with ionization parameter  $U$  shown in Figure 2.

| $U$  | $T_{\text{dust}}$<br>K | $\beta$ |
|------|------------------------|---------|
| -3.0 | 56.0                   | 1.41    |
| -2.6 | 75.5                   | 1.26    |
| -2.3 | 106.8                  | 1.09    |
| -2.0 | 182.5                  | 0.93    |
| -1.6 | 297.3                  | 0.90    |
| -1.3 | 229.7                  | 1.03    |
| -1.0 | 184.1                  | 1.15    |
| -0.6 | 150.4                  | 1.27    |
| -0.3 | 163.2                  | 1.22    |
| 0.0  | 166.0                  | 1.21    |

### 3 Infrared emission models and fitting procedures

In this paper we compare observational data to model SEDs consisting of both a starburst and an AGN related component. A detailed description of the starburst models can be found in Dopita et al. (2004). Groves et al. (2004) present details of the AGN related component. Below we highlight key ingredients of the models and present the procedures used for the comparison with observations.

#### 3.1 Starburst Models

##### 3.1.1 General

The starbursts in the model are a composite of young H II regions and an underlying older stellar population. The stellar populations are modeled with the stellar spectral synthesis code STARBURST 99 (Leitherer et al. 1999). The models assume solar metallicity and the standard Salpeter initial mass function with a range in stellar masses  $1 M_{\odot} < M < 120 M_{\odot}$ . For young ( $< 10$  Myr) starbursts (the lifetime of the O and B stars producing the ionizing radiation) the output of the stellar population code is fed as input to the nebular modeling code MAPPINGS IIIq (Sutherland & Dopita 1993; Dopita et al. 2002a). The models include a 1-D dynamical evolution model of H II regions around massive clusters and relevant dust and gas physics to provide the nebular line, continuum and dust re-emission spectrum. Following Dopita et al. (2004) in total  $10^4$  star clusters of  $10^4 M_{\odot}$  each are assumed to have formed over a period of  $10^8$  yr, normalized to an effective star formation rate of  $1 M_{\odot} \text{ yr}^{-1}$ . This normalized SED is then scaled to the observed SEDs in order to estimate the star formation rates.

##### 3.1.2 Dust and PAH implementation

Dust is modeled using solar abundances. The grain size distribution has a softened power-law shape (with slope  $\alpha = -3.3$ , close to the commonly used MRN model; Mathis et al. 1977) with grain size limits of  $a_{\text{min}} = 0.004 \mu\text{m}$  and  $a_{\text{max}} = 0.25 \mu\text{m}$  for both graphitic and siliceous grains. The implemented distribution extends to smaller sizes than the MRN model ( $0.01 \mu\text{m}$  for silicates). This results in a stronger dust re-emission spectrum below  $25 \mu\text{m}$ , to match the observed *IRAS* colors of starbursts (Dopita et al. 2004).

The models also include a simplified treatment of polycyclic aromatic hydrocarbons (PAHs). PAHs are thought to be the main carriers of many observed IR absorption and emission features. The precise composition of PAHs is still unknown. For simplicity all PAHs are represented with a single type: coronene. The abundance of PAHs is implemented as a constant fraction (61%) of the total number of carbon atoms. However, PAHs are fragile and can be destroyed by the harsh environments of galaxies hosting starbursts or AGN (Voit 1992). Therefore, a dependence on a quantity analogous to the ionization parameter is introduced. If the local radiation field per atom, defined as  $\mathcal{H} = \frac{F_{\text{EUV}}}{cn_{\text{H}}}$  (the *Habing Photodissociation Parameter*; for details see Dopita et al. 2004) exceeds a critical value ( $\mathcal{H} \gtrsim 0.005$ ) then the PAHs are presumed destroyed and the carbon they contain is returned to the gas.

Every embedded H II region has been modeled with MAPPINGSIQ out to a column depth of  $N_{\text{H}} = 10^{21.5} \text{ cm}^{-2}$ . For the assumed dust template this corresponds to  $A_V \sim 3$  mag. This limit was chosen to recreate the PAH emission from photodissociation regions (PDRs) (see Dopita et al. 2004). The resulting spectrum is a superposition of dust emission with a continuous range of temperatures arising at different distances to the central source. The PAH features originate from beyond the distance where the radiation field drops below the critical value.

### 3.1.3 ISM pressure and molecular cloud dissipation timescale

A fundamental ingredient of the models is that they include a dynamical description of the individual H II regions. Young H II regions are envisaged to be small and deeply embedded in their parental molecular clouds. The radiation and mechanical pressure acting on the dust of the molecular cloud will lead to an expansion of the shell. This expansion is slowed by the ambient pressure of the ISM following the formulation by Oey & Clarke (1997). H II regions will remain smaller in higher pressure regions and the dust grains will be closer to their central sources resulting in hotter dust. Figure 1 shows the cumulative SEDs of the older stellar population and the ensemble of H II regions at their respective evolutionary states for ISM pressures  $P/k \sim 10^4, 10^6, \text{ and } 10^7 \text{ cm}^{-3} \text{ K}$ . The peak of the far-IR emission is shifted to shorter wavelengths for higher pressures, indicating the higher average dust temperatures.

Additionally, with the expansion molecular clouds will become “leaky” to radiation from the central source. In the models this is represented through the molecular cloud dissipation time scale  $\tau_{\text{clear}}$ . It is defined as the e-folding timescale over which the covering factor  $f_c$  of molecular clouds decrease:

$$f_c(t) = \exp(-t/\tau_{\text{clear}}).$$

For longer  $\tau_{\text{clear}}$  the older H II regions will dominate the stellar continuum in the SEDs. Furthermore, longer  $\tau_{\text{clear}}$  increase the far-IR fluxes relative to a flatter near-IR stellar continuum, broaden the far-IR bump, and strengthen the PAH features.

The range of temperatures in the models is physically motivated. Increasing  $\tau_{\text{clear}}$  partially counteracts increasing the pressure, because the older H II regions are larger and will increase the emission from cool dust. The resulting degeneracy is not very strong, because the temperature is much more sensitive to the pressure than to the molecular cloud dissipation time scale.

### 3.1.4 Visual extinction

Radiation from the stars that escapes the local H II regions through the “holes” in the dusty shells, may encounter an outer foreground dusty screen. To take this into account, additional attenuation is applied according to a theoretical law similar to the one presented by Fischera et al. (2003) but for the current dust model. This model reproduces the observed Calzetti attenuation law for starbursts closely (Calzetti 2001). It assumes a turbulent screen with a log-normal distribution and that PAHs are the main carriers of the 2175 Å absorption feature. The PAHs are destroyed within the strong UV radiation fields of the diffuse neutral or ionized ISM, explaining the absence of the 2175 Å feature in starbursts. In the models the energy absorbed by this foreground screen is not re-emitted in the FIR but “lost”. This approximation is justified for obscured sources such as ULIRGs because only little UV/optical radiation escapes from the H II region and the largest fraction has already been reprocessed. Therefore, the effective visual attenuation is essentially an independent parameter. It mostly affects the UV through near-IR part of the SED.

## 3.2 AGN torus models

The AGN contribution is modeled as a deeply embedded dusty narrow line region. We used a power-law ionizing source of luminosity  $L_{\text{AGN}}$  and spectral index  $\alpha = -1.4$  as input to the MAPPINGS code with density  $n = 10^4 \text{ cm}^{-3}$ , out to a column depth of  $10^{21.5} \text{ cm}^{-2}$ . Model SEDs for different ionization parameters in the range  $-3.0 \leq \log U \leq -1.0$  are shown in Figure 2. To first order, the FIR portions of these SEDs can be represented by single temperature modified black bodies with dust emissivity proportional to  $\lambda^{-\beta}$ . The effective dust temperatures and  $\beta$ 's are given in Table 1. Clearly, this is not a full description of an embedded AGN, as it describes only reprocessed radiation and no direct radiation.

Some ULIRGs show a clear radiation excess in the near-IR to mid-IR regime. This cannot be accounted for with the obscured AGN model described above. It is likely that for these galaxies the torus surrounding the AGN (as required by orientation based AGN unification models; e.g., Barthel 1989) is inclined such that direct radiation from the AGN and radiation from hot dust close to core become visible.

Many authors have described emission from inclined dusty tori (e.g., Pier & Krolik 1992; Granato & Danese 1994; Efstathiou & Rowan-Robinson 1995; van Bemmell & Dullemond 2003). However, the relevant physics for dusty tori is complex and such models add a significant number of assumptions and parameters. These cannot be properly constrained for most of the galaxies in the present sample. The goal of this paper is to obtain a physical understanding of the parameters controlling the *starburst* related SEDs of ULIRGs. Therefore, we have not aimed to fit the 3–15  $\mu\text{m}$  portion of the SEDs, but rather use theoretical SEDs based on relatively simple physical considerations. We obtain an estimate of the AGN related fraction to the far-IR emission from the fitted dusty narrow-line region. This simple approach is acceptable for estimating the ratios of starburst and AGN related far-IR emission because the largest fraction of AGN related far-IR emission in obscured sources is likely reprocessed emission from the cool outer regions of the narrow-line region. Obviously, it is not suitable for esti-

| Name       | $L_{\text{bol}}^{\text{TAH}}$<br>$L_{\odot}$ | $L_{\text{bol}}^{\text{F03}}$<br>$L_{\odot}$ | $L_{\text{bol}}$<br>$L_{\odot}$ | $\text{SFR}^{\text{TAH}}$<br>$M_{\odot} \text{ yr}^{-1}$ | $\text{SFR}^{\text{F03}}$<br>$M_{\odot} \text{ yr}^{-1}$ | $\text{SFR}_{\text{SB}}$<br>$M_{\odot} \text{ yr}^{-1}$ | $\text{SFR}_{\text{AGN}}$<br>$M_{\odot} \text{ yr}^{-1}$ | $A_V^{\text{TAH}}$<br>mag | $A_V$<br>mag | $F_{\text{agn}}^{\text{F03}}$ | $F_{\text{agn}}$ |
|------------|--|--|---------------------------------|--|--|---|--|---------------------------|--------------|-------------------------------|------------------|
| IRAS 05189 | $3.0 \times 10^{12}$                         | $1.1 \times 10^{12}$                         | $1.4 \times 10^{12}$            | 174  | 136  | 407   | 229  | 4.7                       | 9.0          | 0.3                           | 0.1              |
| IRAS 12112 | $1.7 \times 10^{12}$                         | $1.6 \times 10^{12}$                         | $2.3 \times 10^{12}$            | 268  | 313  | 655   | 229  | 5.4                       | 6.6          | 0.0                           | 0.4              |
| Mrk 231    | $3.4 \times 10^{12}$                         | $3.0 \times 10^{12}$                         | $3.3 \times 10^{12}$            | 557  | 376  | 959   | 541  | 2.8                       | 6.8          | 0.3                           | 0.1              |
| Mrk 273    | $1.4 \times 10^{12}$                         | $1.1 \times 10^{12}$                         | $1.6 \times 10^{12}$            | 228  | 208  | 336   | 208  | 4.9                       | 9.0          | 0.1                           | 0.3              |
| IRAS 14348 | $2.2 \times 10^{12}$                         | $1.6 \times 10^{12}$                         | $2.4 \times 10^{12}$            | 360  | 248  | 655   | 142  | 5.4                       | 9.0          | 0.4                           | 0.6              |
| IRAS 15250 | $1.0 \times 10^{12}$                         | $1.0 \times 10^{12}$                         | $1.3 \times 10^{12}$            | 203  | 56   | 277   | 117  | 4.5                       | 9.0          | 0.6                           | 0.4              |
| Arp 220    | $1.5 \times 10^{12}$                         | $1.1 \times 10^{12}$                         | $1.6 \times 10^{12}$            | 286  | 192  | 370   | 277  | 5.4                       | 5.2          | 0.0                           | 0.0              |
| IRAS 22491 | $1.2 \times 10^{12}$                         | $1.1 \times 10^{12}$                         | $1.7 \times 10^{12}$            | 242  | 48   | 447   | 142  | 4.4                       | 9.0          | 0.7                           | 0.5              |

**Table 2** — Summary of SED fitting results from this paper and work by Takagi et al. (2003, indicated by index TAH) and Farrah et al. (2003, indicated by F03). Total inferred bolometric luminosities  $L_{\text{bol}}$ , star formation rates, visual attenuation, and fractional contribution of AGN to the total IR luminosities are shown (converted to our adopted cosmology).

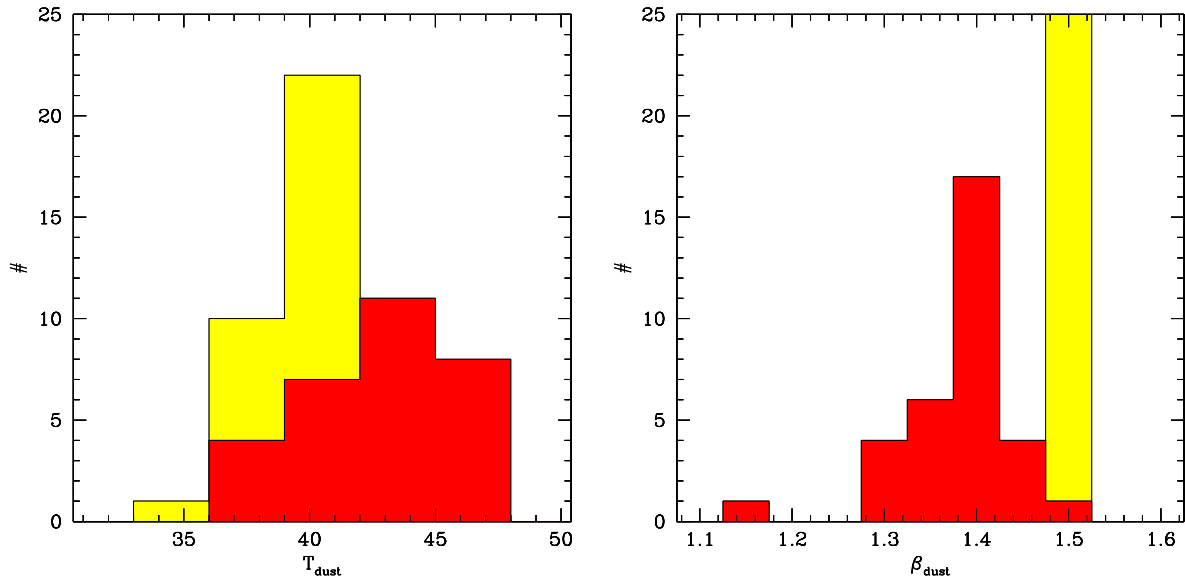


**Figure 3** — Distributions of the dust temperatures (left panel) and dust emissivity proportionality parameter  $\beta$  (right panel). These were inferred from single-temperature modified blackbody fits to the 60–500  $\mu\text{m}$  regime of the best-fit SEDs using SB fits (light grey) and SB+AGN fits (dark grey).

mating the bolometric AGN luminosity because any direct radiation is not considered. When strong emission in the 3–15  $\mu\text{m}$  range is present, our models cannot be applied.

### 3.3 The fitting procedures

Comparing the models to the observations consisted of two steps. First, the observed data were shifted to rest-frame frequencies. Secondly, we constructed a grid of model SEDs for the full set of parameter ranges:

- $\log P/k = 4, 6, 7 \text{ cm}^{-3} \text{ K}$ ,
- $\tau_{\text{clear}} = 1, 2, 4, 8, 16, 32, 100 \text{ Myr}$ ,
- $A_V = 1.0\text{--}9.0$  (41 discrete values),
- $\text{SFR} = 50\text{--}5000 M_{\odot} \text{ yr}^{-1}$  (steps of 10% increase),
- $\log U = -3.0\text{--}0.0$  (10 discrete values),



- $L_{\text{AGN}} = 10^{43}\text{--}10^{47} \text{ erg s}^{-1}$  (steps of 50% increase).

This grid was then searched to obtain the least squares solution of the differences between the observations and all realizations of the model. This fitting method gives most weight to the most energetic data points. For obscured starbursts which emit most radiation in the FIR it is therefore analogous to requiring that the total energy in the starburst is reproduced by the model. As we will see below this means that UV–near-IR data points will be fitted less accurately.

We have performed three sets of fits for the full range of parameter space each. Each set was aimed at obtaining a good fit at the following wavelength regimes:

- FIR-fits: starburst-only fits to the 60–1300  $\mu\text{m}$  range,
- SB-fits: similar to FIR-fits but also include UV–near-IR (0.366–2.2  $\mu\text{m}$ ) and 25–60  $\mu\text{m}$  data,
- AGN+SB-fits: similar to SB-fits but also include mid-IR (15–25  $\mu\text{m}$ ) data and an obscured AGN component.

The FIR-fits attempt to match the peak of the far-IR emission and the slope of the far-IR tail only. This is comparable to the common practice in submillimeter astronomy of inferring star formation rates from modified blackbody fits to the far-IR SEDs of SMGs. A very weak handle on the molecular cloud dissipation time scale can be obtained from the width of the IR bump. The SB-fits include the near-IR data to get a good estimate of the molecular cloud dissipation time-scale and therefore a much improved estimate of the star formation rate. The AGN+SB fits includes also the dusty narrow-line region in order to obtain an estimate of the “contamination” of the far-IR regime by AGN related emission.

Because our models are descriptive, but have not quite the level of sophistication to match observations in detail, we do not quote formal uncertainties on the estimated parameters. From comparing neighboring fits it is found that the uncertainties in the star formation rates are of order  $\sim 50\%$ . The molecular cloud dissipation timescales are accurate to a within a factor of two. The pressure estimates appear not subject to much uncertainty. However, this is a consequence of the sparse sampling of the grid in pressure-space.

## 4 Results

### 4.1 General Results

Table 3 presents an overview of the best-fit parameters for the three sets of fits. The results of the AGN+SB-fits are visualized in Figure 8 with the fit parameters indicated.

Despite the relative simplicity of the models, it is found that generally they can fit the observations well. The main findings are itemized below:

- High pressure models  $P/k \geq 10^6 \text{ cm}^{-3} \text{ K}$  are required in all cases,
- The molecular cloud dissipation timescales are long  $> 8 \text{ Myr}$ ,
- Most star formation rates are in the range 100–250  $\text{M}_{\odot} \text{ yr}^{-1}$  but a few are much higher,
- Inferred values for  $A_V$  span the entire range probed,
- There is a large spread in the fractional contribution of AGN to the 60–1300  $\mu\text{m}$  regime.

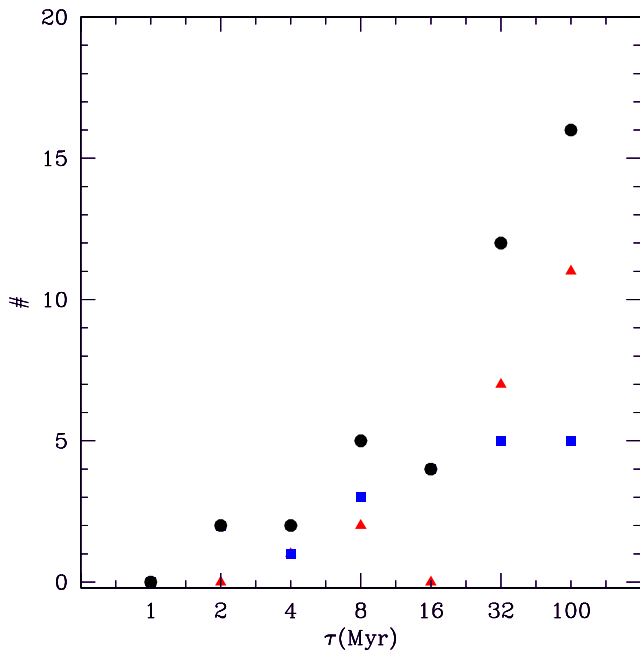


**Figure 4** — Distributions of the inferred molecular cloud dissipation time scales for SB+AGN fits. Circles indicate the full sample, triangles indicate luminous galaxies with  $L_{\text{FIR}} \geq 6.3 \times 10^{11} L_{\odot}$ , and squares indicate galaxies with  $L_{\text{FIR}} < 6.3 \times 10^{11} L_{\odot}$ .

Not all wavelength regimes could be fitted equally well. In approximately 30% of the cases it proved impossible to fit the UV datapoints. These UV components may arise from outer stellar populations that are less obscured than the central starburst. The PAH features cannot be reproduced accurately for the Seyfert sources with an almost flat 3 – 15  $\mu\text{m}$  SED (05189–2524, Mrk231, Mrk273, Mrk463, 15462–0450, 19254–7254). Adding a strong AGN-related component would destroy some PAHs and through an increase of the mid-IR emission hide any features that are left, as required by the observations. Interestingly, there is also a large discrepancy for the archetypical ULIRG Arp 220 for which no signature of an AGN component has been found. The models predict an order of magnitude more PAHs than are observed. In this case the very high star formation rate density may be responsible. It could provide a strong photodissociating UV field destroying a large fraction of the PAHs. For all other sources the SEDs are well matched and produce approximately the correct amount of PAH emission.

## 4.2 Comparison with literature

In order to quantitatively investigate how well the models reproduce the observations, a single temperature modified blackbody spectrum with emissivity proportional to  $\lambda^{-\beta}$  was fitted over the region 60–500  $\mu\text{m}$ . Figure 3 shows the effective temperature and emissivity proportionality coefficients for both SB and SB+AGN fits. All SB fits yield a best-fit value  $\beta = 1.5$ , with effective temperatures  $T = 37\text{--}48$  K (see Table 3). This is in good agreement with what has been found for single temperature fits to bright IRAS galaxies (Dunne et al. 2000). In the SB+AGN fits we have included a hotter component with effective temperatures  $T \sim 55\text{--}160$  K (see Table 1 and Fig. 2). This improves the fits although there is obvious mid-IR excess that is not accounted for in this simple parameterization. In this case we infer temperatures  $T = 37\text{--}57$  K for the

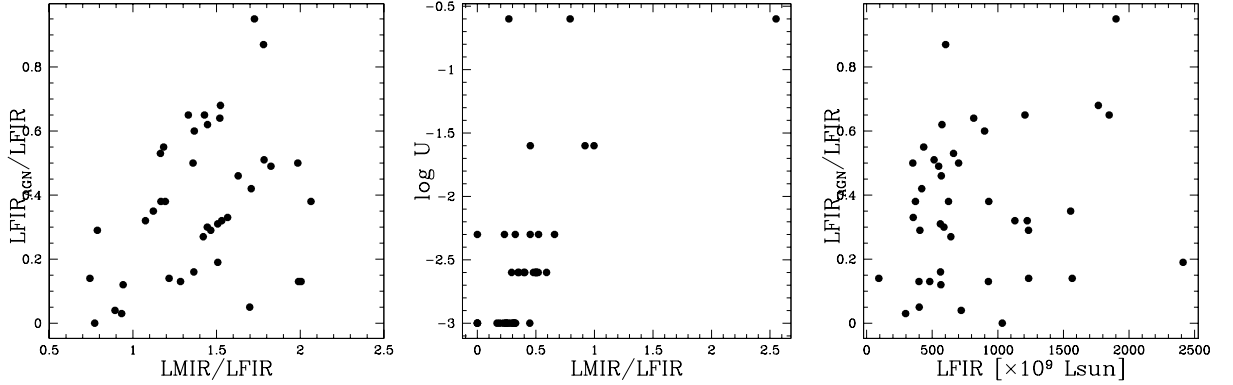


**Figure 5** — Left: The fractional contribution of the AGN related component to  $L_{\text{FIR}}$  as a function of the ratio of mid-IR and far-IR emission. As expected the AGN fraction rises with increasing mid-IR emission. Middle: The ionization parameter of the AGN as a function of mid-IR to far-IR emission. Right: The relative fraction of far-IR emission that is related to the embedded AGN as a function of  $L_{\text{FIR}}$ .

single temperature fits with slightly lower values  $\beta = 0.9\text{--}1.4$ .

Below we compare our results with the results of similar analyses by Takagi et al. (2003) and Farrah et al. (2003) which provide independent estimates for some of the parameters explored in this paper. Takagi et al. (2003) have developed fairly sophisticated SED models for star forming galaxies. In their models the temperature is controlled by the compactness parameter of the galaxies. Deeper potential wells lead to more compact galaxies and higher temperatures. Deeper potential wells would also increase the pressure. Therefore compactness is a tracer of the pressure considered in this paper. The models by Takagi et al. provided an estimate of the visual extinction: the column depth to the starburst region is related to the compactness. Farrah et al. (2003) explored the fractional AGN contribution of ULIRGs, using evolutionary models by Efstathiou et al. (2000).

In Table 2 we present the results of the fits by Takagi et al. and Farrah et al. vis-à-vis our results for those sources that were included in all three programs. The inferred bolometric luminosities  $L_{\text{bol}}$ , and SFRs for the AGN+SB models match the results from Takagi et al. and Farrah et al. to within a factor of two. Especially for Arp 220 and Mrk 231 the three different models agree closely. For Arp 220 the inferred  $A_V$  and  $F_{\text{agn}}$  are also closely matched, but for the other sources the matches are approximate only. Given the very different methods to construct the theoretical SEDs, this result is promising.

## 5 Discussion

### 5.1 Limitations of the models

While our models generally do reproduce the SEDs well, our approach does have some limitations.

- The 3–15  $\mu\text{m}$  regime is not fitted, resulting in bad fits for sources in which the AGN is not fully obscured. If there is strong emission in this regime, the models

are not applicable.

- No ultra-compact H II regions have been included. We might reasonably expect to find relatively more of these in high-pressure regions. This could be responsible for warm dust 12–30 micron components such as seen in Arp 220, and are now often attributed to AGN related emission.
- No cool cirrus component has been included.
- The models assume that all starbursts have an age of 100 Myr. No luminosity or metallicity evolution in the starburst has been incorporated.
- Galaxies are essentially treated as point-sources and less obscured “external” stellar populations are not considered. For ULIRGs the star forming regions are usually compact. However, the data were collected in large apertures possibly explaining why it was not always possible to fit the UV data points.

## 5.2 Pressure

All of the fits for the ULIRGs have far-IR bumps which peak below 100  $\mu\text{m}$  and therefore are characterized by high pressures,  $P/k > 10^6 \text{ cm}^{-3} \text{ K}$  (see Fig. 1 and 8). This result is not unexpected, because the star formation region can only be as compact as it is in ULIRGs if the star formation is occurring in a very high pressure and high density environment. An independent estimate of the pressure in the H II regions can be obtained through measurements of the density-sensitive [S II]  $\lambda 6717, 6731 \text{ \AA}$  doublet. Kewley et al. have applied this technique to warm *IRAS* galaxies and indeed, assuming  $T \sim 10^4 \text{ K}$ , pressures  $P/k > 10^6 \text{ cm}^{-3} \text{ K}$  are inferred for most objects (Kewley et al. 2001a,b).

In the local universe, the dust temperature (but not the amount of dust) inferred from the modified blackbody fits to the far-IR bump in starburst galaxies is found to correlate with the absolute luminosity (Dunne & Eales 2001). High-redshift SMGs display a similar correlation, but shifted to higher luminosity (Blain et al. 2004). At a given luminosity, the dust in SMGs is about 20 K cooler than in ULIRGs in the local universe, and at a given dust temperature, the SMGs are typically 30 times more luminous than their ULIRG counterparts.

What could this mean? Takagi et al. (2003) have found that most ULIRGs have a constant surface brightness of order  $10^{12} L_{\odot} \text{ kpc}^{-2}$  (the few objects with higher surface brightnesses may be post-merger systems). Our results show that this corresponds to an ISM with a pressure of order  $P/k \sim 10^7 \text{ cm}^{-3} \text{ K}$ . These parameters probably characterize a maximal star formation density, above which gas is blown out into the halo of the galaxy and star formation suppressed. Possibly only mergers, which provide an additional ram-pressure confinement of the star formation activity, can exceed this surface brightness. Thus, in order to scale the star formation up to the rates inferred for SMGs ( $\sim 1000\text{--}5000 M_{\odot} \text{ yr}^{-1}$ ), a greater area of the galaxy must be involved in star formation, rather than more star formation occurring in the same volume. To reach a typical far-IR luminosity of  $10^{13} L_{\odot}$  for this upper limit to the star formation rate density, we require star formation over an area of  $\sim 10 \text{ kpc}^2$ . For the most luminous SMGs star formation must be extended over an area of at least  $\sim 100 \text{ kpc}^2$ . Indeed, this is exactly what is found from high resolution optical and radio imaging of 12 luminous SMGs at  $z \sim 2$ . Chapman et al. (2004b) report star formation rates of  $\sim 1700 M_{\odot} \text{ yr}^{-1}$  occurring

within regions of  $\sim 40 \text{ kpc}^2$ , implying star formation rate densities of  $45 \text{ M}_{\odot} \text{ yr}^{-1} \text{ kpc}^{-2}$ . This is comparable to the upper limit found for local starburst galaxies (Meurer et al. 1997) and argues that:

- SMGs host starbursts extended on galaxy-wide scales, rather than the more compact or nuclear starbursts typical of ULIRGs in the local universe.
- Small-scale physical mechanisms that limit the star formation process in SMGs are similar to those operating in the most vigorous systems locally.
- Because of the greater physical extent inferred for the starburst region in the SMGs, the modeling parameters we have derived for local ULIRGs: pressure, molecular gas dissipation timescales, and line of sight attenuations can probably be directly applied to modeling SMGs in the distant universe.

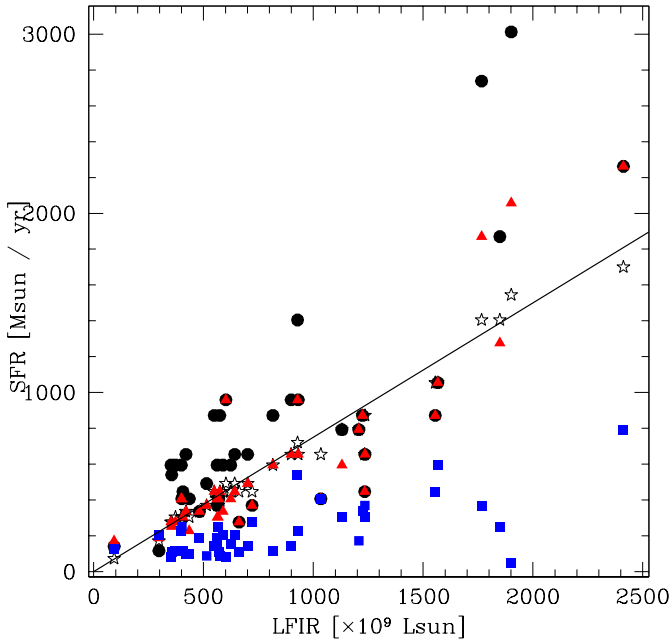
### 5.3 Molecular cloud dissipation time scale

Figure 4 shows a histogram of the inferred molecular cloud dissipation timescales  $\tau_{\text{clear}}$ . This is the timescale on which molecular clouds are destroyed, or, equivalently, the timescale taken for stars to escape from the dense regions of star formation and molecular clouds. It effectively determines the fraction of UV/visual radiation which is intercepted by dust in dense clouds and re-radiated in the far-IR. Therefore it controls the offset between the near-IR and far-IR peaks. AGN+SB fits generally imply longer  $\tau_{\text{clear}}$  than SB fits. This is because an AGN component reduces the fraction of near-IR attributed to the starburst, while the level of the far-IR peak remains mostly related to the starburst. For AGN dominated sources  $\tau_{\text{clear}}$  cannot be reliably determined, because the near-IR is no longer representative of the starburst.

The histogram shows that there is a preference for long dissipation timescales  $\tau_{\text{clear}} \gtrsim 32 \text{ Myr}$ . For such long timescales the dust screen absorbs almost all UV/optical radiation and effectively acts as a bolometer. It is also found that the galaxies with  $L_{\text{FIR}} \gtrsim 6 \times 10^{11} L_{\odot}$  have longer  $\tau_{\text{clear}}$  than lower luminosity sources. This agrees with the result found by Takagi et al. (2003) for ULIRGs, that more active starburst regions tend to be more heavily obscured. More fundamentally, it has been observed also for more regular galaxies that dust obscuration increases both with galaxy mass (Kewley et al. 2002), and with the absolute rate of star formation (e.g., Adelberger & Steidel 2000; Dopita et al. 2002b). The result that  $\tau_{\text{clear}}$  increases with increasing  $L_{\text{FIR}}$  shows that the common practice of assuming that for SMGs and other extreme starbursts all light from the starburst is reprocessed to far-IR wavelengths is not unreasonable.

### 5.4 AGN contribution to MIR and FIR wavelengths and its influence on the inferred star formation rates

There is a longstanding controversy whether AGN or starbursts contribute most to the IR emission of ULIRGs and HyLIRGs. For example, Veilleux et al. (1995) found from optical spectra that the fraction of *IRAS* sources with AGN-like emission line ratios increases with increasing IR luminosity, up to  $\sim 60\%$  at  $L_{\text{IR}} > 10^{12} L_{\odot}$ . In contrast, results from mid-IR spectroscopy show that most ULIRGs ( $\sim 80\%$ ) are powered mainly by starbursts (Genzel et al. 1998; Rigopoulou et al. 1999). More recent observations from near-IR spectroscopy and ISO still give contrasting results (e.g., Veilleux et al.



**Figure 6** — The inferred star formation rates as a function of total far-IR (60–1300 micron) luminosity. Circles indicate the SFRs derived using fits to the far-IR part of the SED only, triangles indicate SFRs inferred from fits to both the near-IR and far-IR, and squares indicate inferred SFRs after including a AGN fraction. The open stars and “best-fit” line indicate the results of SB fits with a fixed molecular cloud dissipation timescale  $\tau_{\text{clear}} = 8$  Myr. Fits to both the near-IR and far-IR yield lower inferred SFRs than fits to the FIR region only.

1999; Tran et al. 2001).

From our modeling we find that both starburst and AGN activity are crucial to our understanding of the ULIRG SEDs. Figure 5 shows three results from our program. It is found that:

- The fractional contribution of AGN emission to  $L_{\text{FIR}}$  is correlated with  $L_{\text{MIR}}/L_{\text{FIR}}$ . This is because we used  $L_{\text{MIR}}$  to scale the narrow-line region.
- As expected, the ionization parameter  $\log U$  (equivalent to dust temperature) increases for larger ratios of  $L_{\text{MIR}}/L_{\text{FIR}}$ .
- The fractional contribution of AGN activity is not correlated with  $L_{\text{FIR}}$ , but almost always less than  $\sim 60\%$ .

Commonly, it is assumed that the AGN contribution to  $L_{\text{FIR}}$  is negligible (e.g., Farrah et al. 2002). However from our analysis this is found not to be strictly true. AGN related emission can constitute more than 40% of  $L_{\text{FIR}}$  in approximately half of the ULIRGs. This is similar to what was found recently by Prouton et al. (2004).

Independent estimates of the AGN contribution could be obtained both through obtaining independent measures of the star formation rate and AGN activity. This could be done through comparison with X-ray observations (e.g., Lutz et al. 2004), reddening corrected optical emission line ratios (e.g., Kewley et al. 2002), relative strengths of the so-called unidentified infrared bands (UIBs) and mid-IR continuum (e.g., Laurent et al. 2000), and sensitive radio observations Prouton et al. (2004). Once such data for a large number of the galaxies of the present sample becomes available, they could provide an important check on our models.

The main driver of this paper is to investigate how inferred star formation rates depend on the SEDs of starburst galaxies. In Figure 6 we have plotted the inferred star formation rates as function of  $L_{\text{FIR}}$  for FIR-fits, SB-fits, and SB+AGN-fits. It shows that increasing the molecular cloud dissipation time scales  $\tau_{\text{clear}}$  lowers the inferred

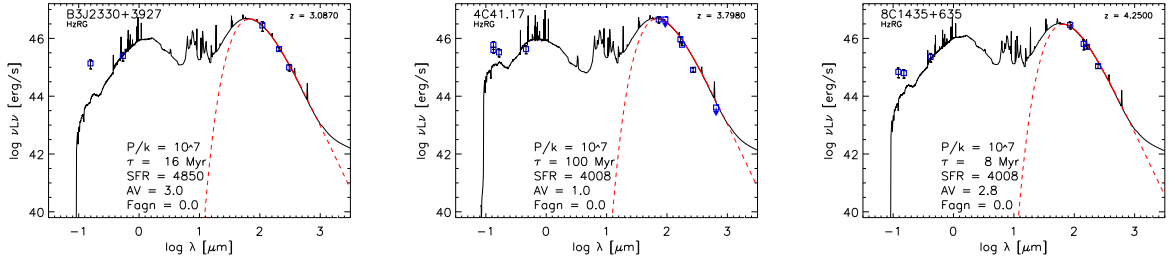


**Figure 7** — Spectral energy distributions of HzRGs, ordered by RA. Upper limits are indicated by a downward arrow. The dotted lines represent modified blackbody fits.

star formation rates significantly. In the FIR-fits these timescales are constrained only by the long-wavelength slope of the FIR-peak. This results in short  $\tau_{\text{clear}}$  because there is a trend for the slopes to be rather steep. Lower pressures and longer  $\tau_{\text{clear}}$  are indistinguishable without a good sampling of the far-IR bump. This illustrates the importance of sensitive mid-IR data for constraining the inferred star formation rates. Taking the near-IR points into account with the SB-fits results in  $\tau_{\text{clear}}$  with a median value of  $\sim 8$  Myr (indicated by the line). Above we argued that AGN frequently may contribute up to 40% to the total  $L_{\text{FIR}}$ . Indeed, Figure 6 shows that taking an AGN component into account often lowers the derived star formation rates by a factor of  $\sim 2$ – $3$ .

### 5.5 Star formation at high redshift

Recently, Blain et al. (2004) investigated a sample ranging from local ULIRGs to distant (up to  $z \sim 5$ ) rest-frame far-IR luminous galaxies. They reported a correlation between the inferred dust temperature and the luminosity of the host galaxy. In the context of this paper, this could indicate a correlation between star formation rate and pressure in the ISM of the galaxies.

To investigate how the characteristics of nearby starbursting galaxies translate to high redshift, we have modeled the SEDs of three  $z > 3$  radio galaxies. The results of SB fits to their SEDs are shown in Figure 7. Star formation rates  $> 4000 M_{\odot} \text{yr}^{-1}$  are inferred. If continued over a dynamical timescale ( $\sim 10^8$  yr) such bursts would convert an amount of gas equivalent to the mass of a  $L_{*}$  galaxy into stars.

Due to the sparse wavelength sampling of the radio galaxy SEDs the fits cannot be tightly constrained. Especially, it is not possible to quantify any AGN contribution to the FIR, despite the fact that a highly active AGN is obviously present. Yet, the far-IR slope for 4C 41.17 (and possibly also for 8C 1435+635) is steeper than can be fitted with  $P/k \sim 10^7 \text{cm}^{-3}\text{K}$ . It seems that to fit the SEDs of HzRGs even higher pressures are required. Such high pressures could be the consequence of the radio source, providing an additional pressure component and possibly inducing star formation (e.g., Begelman & Cioffi 1989; Bicknell et al. 2000).

Assuming equipartition (analogous to a minimum energy requirement), it is possible to calculate lower limits to the pressures associated with the radio emission. This requires estimates of the volume, radio power, and spectral indices of the radio lobes. Using the radio observations by Carilli et al. (1994) and Lacy et al. (1994) for 4C 41.17

and 8C1435+635, typical pressures of  $P/k \gtrsim 0.3 - 1.2 \times 10^7 \text{ cm}^{-3} \text{ K}$  are inferred at distances of  $> 50 \text{ kpc}$  from the center. These high pressures would lead to even more compact H II regions and correspondingly higher typical dust temperatures. Another explanation for the high pressures could be related to mergers. *Hubble* space telescope observations shows that HzRGs consists of many clumps that will merge with the central growing galaxy over dynamical timescales of  $\sim 10^8 \text{ yr}$  (e.g., Pentericci et al. 1998). Optical evidence for elongated structures in SMGs are also interpreted as evidence for ongoing merger activity (Chapman et al. 2003b). But for SMGs the mergers seem more moderate and comparable to those seen in ULIRGs.

These high pressures would increase the typical temperatures and could help shape the IR-luminosity-temperature relation. Such hot dust would radiate more efficiently. Together with a possible AGN contribution this indicates that star formation rates often quoted for high redshift objects (for which usually only rest-frame far-IR data are available) might have to be lowered significantly.

## 6 Conclusion

We have compared theoretical SED models for starburst regions with observations of ULIRGs and HzRGs. These models include a sophisticated treatment of dust and a physically motivated evolution of the individual H II regions. With these models we investigated the properties of these galaxies, such as the SFR, optical depth, molecular cloud dissipation time scale and pressure of the ISM. For the starburst galaxies, the inferred SFRs and optical depths match values from the literature closely. This indicates that the models can be used to derive these properties from the SEDs.

We have included a dusty narrow-line region to help quantify the maximum contribution of hidden nuclear activity to the inferred SFR. From this analysis we find that more luminous sources have a higher absolute contribution from AGN to  $L_{\text{FIR}}$ , but that the fractional AGN contribution does not increase systematically with increasing luminosity. For  $\sim 50\%$  (20/41) of the galaxies we find a clear excess of MIR emission, requiring a significant ( $> 35\%$  to  $L_{\text{FIR}}$ ) contribution of a hidden AGN. In 6 galaxies there is evidence for a power-law spectrum over the UV/optical to FIR range. This is likely related to an AGN which is less obscured than we have modeled. The inferred star formation rates including hidden AGN activity are lower by a factor of 2–3 as compared with models attributing all of the far-IR emission to starburst activity.

From our investigation, it is found that almost all ULIRGs can be best fitted with high-pressure ( $P/k \sim 10^{6-7} \text{ cm}^{-3} \text{ K}$ ) models. Such pressures are much higher than seen normally in the ISM and most likely indicate the importance of dynamical interactions associated with galaxy merging in triggering ULIRGs. We also find that the sources with higher star formation rates are best fitted with models having longer molecular cloud dissipation time scales. This confirms the result found by Takagi et al. (2003) that more active starburst regions tend to be more heavily obscured.

Because ISM densities/pressures may have been higher in the early universe, one might expect high redshift sources to have higher effective temperatures. Evidence for such hot, dusty ultraluminous galaxies at redshift of  $z \sim 2$  has been presented by Chapman et al. (2004a). A significant fraction of these may host a dominant AGN



( $\sim 20\%$ ) or be starburst/AGN hybrids ( $\sim 25\%$ ), but the remainder shows no detectable signs of AGN. The high temperatures in the latter population could be the result of the processes described in this paper.

Higher temperatures would lower the amount of dust for a given far-IR luminosity. Together with a possibly significant (up to  $> 60\%$ ) fraction of AGN related far-IR emission, this indicates that the star formation rates often quoted for high redshift objects (for which until recently only rest-frame far-IR data have been available) may have to be lowered by a factor  $\sim 3$ . Accurate sampling of the MIR to FIR region of the SEDs such as *Spitzer* and ALMA will provide is essential to obtain reliable star formation rates.

## Acknowledgements

We thank Christian Kaiser, Bram Venemans, Andrew Zirm, and Michelle Cappellari for helpful discussions. This work was performed under the auspices of the U.S. Department of Energy, National Nuclear Security Administration by the University of California, Lawrence Livermore National Laboratory under contract No. W-7405-Eng-48. M.D. acknowledges the support of the ANU and the Australian Research Council (ARC) for his ARC Australian Federation Fellowship, and also under the ARC Discovery project DP0208445. M.R. acknowledges the support of a travel grant through M.D.'s ARC Australian Federation Fellowship Support Grant and thanks everybody at the Mt. Stromlo observatories for a very productive visit. This research has made use of the NASA/IPAC Extragalactic Database (NED) which is operated by the Jet Propulsion Laboratory, California Institute of Technology, under contract with the National Aeronautics and Space Administration.

## References

- Adelberger, K. L. & Steidel, C. C. 2000, *ApJ*, 544, 218  
Archibald, E. N., Dunlop, J. S., Hughes, D. H., et al. 2001, *MNRAS*, 323, 417  
Barthel, P. D. 1989, *ApJ*, 336, 606  
Begelman, M. C. & Cioffi, D. F. 1989, *ApJ*, 345, L21  
Benford, D. J. 1999, Ph.D. Thesis  
Bicknell, G. V., Sutherland, R. S., van Breugel, W. J. M., et al. 2000, *ApJ*, 540, 678  
Blain, A. W., Chapman, S. C., Smail, I., & Ivison, R. 2004, *ApJ*, 611, 52  
Calzetti, D. 2001, *PASP*, 113, 1449  
Cardelli, J. A., Clayton, G. C., & Mathis, J. S. 1989, *ApJ*, 345, 245  
Carilli, C. L., Owen, F. N., & Harris, D. E. 1994, *AJ*, 107, 480  
Chambers, K. C., Miley, G. K., & van Breugel, W. J. M. 1990, *ApJ*, 363, 21  
Chapman, S. C., Blain, A. W., Ivison, R. J., & Smail, I. R. 2003a, *Nature*, 422, 695  
Chapman, S. C., Smail, I., Blain, A. W., & Ivison, R. J. 2004a, *ApJ*, 614, 671  
Chapman, S. C., Smail, I., Windhorst, R., Muxlow, T., & Ivison, R. J. 2004b, *ApJ*, 611, 732  
Chapman, S. C., Windhorst, R., Odewahn, S., Yan, H., & Conselice, C. 2003b, *ApJ*, 599, 92  
De Breuck, C., Neri, R., Downes, D., et al. 2004, *A&A*, submitted  
De Breuck, C., Neri, R., Morganti, R., et al. 2003, *A&A*, 401, 911  
de Vaucouleurs, G., de Vaucouleurs, A., Corwin, H. G., et al. 1991, *Third Reference Catalogue of Bright Galaxies (Volume 1-3, XII, 2069 pp. 7 figs.. Springer-Verlag Berlin Heidelberg New York)*  
Dopita, M., Groves, B., Fischera, J., et al. 2004, *ApJ*, in press  
Dopita, M. A., Groves, B. A., Sutherland, R. S., Binette, L., & Cecil, G. 2002a, *ApJ*, 572, 753

- Dopita, M. A., Pereira, M., Kewley, L. J., & Capaccioli, M. 2002b, *ApJ*, 143, 47
- Duc, P.-A., Mirabel, I. F., & Maza, J. 1997, *A&AS*, 124, 533
- Dunne, L., Eales, S., Edmunds, M., et al. 2000, *MNRAS*, 315, 115
- Dunne, L. & Eales, S. A. 2001, *MNRAS*, 327, 697
- Efstathiou, A. & Rowan-Robinson, M. 1995, *MNRAS*, 273, 649
- Efstathiou, A., Rowan-Robinson, M., & Siebenmorgen, R. 2000, *MNRAS*, 313, 734
- Farrah, D., Afonso, J., Efstathiou, A., et al. 2003, *MNRAS*, 343, 585
- Farrah, D., Serjeant, S., Efstathiou, A., Rowan-Robinson, M., & Verma, A. 2002, *MNRAS*, 335, 1163
- Fischera, J., Dopita, M. A., & Sutherland, R. S. 2003, *ApJ*, 599, L21
- Fixsen, D. J., Dwek, E., Mather, J. C., Bennett, C. L., & Shafer, R. A. 1998, *ApJ*, 508, 123
- Genzel, R., Lutz, D., Sturm, E., et al. 1998, *ApJ*, 498, 579
- Granato, G. L. & Danese, L. 1994, *MNRAS*, 268, 235
- Groves, B. A., Dopita, M. A., & Sutherland, R. S. 2004, *ApJ*, 153, 9
- Hauser, M. G. & Dwek, E. 2001, *ARA&A*, 39, 249
- Ivison, R. J., Dunlop, J. S., Hughes, D. H., et al. 1998, *ApJ*, 494, 211
- Kewley, L. J., Dopita, M. A., Sutherland, R. S., Heisler, C. A., & Trevena, J. 2001a, *ApJ*, 556, 121
- Kewley, L. J., Geller, M. J., Jansen, R. A., & Dopita, M. A. 2002, *AJ*, 124, 3135
- Kewley, L. J., Heisler, C. A., Dopita, M. A., & Lumsden, S. 2001b, *ApJ*, 132, 37
- Kim, D.-C. & Sanders, D. B. 1998, *ApJ*, 119, 41
- Klaas, U., Haas, M., Heinrichsen, I., & Schulz, B. 1997, *A&A*, 325, L21
- Klaas, U., Haas, M., Müller, S. A. H., et al. 2001, *A&A*, 379, 823
- Lacy, M., Miley, G., Rawlings, S., et al. 1994, *MNRAS*, 271, 504
- Lagache, G., Dole, H., & Puget, J.-L. 2003, *MNRAS*, 338, 555
- Laurent, O., Mirabel, I. F., Charmandaris, V., et al. 2000, *A&A*, 359, 887
- Leitherer, C., Schaerer, D., Goldader, J. D., et al. 1999, *ApJ*, 123, 3
- Lisenfeld, U., Isaak, K. G., & Hills, R. 2000, *MNRAS*, 312, 433
- Lutz, D., Maiolino, R., Spoon, H. W. W., & Moorwood, A. F. M. 2004, *A&A*, 418, 465
- Madau, P., Ferguson, H. C., Dickinson, M. E., et al. 1996, *MNRAS*, 283, 1388
- Mathis, J. S., Ruml, W., & Nordsieck, K. H. 1977, *ApJ*, 217, 425
- Meurer, G. R., Heckman, T. M., Lehnert, M. D., Leitherer, C., & Lowenthal, J. 1997, *AJ*, 114, 54
- Murphy, T. W., Armus, L., Matthews, K., et al. 1996, *AJ*, 111, 1025
- Oey, M. S. & Clarke, C. J. 1997, *MNRAS*, 289, 570
- Pentericci, L., Röttgering, H. J. A., Miley, G. K., et al. 1998, *ApJ*, 504, 139
- Pier, E. A. & Krolik, J. H. 1992, *ApJ*, 401, 99
- Priddey, R. S. & McMahon, R. G. 2001, *MNRAS*, 324, L17
- Prouton, O. R., Bressan, A., Clemens, M., et al. 2004, *A&A*, 421, 115
- Puget, J.-L., Abergel, A., Bernard, J.-P., et al. 1996, *A&A*, 308, L5+
- Reuland, M., Röttgering, H., van Breugel, W., & De Breuck, C. 2004, *MNRAS*, 353, 377
- Rigopoulou, D., Lawrence, A., & Rowan-Robinson, M. 1996, *MNRAS*, 278, 1049
- Rigopoulou, D., Spoon, H. W. W., Genzel, R., et al. 1999, *AJ*, 118, 2625
- Sanders, D. B. & Mirabel, I. F. 1996, *ARA&A*, 34, 749
- Sanders, D. B., Soifer, B. T., Elias, J. H., et al. 1988a, *ApJ*, 325, 74
- Sanders, D. B., Soifer, B. T., Elias, J. H., Neugebauer, G., & Matthews, K. 1988b, *ApJ*, 328, L35
- Schlegel, D. J., Finkbeiner, D. P., & Davis, M. 1998, *ApJ*, 500, 525
- Scott, S. E., Fox, M. J., Dunlop, J. S., et al. 2002, *MNRAS*, 331, 817
- Scoville, N. Z., Evans, A. S., Thompson, R., et al. 2000, *AJ*, 119, 991
- Smail, I., Chapman, S. C., Blain, A. W., & Ivison, R. J. 2004, *ApJ*, 616, 71
- Spergel, D. N., Verde, L., Peiris, H. V., et al. 2003, *ApJ*, 148, 175
- Spinoglio, L., Malkan, M. A., Rush, B., Carrasco, L., & Recillas-Cruz, E. 1995, *ApJ*, 453, 616
- Spoon, H. W. W., Moorwood, A. F. M., Lutz, D., et al. 2004, *A&A*, 414, 873
- Surace, J. A. & Sanders, D. B. 2000, *AJ*, 120, 604
- Sutherland, R. S. & Dopita, M. A. 1993, *ApJ*, 88, 253
- Takagi, T., Arimoto, N., & Hanami, H. 2003, *MNRAS*, 340, 813
- Tonry, J. L., Schmidt, B. P., Barris, B., et al. 2003, *ApJ*, 594, 1

- Tran, Q. D., Lutz, D., Genzel, R., et al. 2001, *ApJ*, 552, 527  
van Bemmell, I. M. & Dullemond, C. P. 2003, *A&A*, 404, 1  
Veilleux, S., Kim, D.-C., Sanders, D. B., Mazzarella, J. M., & Soifer, B. T. 1995, *ApJ*, 98, 171  
Veilleux, S., Sanders, D. B., & Kim, D.-C. 1999, *ApJ*, 522, 139  
Voit, G. M. 1992, *MNRAS*, 258, 841  
Werner, M. W., Roellig, T. L., Low, F. J., et al. 2004, *ApJ*, 154, 1

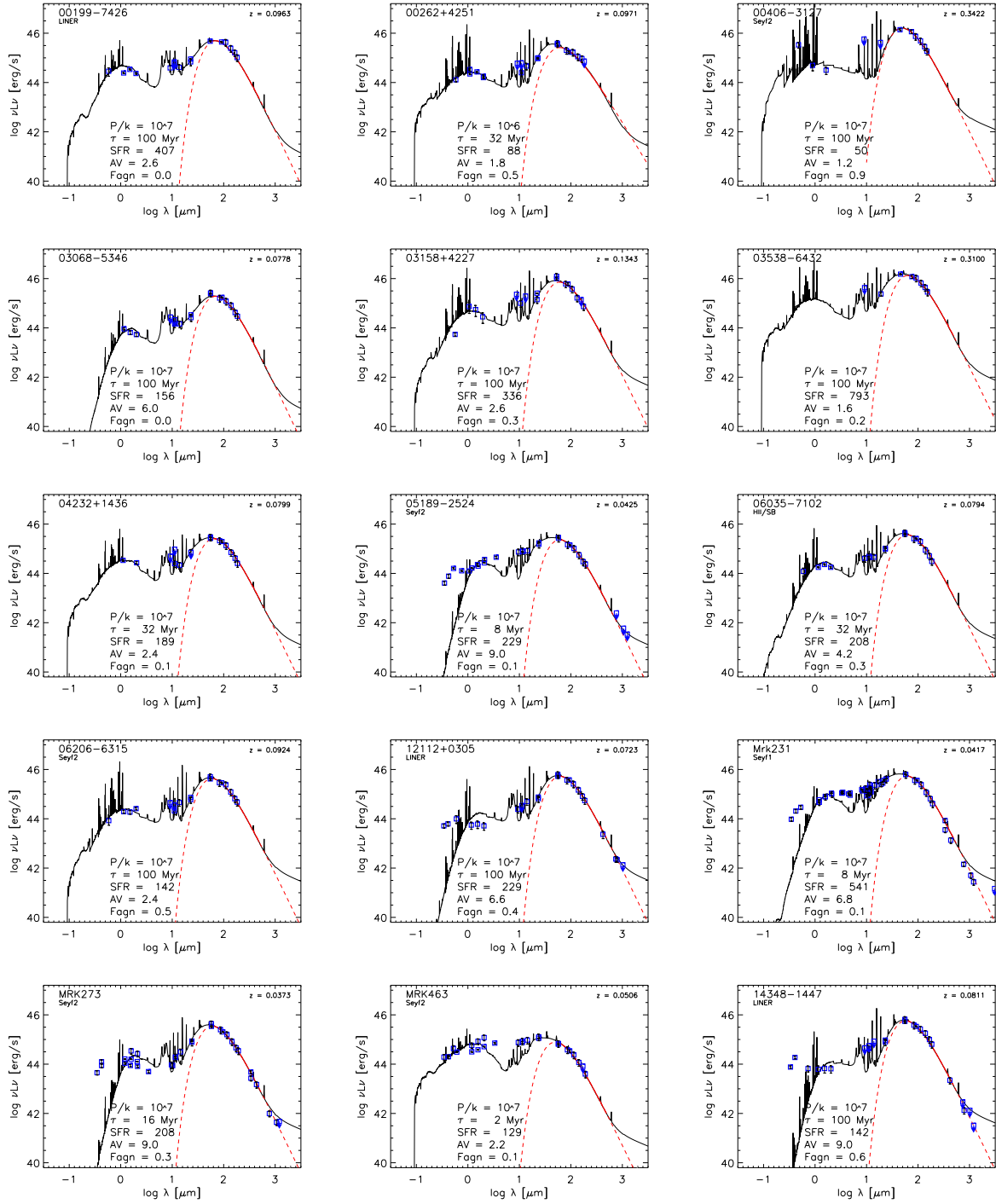


**Figure 8** — Best fit spectral energy distributions of the ULIRGs in our sample, ordered by RA. In each case the solid line is the combined SB+AGN best fit model. Observed data points are overlaid with upper limits indicated by a downward arrow.  $P/k$  represents the pressure in  $\text{cm}^{-3} \text{K}$ ,  $\tau$  the molecular cloud dissipation timescale in Myr, SFR the star formation rate in  $M_\odot \text{yr}^{-1}$ , AV the visual attenuation, and  $F_{\text{agn}}$  the fractional contribution of AGN related emission to the total 60–1300  $\mu\text{m}$  luminosity. The dashed lines represent modified blackbody fits over the range 60–500  $\mu\text{m}$ .

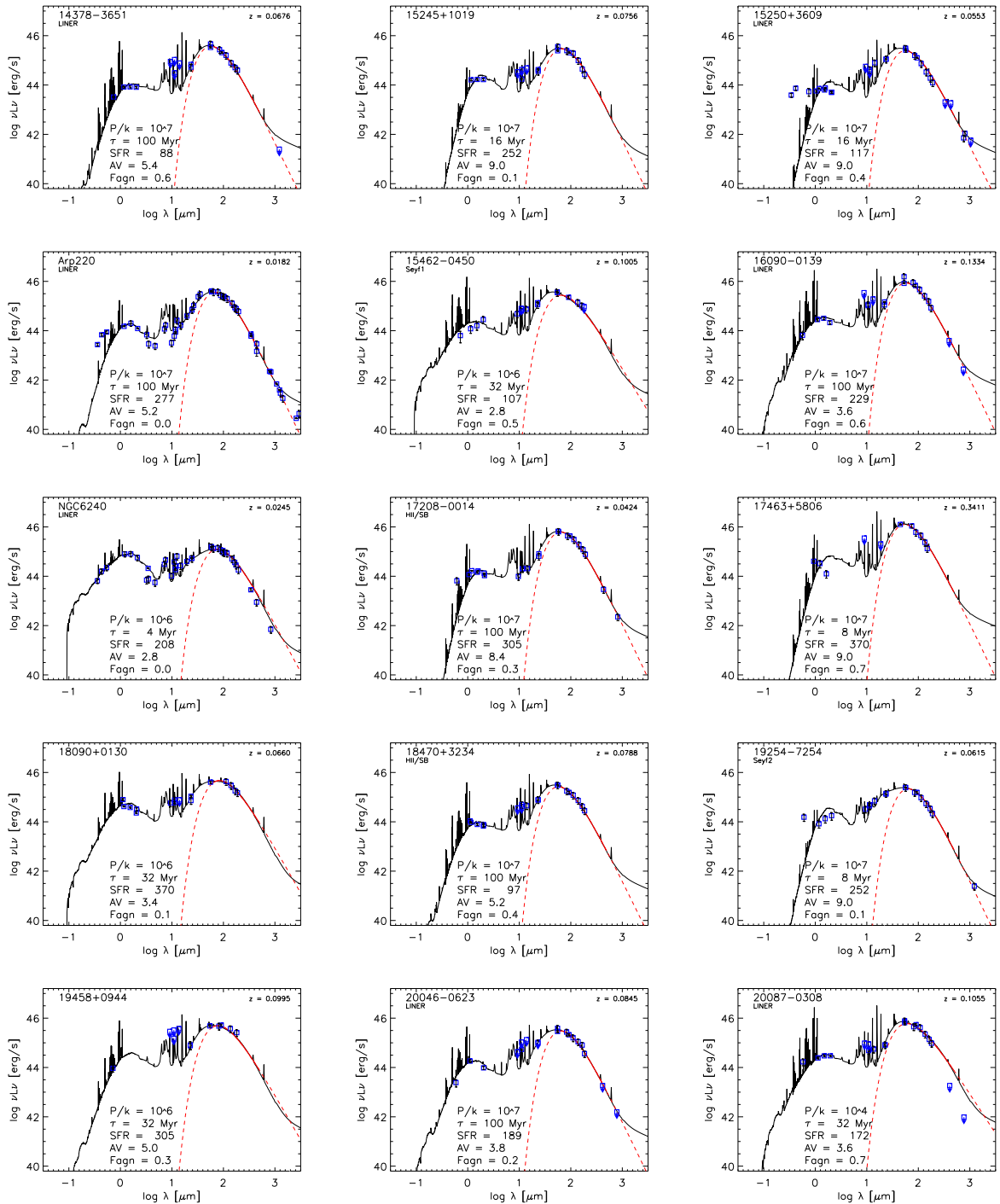


Figure 8 — continued.

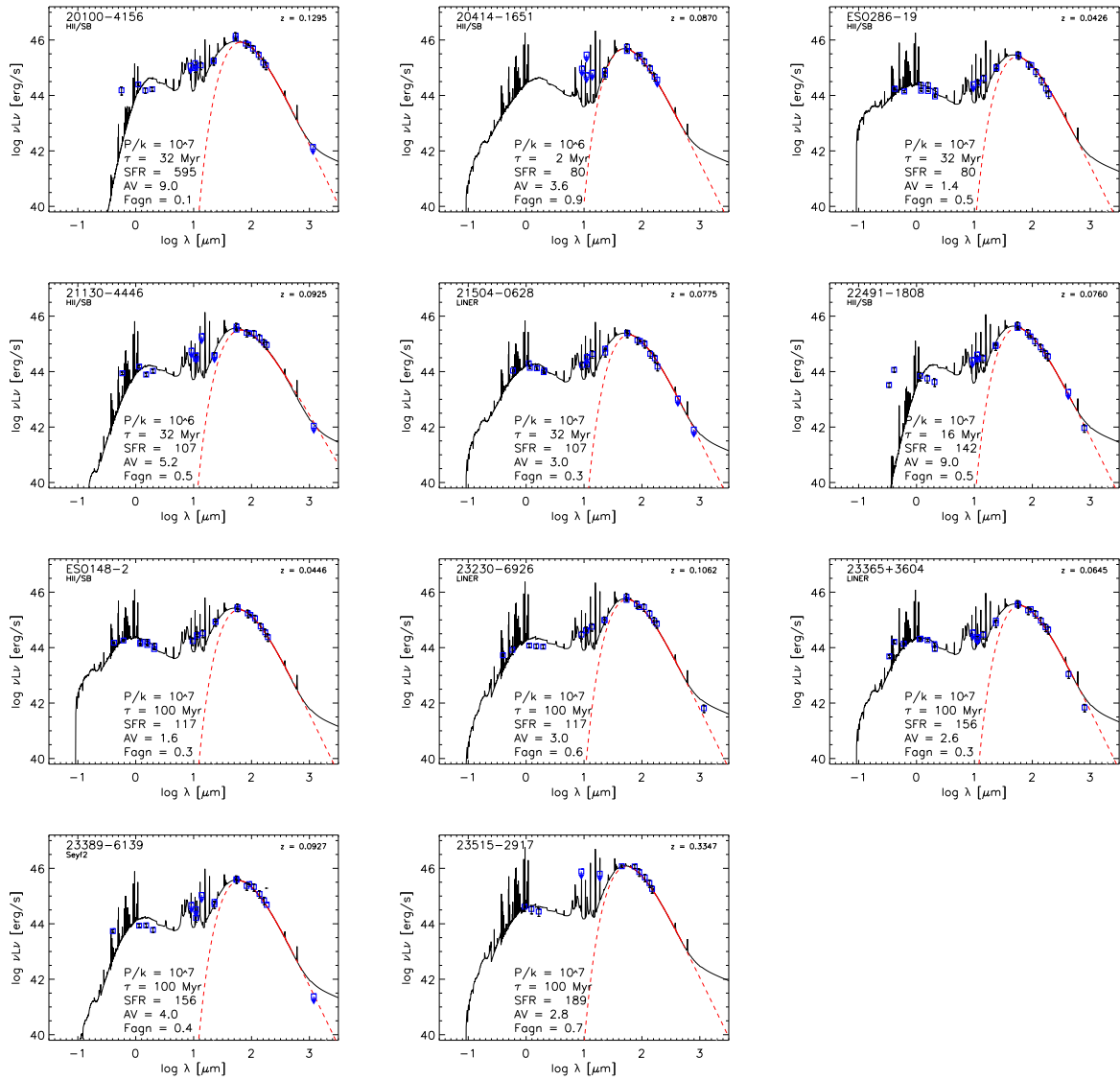


Figure 8 — continued.

| Name       | $z$    | $D$<br>Mpc | $SFR_{\text{FIR}}$<br>$M_{\odot} \text{ yr}^{-1}$ | $SFR_{\text{SB}}$<br>$M_{\odot} \text{ yr}^{-1}$ | $SFR_{\text{SB+AGN}}$<br>$M_{\odot} \text{ yr}^{-1}$ | $P/R_{\text{FIR}}$<br>$\text{cm}^{-3} \text{ K}$ | $P/k_{\text{SB}}$<br>$\text{cm}^{-3} \text{ K}$ | $P/k_{\text{SB+AGN}}$<br>$\text{cm}^{-3} \text{ K}$ | $\tau_{\text{FIR}}$<br>Myr | $\tau_{\text{SB}}$<br>Myr | $\tau_{\text{SB+AGN}}$<br>Myr | $U$  | $L_{\text{AGN}}$<br>$\text{ergs}^{-1}$ | $T_{\text{d}}^{\text{SB}}$<br>K | $\beta^{\text{SB}}$ | $T_{\text{d}}^{\text{SB+AGN}}$<br>K | $\beta^{\text{SB+AGN}}$ |
|------------|--------|------------|---|--|--|--|---|---|----------------------------|---------------------------|-------------------------------|------|--|---------------------------------|---------------------|-------------------------------------|-------------------------|
| 00199-7426 | 0.0963 | 398        | 407   | 407  | 407  | 7  | 7   | 7   | 100                        | 100                       | 100                           | -0.6 | 45.47                                  | 37.31                           | 1.50                | 37.69                               | 1.49                    |
| 00262+4251 | 0.0971 | 401        | 492   | 370  | 88   | 7  | 7   | 7   | 4                          | 8                         | 32                            | -2.6 | 46.87                                  | 39.68                           | 1.49                | 52.27                               | 0.53                    |
| 00406-3127 | 0.3422 | 1338       | 3012  | 2057   | 50   | 7  | 7   | 4   | 2                          | 4                         | 100                           | -3.0 | 47.58                                  | 42.52                           | 1.49                | 54.22                               | 1.40                    |
| 03068-5346 | 0.0778 | 323        | 407   | 229  | 156  | 7  | 7   | 7   | 4                          | 16                        | 100                           | -0.6 | 45.29                                  | 38.34                           | 1.50                | 37.59                               | 1.50                    |
| 03158+4227 | 0.1343 | 551        | 872   | 872  | 336  | 7  | 7   | 7   | 8                          | 8                         | 100                           | -2.6 | 47.05                                  | 39.68                           | 1.49                | 44.55                               | 1.36                    |
| 03538-6432 | 0.3100 | 1221       | 2262  | 2262   | 793  | 7  | 7   | 7   | 4                          | 4                         | 100                           | -2.3 | 47.23                                  | 43.02                           | 1.48                | 42.38                               | 1.38                    |
| 04232+1436 | 0.0799 | 331        | 336   | 336  | 189  | 7  | 7   | 7   | 8                          | 8                         | 32                            | -2.3 | 46.35                                  | 39.78                           | 1.49                | 41.04                               | 1.41                    |
| 05189-2524 | 0.0425 | 177        | 595   | 407  | 229  | 7  | 7   | 7   | 2                          | 4                         | 8                             | -1.6 | 46.52                                  | 42.52                           | 1.49                | 43.78                               | 1.39                    |
| 06035-7102 | 0.0794 | 329        | 655   | 447  | 208  | 7  | 7   | 7   | 4                          | 8                         | 32                            | -2.6 | 46.70                                  | 39.68                           | 1.49                | 43.66                               | 1.38                    |
| 06206-6315 | 0.0924 | 382        | 655   | 447  | 142  | 7  | 7   | 7   | 4                          | 8                         | 100                           | -3.0 | 46.87                                  | 39.68                           | 1.49                | 45.13                               | 1.40                    |
| 12112+0305 | 0.0723 | 300        | 959   | 655  | 229  | 7  | 7   | 7   | 4                          | 8                         | 100                           | -3.0 | 46.87                                  | 39.68                           | 1.49                | 42.89                               | 1.41                    |
| Mrk231     | 0.0417 | 174        | 1405  | 959  | 541  | 7  | 7   | 7   | 2                          | 4                         | 8                             | -1.6 | 46.87                                  | 42.52                           | 1.49                | 43.75                               | 1.39                    |
| Mrk273     | 0.0373 | 156        | 595   | 336  | 208  | 7  | 7   | 7   | 4                          | 16                        | 16                            | -2.6 | 46.70                                  | 38.34                           | 1.50                | 44.64                               | 1.37                    |
| Mrk463     | 0.0506 | 211        | 142   | 172  | 129  | 7  | 7   | 7   | 2                          | 2                         | 2                             | -0.6 | 46.17                                  | 48.02                           | 1.49                | 53.80                               | 1.40                    |
| 14348-1447 | 0.0811 | 336        | 959   | 655  | 142  | 7  | 7   | 7   | 4                          | 8                         | 100                           | -3.0 | 47.05                                  | 39.68                           | 1.49                | 46.46                               | 1.39                    |
| 14378-3651 | 0.0676 | 281        | 872   | 447  | 88   | 7  | 7   | 7   | 2                          | 8                         | 100                           | -3.0 | 46.87                                  | 39.68                           | 1.49                | 47.04                               | 1.39                    |
| 15245+1019 | 0.0756 | 314        | 370   | 305  | 252  | 7  | 7   | 7   | 8                          | 16                        | 16                            | -3.0 | 46.17                                  | 38.36                           | 1.50                | 39.92                               | 1.47                    |
| 15250+3609 | 0.0553 | 230        | 595   | 277  | 117  | 7  | 7   | 7   | 2                          | 8                         | 16                            | -2.3 | 46.70                                  | 39.68                           | 1.49                | 48.75                               | 1.29                    |
| Arp220     | 0.0182 | 76         | 370   | 370  | 277  | 7  | 7   | 7   | 16                         | 16                        | 100                           | -2.3 | 45.99                                  | 38.34                           | 1.50                | 38.34                               | 1.47                    |
| 15462-0450 | 0.1005 | 415        | 407   | 407  | 107  | 7  | 7   | 7   | 8                          | 8                         | 32                            | -2.6 | 46.87                                  | 39.68                           | 1.49                | 49.65                               | 0.54                    |
| 16090-0139 | 0.1334 | 547        | 872   | 872  | 229  | 7  | 7   | 7   | 16                         | 16                        | 100                           | -3.0 | 47.23                                  | 38.34                           | 1.50                | 46.54                               | 1.39                    |
| NGC6240    | 0.0245 | 102        | 117   | 189  | 208  | 7  | 7   | 7   | 100                        | 8                         | 4                             | -1.6 | 45.82                                  | 40.04                           | 1.49                | 38.14                               | 0.96                    |
| 17208-0014 | 0.0424 | 177        | 793   | 595  | 305  | 7  | 7   | 7   | 8                          | 16                        | 100                           | -3.0 | 46.87                                  | 38.34                           | 1.50                | 41.76                               | 1.43                    |
| 17463+5806 | 0.3411 | 1334       | 2738  | 1870   | 370  | 7  | 7   | 7   | 2                          | 4                         | 8                             | -3.0 | 47.40                                  | 42.52                           | 1.49                | 49.14                               | 1.41                    |
| 18090+0130 | 0.0660 | 274        | 655   | 655  | 370  | 6  | 6   | 6   | 8                          | 8                         | 32                            | -2.6 | 46.70                                  | 34.00                           | 0.93                | 36.51                               | 0.74                    |
| 18470+3234 | 0.0788 | 327        | 655   | 336  | 97   | 7  | 7   | 7   | 2                          | 8                         | 100                           | -2.6 | 46.70                                  | 39.68                           | 1.49                | 47.03                               | 1.32                    |
| 19254-7245 | 0.0615 | 256        | 407   | 407  | 252  | 7  | 7   | 7   | 4                          | 4                         | 8                             | -0.6 | 46.35                                  | 42.52                           | 1.49                | 41.33                               | 1.45                    |
| 19458+0944 | 0.0995 | 411        | 447   | 447  | 305  | 7  | 7   | 7   | 100                        | 100                       | 32                            | -3.0 | 46.87                                  | 37.31                           | 1.50                | 39.58                               | 0.71                    |
| 20046-0623 | 0.0845 | 350        | 370   | 305  | 189  | 7  | 7   | 7   | 8                          | 16                        | 100                           | -2.3 | 46.52                                  | 38.51                           | 1.49                | 41.50                               | 1.40                    |
| 20087-0308 | 0.1055 | 435        | 793   | 793  | 172  | 7  | 7   | 7   | 8                          | 8                         | 32                            | -3.0 | 47.23                                  | 39.68                           | 1.49                | 56.32                               | 0.29                    |
| 20100-4156 | 0.1295 | 532        | 1055  | 1055   | 595  | 7  | 7   | 7   | 8                          | 8                         | 32                            | -2.3 | 46.87                                  | 39.68                           | 1.49                | 40.87                               | 1.42                    |
| 20414-1651 | 0.0870 | 360        | 959   | 959  | 80   | 7  | 7   | 7   | 2                          | 2                         | 2                             | -3.0 | 47.05                                  | 48.14                           | 1.49                | 53.77                               | 1.34                    |
| ESO286-19  | 0.0426 | 178        | 595   | 277  | 80   | 7  | 7   | 7   | 2                          | 8                         | 32                            | -2.6 | 46.70                                  | 39.68                           | 1.49                | 49.90                               | 1.30                    |
| 21130-4446 | 0.0925 | 383        | 277   | 277  | 107  | 7  | 7   | 7   | 100                        | 100                       | 32                            | -3.0 | 46.87                                  | 37.55                           | 1.50                | 47.48                               | 0.67                    |
| 21504-0628 | 0.0775 | 322        | 541   | 252  | 107  | 7  | 7   | 7   | 2                          | 8                         | 32                            | -2.6 | 46.52                                  | 39.68                           | 1.49                | 45.09                               | 1.36                    |
| 22491-1808 | 0.0760 | 315        | 872   | 447  | 142  | 7  | 7   | 7   | 2                          | 8                         | 16                            | -2.6 | 46.87                                  | 39.68                           | 1.49                | 49.61                               | 1.32                    |
| ESO148-2   | 0.0446 | 186        | 447   | 305  | 117  | 7  | 7   | 7   | 4                          | 8                         | 100                           | -2.6 | 46.52                                  | 39.68                           | 1.49                | 43.73                               | 1.37                    |
| 23230-6926 | 0.1062 | 438        | 872   | 595  | 117  | 7  | 7   | 7   | 4                          | 8                         | 100                           | -3.0 | 47.05                                  | 39.68                           | 1.49                | 47.76                               | 1.38                    |
| 23365+3604 | 0.0645 | 268        | 595   | 407  | 156  | 7  | 7   | 7   | 4                          | 8                         | 100                           | -2.6 | 46.70                                  | 39.68                           | 1.49                | 44.28                               | 1.36                    |
| 23389-6139 | 0.0927 | 383        | 595   | 407  | 156  | 7  | 7   | 7   | 4                          | 8                         | 100                           | -3.0 | 46.70                                  | 39.68                           | 1.49                | 42.96                               | 1.41                    |
| 23515-3127 | 0.3347 | 1311       | 1870  | 1277   | 189  | 7  | 7   | 7   | 4                          | 8                         | 100                           | -3.0 | 47.40                                  | 39.68                           | 1.49                | 49.22                               | 1.38                    |

**Table 3** — Summary of the best-fit parameters for fits to the SEDs of the 41 ULIRGs shown in Figure 8 ordered by RA. The columns show the source name, redshift, distance, star formation rate, the logarithm of the pressure of the interstellar medium, molecular cloud dissipation timescale, ionization parameter, total luminosity of the reprocessed AGN light, and temperature obtained with modified blackbody fit to the regime 60–500  $\mu\text{m}$  with proportionality index  $\beta$ . The indices FIR, SB, and SB+AGN refer to the fitting procedures outlined in §3.3.





---

## Chapter 6

---

# Giant Ly $\alpha$ nebulae associated with high redshift radio galaxies

Michiel Reuland, Wil van Breugel, Huub Röttgering, Wim de Vries, S.A. Stanford, Arjun Dey, Mark Lacy, Joss Bland-Hawthorn, Michael Dopita, and George Miley, The Astrophysical Journal, Vol. 592, p. 755, 2003

We report deep Keck narrow-band Ly $\alpha$  images of the luminous  $z > 3$  radio galaxies 4C 41.17, 4C 60.07, and B2 0902+34. The images show giant, 100–200 kpc scale emission line nebulae, centered on these galaxies, which exhibit a wealth of morphological structure, including extended low surface brightness emission in the outer regions, radially directed filaments, cone-shaped structures and (indirect) evidence for extended Ly $\alpha$  absorption. We discuss these features within a general scenario where the nebular gas cools gravitationally in large Cold Dark Matter (CDM) halos, forming stars and multiple stellar systems. Merging of these “building” blocks triggers large scale starbursts, forming the stellar bulges of massive radio galaxy hosts, and feeds super-massive black holes which produce the powerful radio jets and lobes. The radio sources, starburst superwinds and AGN radiation then disrupt the accretion process limiting galaxy and black hole growth, and imprint the observed filamentary and cone-shaped structures of the Ly $\alpha$  nebulae.

## 1 Introduction

**H**IGH redshift radio galaxies (HzRGs;  $z > 2$ ) are great beacons for pinpointing some of the most massive objects in the early universe, whether these are galaxies, super-massive black holes or even clusters of galaxies (van Breugel et al. 2002).

Powerful, non-thermal radio sources are uniquely associated with massive, multi  $L_*$  elliptical galaxies. At *low* redshifts this has been known since the first optical identifications of extra-galactic radio sources were made possible using radio interferometers (Cygnus A; Carilli & Barthel 1996). The large, twin-jet, double-lobe morphologies and enormous radio luminosities ( $P_{178\text{MHz}} \sim 5 \times 10^{35} \text{ erg s}^{-1} \text{ Hz}^{-1}$ ) suggested already early on that such galaxies must have spinning, super-massive black holes (SMBHs) in their centers (Rees 1978; Blandford & Payne 1982). We now know that the masses of the stellar bulges of galaxies and their central black holes are closely correlated ( $M_{\text{SMBH}} \sim 0.006 M_{\text{bulge}}$ ; Magorrian et al. 1998; Gebhardt et al. 2000; Ferrarese & Merritt 2000), indicating a causal connection and it is no longer a surprise that their parent galaxies occupy the upper end of the galaxy mass function ( $\gtrsim 2 \times 10^{11} M_{\odot}$ ).

At *high* redshifts the evidence is more recent but equally compelling. The combined near-infrared “Hubble”  $K - z$  relation for radio and field galaxies (De Breuck et al. 2002; Jarvis et al. 2001) shows that radio-loud galaxies are the most luminous at any redshift  $0 < z < 5.2$ . This is despite considerable changes in their rest-frame morphologies from smooth ellipticals at  $z \sim 1$  (Best, Longair, & Röttgering 1998) to large ( $\sim 50 - 70$  kpc) multi-component, structures aligned with the radio source at  $z > 2$  (Pentericci et al. 1999; van Breugel et al. 1998).

Evidence that the HzRGs are young forming galaxies has been provided by the direct detection of absorption lines and P Cygni-like features from young hot stars (Dey et al. 1997) and strong sub-mm continuum emission (Dunlop et al. 1994; Ivison et al. 1998; Archibald et al. 2001; Reuland et al. 2004). The sub-mm observations imply “hyper” luminous rest-frame far-infrared luminosities ( $L_{FIR} \gtrsim 10^{13} L_{\odot}$ ) and huge ( $> 1000 M_{\odot} \text{ yr}^{-1}$ ) star formation rates (SFRs). Large amounts of star formation are also indicated by the recent detections in several HzRGs of very extended ( $\sim 30 - 50$  kpc) molecular gas and dust clouds (Papadopoulos et al. 2000; De Breuck et al. 2002b), showing that the star formation in these systems occurs on galaxy wide scales.

There are great practical advantages in using HzRGs to study the formation and co-evolution of massive galaxies and their central black holes. Radio source identifications are unbiased with respect to heavy obscuration by dust, which is especially important in young galaxies with large amounts of star formation. Furthermore, HzRGs are the most extended and luminous galaxy-sized structures at many wavelengths and can therefore be studied in great detail over nearly the entire electromagnetic spectrum. Some specific questions that one might hope to address are: Do the stellar bulges of massive elliptical galaxies form mostly during one major, “monolithic” collapse or over a longer period through the merging of smaller components? Does outflow and radiation from starburst and AGN affect the galaxy formation process? Are active, massive forming galaxies capable of enriching the intra-cluster media with metals and thus affect cluster evolution?

It is well established that radio galaxies at low to moderately high redshifts ( $z < 2$ ) often have bright, extended (100 – 200 kpc), emission line nebulae which are aligned with the radio sources (see McCarthy 1993, and references therein). The morphologies, kinematics and ionization of these nebulae have been studied extensively (e.g., van Breugel et al. 1985; Baum, Heckman, & van Breugel 1992; McCarthy 1993; van Ojik et al. 1997; Villar-Martín et al. 1999; Best, Röttgering, & Longair 2000b; Tadhunter et al. 2000; Inskip et al. 2002a). From this work one can conclude that (i) the gas is probably leftover material from earlier galaxy merging events which involve at least one gas rich galaxy, (ii) the kinematics of the gas along the radio source axes is disturbed due to interaction with the radio lobes and jets, (iii) the merging events may have triggered star formation and radio AGN activity at the galaxy centers, and (iv) the gas is ionized in part by shocks induced by the radio sources and in part by photoionization from the AGN (Villar-Martín et al. 1999; Tadhunter et al. 2000; Best, Röttgering, & Longair 2000a,b; Inskip et al. 2002a,b).

Few images exist of extended emission-line (Ly $\alpha$ ) nebulae at much higher redshifts ( $z > 3$ ). Most known nebulae are *radio-loud*, being associated with radio galaxies, but some are *radio-quiet* (Steidel et al. 2000; Francis et al. 2001). Nearly all these nebulae

were imaged with 4 m class telescopes and little morphological detail can be discerned because of limited signal-to-noise and often moderately poor seeing. Higher quality images are of great interest because of the potential diagnostics they may provide about the very early stages of galaxy formation, and about starburst/AGN feedback and chemical enrichment during this process.

For example, the existence of radio-quiet Ly $\alpha$  nebulae without obvious central sources of ionization and/or outflow suggests that they may be due to accretion of cooling gas in the gravitational fields of CDM halos (Steidel et al. 2000; Chapman et al. 2001; Fardal et al. 2001; Francis et al. 2001). Such nebulae might be the very first stage in the formation of large galaxy, or its building blocks, a group of smaller galaxies. The radio-loud Ly $\alpha$  nebulae could be the next phase, during which the central galaxy develops a large scale starburst as a result of galaxy merging and a super-massive black hole is activated. The ensuing outflow and ionizing radiation might then heat and expel the accreting gas, while adding enriched material from the central starburst to the mix, effectively stopping further galaxy growth until starburst and AGN activity subside. Such a self regulated process of galaxy growth has been invoked as a possible explanation for the surprisingly tight SMBH/stellar bulge correlation (Silk & Rees 1998; Haiman & Rees 2001). Could it be that in the case of radio galaxies, which are the most massive systems at any redshift, this process is further aided by radio jets and lobes?

To investigate the nature of Ly $\alpha$  nebulae associated with HzRGs and exploit their diagnostic value we have obtained deep narrow-band Ly $\alpha$  images of three  $3 < z < 4$  radio galaxies using the W.M. Keck Observatory 10 m telescopes. Here we discuss the morphologies of these nebulae, their relationship to other pertinent imaging data (radio, infrared, mm), and the possible implications for understanding the formation and coevolution of massive galaxies and super-massive black holes.

Our paper is organized as follows. In Section 2 we describe the target selection, observations and data analysis. The observational results for the individual objects are presented in Section 3 and some physical parameters are deduced. In Section 4, we discuss possible scenarios for the origin of the outer nebulae and the features in the central region. We summarize our conclusions in Section 5. Throughout we adopt a flat universe cosmology with  $\Omega_M = 0.3$ ,  $\Omega_\Lambda = 0.7$ , and  $H_0 = 65 \text{ km s}^{-1} \text{ Mpc}^{-1}$ . Note that at the high redshifts of our targets a slightly different choice of cosmological parameters can make a significant difference to the derived parameters. To emphasize this we quote our numbers while retaining the scale factor  $h_{65} = 1$ . At the redshifts of our galaxies ( $z = 3.4 - 3.8$ ) and using the adopted cosmology we find look-back times  $\sim 12.8 h_{65}^{-1} \text{ Gyr}$ , galaxy ages  $\lesssim 1.7 h_{65}^{-1} \text{ Gyr}$ , and angular scales of  $\sim 7.6 h_{65}^{-1} \text{ kpc arcsec}^{-1}$ .

## 2 Sample Selection and Observations

The observations presented here include sensitive optical narrow-band and broad-band imaging of three  $z > 3$  radio galaxies using the Keck telescopes and previously unpublished Hubble Space Telescope (HST) imaging of 4C 60.07. Our targets were selected on the basis of their high redshifts and the availability of data at many other wavelengths.

| Object     | Coordinates <sup>a</sup> |                | Narrow-band                  |                          |  | R-band                   |  |
|------------|--------------------------|----------------|------------------------------|--------------------------|--|--------------------------|--|
|            | RA<br>(J2000)            | DEC<br>(J2000) | Gal.Ext. <sup>b</sup><br>mag | t <sub>obs</sub><br>(ks) | 1 $\sigma$ det.surf.br. <sup>c</sup><br>(AB mag) | t <sub>obs</sub><br>(ks) | 1 $\sigma$ det.surf.br. <sup>c</sup><br>(AB mag) |
| B2 0902+34 | 09 05 30.11              | 34 07 55.9     | 0.101                        | 9.6                      | 29.04, 27.4                                      | 2.4                      | 29.70, 28.3                                      |
| 4C 60.07   | 05 12 55.17              | 60 30 51.1     | 1.609                        | 7.2                      | 28.85, 27.3                                      | 2.0                      | 29.64, 28.1                                      |
| 4C 41.17   | 06 50 52.14              | 41 30 30.7     | 0.393                        | 27.6                     | 29.85, 28.1                                      | 4.0                      | 30.08, 28.7                                      |

**Table 1** — Summary of Keck observations<sup>a</sup> Position of the radio core (Carilli et al. 1994, 1997; Carilli 1995)<sup>b</sup> Galactic extinction at the central wavelength of the narrow-band filters<sup>c</sup> Formal 1 $\sigma$  detection limit: in the seeing disc and in a 3'' diameter aperture respectively

## 2.1 Sample Selection

### 4C 41.17

4C 41.17 at  $z = 3.798$  was chosen because its Ly $\alpha$  halo is one of the most luminous and extended known. Previous imaging observations showed a bright elliptical-shaped Ly $\alpha$  halo with a major axis of  $\sim 15''$  directed along the radio axis (Chambers et al. 1990; Hippelein & Meisenheimer 1993; Adam et al. 1997; Rocca-Volmerange 1999), and spectroscopic evidence indicated that the Ly $\alpha$  might extend to  $\gtrsim 18''$  (Dey 1999). The radio source has a multiple component, asymmetric, “double-double” FR II morphology, with the radio axis of the inner source having a position angle different from the outer source (Chambers et al. 1990; Carilli et al. 1994). It was the first HzRG in which a large dust mass has been detected through sub-mm observations (Dunlop et al. 1994), implying a large SFR in the range of  $2000 - 3000 M_{\odot} \text{ yr}^{-1}$ .

The galaxy has a clumpy rest-frame UV morphology, with the brightest components aligned with the inner radio source (van Breugel et al. 1999). This light is unpolarized between  $\lambda_{\text{rest}} \sim 1400 - 2000 \text{ \AA}$ , and thus not due to scattering from a hidden quasar-like AGN (Dey et al. 1997). Instead, the observations show absorption line features from young hot stars which resemble those seen in  $z \approx 2 - 3$  star-forming galaxies and nearby starburst systems. Dey et al. derive a SFR of  $140 - 1100 M_{\odot} \text{ yr}^{-1}$  for the central  $10 \text{ kpc} \times 20 \text{ kpc}$  of 4C 41.17 or  $400 - 3200 M_{\odot} \text{ yr}^{-1}$  after correction for local extinction. These values are consistent with those derived from the sub-mm observations. In this radio source aligned star formation is thought to have been triggered by radio jets colliding with a large, dense cloud in the forming galaxy (Dey et al. 1997; van Breugel et al. 1999; Bicknell et al. 2000).

### 4C 60.07

4C 60.07 ( $z = 3.791$ ; Chambers et al. 1996) is close to the Galactic plane ( $b_{\text{II}} = 12^{\circ}$ ) and suffers significant Galactic extinction (see, Table 2). Despite this unfortunate circumstance, we selected 4C 60.07 as one of our targets because its redshift is close to that of 4C 41.17 and it is a strong sub-mm emitter and one of only three HzRGs in which CO has been detected (Papadopoulos et al. 2000; De Breuck et al. 2002b). The large extent ( $7'' \sim 50 h_{65}^{-1} \text{ kpc}$ ) and dynamical mass ( $\sim 1 - 7 \times 10^{11} M_{\odot}$ ) of the cold gas are some of the best evidence that 4C 60.07 is indeed a massive forming galaxy. A low signal-to-noise image of 4C 60.07 shows a  $2''$  Ly $\alpha$  feature aligned with the radio source. The source displays a simple edge brightened FR II morphology (Fanaroff & Riley 1974),

unlike the other two objects in our sample (Carilli et al. 1994; Chambers et al. 1996).

### B2 0902+34

Our third target, B2 0902+34 ( $z = 3.395$ ; Lilly 1988), was selected because of its extended, very diffuse optical morphology (Eisenhardt & Dickinson 1992), which is very unlike that of the elongated, radio source aligned structures seen in 4C 41.17 and 4C 60.07. It is also the only HzRG for which 21 cm neutral hydrogen has been detected in absorption against the radio continuum (Uson, Bagri, & Cornwell 1991; Briggs et al. 1993). No other evidence for cold gas or dust has been found in B2 0902+34. No strong absorption in the Ly $\alpha$  emission has been detected through spectroscopy (Martin-Mirones et al. 1995) and no significant sub-mm signatures of thermal dust emission have been found (Archibald et al. 2001). Eisenhardt & Dickinson (1992) published a shallow Ly $\alpha$  image for B2 0902+34 that showed its halo to be relatively bright but did not reveal much detail. They argued that it is a true protogalaxy, based on its relatively flat UV-optical spectral energy distribution, indicative of a dominant population of young stars. The radio structure resembles that of quasars with a flat spectrum nucleus, a bright knotty jet with a sharp 90° bend in the north, and a disembodied double hotspot to the south. Carilli (1995) explained its unusual properties, inferring that the radio axis is close to the line of sight.

## 2.2 Keck Imaging

### 2.2.1 Ly $\alpha$ imaging

We observed 4C 41.17, 4C 60.07 and B2 0902+34 using two custom-made, high throughput narrow-band filters. The central wavelengths and bandpasses were chosen to cover redshifted Ly $\alpha$  within a velocity range of  $\pm 1500 \text{ km s}^{-1}$  for each object, which is the typical maximum width of the emission lines of HzRGs (e.g., Dey et al. 1997; van Ojik et al. 1997). 4C 41.17 and 4C 60.07 are close in redshift and fit in the same filter, although for 4C 60.07 emission at velocities larger than  $1000 \text{ km s}^{-1}$  blueward from the systemic velocity falls outside the bandpass. The transmission curve of this filter ( $\lambda_c = 5839.0 \text{ \AA}$  and  $\Delta\lambda = 65.0 \text{ \AA}$ ) averages  $\sim 84\%$  over the bandpass. The narrow-band filter for B2 0902+34 has  $\lambda_c = 5342.4 \text{ \AA}$  and a FWHM of  $\Delta\lambda = 56.8 \text{ \AA}$ , with an average transmission of 73%. The fields of view through the 10 cm  $\times$  10 cm filters were vignetted slightly, resulting in an useful sky coverage of  $\sim 2' . 0 \times 1' . 7$ .

The observations were made during the nights of UT 2000 December 27, 28 and UT 2001 February 25 using the Echelle Spectrograph and Imager (ESI; Sheinis et al. 2000) at the Cassegrain focus of the Keck II 10 m telescope in imaging mode. The detector used is a high-resistivity MIT-Lincoln Labs 2048  $\times$  4096 CCD, has a plate scale of  $0' . 154 \text{ pixel}^{-1}$ , and is only partly illuminated in imaging mode. Exposures were broken into integrations of 1200 seconds and we performed  $15''$  offsets between each integration. This facilitated removal of cosmic rays and bad pixels on the CCD. The data were taken during photometric conditions and good seeing (FWHM  $0' . 6 - 0' . 8$  in the co-added images) and were reduced using standard methods in IRAF (including registering and stacking the individual integrations). Flatfielding was done with twilight sky flats only (as opposed to creating field flats from unregistered images) to prevent suppression of faint diffuse emission.

The data were flux calibrated using the spectrophotometric standard stars Feige 34, PG 1121+145, and PG 1545+035 (Massey et al. 1988). All magnitudes and colors quoted in this paper are on the AB system and the individual calibrations agree to within approximately 10%, which we take to be the systematic photometric uncertainty. We corrected for Galactic extinction using the  $E(B-V)$  values based upon IRAS 100 $\mu$ m cirrus emission maps (Schlegel, Finkbeiner, & Davis 1998) and extrapolating following Cardelli, Clayton, & Mathis (1989). A summary of the total integration times, surface brightness limits, and Galactic extinction corrections is given in Table 2. With  $1\sigma$  surface brightness limits of NB  $\sim 29 - 30$  mag within an aperture of the seeing disk ( $\sim 0.7''$ ) these are the deepest narrow-band exposures of Ly $\alpha$  nebulae ever obtained.

### 2.2.2 Broad-band imaging

We also obtained emission line free  $R$ -band images during the same nights to allow continuum subtraction from the narrow-band exposures and create pure Ly $\alpha$  images. For 4C 41.17 and 4C 60.07 the  $R$ -band ( $\lambda_c = 6700 \text{ \AA}$ ; FWHM = 1400  $\text{\AA}$ ) is just redward of Ly $\alpha$  and free of strong emission lines (all emission lines that fall within the filter bandpass have observed equivalent widths  $\lesssim 10 \text{ \AA}$ ; Dey et al. 1997, Chapter 7;). In the case of B2 0902+34 the  $R$ -band contains the C IV  $\lambda 1548, 1551$  doublet and He II  $\lambda 1640$ . The spectrum by Martin-Mirones et al. (1995) shows that C IV and He II have observed equivalent widths of  $\sim 55 \text{ \AA}$ , and  $\sim 40 \text{ \AA}$ , respectively. The average total contribution of these emission lines to the total flux received in the broad-band filter is  $\lesssim 7\%$  indicating that they are only minor contaminants. However, the relative contribution could depend on the region of interest. There is no easy way to correct for this, but compared to the large equivalent width Ly $\alpha$  line continuum subtraction is only a small correction and does not change any morphological features of interest for this paper. These  $R$ -band images have fields of view of  $3' . 3 \times 1' . 7$ , were broken into 400 s exposures and were reduced following standard methods.

## 2.3 HST Imaging

4C 60.07 was observed during Cycle 6 with the Wide Field Planetary Camera 2 (WFPC2; Trauger et al. 1994) on the HST. The object was placed on the PC chip, which utilizes an  $800 \times 800$  pixel Loral CCD as detector with a plate scale of  $0'' . 0455 \text{ pixel}^{-1}$ . In two pointings 9 broad-band exposures of 2900 s each were obtained for a total exposure time of 26.1 ks through the F702W filter, which has a central wavelength  $\lambda_c = 6944.3 \text{ \AA}$  and a FWHM of  $\Delta\lambda = 1384.7 \text{ \AA}$ . For 4C 60.07 this filter includes the C IV doublet with a combined observed equivalent width of  $\sim 300 \text{ \AA}$  (Chapter 7), but is free from other strong emission lines. After cosmic ray removal these images were co-added. The data were severely affected by light scattering off of the Earth atmosphere. However, the scattered light pattern was fixed with respect to the CCD. This allowed for using the small offsets between the unregistered images of the two pointings to construct a scattering model. After subtraction of this model, the resulting image was virtually fully corrected.

Deep (21.6 ks) F702W observations of 4C 41.17 were obtained using the PC section of WFPC2 (for details see van Breugel et al. 1999; Bicknell et al. 2000). Observations

with the F702W filter are slightly contaminated by the C IV doublet, which has a combined observed equivalent width of  $\sim 104 \text{ \AA}$  (Dey et al. 1997).

Eisenhardt and Dickinson observed B2 0902+34 during Cycle 4 for 21.6 ks using the PC of WFPC2 with the filter F622W, which is centered at  $\lambda_c = 6189.6 \text{ \AA}$ , has a FWHM of  $\Delta\lambda = 917.1 \text{ \AA}$ , and is free of emission from the Ly $\alpha$  and C IV lines. These data were obtained from the archives.

## 2.4 Relative Astrometry

Astrometric calibration of the Keck images was performed using the USNO-A2.0 catalog (Monet 1998). For the broad-band images 15 catalog stars were typically available in each field, of which about 10 were unsaturated and suitable for astrometry. In all cases this resulted in astrometry accurate to approximately  $0''.15$  rms with respect to the USNO catalog. The catalog itself has a rms uncertainty of  $\sim 0''.25$  with respect to the International Celestial Reference Frame (ICRF), while the astrometric uncertainties of the radio images are  $\lesssim 0''.2$  with respect to the ICRF (for a concise discussion of relative astrometric uncertainties see De Breuck et al. 2002, and references therein). The narrow-band image of B2 0902+34 contains only few stars and the astrometry had to be bootstrapped from the broad-band image which has more stars in the field. To do this, the narrow-band image was registered relative to the *R*-band image to better than a fraction of a pixel using a second order polynomial function. Similarly, the HST images were matched to the respective Keck images resulting in relative optical astrometry better than  $0''.1$  rms, and astrometry relative to the radio maps of comparable accuracy as for the Keck imaging.

Generally, for the 5 GHz and 8 GHz VLA radio images (Carilli et al. 1994; Carilli 1995; Carilli et al. 1997), we used the astrometry as given by the observations of the phase calibrators. However, in the case of 4C 41.17 there was a faint optical counterpart with a well defined centroid to the serendipitous source to the SE in the 5 GHz map (Source E in Chambers et al. 1996). We used this source to register the radio and optical images to better than  $0''.1$ . A change of only  $+0''.15$  in right ascension and  $+0''.2$  in declination was required to align the images. These shifts agree with typical uncertainties in the match between the optical and radio reference frames as cited above. Therefore, we believe that, generally, relative astrometry between the radio and optical is better than  $\lesssim 0''.35$  rms, while it is better than  $0''.1$  rms in the case of 4C 41.17.

## 2.5 Continuum subtraction

Pure emission line images were constructed as follows: First, the point spread functions (PSFs) of the narrow-band images were matched to the broader PSFs of the *R*-band images. For this we selected a suitable star close to the galaxy in both images and calculated a convolution kernel using the IRAF task `psfmatch`. Subsequently, the Ly $\alpha$  image was convolved with this kernel to obtain a new image with a PSF similar to the *R*-band image.

The registered *R*-band images were then divided by a scaling factor, and subtracted from the narrow-band images in order to remove continuum emission. This scaling factor was determined for each radio galaxy by convolving high quality spectra (Dey

| Object     | $z$   | NB <sup>a</sup><br>mag | BB–NB<br>mag | F <sub>Ly<math>\alpha</math></sub> <sup>b</sup><br>erg s <sup>-1</sup> cm <sup>-2</sup> | log L <sub>Ly<math>\alpha</math></sub> <sup>c</sup><br>erg s <sup>-1</sup> | Extent<br>" $\times$ " | Size <sup>c</sup><br>kpc $\times$ kpc | Mass <sup>d</sup><br>10 <sup>8</sup> M <sub><math>\odot</math></sub> | SFR <sup>e</sup><br>M <sub><math>\odot</math></sub> yr <sup>-1</sup> |
|------------|-------|------------------------|--------------|---|--|------------------------|---------------------------------------|--|--|
| B2 0902+34 | 3.395 | 19.20 $\pm$ 0.004      | 2.81         | 4.9 $\times$ 10 <sup>-15</sup>  | 44.77  | 10 $\times$ 8          | 80 $\times$ 64                        | 30 $f_v^{-\frac{1}{2}}$  | > 450 $f_{\text{esc}}^{-1}$  |
| 4C 60.07   | 3.791 | 19.97 $\pm$ 0.050      | 3.26         | 8.8 $\times$ 10 <sup>-15</sup>  | 45.14  | 9 $\times$ 7           | 68 $\times$ 53                        | 30 $f_v^{-\frac{1}{2}}$  | > 1100 $f_{\text{esc}}^{-1}$   |
| 4C 41.17   | 3.798 | 18.76 $\pm$ 0.001      | 3.38         | 9.0 $\times$ 10 <sup>-15</sup>  | 45.15  | 25 $\times$ 17         | 190 $\times$ 130                      | 130 $f_v^{-\frac{1}{2}}$   | > 1100 $f_{\text{esc}}^{-1}$   |

**Table 2** — Properties of the Ly $\alpha$  nebulae

<sup>a</sup> Determined using SExtractor (Bertin & Arnouts 1996) with automatic aperture selection and deblend parameter optimized for detecting large structures. The uncertainties quoted are the formal error estimates given by SExtractor. The magnitudes were also determined in IRAF using a curve of growth for the cumulative magnitude in increasing radii which resulted in magnitudes differing by at most 0.3 mag.

<sup>b</sup> Corrected for Galactic extinction

<sup>c</sup> Assuming a cosmology with  $\Omega_M = 0.3$ ,  $\Omega_\Lambda = 0.7$ , and  $H_0 = 65 \text{ km s}^{-1} \text{ Mpc}^{-1}$

<sup>d</sup> These mass estimates are derived from  $M = n_e m_p f_v V$  and  $L_{\text{Ly}\alpha} = 4 \times 10^{-24} n_e^2 f_v V \text{ erg s}^{-1}$  (e.g., McCarthy et al. 1990) assuming cylindrical symmetry and case B recombination. We have assumed a filling factor  $f_v = 10^{-5}$ , which is extremely uncertain (Heckman et al. 1982).

<sup>e</sup> The estimated  $SFR \geq 8.12 \times 10^{-43} f_{\text{esc}}^{-1} L_{\text{Ly}\alpha}$  is very uncertain and based on the assumption that all of the Ly $\alpha$  flux is the result of Case B recombination of photoionization by a young stellar population (see Section 3.1).

et al. 1997, Chapter 7); after removal of the Ly $\alpha$  emission line, with the  $R$ -band and narrow-band filter curves. For each galaxy this resulted in an expected ratio of continuum flux densities within both filters. These expected ratios are based only on the filter curves, while telescope and CCD efficiencies should be taken into account as well. We corrected for this by adjusting the scaling factor by  $\sim 10\%$ , which was the difference between the predicted and observed ratios for the spectrophotometric standards.

### 3 Results

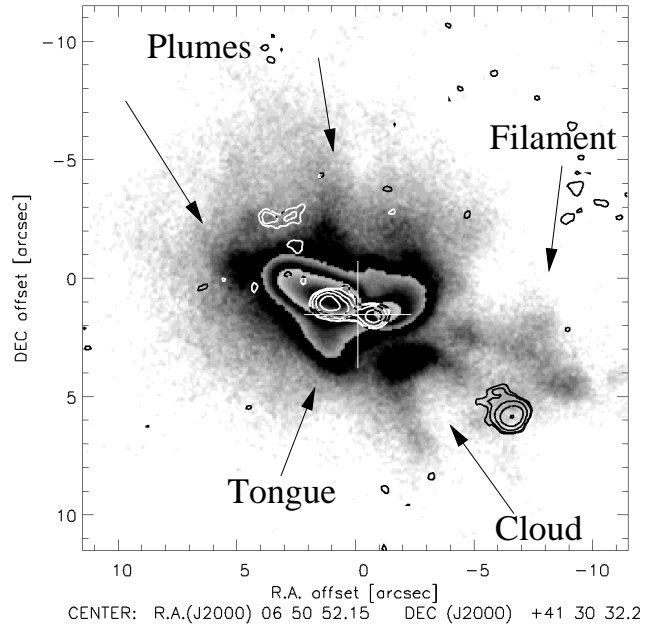
Our narrow-band images show unprecedented detail in the spectacular nebulae that surround the radio galaxies. The nebulae extend over more than 100 kpc and display complex morphologies such as filamentary structures, conical shapes, and distinct regions of high and low intensity. Grayscale representations (colorcycled to show both low and high surface-brightness regions) of the pure emission line images and contour plots of the narrow-band images (including continuum) are shown in Figures 1–8. In the following, we discuss the morphological features of the nebulae in detail. A summary of their global properties is given in Table 2. This table also gives estimates for the mass of the ionized gas and star formation rates. Despite being subject to considerable uncertainties these might help provide some insight in the nature of the nebulae.

#### 3.1 4C 41.17

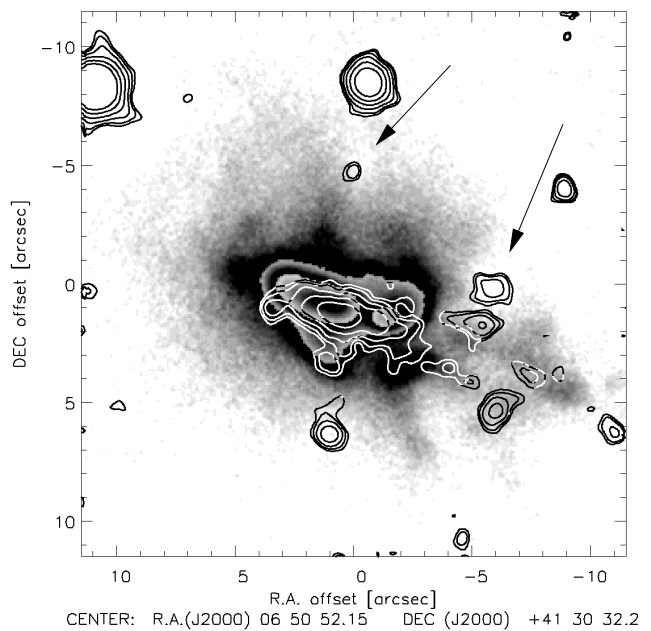
The co-added continuum-subtracted narrow-band image for 4C 41.17 overlaid with a 5 GHz VLA radio map (Carilli et al. 1994) is shown in Figure 1, while Figure 2 shows the same image overlaid with a Keck  $K$ -band image (Graham et al. 1994). Figure 3 shows an overlay of the HST image with the narrow-band image (including continuum). The Ly $\alpha$  nebula is seen to extend over  $25'' \times 17''$  ( $\sim 190 h_{65}^{-1} \text{ kpc} \times 130 h_{65}^{-1} \text{ kpc}$ ), nearly twice



**Figure 1** — Grayscale Ly $\alpha$  image of 4C 41.17 with a contour representation of the 4.9 GHz VLA map (Carilli et al. 1994) overlaid. The grayscale has been colorcycled to show the details of the high and low surface brightness simultaneously. The radio core is identified with a cross, and the contour levels are 0.07, 0.11, 0.4, 1.6 and 6.4 mJy beam $^{-1}$ . The arrows indicate “plumes” of enhanced emission on both sides of the Northern Lobe, a separate emission line cloud with filaments extending to the SSW and SW, a large filament, and a Ly $\alpha$  tongue corresponding to a region which appears unaffected by the radio source.



**Figure 2** — Similar to Figure 1 but with  $K$ -band image (contours; Graham et al. 1994) overlaid. The contours are at arbitrary levels and have been chosen to show the desired components. Some dips in the outer halo are co-spatial with  $K$ -band galaxies (indicated with arrows), suggesting that these galaxies are absorbing systems close in redshift to 4C 41.17.



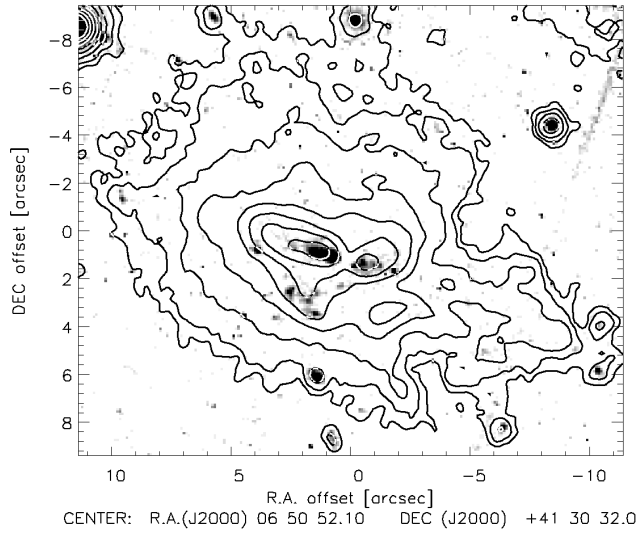


**Figure 3** — HST F702W image (van Breugel et al. 1999) of 4C 41.17 with narrow-band image (contours; including continuum) overlaid. The contours indicate observed surface brightness levels at  $6.7 \times 10^{-19} \times (6, 12, 25, 50, 100, 200, 400, 800) \text{ erg s}^{-1} \text{ cm}^{-2} \text{ arcsec}^{-2}$ . Note the group of kpc-sized clumps in the extended diffuse emission tongue  $2''$  south of the central peak, which is not aligned with the radio axis.

the size previously seen in the images obtained with 4m class telescopes, and shows a wealth of structure.

#### Central region

The bright inner region was observed and discussed in detail by Chambers et al. (1990). It is aligned with the inner radio source and of approximately the same size, while the radio core is located in a central dip in the Ly $\alpha$  emission. This has been noticed before (Hippelein & Meisenheimer 1993; Adam et al. 1997), and Hippelein & Meisenheimer (1993) interpret the dip as absorption by a foreground Lyman-forest cloud unrelated to the radio galaxy. However, as proposed by Dunlop et al. (1994), it seems more likely that the absorption is due to a dust lane orthogonal to the major axis of the galaxy and its radio source, obscuring the center of the galaxy near the position of the radio core. This would provide a natural explanation for both the observed sub-mm emission and the gap in the UV continuum seen in the HST image (Fig. 3). Graham et al. (1994) also mention that their *K*-band image (Fig. 2; strongly contaminated with and  $H\beta$ ) shows evidence for a double peaked structure. They could not ascertain whether this was also true for a line-free *Ks* image.

#### Galaxy scale

The Keck *K*-band and HST F702W “R”-band images (rest-frame B-band and  $1500\text{\AA}$  respectively) show a multi-component galaxy spread out over a region of  $9'' \times 5''$  ( $\sim 68h_{65}^{-1} \text{ kpc} \times 38h_{65}^{-1} \text{ kpc}$ ) near the center of the Ly $\alpha$  nebula. A Ly $\alpha$  tongue sticks out just SE of the nucleus and overlaps with continuum emission seen in the Keck and HST images. The HST image shows that this is a small group of kpc-sized clumps, embedded in low surface brightness emission of  $\sim 12h_{65}^{-1} \text{ kpc}$  diameter, which appears to be unaffected by the radio source. From the total UV $_{rest}$  continuum for this region van Breugel et al. (1999) derive a star formation rate of  $33 M_{\odot} \text{ yr}^{-1}$  (for the cosmological parameters used in the present paper). For this same region we derive from our Keck observations an integrated Ly $\alpha$  flux of  $3 \times 10^{-16} \text{ erg s}^{-1} \text{ cm}^{-2}$ , or  $L_{\text{Ly}\alpha} = 5 \times 10^{43} \text{ erg s}^{-1}$ .

We can convert the Ly $\alpha$  luminosity into an estimate of the star formation rate if we make a couple of assumptions. With the assumption that all the Ly $\alpha$  is due to Case B

recombination of photoionization by stars we obtain  $SFR \geq 8.12 \times 10^{-43} f_{\text{esc}}^{-1} L_{\text{Ly}\alpha}$ . This assumption, while unlikely to be correct for most of the halo, may be reasonable for the undisturbed region. The estimated  $SFR$  constitutes a lower limit as it assumes that a fraction  $f_a = 1$  of the ionizing photons will be absorbed. The typical escape fraction found locally is  $f_{\text{esc}} \leq 0.1$  (Leitherer et al. 1995). However for the  $z \sim 3$  Lyman break galaxy (LBG) population (Steidel et al. 1996)  $f_{\text{esc}} \sim 0.5 - 1.0$  is typically found (Steidel, Pettini, & Adelberger 2001) and these LBG values may be more appropriate for HzRGs.

From the inferred  $L_{\text{Ly}\alpha}$  we obtain a lower limit to the star formation rate of  $40 f_{\text{esc}}^{-1} M_{\odot} \text{yr}^{-1}$ , rather similar to the estimate based on the UV continuum. However, both the UV-continuum and Ly $\alpha$  based SFR estimates are probably lower limits since they assume no extinction, which may very well be important given the detection of dust in 4C 41.17.

#### *Outer region and filamentary structure*

Perhaps the most striking morphological feature of the 4C 41.17 Ly $\alpha$  nebula is the cone-shaped structure emanating from the center of the galaxy, with long filaments and a crescent-shaped cloud with horns. The SW outer radio lobe is located within the cone and extends further from the core than its, much fainter, NE counterpart. It suggests that the SW radio lobe may have encountered less dense material on its way out. This also agrees with the emission-line and radio surface brightness asymmetry near the center: the line emission and radio emission of the inner radio source are brighter on the NE side. Such optical/radio asymmetry correlations have also been seen in nearby radio galaxies (McCarthy, Spinrad, & van Breugel 1995). They are thought to be due to local gas density asymmetries, with denser gas blocking radio jets, resulting in brighter line and radio emission.

The filamentary/plume features of the nebula are probably caused by AGN activity and/or the radio source: the long SW filament ( $\sim 8''$ ,  $60 h_{65}^{-1}$  kpc) is about the same size as the distance between the nucleus and the SW hotspot, the NE lobe appears to be embraced by two short “plumes” of enhanced Ly $\alpha$  emission, and the apex of the two  $\sim 4''$  ( $30 h_{65}^{-1}$  kpc) SW cloud horns projects close to the nucleus.

Another point of interest is the *absence* of Ly $\alpha$  emission near several faint  $K$ -band companions around 4C 41.17 (Fig. 2; Graham et al. 1994). Based on their red colors ( $R - K_s \sim 4 - 5$ ) Graham et al. concluded that these are probably multiple  $L_*$  galaxies at the same redshift as 4C 41.17. Graham’s objects 4, 9 and 12 are all near Ly $\alpha$  “gaps”. It suggests that they are dusty galaxies in the local foreground to the Ly $\alpha$  nebula, absorbing the Ly $\alpha$  photons along the line of sight. If the sizes of the gaps are larger than the  $K$ -band objects this could be evidence for galactic envelopes (e.g., Chen, Lanzetta, & Webb 2001). This is hard to test, given the limited signal-to-noise of the  $K$ -band objects, but visual inspection of Figure 2 shows that they are consistent with having similar sizes. The scale of the Ly $\alpha$  absorption halos ( $15 h_{65}^{-1}$  kpc  $< D < 25 h_{65}^{-1}$  kpc) suggests that these represent objects which have already collapsed to “normal” galaxian dimensions by this redshift.

The 4C 41.17 field also shows an over-density of dusty galaxies on a much larger scale ( $\sim 2.5'$  diameter,  $\sim 1 h_{65}^{-1}$  Mpc; Ivison et al. 2000), suggesting that 4C 41.17 may be at the center of a “proto-cluster”.

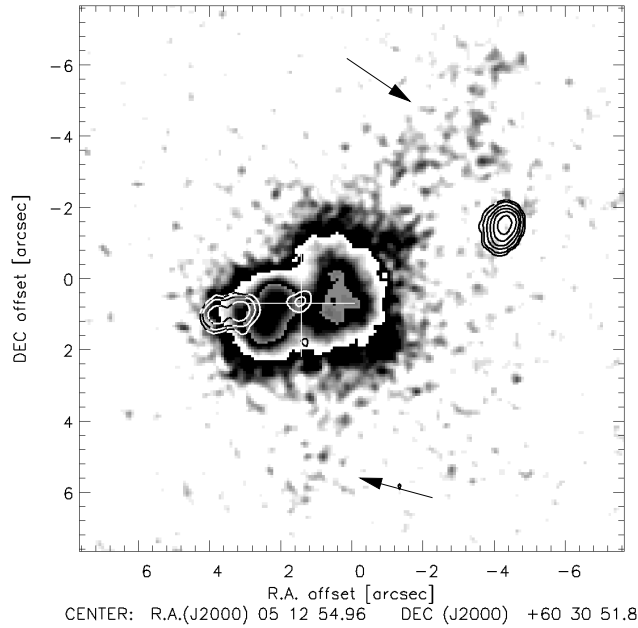


**Figure 4** — Ly $\alpha$  image of 4C 60.07 (grayscale) with 4.7 GHz VLA map (contours; Carilli et al. 1997) overlaid. The radio core is indicated with a cross, and the contour levels are 0.2, 0.4, 1.0, 2.0, 4.0 and 8.0 mJy beam $^{-1}$ . A very extended NW filament and tentative evidence for a SE filament are indicated with arrows.

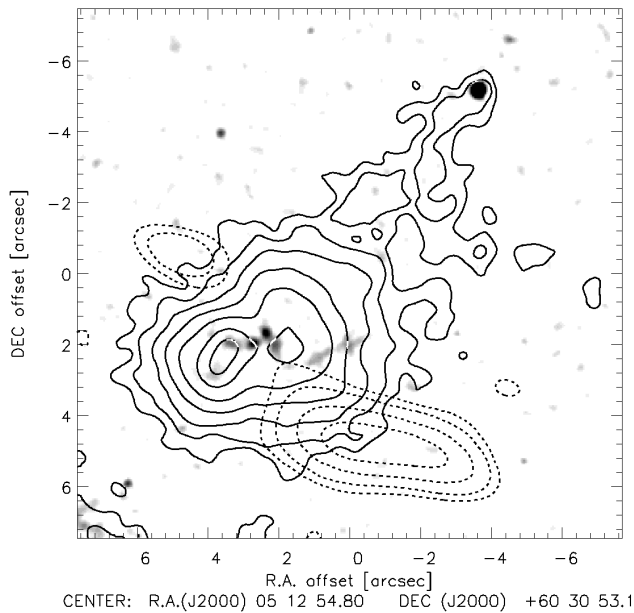
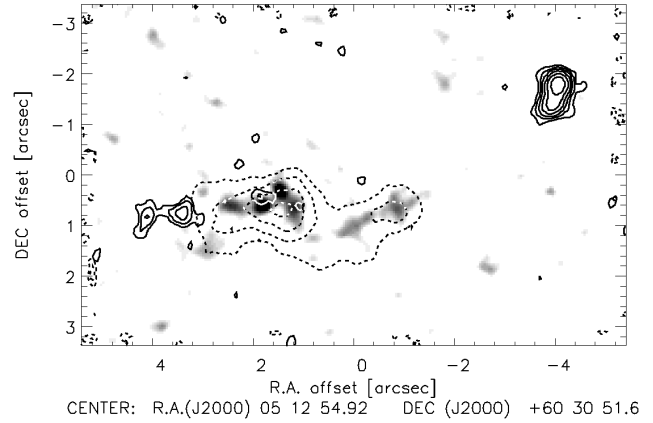


**Figure 5** — HST F702W image of 4C 60.07 with narrow-band image (solid contours, not extinction corrected, including continuum) and 1.25 mm map (dashed contours; Papadopoulos et al. 2000) overlaid. The narrow-band image has been heavily smoothed to bring out the low surface brightness filament and contour levels are  $6.7 \times 10^{-19} \times (5, 10, 20, 40, 80, 160, 240)$  erg s $^{-1}$  cm $^{-2}$  arcsec $^{-2}$ . The levels for the 1.25 mm emission are at 1.2, 1.6, 2.0, and 2.5 mJy, with  $\sigma = 0.6$  mJy beam $^{-1}$ , showing that the NE component is a tentative detection comparable in size and shape to the restoring beam. The galaxy at the tip of the narrow-band filament is foreground at  $z = 0.891$ .

### 3.2 4C 60.07

In Figure 4 we show the continuum-subtracted image of 4C 60.07 overlaid with the 5 GHz VLA radio map of Carilli et al. (1997). Contour overlays of the narrow-band image and 1.25 mm Plateau de Bure map (Papadopoulos et al. 2000) on top of the newly obtained HST image are shown in Figure 5. A zoomed-in version of this HST image with a high resolution 8 GHz VLA map is shown separately in Figure 6 to better bring out the morphological details.

**Figure 6** — Zoomed in grayscale representation of the HST F702W image of 4C 60.07 with 8.2GHz VLA map overlaid (solid contours; Carilli et al. 1997). The image has been smoothed to a resolution of  $0.25''$ , and ESI R-band contours (dashed) are overlaid to better show the shape of the galaxy. The knotty, Z-shaped structure of the aligned restframe UV continuum is apparent, while the radio core might be coincident with the central gap between the two brightest emission peaks. The radio contour levels are 0.08, 0.16, 0.3, 0.6, 1.2, and  $2.4 \text{ mJy beam}^{-1}$ .



### *Central region*

The radio core appears to fall into a gap in the bright central  $\text{Ly}\alpha$  emission, and is possibly coincident with a lack of UV continuum emission in the HST images (Figs. 5,6) similar to 4C 41.17. There is enhanced emission on either side of the nucleus, and the  $\text{Ly}\alpha$  emission is brightest between the nucleus and the eastern lobe which is closest to the nucleus. This emission-line/radio asymmetry correlation is again similar to 4C 41.17 and other radio galaxies.

### *Galaxy scale*

The HST images shown in Figures 5 and 6 show a string of knots subtending at least  $5''$  ( $\sim 38h_{65}^{-1} \text{ kpc}$ ). The two brightest knots appear to be on either side of the radio core. There is a prominent Z-shaped structure, both ends of which approximately point toward the radio lobes, making it a typical case of the radio-optical alignment effect. By comparing the HST morphology with the  $\text{Ly}\alpha$  emission, it seems that the Z-shaped structure goes around the western peak of the halo (Fig. 5).

### *Outer region and filamentary structure*

On a larger scale the halo extends over approximately  $9'' \times 7''$  ( $\sim 68h_{65}^{-1} \text{ kpc} \times 53h_{65}^{-1} \text{ kpc}$ ) and shows a cone shaped structure bounded on one side by a  $10''$  ( $\sim 76h_{65}^{-1} \text{ kpc}$ ) long filament. The maximum projected sizes of the  $\text{Ly}\alpha$  and radio structures are fairly similar, although the filament extends beyond the radio hotspot by  $4''$  ( $30h_{65}^{-1} \text{ kpc}$ ). The tip of the filament is co-spatial with a galaxy (Fig. 5). Although it is tempting to infer a connection between the two, spectroscopic observations show that the galaxy is foreground at  $z = 0.891$  (Chapter 7) and cannot be related. There is also a hint of a filament extending out to the SE.

Interestingly, the mm emission shown in Figure 5 seems almost completely anti-correlated with the  $\text{Ly}\alpha$ . The  $\text{Ly}\alpha$  cone and filament appear nearly orthogonal to the cold gas and dust. This morphology seems indicative of an outflow as it resembles luminous starburst galaxies such as M 82. In starburst galaxies this is usually interpreted as being caused by a starburst driven superwind which blows out stellar debris and interstellar gas and dust from the central part of the galaxy (e.g., Strickland & Stevens 2000; Ohya et al. 2002).

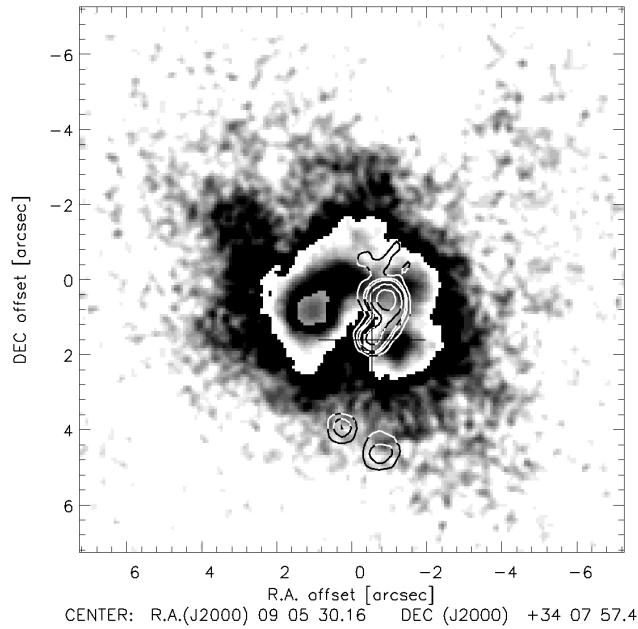


**Figure 7** — A continuum-subtracted Ly $\alpha$  image (grayscale) of B2 0902+34 with high resolution 4.9 GHz VLA radio map (contours; Carilli 1995) overlaid. The radio core is identified with a cross, and the contour levels are 0.2, 0.8, 1.6, 6.4, and 25.6 mJy beam $^{-1}$ .

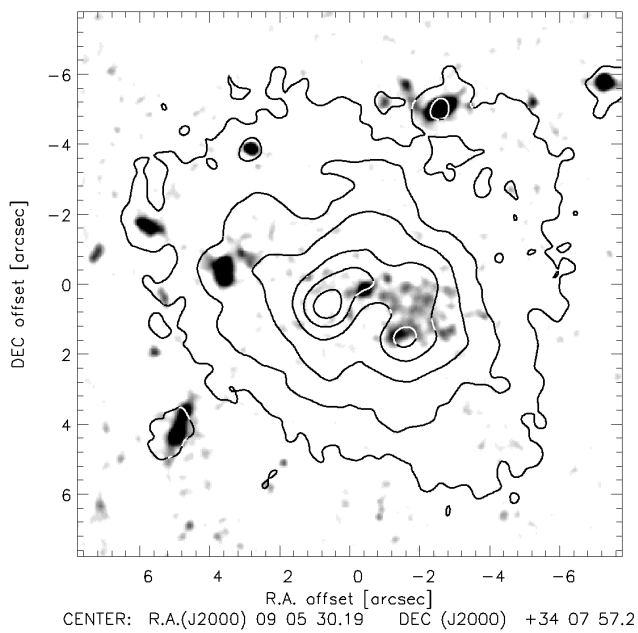


**Figure 8** — Narrow-band image contours of B2 0902+34 superposed on the HST F622W image. The contour levels are  $8.4 \times 10^{-19} \times (8, 20, 40, 80, 120, 160)$  ergs $^{-1}$  cm $^{-2}$  arcsec $^{-2}$ , include continuum emission, and have not been corrected for extinction.

### 3.3 B2 0902+34

Figure 7 shows the Ly $\alpha$  image and radio map overlay of B2 0902+34. The HST image with narrow-band contours is shown in Figure 8.

#### *Central region*

Unlike in 4C 41.17 and 4C 60.07 the central part of the Ly $\alpha$  and continuum emission in B2 0902+34 is not dominated by a high surface brightness elongated, radio-aligned structure. Instead the overall morphology appears more diffuse and bimodal, surrounding the radio core and a curved jet to the north (consistent with Carilli 1995; Pentericci et al. 1999; Fabian, Crawford, & Iwasawa 2002). Figure 8 shows that while there is faint continuum emission to the west co-spatial with the lower luminosity Ly $\alpha$  peak, there seems to be little continuum emission associated with the brightest peak. Dust is not likely to be an important factor in obscuring any continuum on the E, because the Ly $\alpha$  should then be completely extinguished in contrast to the observations and because Archibald et al. (2001) did not find strong signatures of thermal dust emission in the sub-mm. Therefore, the source of ionization in this region remains somewhat unclear, reminiscent of the radio-quiet Ly $\alpha$  halos but with the important distinction that there is a luminous AGN nearby. Given that the radio axis of the source is oriented close to the line of sight (Carilli 1995), beaming effects are expected to be important. A possibility is that the bright Ly $\alpha$  is due to scattered light from the AGN or the result of collisional excitation. Based on the relatively flat UV-optical spectral energy distribution, Eisenhardt & Dickinson (1992) argued for the presence of a large population of young stars. Both the inner Ly $\alpha$  morphology and the HST continuum might be better understood as being due to a shocked cocoon of gas and possibly shock-induced star formation associated with the approaching radio lobe.

#### *Outer region and filamentary structure*

The extended emission line region subtends approximately  $10'' \times 8''$  on the sky ( $\sim 80h_{65}^{-1} \text{ kpc} \times 64h_{65}^{-1} \text{ kpc}$ ). Again the radio and Ly $\alpha$  structures are roughly comparable in size, and the brightest radio and line emission are on the same side of the core. However, the radio emission near bright Ly $\alpha$  emission is strongly polarized, unlike 4C 41.17 and 4C 60.07. This could be understood if the radio jet in B2 0902+34 is pointed towards us. The shorter line of sight through the gaseous medium would cause less depolarization (the Laing-Garrington effect; Garrington & Conway 1991), and at the same time would boost the core and jet emission due to relativistic beaming.

There are few signs of large scale filamentary emission in B2 0902+34. They could be hidden if the filaments preferentially follow the radio axis and are similarly elongated along our line of sight.

## 4 Discussion

Our deep, sub-arcsecond seeing narrow-band imaging observations show previously unknown, complex morphologies in giant Ly $\alpha$  nebulae around three HzRGs. Since the nebulae are centered on massive forming galaxies these structures may provide new insights about this galaxy formation process and the importance of starburst/AGN feedback. We will discuss some of the general conclusions that can be drawn from these data. A more in-depth understanding of the nature of the nebulae will require

analysis of spectroscopic observations, which will be presented in a following paper. For now we note that these and other spectroscopic evidence for HzRGs show that the nebulae, at least along the *major* axes of the radio sources, are enriched and ionized i.e. are not composed of pure primordial (H, He) gas and not due to Ly $\alpha$  scattering off cold gas (HI). This is based on the detection of C and O along the radio sources over many tens of kpc (e.g., Overzier et al. 2001; Maxfield et al. 2002; van Breugel et al. 2002; Jarvis et al. 2002; Villar-Martín et al. 2002), including evidence for enriched material C IV in undisturbed regions *beyond* radio hotspots (Maxfield et al. 2002; Villar-Martín et al. 2002).

Some of the properties of radio galaxy Ly $\alpha$  nebulae, to the extent that they could be studied with mostly 4 m class telescopes, have been discussed by others (e.g., Chambers et al. 1990; Eisenhardt & Dickinson 1992; Hippelein & Meisenheimer 1993; McCarthy 1993; van Ojik et al. 1996; van Ojik et al. 1997; Rocca-Volmerange 1999; Venemans et al. 2002). Here we will focus on the newly discovered features in our images: the very large low surface brightness outer regions, the long radial filaments and cone-shaped structures, and the (indirect) evidence for extended Ly $\alpha$  absorption. It is important to reiterate that radio-quiet Ly $\alpha$  nebulae also exist (Steidel et al. 2000; Francis et al. 2001). It is not known whether the gas in these nebulae is enriched or not, and the available images are of insufficient detail to determine whether they exhibit similar filamentary structures as the HzRG nebulae.

A plausible scenario for explaining the origin of Ly $\alpha$  nebulae is one in which cold gas from the “Dark Ages” is accreted in large Cold Dark Matter halos. In contrast to the classical picture of gas cooling from the virial temperature,  $T \sim 10^6$  K for a typical dark matter halo, recent theoretical models predict that most of the infalling gas may not heat to virial temperatures but remains at  $T \sim 10^4$  K because of efficient Ly $\alpha$  cooling (Fardal et al. 2001; Haiman, Spaans, & Quataert 2000). There is strong evidence that HzRGs reside in (proto)-clusters (e.g., Pentericci et al. 2000; Venemans et al. 2002), and a viable scenario to explain these nebulae might then be that they are signatures of cooling flows.

As the gas accretes it will condense into stars and galaxies, and thus cooling flow and star formation are intimately linked. The Ly $\alpha$  emission associated with the release of gravitational potential energy is expected to be more spatially extended than emission related to the starburst and they are expected to be of similar magnitude in the most luminous objects (Fardal et al. 2001). The fairly smooth and very extended outer regions orthogonal to the radio sources suggest that these could be the remnants of these initial, undisturbed accretion flows. The surface brightness profile in the outer parts of the SE corner of 4C 41.17, which appears to be the least disturbed part of the nebula, drops with radius as approximately  $I(r) \propto r^{-2}$  and would be consistent with theoretical predictions for cooling halos (Haiman, Spaans, & Quataert 2000).

What about the radial filamentary and cone-shaped structures? How did these form in such a scenario? Here some lessons might be learned from nearby cooling flow clusters, Abell 1795 (Fabian et al. 2001) and NGC 1275 (Conselice, Gallagher, & Wyse 2001; Fabian et al. 2001), starburst superwinds such as in M 82, Arp 220 (e.g., Heckman, Armus, & Miley 1990), and Seyfert II’s (NGC 1068; Dopita et al. 2002).



#### 4.1 Cooling flows and radio lobes

In Abell 1795 there is a long,  $\sim 80$  kpc (projected size), radially directed emission-line and X-ray filament associated with the central cD galaxy. Fabian et al. (2001) consider several possible scenarios to explain this, including a “conrail” induced by ram pressure from the radio source. However, based on kinematic and cooling time considerations, and the fact that the cD galaxy is not quite centered at the X-ray halo, Fabian et al. conclude that the simplest explanation would be that the filament is a cooling wake behind the galaxy as it moves within the X-ray halo. It is possible that the bright, single filament in 4C 60.07 might be explained in this way but we consider this unlikely because of evidence for a very low surface brightness cone-like structure (Fig. 4). The multiple radially directed filaments in 4C 41.17 would also be inconsistent with such a model.

In NGC 1275 numerous radial emission-line filaments are found up to  $\sim 50$  kpc from the central AGN, with some tangential features at large radii. These features overlap with a large radio halo centered on the galaxy. The fairly constant surface brightness along the lengths of the filaments and inferred physical parameters suggest that the filaments formed as a result of compression of the intracluster gas by the expanding radio source (Conselice, Gallagher, & Wyse 2001). The correlation between emission-line and radio source asymmetries in each of the three radio galaxies shows that radio jets and lobes must indeed have a significant impact on the ambient gas emissivity and emission-line morphology. Also, the eastern radio lobe of 4C 41.17 appears to have associated “plumes” of enhanced emission straddling the lobe at both the SW and SE, and the sizes of the radio structures are comparable to those of the emission line gas.

We note that even if the filaments are at a significant distance from the observed radio source components, such as the SW lobe of 4C 41.17, there still is a good reason to believe that they may be causally related, in particular if there is supporting kinematic evidence (see 4C 29.30 for a nearby example; van Breugel et al. 1986). In the canonical picture of radio sources the hotspots and lobes are surrounded by bowshocks and cocoons of radio quiet, shock heated gas with scale sizes which are significantly larger than the observed radio emission (Carilli, Perley, & Dreher 1988; Begelman & Cioffi 1989). The emission-line filaments are then located at the interface of the cocoons and the ambient gas and are not in direct contact with the radio lobes or hotspots and can even extend *beyond* radio hotspots (Figs. 1,4; Maxfield et al. 2002) if one accounts for projection effects and the fact that the radio observations only show the highest surface brightness regions.

#### 4.2 Starburst superwinds

Although HzRGs may not resemble “normal” starburst systems in the strictest sense, it seems reasonable to explore whether galactic superwinds can explain the emission-line morphologies. Observations of low redshift starburst galaxies show weakly collimated bipolar outflows of gas with outflow velocities of several hundred  $\text{km s}^{-1}$  and up to scales of  $\sim 10$  kpc (Heckman, Armus, & Miley 1990).  $\text{H}\alpha$  emission line observations that trace this gas show filaments and arclike structures which are possibly not too

dissimilar from the filaments that we can discern in the higher redshift Ly $\alpha$  nebulae. Spectroscopic evidence for galactic outflows has been found also at high redshifts (e.g., Pettini et al. 1998; Pettini et al. 2001; Dawson et al. 2002) from metal absorption lines that are blue-shifted by a few hundred to a few thousand km s $^{-1}$  relative to the estimated systemic velocity of the galaxies. Recent observations of C IV absorptions systems along the lines of sight to QSOs indicate enrichment of the intra-cluster medium (ICM) even at redshifts higher than  $z \sim 5$  (Rauch et al. 2001) which may have been caused by these outflows.

For a galactic outflow powered by a superwind to occur, the star formation rate per unit area  $\Sigma_{\text{SFR}}$  must satisfy the empirical relation  $\Sigma_{\text{SFR}} \gtrsim 0.1 \text{ M}_{\odot} \text{ yr}^{-1} \text{ kpc}^{-2}$  (e.g., Heckman 2001). As we have argued above, based on sub-mm detections and direct observations of stellar absorption lines, HzRGs are massive star forming systems, with SFRs of approximately  $1000\text{--}2000 \text{ M}_{\odot} \text{ yr}^{-1}$ . This implies SFR surface densities of  $\Sigma_{\text{SFR}} \gtrsim 0.4 \text{ M}_{\odot} \text{ yr}^{-1} \text{ kpc}^{-2}$  for the regions corresponding to the extent of the  $K$ -band (rest-frame  $B$ ) continuum. Therefore, the minimum condition for an outflow can be satisfied easily. Similarly, the SFR surface density based on the UV flux and extent of the “undisturbed” southern region in 4C 41.17  $\Sigma_{\text{SFR}} \gtrsim 33 \text{ M}_{\odot} \text{ yr}^{-1} / 100 \text{ kpc}^2 \gtrsim 0.3 \text{ M}_{\odot} \text{ yr}^{-1} \text{ kpc}^{-2}$  would also support a galactic wind.

Models show that starburst outflows fill an over-pressured cavity of hot gas and expand into superbubbles, but they are usually not energetic enough for the bubbles to burst and the gas to escape from the host galaxy (Heckman 2001). This means that for the massive HzRGs this material is likely to reside at large radii but still within the potential well of the galaxy. Taniguchi & Shioya (2000) modelled the outflow of gas and find the following relation for the radii of the shells:

$$r_{\text{shell}} \sim 110 L_{\text{mech},43}^{0.2} n_{\text{H},-5}^{-0.2} t_8^{0.6} \text{ kpc},$$

with  $L_{\text{mech}} \sim 10^{43} \text{ erg s}^{-1} \text{ M}_{\odot}^{-1}$  the mechanical luminosity released by supernovae in the starburst,  $n_{\text{H},-5}$  the hydrogen density in units of  $10^{-5} \text{ cm}^{-3}$  and  $t_8$  the age of the starburst in units of  $10^8 \text{ yr}$ . Dey et al. (1997) modelled the stellar population of 4C 41.17 with a starburst of duration  $1.6 \times 10^7 \text{ yr}$  and an older population of stars younger than  $6 \times 10^8 \text{ yr}$ . This gives a lower and upper limit for  $t_8$  and Chambers et al. (1990) estimated  $n_{\text{H}} \sim n_e f_v$  with  $n_e$  the electron density and  $f_v$  the volume filling factor of the clouds to be of order  $20 \times 10^{-5} \text{ cm}^{-3}$ . Applying these estimates to 4C 41.17 we obtain:  $20 \text{ kpc} \leq r_{\text{shell}} \leq 170 \text{ kpc}$ , resulting in a characteristic extent of the superwind shells  $l = 2r_{\text{shell}} \sim 150 \text{ kpc}$ , consistent with the sizes for the nebulae presented here.

### 4.3 Radiation pressure driven outflows

Recently, Dopita et al. (2002) presented a model to explain the origin and kinematics of the narrow line regions in Seyfert Galaxies. In this model ionized gas and dust are electrically locked together and streaming from ionization fronts around photo-evaporating clouds located in the ionization cones of the AGN. A similar process might be envisaged in HzRGs. If the dust is destroyed somewhere along the outflow, then the gas will continue to flow outward from the cloud, but radiation pressure will no longer dominate the dynamics. Aguirre et al. (2001) also found that dusty outflows

might be radiation pressure driven and can reach distances of up to a few 100 kpc. These models suggest that radiative ablation by the central source may be a significant if not dominant contributor to outflows.

Such a scenario would explain why the filaments are all oriented radially, and why the focal point of the tails of the SW emission line cloud in 4C 41.17 seems to be the radio core while there is no obvious connection with the radio emission.

#### 4.4 Obscured AGN

For all three galaxies in the sample, and for 4C 23.56 which was extensively studied by Knopp & Chambers (1997), the radio core appears to be located in a hole or at least a depression in the bright central part of the Ly $\alpha$  line emission. The best example of this is 4C 41.17 where the UV continuum also shows a gap of approximately  $0''.4$  ( $\sim 3h_{65}^{-1}$  kpc). Because the dips are also apparent in the UV continuum and because there appears to be very bright emission on either side, the gap must be due to an obscuring medium of high optical depth. MRC 1243+036 is the only HzRG with a well studied Ly $\alpha$  halo for which the radio core appears associated with a peak in Ly $\alpha$  (van Ojik et al. 1996). However, the central shape of MRC 1243+036 bears close resemblance to the central cone shapes of 4C 60.07, and it is quite possible that the central region would show two distinct components with the radio core being in between if it were observed at higher resolution.

Hippelein & Meisenheimer (1993) were the first to notice the gap in the Ly $\alpha$  image of 4C 41.17 and interpreted it as being due to a foreground absorber being part of the Ly $\alpha$  forest. The strong sub-mm dust detection of 4C 41.17 led Dunlop et al. (1994) to speculate that this gap might rather be due to a dusty disk. While this remains a viable option, in the case of 4C 60.07 which shows a similar UV continuum and emission line dip, sub-mm observations show that *most* of the dust is located “outside” the galaxy.

At least two of the three radio galaxies that we present here, show a distinct biconical shape in the brightest parts of their nebulosities. This morphology suggests that the nucleus contributes significantly to the photoionization, and is surrounded by an obscuring torus which we observe under an angle as favored by the quasar-radio galaxy unification scheme (Barthel 1989). This putative torus would be much larger than what is traditionally assumed and it would be more appropriate to refer to this feature as a dust lane. Dust lanes have been studied in nearby FR I radio galaxies (Verdoes Kleijn et al. 1999), and appear to be orthogonal to the radio axis independent of the orientation of the galactic disk. Verdoes et al. found that these features typically range from 200 pc to 4.5 kpc, while features larger than  $\sim 1$  kpc show peculiar morphologies and are possibly still settling towards stable orbits. This suggests that the large sizes seen in HzRGs might be the result of the availability of substantial amounts of debris and that the torus/dust lane is still forming and has not yet reached its final configuration.

## 5 Conclusions

We have presented a morphological study of the Ly $\alpha$  emission line nebulae of three radio galaxies at redshifts  $z \sim 3.4 - 3.8$ .

Our new findings are that the emission line nebulae show giant, 100 - 200 kpc low surface brightness emission and large (up to 80 kpc) filamentary and cone-shaped structures, which are even more extended than known previously. We have also found indirect evidence for extended Ly $\alpha$  absorption due to neighboring galaxies in the local foreground to the 4C 41.17 nebula and, in all three cases, that the AGN appear obscured by surrounding dust.

In order to explain these observations, we have presented a scenario in which primordial cooling flows in Cold Dark Matter halos form multiple stellar systems which merge, building the stellar bulges of future massive galaxies and triggering (radio-loud) SMBH activity. The radio jets, starburst superwinds and radiative ablation from the AGN may all contribute to cause the observed radially directed filamentary structures, in at least two of the three objects studied, and may provide a feedback mechanism which regulates stellar bulge and SMBH growth. To study these processes will require further observations of the physical properties of the gas, and numerical simulations of the effects of jets and AGN radiation on dusty, astrophysical plasmas. Some regions of the outermost halos appear unaffected by any radio/AGN activity. This suggests that this gas must either be infalling for the first time or be a remnant of previous outflows.

Deep spectroscopy targeting non-resonant emission lines are important to constrain the various scenarios, and determine the gas kinematics, metallicities and sources of ionization. The observations presented here also show that filamentary structure is not always aligned with the radio axis, and that long slit spectroscopy can easily miss large, bright filaments. Therefore, to fully exploit narrow-band emission-line images as a tool for studies of galaxy formation requires the use of "3-Dimensional" (2-D spatial + 1-D spectral) imaging devices on large telescopes (van Breugel & Bland-Hawthorn 2000). Several such devices are currently being build, including the LLNL Imaging Fourier Transform Spectrometer (Wurtz et al.2001), and the OSIRIS imaging spectrograph for the Spanish 10.4 m telescope GTC at La Palma (Cepa et al.2001).

## Acknowledgements

It is a pleasure to thank Chris Carilli for making available the VLA radio maps, Padelis Papadopoulos for providing us with the PdB images, Björn Heijligers for IDL tips and tricks, and the staff at W.M. Keck Observatory for their efficient assistance. We thank the referee, Montse Villar-Martín for many helpful suggestions that improved the manuscript. The work of M.R., W.d.V., W.v.B., A.S., and M.L. was performed under the auspices of the U.S. Department of Energy, National Nuclear Security Administration by the University of California, Lawrence Livermore National Laboratory under contract No. W-7405-Eng-48. W.v.B. also acknowledges NASA grants GO 5429, 5765, 5940, 6608, and 8183 in support of HzRG research with HST at LLNL. M.L. performed part of this work at the Jet Propulsion Laboratory, California Institute of Technology, under contract with NASA. M.D. acknowledges the support of the ANU and the Australian Research Council (ARC) for his ARC Australian Federation Fellowship, and also under the ARC Discovery project DP0208445. This research has made use of the USNOFS Image and Catalogue Archive operated by the United States

Naval Observatory, Flagstaff Station (<http://www.nofs.navy.mil/data/fchpix/>), and the NASA/IPAC Extragalactic Database (NED) which is operated by the Jet Propulsion Laboratory, California Institute of Technology, under contract with the National Aeronautics and Space Administration.

## References

- Adam, G., Rocca-Volmerange, B., Gérard, S., Ferruit, P. & Bacon, R., 1997, *A&A*, 326, 501  
Aguirre, A., Hernquist, L., Schaye, J., Katz, N., Weinberg, D.H. & Gardner, J., 2001, *ApJ*, 561, 521  
Archibald, E.N., Dunlop, J.S., Hughes, D.H., Rawlings, S., Eales, S.A. & Ivison, R.J., 2001, *MNRAS*, 323, 417  
Barthel, P.D., 1989, *ApJ*, 336, 606  
Baum, S.A., Heckman, T.M., & van Breugel, W., 1992, *ApJ*, 389, 208  
Begelman, M. C. & Cioffi, D. F. 1989, *ApJ*, 345, L21  
Bertin, E. & Arnouts, S., 1996, *A&A*, 117, 393  
Best, P.N., Longair, M.S. & Röttgering, H.J.A., 1998, *MNRAS*, 295, 549  
Best, P. N., Röttgering, H. J. A., & Longair, M. S. 2000a, *MNRAS*, 311, 1  
Best, P. N., Röttgering, H. J. A., & Longair, M. S. 2000b, *MNRAS*, 311, 23  
Bicknell, G., Sutherland, R., van Breugel, W., Dopita, M., Dey, A. & Miley, G. 2000, *ApJ*, 540, 678  
Binette, L., Kurk, J. D., Villar-Martín, M., & Röttgering, H. J. A. 2000, *A&A*, 356, 23  
Blandford, R. D. & Payne, D. G. 1982, *MNRAS*, 199, 883  
Briggs, F. H., Sorar, E. & Taramopoulos, A., 1993, *ApJ*, 415, L99  
Cardelli, J.A., Clayton, G.C. & Mathis, J.S. 1989, *ApJ*, 345, 245  
Carilli, C. L., Perley, R. A., & Dreher, J. H. 1988, *ApJ*, 334, L73  
Carilli, C.L., Owen, F.N. & Harris, D.E. 1994, *AJ*, 107, 480  
Carilli, C.L., 1995, *A&A*, 298, 77  
Carilli, C. L. & Barthel, P. D. 1996, *A&A Rev.*, 7, 1  
Carilli, C.L., Röttgering, H.J.A., van Ojik, R., Miley, G.K. & van Breugel, W.J.M. 1997, *ApJ*, 109, 1  
Cepa, J., González-Serrano, J. I., & del Río, M. S. 2001, *The Promise of the Herschel Space Observatory*.  
Eds. G.L. Pilbratt, J. Cernicharo, A.M. Heras, T. Prusti, & R. Harris. ESA-SP 460, p. 373, 460, 373  
Chambers, K.C., Miley, G.K. & van Breugel, W.J.M., 1990, *ApJ*, 363, 21  
Chambers, K.C., Miley, G.K., van Breugel, W.J.M., Bremer, M.A.R., Huang, J.S. & Trentham, N.A. 1996,  
*ApJ*, 106, 247  
Chapman, S.C., Lewis, G.F., Scott, D., Richards, E., Borys, C., Steidel, C.C., Adelberger, K.L., & Shapley,  
A.E., 2001, *ApJ*, 548, L17  
Chen, H-W., Lanzetta, K. & Webb, J. 2001, *ApJ*, 556, 158  
Conselice, C. J., Gallagher, J. S., & Wyse, R. F. G. 2001, *AJ*, 122, 2281  
Dawson, S., Spinrad, H., Stern, D., Dey, A., van Breugel, W., de Vries, W. & Reuland, M., 2002, *ApJ*, 570,  
92  
De Breuck, C., van Breugel, W., Stanford, S.A., Röttgering, H., Miley, G. & Stern, D., 2002a, *AJ*, 123, 637  
De Breuck, C. et al., 2002b, submitted.  
Dey, A., van Breugel, W., Vacca, W.D. & Antonucci, R., 1997, *ApJ*, 490, 698  
Dey, A., 1999, in *Proc. KNAW Colloq.* 49, 19  
Dopita, M.A., Groves, B.A., Sutherland, R.S., Binette, L. & Cecil, G., 2002, *astro-ph/0203360*  
Dunlop, J. S., Hughes, D. H., Rawlings, S., Eales, S. A., & Ward, M. J., 1994, *Nature*, 370, 347  
Eisenhardt, P. & Dickinson, M., 1992, *ApJ*, 399, L47  
Fabian, A. C., Sanders, J. S., Ettori, S., Taylor, G. B., Allen, S. W., Crawford, C. S., Iwasawa, K., & John-  
stone, R. M. 2001, *MNRAS*, 321, L33  
Fabian, A. C., Crawford, C. S. & Iwasawa, K., 2002, *MNRAS*, 331, L57  
Fanaroff, B. L. & Riley, J. M. 1974, *MNRAS*, 167, 31P  
Fardal, M. A., Katz, N., Gardner, J. P., Hernquist, L., Weinberg, D. H., & Davé, R., 2001, *ApJ*, 562, 605  
Ferrarese, L. & Merritt, D., 2000, *ApJ*, 539, L9  
Francis, P. J. et al. 2001, *ApJ*, 554, 1001

- Garrington, S.T. & Conway, R.G., 1991, MNRAS, 250, 198
- Gebhardt, K. et al., 2000, ApJ, 539, 13
- Graham, J. R. et al., 1994, ApJ, 420, L5
- Haiman, Z., Spaans, M. & Quataert, E., 2000, ApJ, 537, L5
- Haiman, Z. & Rees, M.J., 2001, ApJ, 556, 87
- Heckman, T. M., Miley, G. K., Balick, B., van Breugel, W. J. M., & Butcher, H. R. 1982, ApJ, 262, 529
- Heckman, T. M., Armus, L., & Miley, G. K. 1990, ApJ, 74, 833
- Heckman, T.M., 2001, astro-ph/0107438
- Hippelein, H. & Meisenheimer, K., 1993, Nature, 362, 224
- Inskip, K. J., Best, P. N., Rawlings, S., Longair, M. S., Cotter, G., Röttgering, H. J. A., & Eales, S. 2002a, MNRAS, accepted, astro-ph/0208548
- Inskip, K. J., Best, P. N., Röttgering, H. J. A., Rawlings, S., Cotter, G., & Longair, M. S. 2002b, MNRAS, accepted, astro-ph/0208549
- Iverson, R. J. et al. 1998, ApJ, 494, 211
- Iverson, R.J., Dunlop, J.S., Smail, I., Dey, A., Liu, M.C. & Graham, J.R., 2000, ApJ, 542, 27
- Jarvis, M. J., Rawlings, S., Eales, S., Blundell, K. M., Bunker, A. J., Croft, S., McLure, R. J., & Willott, C. J. 2001, MNRAS, 326, 1585
- Jarvis, M. J., Wilman, R.J, Röttgering, H.J.A & Binette, L., 2002, MNRAS, accepted
- Knopp, G.P. & Chambers, K.C. 1997, ApJ, 109, 367
- Leitherer, C., Ferguson, H. C., Heckman, T. M., & Lowenthal, J. D. 1995, ApJ, 454, L19
- Lilly, S.J., 1988, ApJ, 333, 161
- Magorrian, J. et al., 1998, AJ, 115, 2285
- Martín-Mirones, J.M., Martínez-Gonzalez, E., Gonzalez-Serrano, J.I. & Sanz, J.L., 1995, ApJ, 440, 191
- Massey, P., Strobel, K., Barnes, J.V. & Anderson, E., 1988, ApJ, 328, 315
- Maxfield, L., Spinrad, H., Stern, D., Dey, A., & Dickinson, M. 2002, AJ, 123, 2321
- McCarthy, P. J., Spinrad, H., Dickinson, M., van Breugel, W., Liebert, J., Djorgovski, S., & Eisenhardt, P. 1990, ApJ, 365, 487
- McCarthy, P. J., 1993, ARA&A, 31, 639
- McCarthy, P. J., Spinrad, H., & van Breugel, W. 1995, ApJ, 99, 27
- Monet, D. G. 1998, American Astronomical Society Meeting, 193, 112003
- Ohyama, Y. et al. 2002, astro-ph/0209442
- Overzier, R. A., Röttgering, H. J. A., Kurk, J. D., & De Breuck, C. 2001, A&A, 370, L39
- Papadopoulos, P.P., Röttgering, H.J.A., van der Werf, P.P., Guilloteau, S., Omont, A., van Breugel, W.J.M. & Tilanus, R.P.J., 2000, ApJ, 528, 626
- Pentericci, L., Röttgering, H.J.A., Miley, G.K., McCarthy, P., Spinrad, H., van Breugel, W.J.M. & Macchetto, F., 1999, A&A, 341, 329
- Pentericci, L. et al. 2000, A&A, 361, L25
- Pettini, M., Kellogg, M., Steidel, C., Dickinson, M., Adelberger, K. & Giavalisco, M., 1998, ApJ, 508, 539
- Pettini, M., Shapley, A.E., Steidel, C.C., Cuby, J., Dickinson, M., Moorwood, A.F.M., Adelberger, K.L. & Giavalisco, M., 2001, ApJ, 554, 981
- Rauch, M., Sargent, W. L. W., & Barlow, T. A. 2001, ApJ, 554, 823
- Rees, M. J. 1978, Nature, 275, 516
- Reuland, M., Röttgering, H., van Breugel, W., & De Breuck, C. 2004, MNRAS, 353, 377
- Rocca-Volmerange, B. 1999, The Most Distant Radio Galaxies, 245
- Schlegel, D.J., Finkbeiner, D.P. & Davis, M., 1998, ApJ, 500, 525
- Sheinis, A.I., Miller, J.M., Bolte, M. & 2000, Proc. SPIE, 4008, 522
- Silk, J. & Rees, M. J. 1998, A&A, 331, L1
- Steidel, C.C., Giavalisco, M., Pettini, M., Dickinson, M. & Adelberger, K.L. 1996, ApJ, 462, L17
- Steidel, C. C., Adelberger, K. L., Shapley, A. E., Pettini, M., Dickinson, M., & Giavalisco, M. 2000, ApJ, 532, 170
- Steidel, C. C., Pettini, M., & Adelberger, K. L. 2001, ApJ, 546, 665
- Strickland, D. K. & Stevens, I. R., 2000, MNRAS, 314, 511
- Tadhunter, C. N., Villar-Martin, M., Morganti, R., Bland-Hawthorn, J., & Axon, D. 2000, MNRAS, 314, 849

- Taniguchi, Y. & Shioya, Y. 2000, *ApJ*, 532, L13
- Trauger, J. T. et al. 1994, *ApJ*, 435, L3
- Uson, J. M., Bagri, D. S., & Cornwell, T. J. 1991, *Physical Review Letters*, 67, 3328
- van Breugel, W., Miley, G., Heckman, T., Butcher, H. & Bridle, A., 1985, *ApJ*, 290, 496
- van Breugel, W. J. M., Heckman, T. M., Miley, G. K. & Filippenko, A. V., 1986, *ApJ*, 311, 58
- van Breugel, W.J.M., Stanford, S.A., Spinrad, H., Stern, D. & Graham, J.R., 1998, *ApJ*, 502, 614
- van Breugel, W. et al. 1999 in *Proc. KNAW Colloq.* 49, 49
- van Breugel, W. & Bland-Hawthorn, J. 2000, *PASP*, 112, 579
- van Breugel, W. et al. 2002, *astro-ph/0209173*
- van Ojik, R., Röttgering, H.J.A., Carilli, C.L., Miley, G.K., Bremer, M.N. & Macchetto, F., 1996, *A&A*, 313, 25
- van Ojik, R., Röttgering, H.J.A., Miley, G.K. & Hunstead, R.W., 1997, *A&A*, 317, 358
- Venemans, B. P. et al. 2002, *ApJ*, 569, L11
- Verdoes Kleijn, G. A., Baum, S. A., de Zeeuw, P. T., & O'Dea, C. P. 1999, *AJ*, 118, 2592
- Vernet, J., Fosbury, R. A. E., Villar-Martín, M., Cohen, M. H., Cimatti, A., di Serego Alighieri, S., & Goodrich, R. W. 2001, *A&A*, 366, 7
- Villar-Martín, M., Tadhunter, C., Morganti, R., Axon, D., & Koekemoer, A. 1999, *MNRAS*, 307, 24
- Villar-Martín, M., Vernet, J, di Serego Alighieri, S., Fosbury, R., Pentericci, L., Cohen, M., Goodrich, R. & Humphrey, A., 2002, *MNRAS*, accepted, *astro-ph/0206118*
- Wurtz, R., Wishnow, E., Blais-Ouellette, S., Cook, K., Carr, D., Grandmont, F., Lewis, I. & Stubbs, C., 2001, *Galaxies: the Third Dimension*. Eds. M. Rosado, L. Binette, L. Arias, *ASP Conf. Ser.* *astro-ph/0203501*





---

# Chapter 7

---

## Metal enriched gaseous halos around distant radio galaxies

Michiel Reuland, Wil van Breugel, Wim de Vries, Huub Röttgering, Michael Dopita, Mark Lacy, Arjun Dey, George Miley, S.A. Stanford, Bram Venemans, Hyron Spinrad, Steve Dawson, Daniel Stern, *Astronomy and Astrophysics*, submitted

We present the results of an optical and near-IR spectroscopic study of giant nebular emission line halos associated with the  $z > 3$  radio galaxies 4C 41.17, 4C 60.07 and B2 0902+34. Previous deep narrow-band rest-frame Ly $\alpha$  imaging revealed cone shapes and filamentary structures (with sizes up to 100 kpc), possibly connected to AGN and starburst feedback. In agreement with previous studies we find that the inner high surface-brightness regions exhibit disturbed kinematics with velocity dispersions  $>1000 \text{ km s}^{-1}$  that seem to be closely related to the radio source. The outer regions of the halos exhibit kinematics with typical velocity dispersions of a few hundred  $\text{km s}^{-1}$ , and velocity characteristics consistent with rotation.

Spectroscopic evidence for the presence of enriched material (oxygen) throughout the nebula of 4C 41.17 (up to a distance of  $\sim 60$  kpc along the radio-axis) is presented. The oxygen emission has a similar spatial and kinematic distribution as the Ly $\alpha$  emission. We argue that this implies that the Ly $\alpha$  cannot be purely scattered light, and that the halo had already been enriched by a previous generation of stars when the Universe was approximately 10% of its current age. It is also possible that the extended oxygen has been transported from the central starburst region aided by the radio source. We discuss various feedback processes and their implications for galaxy formation in the context of the nature and origin of these halos.

### 1 Introduction

**U**NDERSTANDING the coevolution of galaxy spheroids and their central massive black holes is one of the key issues in modern cosmology. There are at least two reasons why high redshift radio galaxies (HzRGs;  $z > 3$ ) are prime objects for studying the processes involved. First, because they are among the most luminous and massive known galaxies in the early Universe (e.g., De Breuck et al. 2002), they can be studied in great detail. Secondly, we observe them early in their formation process when their super-massive black holes (SMBHs) are highly active.

Within standard Cold Dark Matter (CDM) scenarios, massive galaxies grow in hierarchical fashion through merging of smaller stellar structures and their central black holes likely grow in similar fashion or may be primordial (Loeb 1993; Silk & Rees 1998; Kauffmann & Haehnelt 2000). In either way, outflows and radiation from active SMBHs are expected to affect profoundly the evolution of their parent galaxies and their environment. Models describing the formation of massive galaxies and clusters also indicate the importance of feedback, because heating is required to prevent the condensation of more (massive) galaxies than are observed (e.g., Benson et al. 2003). Additionally, outflows could provide a source for the chemical enrichment of the intergalactic medium seen at high redshifts (e.g., Rauch et al. 2001; Aguirre et al. 2001). While there is consensus that feedback in some form must be important, there is an ongoing debate about which manifestations dominate and the scales on which they operate.

Most HzRGs are known to be embedded in dense gaseous environments (e.g., McCarthy 1993; Hippelein & Meisenheimer 1993; van Ojik et al. 1996; Athreya et al. 1998; Pentericci et al. 2000; Papadopoulos et al. 2000; Wilman et al. 2004). Because of their large spatial extents these gaseous reservoirs are excellent laboratories for studying feedback processes at high redshift in detail.

In paper I of this series (Reuland et al. 2003) we presented narrow-band images with unprecedented sensitivity of three HzRGs (B2 0902+34, 4C 60.07, and 4C 41.17). These images were obtained at the Keck II 10 m telescope using custom-made, high-throughput interference filters with bandpasses centered at the redshifted Ly $\alpha$  line. The observations showed very luminous ( $L_{\text{Ly}\alpha} \simeq 10^{45} \text{ erg s}^{-1}$ ) and extended ( $\sim 200$  kpc) emission line nebulae with spectacular filamentary structures, ionization cones, and multiple sharply bounded regions of enhanced emission, all indicative of strong interactions as expected from the scenario painted above. We argued that the extended Ly $\alpha$  nebulae may represent gas cooling in massive CDM halos, supplying material for the continued growth of the galaxies at their center. This growth process then could be responsible for feedback mechanisms through radio jets, supernova explosions, and radiation pressure from the active galactic nucleus (AGN), resulting in large scale outflows. The extended X-ray halo around 4C 41.17 provides further evidence for a highly interactive environment in such systems (Scharf et al. 2003).

While the morphologies of the nebulae were revealing some connection to the central AGN/starburst and radio source, several key questions remained. First among these is whether the nebulae are actually ionized or, because Ly $\alpha$  is a resonance line, may be due to scattering of Ly $\alpha$  photons produced by the central AGN/starburst off surrounding, neutral hydrogen halos. In the latter case this could be primordial gas from the recombination epoch. Other questions are: what is the source of ionization and what is the chemical composition of the gas, what can we learn from the kinematics of various halo features (inner and outer regions, filaments, clouds interacting with radio jets etc.), can outflowing gas expel metals from the deep potential wells and enrich the intergalactic medium, and could this possibly affect accretion onto the massive forming galaxy and growth of its central black hole? AGN / gas feedback has been proposed as possible way to regulate galaxy and black hole growth (e.g., Silk & Rees 1998; King 2003; Sazonov et al. 2004), which might explain the close correlation

**Table 1** — Radio galaxies spectrographically observed. Positions of the radio core (Carilli et al. 1994, 1997; Carilli 1995) and the systemic redshifts based on the He II line adopted as the frame of reference in this paper.

| Source     | RA (J2000)  | DEC (J2000) | $z$   |
|------------|-------------|-------------|-------|
| B2 0902+34 | 09 05 30.11 | 34 07 55.9  | 3.389 |
| 4C 60.07   | 05 12 55.17 | 60 30 51.1  | 3.789 |
| 4C 41.17   | 06 50 52.14 | 41 30 30.7  | 3.798 |

between stellar system and black hole masses (e.g., Magorrian et al. 1998; Gebhardt et al. 2000; Ferrarese & Merritt 2000).

To help answer these questions we obtained optical and near-infrared spectra of these galaxies with the Keck telescopes. The observations were aimed at measuring the extent, intensity, and kinematics of Ly $\alpha$  and the luminous *non-resonance* lines, [O II]  $\lambda$ 3727 and [O III]  $\lambda$ 5007, at various position angles across the nebulae. This paper presents the results of these observations and considers their implications for the nature of the line emitting gas.

The structure of the paper is as follows: The choice of targets, observations and data analysis are described in §2. In §3 we present results for each of the targets. §4 is a discussion of the observed kinematics and line ratios of the halos. The implications for the origin and fate of the emission line halos are discussed in §5 and we provide a summary of our conclusions in §6.

We adopt cosmological parameters of  $\Omega_M = 0.3$ ,  $\Omega_\Lambda = 0.7$ ,  $H_0 = 65 \text{ km s}^{-1} \text{ Mpc}^{-1}$ , for which the age of the Universe is  $\sim 1.7 \text{ Gyr}$  at the redshifts ( $z = 3.4 - 3.8$ ) of our galaxies, and the angular-to-linear transformation is  $\sim 7.6 \text{ kpc arcsec}^{-1}$ .

## 2 Observations and data analysis

### 2.1 Sample Selection

The three objects selected for spectroscopic follow-up observations are shown in Table 1, with their positions and adopted redshifts. They were selected from amongst the galaxies observed in the course of our Keck imaging program described in Paper I.

The galaxy 4C 41.17 at  $z = 3.8$ , was one of the first  $z > 3$  galaxies to be discovered (Chambers et al. 1990) and for many purposes serves as an archetype HzRG. Optical (Dey et al. 1997) as well as sub-mm wavelength observations (Dunlop et al. 1994) have shown that it is a massive forming galaxy with a star formation rate of up to several thousand  $M_\odot \text{ yr}^{-1}$ . Recently, very extended X-ray emission was found around 4C 41.17, whose appearance follows the Ly $\alpha$  morphology closely (Scharf et al. 2003).

We selected 4C 60.07 ( $z = 3.8$ ; Chambers et al. 1996; Röttgering et al. 1997) because it shows both spatially and kinematically resolved CO emission (Papadopoulos et al. 2000; Greve et al. 2004). Interestingly, in Paper I it was found that the Ly $\alpha$  halo has a very extended (76 kpc) filament which appears orthogonal to the major axis of the CO and dust emission.

B2 0902+34 ( $z = 3.4$ ; Lilly 1988) is thought to be a protogalaxy, dominated by young stars (Eisenhardt & Dickinson 1992). So far, it is one of only two HzRGs for which neutral hydrogen has been detected in absorption against the radio continuum (Uson et al. 1991; Cody & Braun 2003).

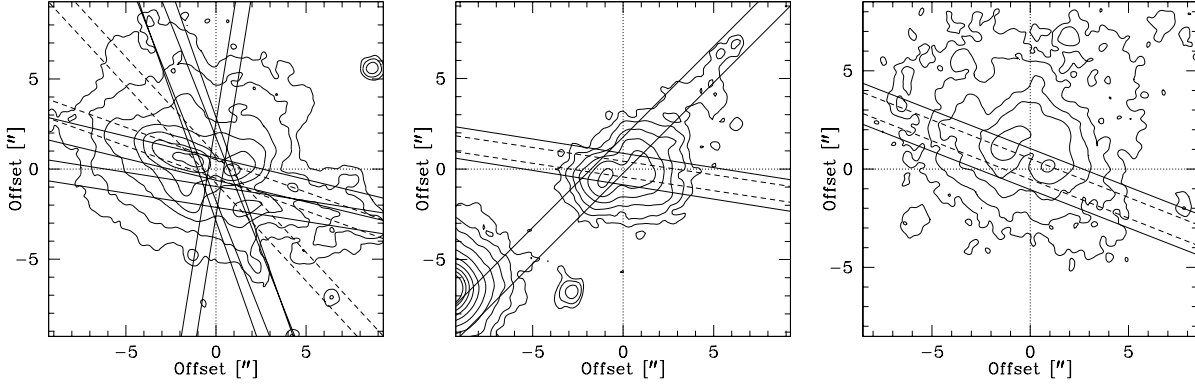


**Figure 1** — Contour representations of the narrow-band images of the Ly $\alpha$  emission line halos around 4C 41.17, 4C 60.07, and B2 0902+34 (left, middle, right) with the various PAs at which they were studied overlaid. The solid and dashed lines correspond with slit positions of the optical and near-IR spectroscopy respectively and the dotted crosshairs indicate the positions of the radio cores. North is up, East is to the left.

| Object     | UT Date    | Instrument | Setup        | Seeing<br>" | Slitwidth<br>" | Resolution<br>$\text{\AA}$ | Wavelength coverage<br>$\text{\AA}$ | P.A.<br>$^\circ$ | $t_{\text{obs}}$<br>s         |
|------------|------------|------------|--------------|-------------|----------------|----------------------------|-------------------------------------|------------------|-------------------------------|
| B2 0902+34 | 16/01/2002 | LRIS       | LS 600/5000  | 0.9         | 1.5            | 4                          | 5150–7650                           | 68.7             | 2 $\times$ 1800               |
| 4C 60.07   | 07/01/2002 | NIRSPEC    | Low Disp. N5 | 0.9         | 0.76           | 14                         | 14600–17400                         | 68.5             | 6 $\times$ 900                |
|            | 15/01/2002 | LRIS       | LS 600/7500  | 0.7         | 1.5            | 4                          | 5450–7600                           | 81.0             | 2 $\times$ 1800               |
| 4C 41.17   | 25/02/2001 | ESI        | Low Disp.    | 0.8         | 1.0            | 13 <sup>a</sup>            | 4000–9600                           | 135.2            | 3.5 $\times$ 1800             |
|            | 07/01/2002 | NIRSPEC    | Low Disp. N6 | 0.9         | 0.76           | 14                         | 15600–19800                         | 81.4             | 6 $\times$ 900                |
|            | 24/02/2001 | LRIS       | LS 600/7500  | 0.7         | 1.5            | 6                          | 5200–6100                           | 19.4             | 3 $\times$ 1800               |
|            | 23/02/2001 | LRIS       | MOS 300/5000 | 0.6         | 1.0            | 4                          | 4300–6600                           | 21.6             | 4 $\times$ 1800               |
|            | 10/12/1996 | LRISp      | LS 400/8500  | 0.9         | 1.0            | 8                          | 5500–9280                           | 76.5             | 28 $\times$ 1200 <sup>b</sup> |
|            | 15/01/2002 | LRIS       | MOS 400/8500 | 0.7         | 1.0            | 6                          | 5300–8000                           | 81.0             | 3 $\times$ 1800               |
|            | 03/02/1997 | LRIS       | LS 600/5000  | 0.9         | 1.0            | 5                          | 4320–6850                           | 170.8            | 3 $\times$ 1800               |
|            | 07/01/2002 | NIRSPEC    | Low Disp. N6 | 0.9         | 0.76           | 14                         | 15600–19800                         | 70.2             | 5 $\times$ 900                |
|            | 07/01/2002 | NIRSPEC    | Low Disp. N7 | 0.9         | 0.76           | 14                         | 20300–25000                         | 67.8             | 4 $\times$ 900                |

**Table 2** — Summary of observations and instrumental setups sorted by position angle (P.A.)

<sup>a</sup> Near the redshifted Ly $\alpha$  line at  $\lambda = 5825 \text{ \AA}$ ; the resolution varies roughly linearly from  $3 \text{ \AA}$  at  $3900 \text{ \AA}$  to  $40 \text{ \AA}$  at  $11000 \text{ \AA}$ .

<sup>b</sup> Spectropolarimetric observations, a detailed analysis of which was presented in Dey et al. (1997).

## 2.2 Optical and Near-Infrared Spectroscopy

We conducted both optical and near-IR spectroscopic observations using the LRIS, ESI, and NIRSPEC spectrographs at the Keck telescopes. The details of the specific instrumental setups are given in Table 2 and the data reduction techniques are described below. Figure 1 shows the slit position angles used in the program overlaid on contour representations of the narrow-band images of the nebulae. In contrast to many previous spectroscopic studies of HzRGs, most of the slits were not placed directly along the radio axes.

### 2.2.1 LRIS

Most of the optical observations were carried out using the Low-Resolution Imaging Spectrometer (LRIS; Oke et al. 1995) at the Cassegrain focus on the 10 m Keck I Telescope. The data were collected with various instrumental setups using both the long-

slit mode and multi-slit masks designed to obtain spectra for  $\sim 15$  targets in the field simultaneously (part of a survey looking for associated galaxies in a proto-cluster; Croft et al. 2005 in preparation). The red-sensitive LRIS-R camera was employed, which uses a Tektronix  $2048 \times 2048$  CCD detector with a pixel scale of  $0''.215 \text{ pixel}^{-1}$ .

All of the spectroscopic reductions were performed using standard methods and the NOAO IRAF<sup>1</sup> package (Tody 1993). Skylines were used to improve the first order wavelength calibration based on arc spectra to better than  $0.3 \text{ \AA}$  rms. The instrumental resolution was measured from unblended skylines. The flux calibrations were performed using observations of standard stars such as Feige 110 and Feige 34 (Massey et al. 1988). The extended emission of 4C 41.17 filled the narrow slits of the multi-object spectroscopic program, rendering accurate sky subtraction difficult. This does not seriously affect the kinematics or relative fluxes discussed in this paper.

### 2.2.2 ESI

One set of observations along the filament of 4C 60.07 was made during the night of UT 2001 February 25, using the Echelle Spectrograph and Imager (ESI; Sheinis et al. 2000) at the Cassegrain focus of the Keck II 10 m telescope in low-dispersion mode. The detector used is a high-resistivity MIT-Lincoln Labs  $2048 \times 4096$  CCD with a plate scale of  $0''.154 \text{ pixel}^{-1}$ . Exposures were broken into integrations of 1800 seconds each, one of which had to be halved because of time constraints. We performed  $6''$  offsets along the slit between each integration to improve skysubtraction. The data reduction was done using standard methods in IRAF. Prior to stacking the data, they were rotated over an angle depending on the position of the object on the slit, to align the dispersion axes. The wavelength calibration varies slightly with slit position, hence we shifted the spectra along the dispersion axes. This first order approximation is sufficiently accurate for the region of interest  $4300 \text{ \AA} - 9200 \text{ \AA}$  ( $900 \text{ \AA} - 1920 \text{ \AA}$  rest-frame).

### 2.2.3 NIRSPEC

The near-infrared spectra were obtained with the 10 m Keck II Telescope using the facility Near-Infrared Spectrograph (NIRSPEC; McLean et al. 1998). We employed  $0.76'' \times 42''$  slits to achieve low-resolution ( $R \sim 1400 - 1900$ ) spectra in wavelength ranges including their  $H\beta$ , [O II] and [O III] lines (see Table 2 for details). In this low-resolution mode, the  $1024 \times 1024$  ALADDIN InSb detector has a plate scale of  $0''.143 \text{ pixel}^{-1}$ . We obtained sets of 900 s integrations each with  $\sim 5 - 10''$  spatial offsets between exposures.

The NIRSPEC spectra need to be corrected for the slight curvature and distortions caused by the high-throughput optics. A general correction would require rectification onto a slit position-wavelength grid based on a wavelength solution from skylines and coadded exposures of a standard star. However, since no continuum emission is apparent in our 2-D spectra, we have extracted small regions close to the emission lines

---

<sup>1</sup>IRAF is distributed by the National Optical Astronomy Observatories, which are operated by the Association of Universities for Research in Astronomy, Inc., under cooperative agreement with the National Science Foundation.

only. This approach avoids interpolations because it requires just a simple rotation over an angle that depends on the wavelength of interest.

The data were flat-fielded and corrected for cosmic rays and bad pixels in the standard fashion. In order to remove the strong near-IR skylines, a sky frame scaled to the brightness of unsaturated sky lines near the emission line of interest was subtracted. Subsequently, the frames were cropped, rotated, and coadded. Flux calibration was done with stars of spectral type A0V, B3, and G4 from the 2MASS survey, and was consistent to within 10%.

### 2.3 Data analysis

For the data analysis the spectra were registered in position with radio maps from the literature (Carilli et al. 1994; Carilli 1995; Carilli et al. 1997). The zero points of the spatial scales were registered as closely as possible with the radio core. This was achieved by identifying the core with the centroid of the continuum emission (e.g., the optical spectra of B2 0902+34, 4C 60.07, 4C 41.17). If no continuum emission was visible, we either identified the core with the region that shows the broadest line emission or bootstrapped the spatial solution to spectra for which the radio core could be easily identified. These results were then checked with the narrow-band images, matching peaks and dips in the observed intensity on the basis of our assumptions. This resulted in a total uncertainty less than 0.5 " rms in the relative spatial offsets.

The velocity scale used in the analysis is relative to the systemic velocity derived from the He II  $\lambda 1640$  line (the adopted systemic redshifts are given in Table 1). The kinematic information was obtained from the 2-D spectra using a program written in IDL making use of the publicly available fitting routine MPFIT<sup>2</sup>. The individual pixel-wide traces were binned to aperture sizes corresponding with the seeing in order to increase signal-to-noise and to ensure that the extracted spectra are not correlated. We then determined the velocity centroid, FWHM (corrected for instrumental broadening measured from unsaturated skylines), peak and baseline fluxes by fitting a single Gaussian curve to each trace. To fit the central multiple absorption profiles accurately would require Gaussian fits with multiple Voigt profiles. However, since single Gaussians provide good fits to the spectra of the outer regions and it is preferable for a direct comparison to treat the central regions similarly, we have chosen to treat all regions consistently using the simpler approach. Therefore, the fits always represent the regions of high surface brightness emission, occasionally resulting in breaks when these regions are embedded in more smoothly varying large scale low surface brightness envelopes.

## 3 Results

Figures 2 and 3 show the extracted optical spectra of 4C 60.07 and B2 0902+34 respectively. The apertures were matched to the continuum emission from the central  $<3$  " regions. The rest-frame UV continuum of 4C 41.17 was discussed in detail by Dey et al. (1997). It showed absorption lines similar to those seen in starbursting galaxies,

---

<sup>2</sup>Available at <http://cow.physics.wisc.edu/~craigm/idl/fitting.html>

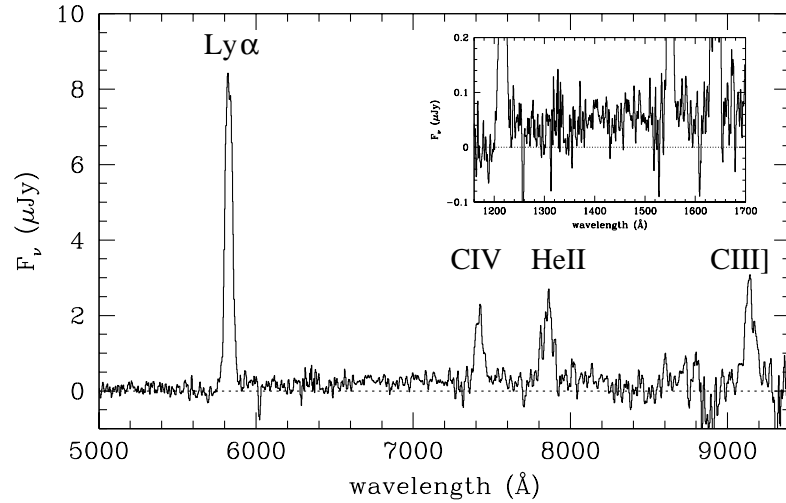


**Figure 2** — Optical 1-D spectrum of 4C 60.07 extracted in a  $3''$  aperture along the continuum emission. The prominent Ly $\alpha$ , C IV, He II, and C III] features are indicated. A redshift  $z = 3.7887 \pm 0.0007$  is inferred based on the He II  $\lambda 1640$  line. The inset shows the rest-frame UV continuum. It is of insufficient sensitivity to allow identification of reliable absorption features.

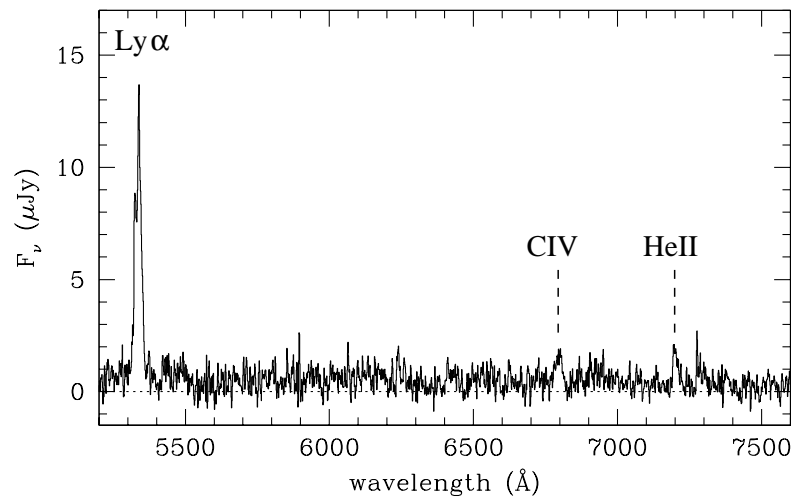


**Figure 3** — Optical 1-D spectrum of B2 0902+34 extracted in a  $3''$  aperture along the continuum emission. The Ly $\alpha$ , C IV, and He II emission lines are indicated. A redshift  $z = 3.3886 \pm 0.0003$  is inferred based on the He II  $\lambda 1640$  line. No strong absorption features can be discerned against the continuum.

indicating that the UV continuum is dominated by stars. The spectra of 4C 60.07 and B2 0902+34 are of insufficient sensitivity to allow a similar detailed analysis. However, since the main interest of this paper is the extended emission, we instead focus our discussion on the nebular lines.

The 2-D optical and near-IR spectra of 4C 41.17, 4C 60.07, and B2 0902+34 centered at the emission lines most relevant to our discussion are shown in Figures 4, 7, and 11. The vertical lines indicate the systemic redshifts of the galaxies as derived from the He II  $\lambda 1640$  line. The horizontal lines indicate the positions of the outer edges of the radio lobes and radio core projected onto the slit. It is immediately obvious that many of the lines are very extended, and that they show strong spatial variation of their velocity centroids and FWHMs.

An important result is that for both 4C 41.17 and 4C 60.07 the oxygen line profiles resemble those from the bright inner parts of the Ly $\alpha$  emission closely. Since self-absorption cannot be important in the strong forbidden lines, this suggests that information about the kinematic structure is preserved in the Ly $\alpha$  line despite it being subject to resonance scattering. If this is true also in the outer regions, it then follows that we can hope to obtain kinematic information using Ly $\alpha$  for those parts where other lines are too faint to have been detected.

Figure 5, 6, 8, and 12, show plots of the velocity centroids, FWHMs, and normalized flux densities of the halos as a function of distance from the radio cores for all position angles observed. In §4.3 we will discuss the general implications of these diagrams. First, we describe the individual sources.

### 3.1 Notes on individual objects

#### 3.1.1 4C 41.17

Dey et al. (1997) have discussed the brightest part ( $2'' \times 1''$ ) of the extracted 1-D optical spectrum of 4C 41.17 at PA =  $76^\circ$  in detail. They determined a redshift  $z = 3.79786 \pm 0.00024$  based on the He II line. Furthermore they found evidence for stellar absorption lines, and low polarization indicating that a young stellar population contributes significantly to the rest-frame UV continuum emission.

The 2-D spectra along the radio axis (PA  $76^\circ$ ; Fig. 4) show that the Ly $\alpha$ , [O II]  $\lambda 3727$ , and [O III]  $\lambda 5007$  emission line regions are very extended (over  $\sim 20''$ ,  $10''$ , and  $6''$ , respectively). The H $\beta$  line is much fainter, but also appears extended. As has been noted above, the velocity structure of the Ly $\alpha$  emission resembles that of oxygen closely despite the resonant broadening of Ly $\alpha$ . The Ly $\alpha$  and [O III] lines both consist of two separate components straddling the radio core with peak fluxes separated by about  $3''$ . Careful inspection reveals that these components are present also in the [O II] line, with the red part of the western component missing due to a skyline near  $\lambda = 17880 \text{ \AA}$ . The dip in between the emission peaks is expected since the narrow-band Ly $\alpha$  and radio image overlays showed the core to be highly obscured (see Paper I). This suggests that the lack of Ly $\alpha$  near the core is caused by a dusty medium, and not only by large columns of neutral hydrogen.

The image overlays indicated that the position of the radio core is offset by  $0.5''$  to the NE from the center of the dip in the line emission. Figure 4 provides further



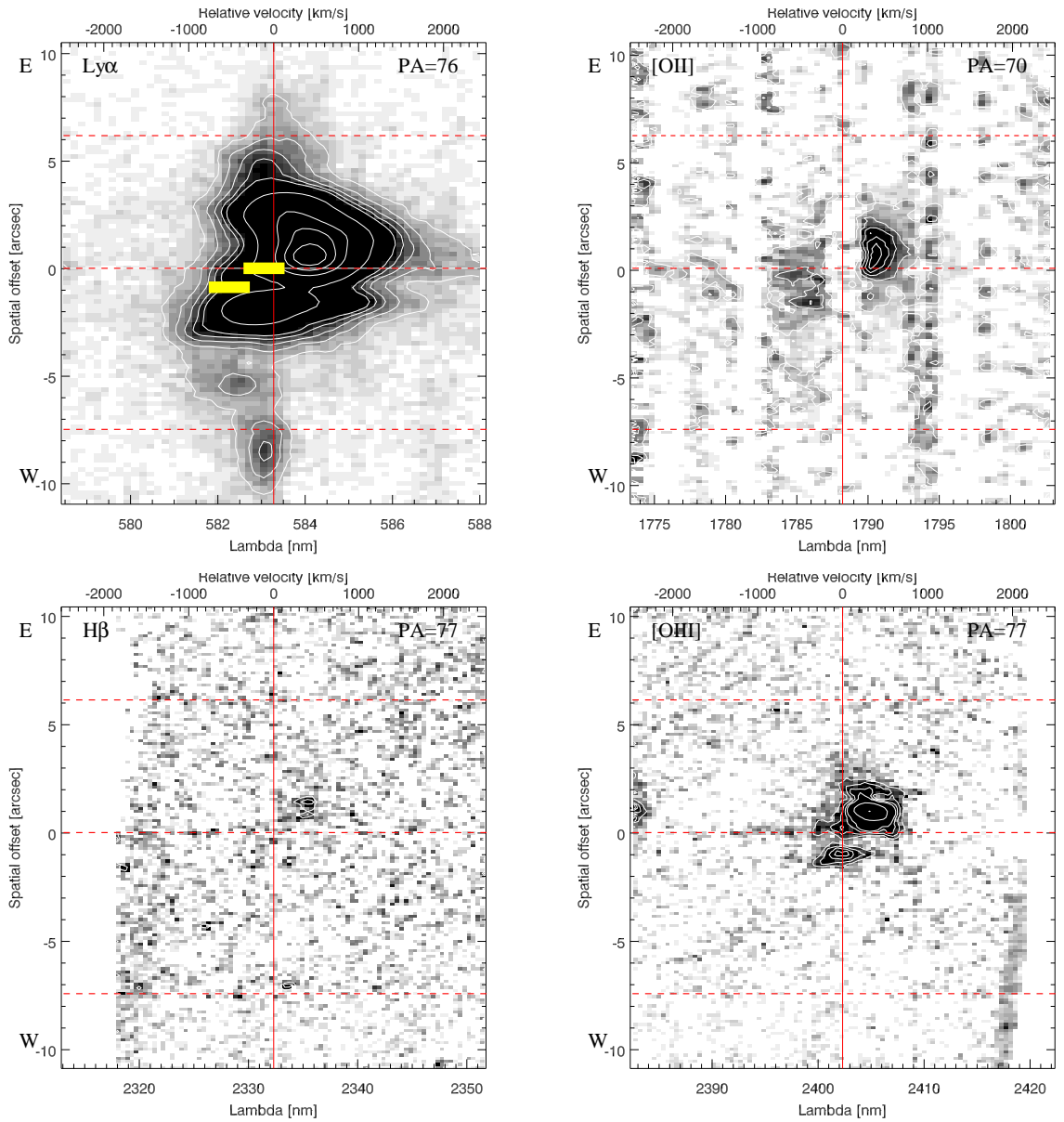


**Figure 4** — Grayscale representations of the 2-D spectra of 4C 41.17 centered at the  $\text{Ly}\alpha$ ,  $[\text{O II}] \lambda 3727$ ,  $\text{H}\beta$ , and  $[\text{O III}] \lambda 5007$  lines. The velocities are indicated relative to the systemic redshift determined from the  $\text{He II}$  line. The zero points of the spatial scales correspond with the position of the radio core as identified with the broad line and continuum emission. Note that the peaks of the line emission corresponding with the position of radio knot B2 in Carilli et al. (1994) are  $1''$  E of the nucleus. Furthermore it can be seen (most easily in the  $[\text{O III}] \lambda 5007$  spectrum) that there are  $0.5''$  offsets between the broad lines and the center of the depression. The  $[\text{O II}]$  spectrum is rich in skylines. These have been masked to better show the structure of the  $[\text{O II}]$  line emission. The dashed lines correspond to the positions of the outer radio lobes and radio core projected onto the slit. The vertical line represents the adopted systemic velocity of the galaxy. The thick lines in the  $\text{Ly}\alpha$  panel indicate the two velocity regimes and the projected spatial positions for which CO emission has been detected (De Breuck et al. 2004). The position angles of the slits are indicated in the top right corner.

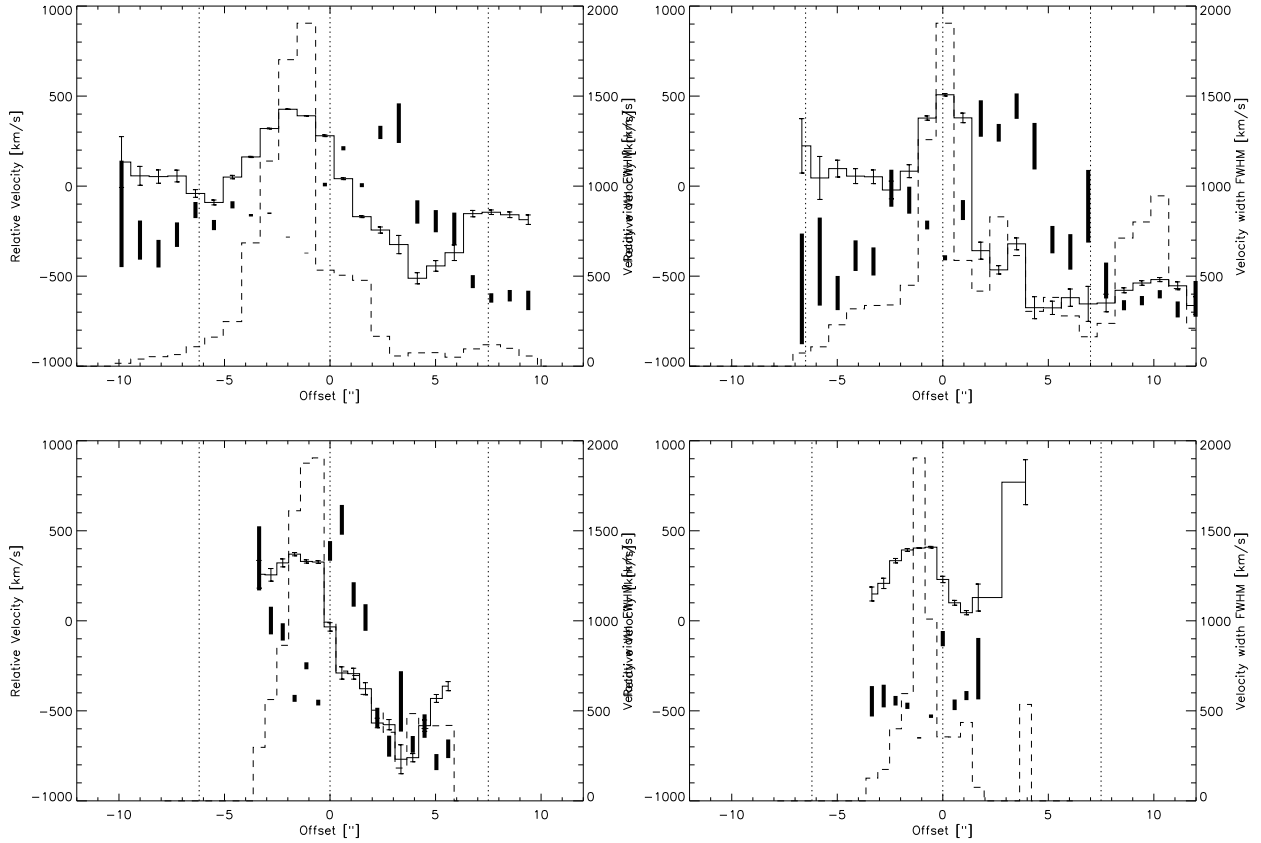


**Figure 5** — Relative velocities (solid lines), velocity dispersion (bars), and normalized surface brightness profiles (dashed lines) as determined from spectra with slit positions parallel to the radio axis of 4C 41.17. Top panels: Ly $\alpha$  for PA=76° (left), Ly $\alpha$  for PA=81° (right). Bottom panels: [O II] for PA=70° (left), and [O III] for PA=68° (right). The spatial zero points correspond with the position of the radio core and the dotted lines represent the position of the radio lobes projected on the slit. Bar and symbol size indicate the  $1\sigma$  uncertainties on the measurements. The left axis indicates the scale for the relative velocities, the right axis for the FWHMs. In the central region of 4C 41.17 the formal errorbars on the fitted FWHMs are very small. However they are not representative of the diffuse extended halo. Note that the fits to the [O II] emission are affected by the strong skylines and that the slit with PA=81° did not intersect the radio core.

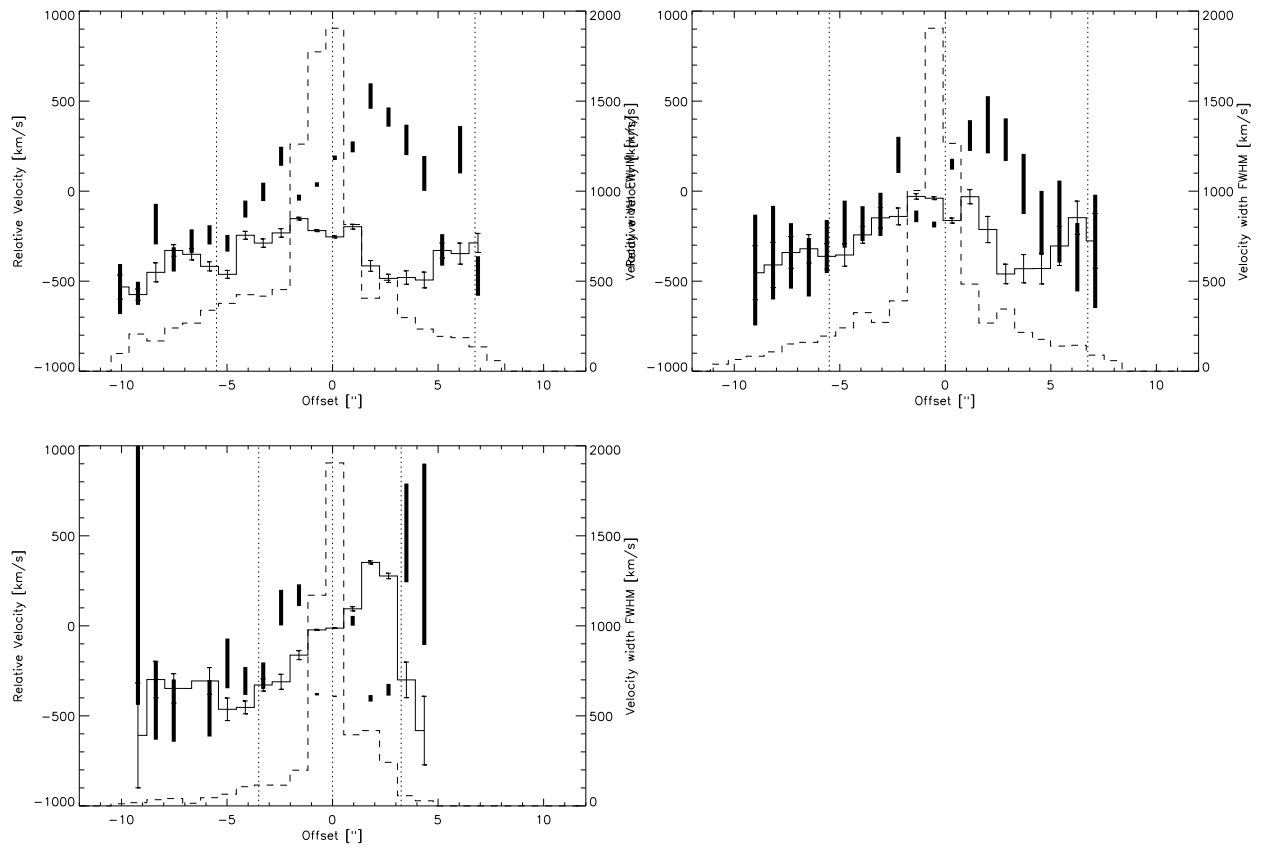


**Figure 6** — Similar to Fig. 5 but for Ly $\alpha$  emission along the slits that are approximately perpendicular to the radio axis of 4C 41.17. PA=19° (top right), PA=22° (top left), and PA=171° (bottom).

evidence for this without relying on relative astrometry: in the spectra, the position of the radio core is identified with a narrow ( $\lesssim 0.9''$ ) tail of broad ( $1000 \text{ km s}^{-1}$  FWHM) [O III]  $\lambda 5007$  emission starting at  $\lambda \sim 23930 \text{ \AA}$ , which appears to be symmetrically distributed around the systemic velocity.

### *Kinematics*

Figure 5 shows that for  $\text{Ly}\alpha$  the central regions show high ( $\sim 800 \text{ km s}^{-1}$ ) velocity dispersions which extend along the radio axis to the outer radio lobes. The velocity dispersions inferred from [O III] are similarly high ( $\sim 500 \text{ km s}^{-1}$ ) in the region for which they could be determined. Beyond the radio lobes there is a break and the  $\text{Ly}\alpha$  kinematics become more quiescent ( $\sim 400 \text{ km s}^{-1}$ ) and the velocity centroids change from being blue-ward shifted ( $-500$  to  $-700 \text{ km s}^{-1}$  along the (south-)western lobe) to near systemic. Perpendicular to the radio axis (see Fig. 6) the kinematics follow a smooth gradient with the high FWHMs more limited to the central region of  $\sim 3''$  ( $\sim 20 \text{ kpc}$ ) wide that is identified by the break in peak surface brightness distribution.

A very important result from the near-IR spectroscopy is that there is [O II] emission in the velocity regime  $-200$  to  $-1000 \text{ km s}^{-1}$  extending from the nucleus to  $7\text{-}8''$  west of the nucleus, whereas the [O III] emission is much more centrally concentrated. We will discuss this further in §4.1 and §4.2.

If one neglects possible radiative transfer and obscuration effects in the  $\text{Ly}\alpha$  emission (as seems justified by the similarity to the oxygen emission), there appears to be a velocity shear in the outer parts (undisturbed by the radio source) along the radio axis. The kinematic profiles with slit positions perpendicular to the radio axis (Fig. 6) show a fairly symmetric velocity distribution.

Interestingly, the velocity structure of the bulk of the emission line gas is predominantly redward shifted in the O,  $\text{H}\beta$ , and  $\text{Ly}\alpha$  lines with respect to the systemic velocity inferred from the He II emission line. We will discuss this in §4.4.

#### 3.1.2 4C 60.07

Figure 2 shows the 1-D extraction of the ESI spectrum of 4C 60.07 (PA =  $135^\circ$ ) in a  $3''$  aperture to include all continuum emission. Based on the He II line at  $7855.7 \pm 1.1 \text{ \AA}$  we infer a redshift  $z = 3.7887 \pm 0.0007$ , in agreement with Röttgering et al. (1997).

The 2-D spectra are presented in Figure 7. The top panels show the  $\text{Ly}\alpha$  and C IV emission lines along PA =  $135^\circ$ . The two bottom panels show that, as was the case for 4C 41.17, the morphologies of the  $\text{Ly}\alpha$  and [O II] emission line velocity structures (PA =  $81^\circ$ ) are remarkably similar, providing further justification for the use of  $\text{Ly}\alpha$  as a tracer of the dynamics of these systems. There is one significant difference between [O II] and  $\text{Ly}\alpha$  however: the [O II] line exhibits two emissions peaks at both sides of the location of the radio core, while the  $\text{Ly}\alpha$  emission near the systemic velocity shows a smooth gradient from one side to the other.

The 2-D  $\text{Ly}\alpha$  emission line for PA =  $135^\circ$  is presented at a different stretch in Figure 9, emphasizing the difference between high and low surface brightness regions. Interesting structure is apparent: crescent shaped clouds surround a 'gap' at the position of the radio core near the systemic velocity of the galaxy. We will discuss this further in §4.2.

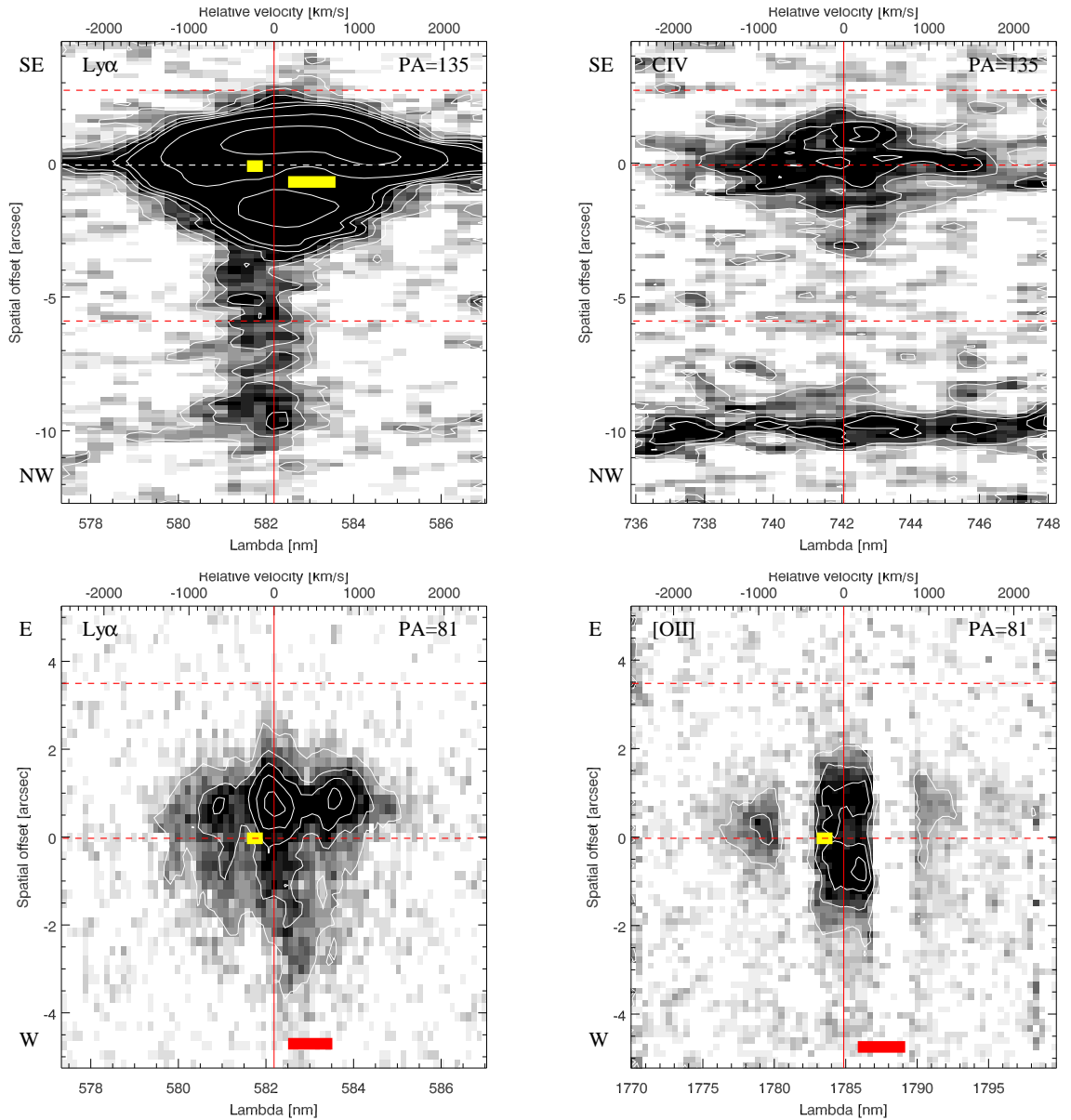


**Figure 7** — Similar to Fig. 4. Grayscale representations of the 2-D spectra of the emission line halo around 4C 60.07. The top left and top right panel respectively show Ly $\alpha$  and CIV emission along the filament with PA = 135°. The bottom left and right panel show Ly $\alpha$  and [OII]  $\lambda$ 3727 along the radio axis with PA = 81° and have a different scale to bring out more details. Therefore, in the two bottom panels the projection of the western radio lobe (at 6'') falls outside the figure. Two CO components have been detected for this galaxy (Papadopoulos et al. 2000; Greve et al. 2004). The thick lines indicate their velocities and positions as projected on the slit.

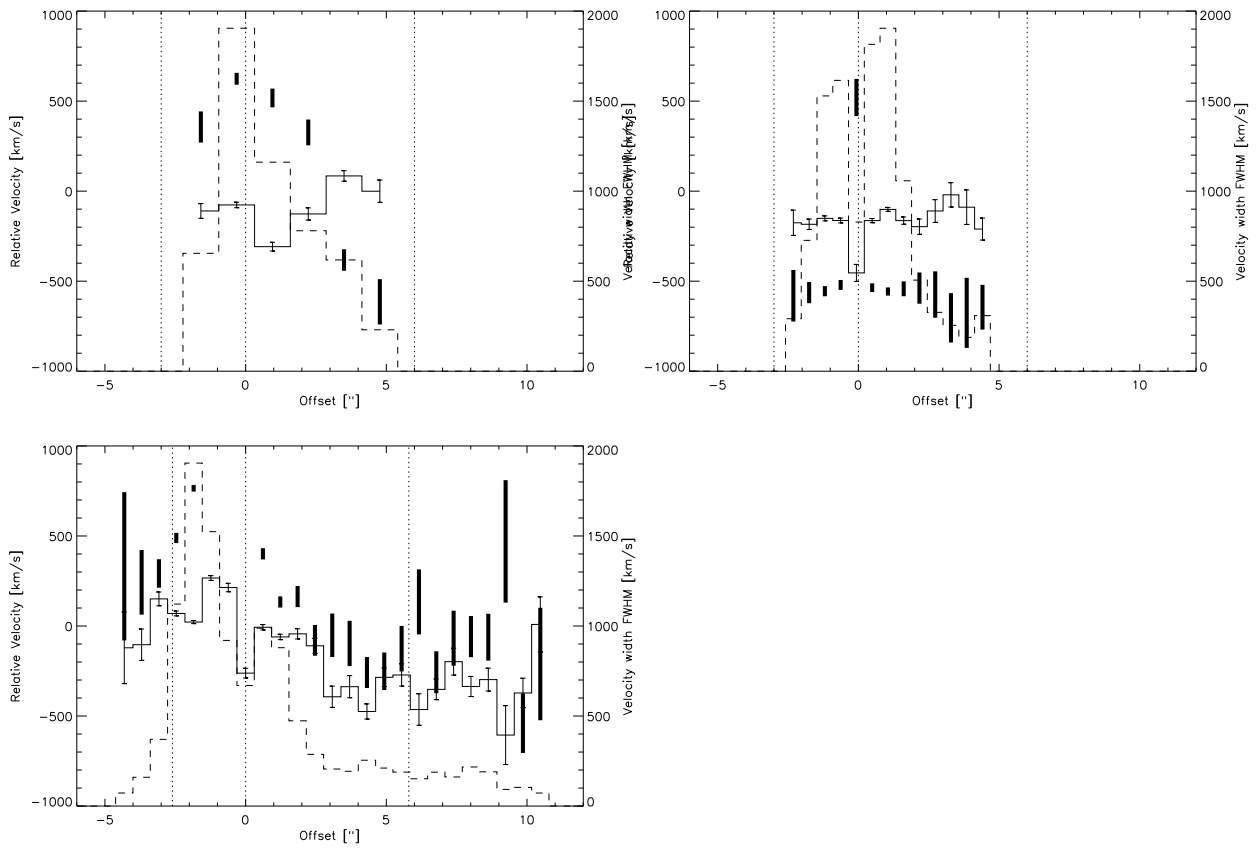
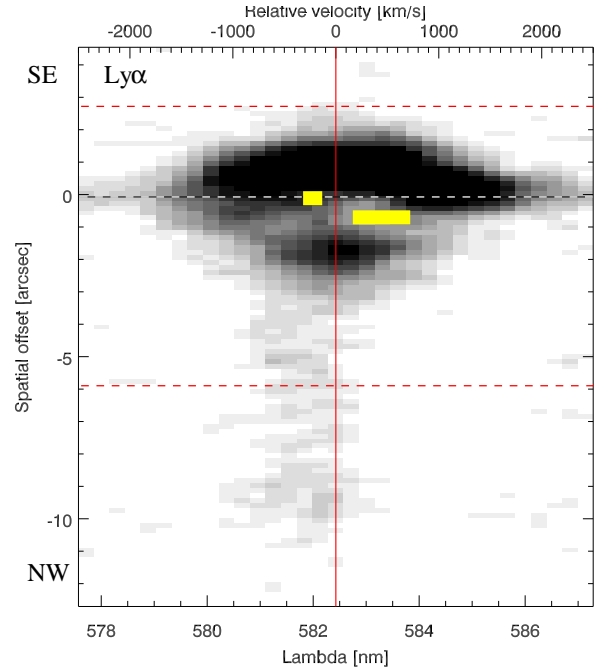


**Figure 8** — Similar to Fig. 5 but for 4C 60.07. Ly $\alpha$  (top left) and [O II] (top right) emission along PA=81 $^\circ$  and Ly $\alpha$  emission along PA=135 $^\circ$  (bottom). The datapoints representing the fitted FWHMs for the center region fall outside the plot. See the text for details.

**Figure 9** — Similar to the Ly $\alpha$  emission line at PA = 135° in Figure 7. The contrast has been adjusted to bring out crescent shaped arcs surrounding a depression in the emission that is identified with the location of the radio core and unobscured optical nucleus.



### Kinematics

Figure 8 shows that both the Ly $\alpha$  and [O II] lines at PA = 81° have very high velocity FWHMs of  $\sim 1600 - 1700 \text{ km s}^{-1}$ , rather large for HzRGs. These are however smaller than for the spectrum at PA = 135° which shows a FWHM of  $2600 \text{ km s}^{-1}$  near location of the ‘Ly $\alpha$  gap’ discussed before.

For the central (+2'' to -3'') region of Ly $\alpha$  and C IV at PA=135°, emission at the eastern side seems preferentially blue-shifted by  $\sim 100-200 \text{ km s}^{-1}$ . In contrast, most of emission at the western side is redshifted by a comparable amount. Ly $\alpha$  and [O II] at PA=81° show similar structure.

### The Ly $\alpha$ Filament

The most striking feature of the emission line nebula surrounding 4C 60.07 is the extended Ly $\alpha$  filament. Imaging showed this filament to have approximately constant surface brightness, sharply bounded on the NE side, and more “fluffy” on the SW side. The tip of the filament is co-spatial with a small galaxy suggesting a possible physical connection. In Figure 10 we present the full 2-D spectrum of this filament obtained with ESI.

Figures 8 and 9 show that the filament is offset from the systemic velocity of the radio source with evidence for a velocity gradient across the filament. The gas seems to be moving at a relative velocity of  $-100 \text{ km s}^{-1}$  near the tip, with the absolute velocity offset gradually increasing to  $-400 \text{ km s}^{-1}$  close to the galaxy. The central wavelength fit by a single Gaussian to the coadded filament yields  $\lambda \sim 5818.1 \pm 0.3 \text{ \AA}$  or  $-175 \text{ km s}^{-1}$  relative to a systemic velocity at  $z = 3.789$  with a FWHM of  $20 \pm 1 \text{ \AA}$  corresponding to a deconvolved velocity dispersion of  $\sim 700 \text{ km s}^{-1}$ .

Both spectroscopy and imaging show the filament to be of approximately constant surface brightness with well defined spatial limits. However, the apparent sharp

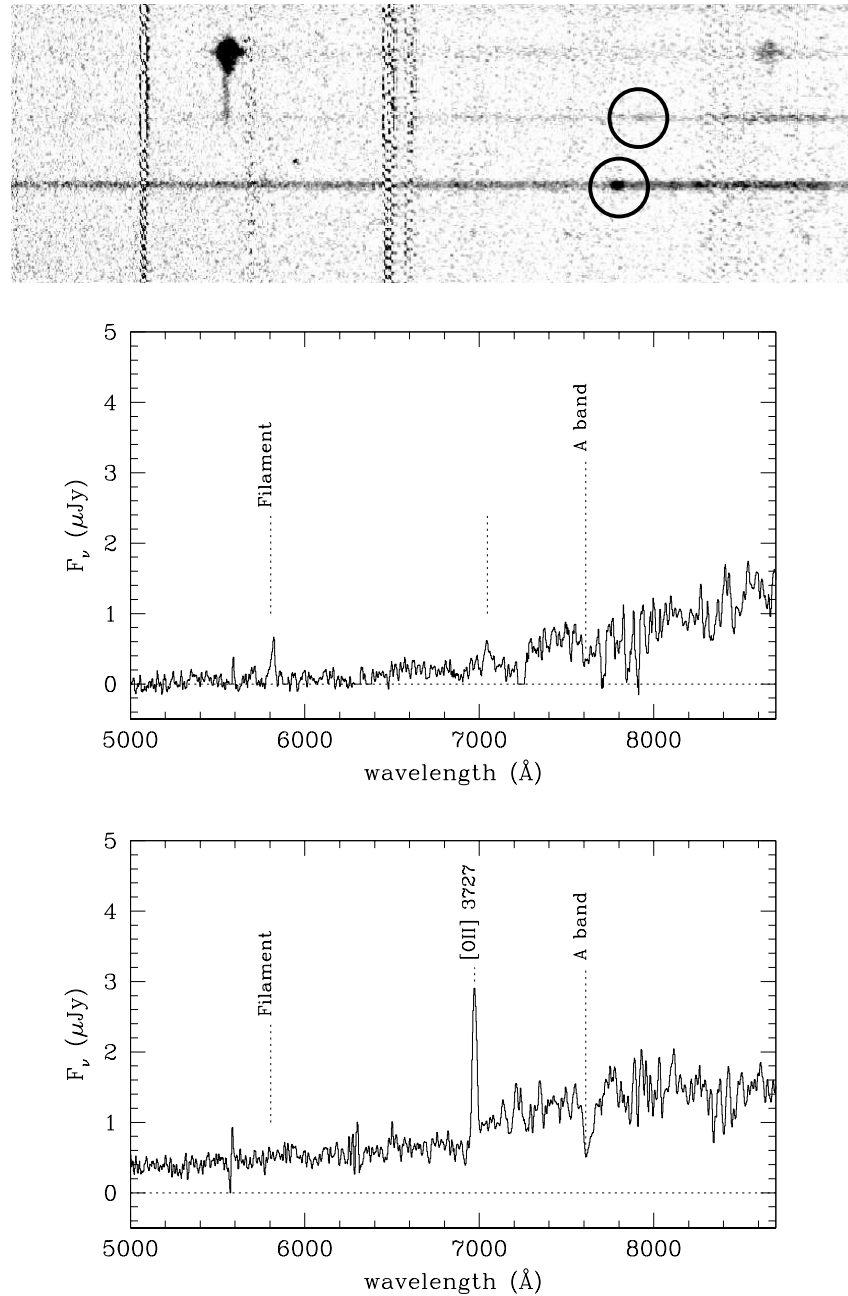


**Figure 10** — 2-D (Top panel) and 1-D spectrum (Middle panel) of the galaxy at the extremity of the  $\text{Ly}\alpha$  filament of 4C 60.07. No strong redshift constraints could be obtained based on this spectrum. A possibility is that the galaxy is at  $z \sim 0.9$ , close to that of brighter foreground galaxy ( $z = 0.871$ ) that was also on the slit and is plotted in the bottom panel. The circles indicate emission lines which could be identified with redshifted [O II]  $\lambda 3727$ . It is also possible that the galaxy is at a redshift similar to 4C 60.07. See the text for details.



boundary of the filament could be due to the filter bandpass whose response cuts off sharply at the blueward limit of the wavelength observed (the lower limit of the narrow-band filter is 5806 Å). If the filament is part of larger scale structure with coherent motion extending blueward this would fall outside the filter, explaining the seemingly sharp boundary, and the observed velocity structure would be a function of the position selected.

#### *Galaxy at the tip of the filament*

As shown in Paper I there is a galaxy co-spatial with the observed extremity of the Ly $\alpha$  filament. Figure 10 shows the 2-D and 1-D spectra of this galaxy. The spectra show faint continuum emission which extends blueward from the Ly $\alpha$  filament, a possible faint emission line near 7050 Å and a steady rise of the continuum longward of approximately 7200 Å. Unfortunately, strong redshift constraints cannot be obtained from these spectra. One possibility is that the redshift is very similar to that of a nearby brighter galaxy which was also on the slit. The brighter galaxy shows a line and break near 7000 Å. The bright emission line is best identified with [O II]  $\lambda$ 3727 at  $z = 0.871$ . If the possible emission line near 7050 Å is also identified with [O II]  $\lambda$ 3727 and/or the rise in the continuum emission with a Balmer/4000 Å break, then a redshift of  $z \sim 0.9$  is inferred for the galaxy at the tip of the filament, possibly suggesting that 4C 60.07 is observed through a foreground group.

Alternatively, it is possible that the galaxy at the tip of the filament is actually at a redshift similar to 4C 60.07. The following arguments are in favor of this interpretation: (i) The location. Although a chance superposition is possible, it seems that the Ly $\alpha$  filament ends exactly at the position of this galaxy suggesting a physical connection. (ii) The galaxy has colors which are redder than for 4C 60.07 and the brighter galaxy, as expected for distant galaxies without an AGN. (iii) In the CO map of Papadopoulos et al. (2000) there is a hint of CO line emission at the location of the galaxy. If correct, then this galaxy would most likely be a dusty starburst galaxy without strong emission lines, at the redshift of 4C 60.07.

#### 3.1.3 B2 0902+34

Our optical spectrum of B2 0902+34 shown is the most sensitive exposure at a fixed PA yet obtained (e.g., Lilly 1988; Martin-Mirones et al. 1995). The 1-D spectrum (Fig. 3) shows that the integrated continuum emission (3" aperture) has an almost constant surface brightness and a faint break blueward of Ly $\alpha$ . We consider the He II line at  $7199.4 \pm 0.5$  Å, extracted in a 3" wide aperture centered at the radio core, to be most representative of the systemic velocity of the galaxy. Accordingly, we infer a redshift  $z = 3.3886 \pm 0.0003$ . This value for the redshift is slightly less than reported previously (Lilly (1988) and Martin-Mirones et al. (1995) inferred  $z = 3.395$  and  $z = 3.391$  respectively) but entirely consistent with the redshift estimate from fitting the Ly $\alpha$  line with a Gaussian envelope and strong Voigt absorption profile in the same aperture.

From the 2-D spectra we detect Ly $\alpha$  emission over an extent of  $\sim 10''$ , having a complex multi-component spatial and velocity structure (c.f., Fig 11). The 2-D structures of the C IV and He II lines differ significantly from the overall shape of the Ly $\alpha$ . Inferred redshifts for B2 0902+34 depend on both the emission line and aperture used.

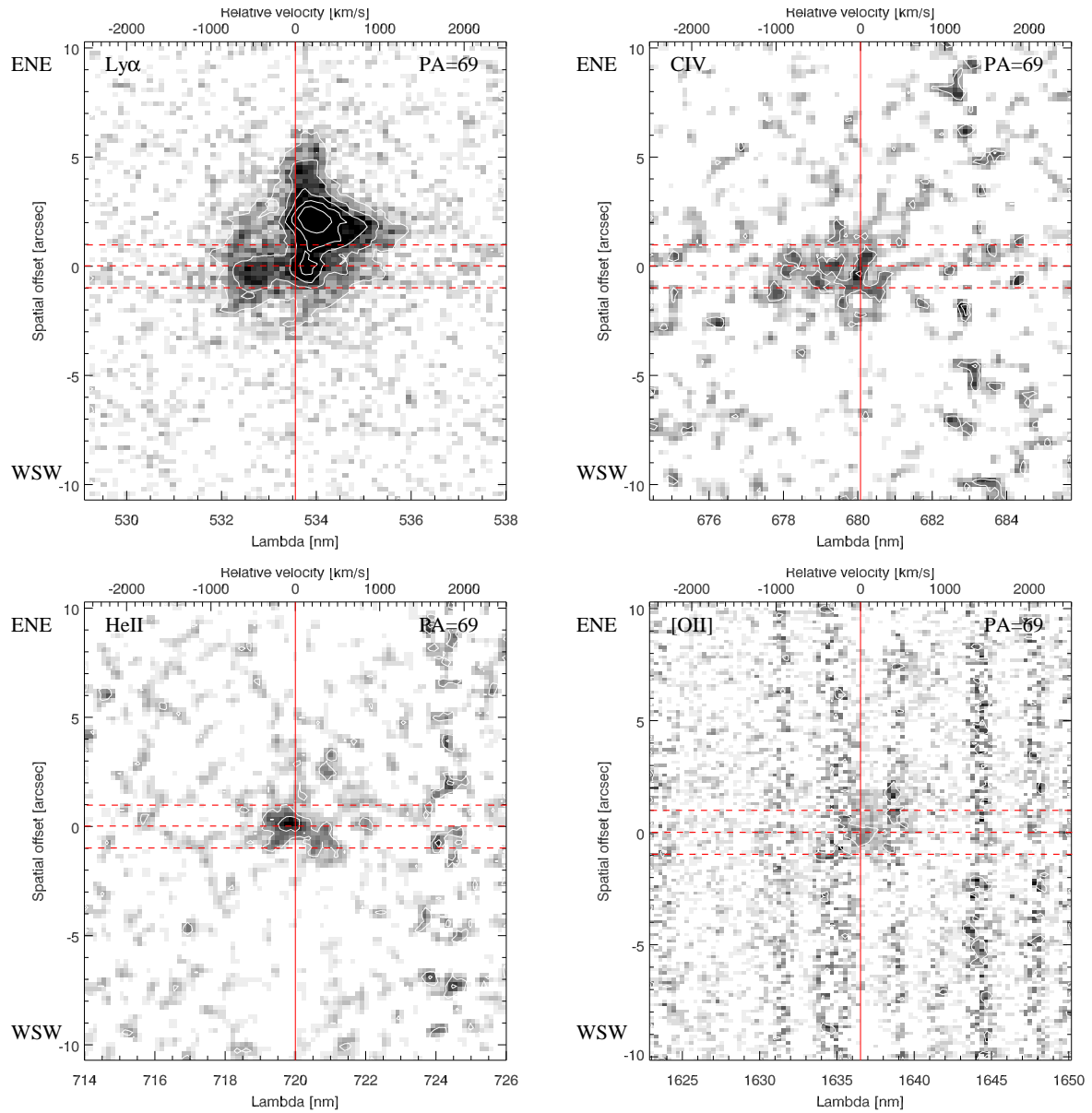


**Figure 11** — Similar to Fig. 4, but for B2 0902+34. The top left panel shows the line emission profile for Ly $\alpha$ , top right C IV, bottom left He II, and bottom right [O II].

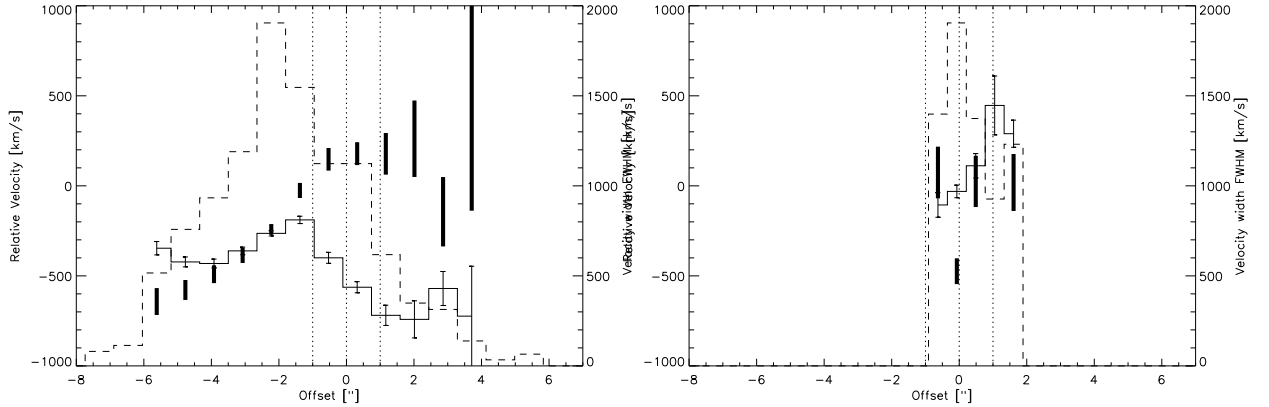


**Figure 12** — Similar to Fig. 5 but for B2 0902+34. Ly $\alpha$  (left) and [O II] (right) both along PA=69 $^\circ$ .

This illustrates the difficulty of assigning single redshifts to such complex systems and explains the small discrepancies with redshifts from the literature discussed above.

The [O II] spectrum is too shallow to allow a detailed comparison with the Ly $\alpha$  emission, but is consistent with [O II] being similarly distributed.

Given that B2 0902+34 shows associated H I absorption against the radio continuum it is important to see whether this is present also in the Ly $\alpha$  profile, since no signatures of this have been seen previously in the optical. Associated OH emission has been reported also, but follow-up observations have failed to confirm this (Cody & Braun 2003).

The spectrum with an aperture encompassing all Ly $\alpha$  emission shows an absorption feature blueward of the Ly $\alpha$  line at  $\lambda = 5331.58$  ( $z = 3.3857$ ), which can be fitted with a Voigt profile with a column density of  $1.8 \times 10^{14} \text{ cm}^{-2}$  and Doppler parameter  $b = 195 \pm 11 \text{ km s}^{-1}$ . This however cannot be the same gas that causes absorption against the radio continuum, since Briggs et al. (1993) and Cody & Braun (2003) infer a redshift  $z_{\text{abs}} = 3.3962$  with  $N_{\text{H}} = 3 \times 10^{21} \text{ cm}^{-2}$  and FWHM =  $120 \text{ km s}^{-1}$  for the absorbing gas. At this redshift a weak feature exists that can be fitted with a small additional Voigt profile at  $\lambda = 5343.0 \pm 0.3$  with Doppler parameter  $b = 104 \pm 76 \text{ km s}^{-1}$  and column density  $N_{\text{H}} = 1.7 \times 10^{13} \text{ cm}^{-2}$ . This is unlikely to be the same gas however, because the inferred column density is eight orders of magnitude smaller than estimated from the radio observations. This second ‘absorption’ feature is more easily explained as an artefact of representing the triangular shape of the Ly $\alpha$  emission and the low surface brightness emission with a single spectral profile.

### Kinematics

None of the emission lines show strong indications for rotation or any ordered motion. The kinematics of the Ly $\alpha$  emission is very interesting however, as it seems to consist of two components. One component being the typical triangular shape resulting from spatially extended absorption that is blue-shifted relative to the systemic velocity (c.f., Dey 1999). The other component is the Ly $\alpha$  emission near the position of the radio core, but at a relative velocity of  $-500 \text{ km s}^{-1}$ . The C IV emission is preferentially blue-shifted with respect to the systemic velocity of the galaxy. It covers a velocity

range of approximately  $-1200 \text{ km s}^{-1}$  to  $+400 \text{ km s}^{-1}$ . The centroid is at  $-400 \text{ km s}^{-1}$ , close to the centroid ( $-500 \text{ km s}^{-1}$ ) of the blue-shifted  $\text{Ly}\alpha$  near the postulated position of the radio core.

## 4 Discussion

We now discuss the implications of our observations. We address the following questions: What processes are ionizing these halos? Can  $\text{Ly}\alpha$  be used as a reliable tracer of the velocity field of the gas? What are the small scale and large scale kinematics of the halos and outflows? What are the metallicities of the gas and the estimated masses of the galaxies? Can outflows from the HzRGs escape the deep potential wells and enrich the IGM? What is the impact of these outflows on the radio galaxies themselves?

### 4.1 Ionizing source

In studying the nature of the ionized gas halos one of the most important questions concerns the nature of the mechanism that is responsible for ionizing the extended emission line nebulae. The most likely candidates are: photoionization by radiation from an AGN or stars, shock heating, and shocks with precursors that photoionize the region ahead of the shock by radiation from the gas (e.g., Allen et al. 1998, and references therein).

Studies of  $z \sim 1$  radio galaxies have shown that the dominant ionization mechanism may depend on the evolutionary state of the radio source (e.g., Best et al. 2000; Inskip et al. 2002). Generally, it was found that the emission line gas of small (i.e. young) sources is shock ionized, but as the radio source expands beyond the host galaxy, interactions with the gas decrease and photoionization by the AGN takes over. As De Breuck et al. (2000) noted, for HzRGs the situation is likely to be more complex because of ongoing merging of galaxies and their halos, jet-induced star formation, entrainment by the radio source and outflows.

The total  $\text{Ly}\alpha$  luminosities  $L_{\text{Ly}\alpha} \simeq 10^{45} \text{ erg s}^{-1}$  (Paper I) can be explained both by (i) an embedded QSO with a power-law spectrum with index  $\alpha = -1.4$  ( $f_\nu \sim \nu^\alpha$ ) and combined ionizing and mechanical energy flux of at least  $1 \times 10^{46} \text{ erg s}^{-1}$  and (ii) by a starburst with a star formation rate  $\gtrsim 1000 M_\odot \text{ yr}^{-1}$ . The required star formation rate is remarkably close to what is deduced from rest-frame far-IR observations (Dunlop et al. 1994; Stevens et al. 2003). However, based on detailed modeling Bicknell et al. (2000) argue that the dominating ionizing mechanism is shock excitation through jet-cloud interactions with fast  $\sim 1000 \text{ km s}^{-1}$  shocks. Scharf et al. (2003) proposed that X-ray emission could be responsible for ionizing the outermost parts of the halo.

Allen et al. (1998) showed that a combination of rest-frame UV ( $\text{C IV } \lambda 1549 / \text{He II } \lambda 1640$ ) and rest-frame optical ( $[\text{O III}] \lambda 5007 / \text{H}\beta$ ) line fluxes can help to separate pure photoionization from shock dominated mechanisms. This diagram is relatively insensitive to the effects of dust extinction as the ratios are determined from lines close in wavelength. Iwamuro et al. (2003) conducted a rest-frame UV-optical emission line study of 15 radio galaxies with  $2 < z < 2.6$ . They found that there is a range in observed line-ratios suggesting that some objects are best explained with photoionization of low metallicity gas while others are consistent with the shock+precursor model.

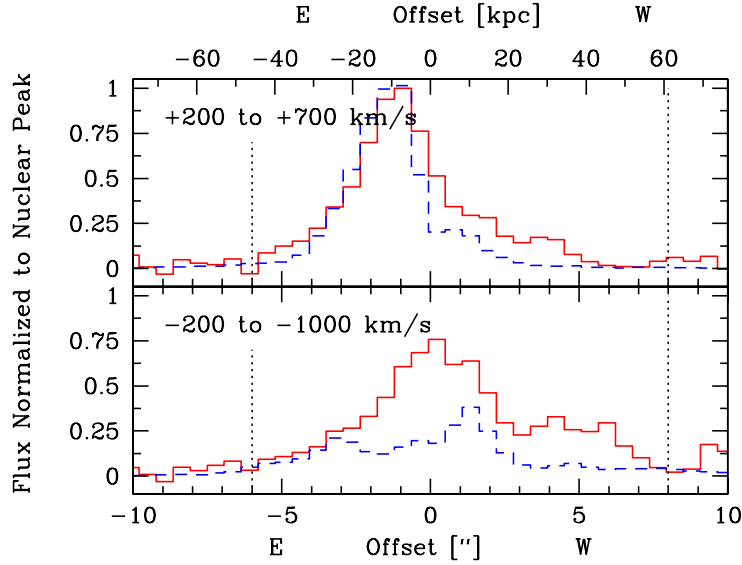


**Figure 13** — Top: Normalized surface brightness profiles of the [O II] (solid line) and Ly $\alpha$  (dashed line) emission along the inner radio axis and south-west filament of 4C 41.17 in the velocity range +200 to +700 km s<sup>-1</sup>, showing extended [O II]. The spatial zero-point corresponds to the position of the radio core. Bottom: Similar to top panel but for the velocity range -200 to -1000 km s<sup>-1</sup>. The [O II] emission is detected out to  $\sim 8''$  ( $\sim 60$  kpc) west of the nucleus, where it is blue-shifted by  $\sim -600$  km s<sup>-1</sup> relative to the He II line. The projected distance of the south-west and north-east radio lobes along the slit direction are indicated (dotted lines). The +200 to -200 km s<sup>-1</sup> range for [O II] is affected by near-infrared sky lines and is not shown.

Carson et al. (2001) and Maxfield et al. (2002) found evidence for changing line ratios *within* sources, suggesting that the dominant ionization process depends on the region of interest. The different distributions of the [O II] and [O III] emission for 4C 41.17 also suggest a change in ionizing mechanism. Therefore, we discuss the central and extended regions separately.

#### 4.1.1 Central region

Based on previously published values of [O III]/H $\beta$   $\sim 3.4$  and  $2.8$  for 4C 41.17 and B2 0902+34 respectively (Eales & Rawlings 1993) it seemed that pure photoionization models could be ruled out. However the H $\beta$  detections were marginal, and using the total integrated line fluxes for 4C 41.17 from the present study we derive ratios of [O III]  $\lambda 5007$ /H $\beta$   $\sim 9.6$  for the central region, and [O III]  $\lambda 5007$ /H $\beta$   $\sim 11.8$  for the spatially integrated spectrum. These are much larger than the values reported by Eales and Rawlings and suggest either a pure photoionization or a shock+precursor model.

#### 4.1.2 Extended region along the radio axis

The degree of ionization in the extended regions, at large distances from the AGN, appears different from that near the galaxy centers. As discussed in §3.1.1, for 4C 41.17, [O II] emission was detected as far as  $\sim 60$  kpc from the nucleus. Figure 13 shows the velocity integrated relative intensities of Ly $\alpha$  and [O II] as a function of distance from the nucleus for a red-shifted (+200 to +700 km s<sup>-1</sup>) and a blue-shifted (-200 to

$-1000 \text{ km s}^{-1}$ ) velocity regime. The red-shifted [O II] follows the  $\text{Ly}\alpha$  closely, while the blue-shifted [O II] shows a relative enhancement over the range  $3-8''$  W of the nucleus. In this regime no evidence for [O III] is found (Fig. 4), whereas the [O III] emission in the nuclear region is much brighter than the [O II]. The [O III]/[O II] ratio is a tracer of the ionization parameter. It changes from  $\sim 3-4$  in the center to  $< 0.5$  in the outer regions. Naively, one could interpret this as a natural result of softening of the ionizing spectrum with increasing distance from the central source. However, representing the entire emission line region with a single H II region is not realistic. The halo is better described with a multi-phase medium, in which cool, dense clouds are in pressure equilibrium with a hot surrounding medium. In this scenario the extended [O II] emission depends on the detailed ionization balances of many individual clouds. Explaining the observed spectrum with photoionization from a central region would require fine tuning the density distribution of these clouds. The extended [O II] emission is therefore much better described as the result of shocks related to the radio source interacting locally with the emission line clouds. This is sensible since the emission is located along the radio-axis and both the  $\text{Ly}\alpha$  and [O II] are blue-shifted by  $\sim 600 \text{ km s}^{-1}$ , likely related to the expansion of the radio cocoon.

#### 4.2 Radiative transport: to scatter or not to scatter

As mentioned already in §3 one important result of the near-IR spectroscopy is that for both 4C 41.17 and 4C 60.07 (and possibly also B2 0902+34, but the spectrum is not as sensitive) the velocity structures of  $\text{Ly}\alpha$  resembles those of oxygen closely. This is unexpected since  $\text{Ly}\alpha$  is subject to resonant broadening in the damping wings. However, in the previous section we have argued that the extended filaments along the radio axis are actually locally ionized. It may be that these extended parts are not sufficiently dense for significant line broadening of the  $\text{Ly}\alpha$  emission to occur. The  $R$ -band image shown in Paper I is free from strong emission lines. Yet, it shows a close correlation with the narrow-band  $\text{Ly}\alpha$  image. This indicates that morphological information about the ionizing continuum is contained in the narrow-band image despite the expected resonant scattering of the  $\text{Ly}\alpha$ . Together, we believe this justifies our use of  $\text{Ly}\alpha$  as a tracer of the underlying kinematics in those regions where other emission lines are too faint to have been detected.

In contrast to what was found for the extended regions, resonant scattering appears to play a significant role in the central regions. Figure 9 shows that in the  $\text{Ly}\alpha$  spectrum of 4C 60.07 at  $\text{PA} = 135^\circ$  there is a ‘gap’ at the position of the radio core. A comparable ‘hole’ in  $\text{Ly}\alpha$  emission near the systemic velocity of a galaxy has been found for SSA-22  $\text{Ly}\alpha$  Blob 1 (Bower et al. 2004) with the SAURON integral field spectrograph. It seems reasonable to attribute these velocity profiles to complex radiative transport effects of the resonantly scattered  $\text{Ly}\alpha$  emission in dense (dusty) media (e.g., Neufeld 1990; Ahn 2004) since both sources are strong submillimeter (rest-frame far-IR) emitters (Papadopoulos et al. 2000; Chapman et al. 2001). The emission line profile across the  $\text{Ly}\alpha$  gap can be fitted with two Gaussian components with central wavelengths of  $5839.9 \pm 0.5 \text{ \AA}$  and  $5806.8 \pm 0.4 \text{ \AA}$  and FWHMs of  $12.8 \pm 0.5 \text{ \AA}$  and  $10.6 \pm 0.3 \text{ \AA}$  respectively. This double peaked structure is very similar to the one inferred for static halos with coherent scattering and complete redistribution for an optical depth  $\tau \gtrsim 10$

(c.f., Fig. 1 in Meinköhn & Richling 2002). Figure 8 shows that Ly $\alpha$  and [O II] at PA = 81° both have very high velocity FWHMs of  $\sim 1600 - 1700 \text{ km s}^{-1}$ . The spectrum at PA = 135° shows the ‘Ly $\alpha$  gap’ and has a much broader FWHM of  $2600 \text{ km s}^{-1}$ .

It seems that the high HI densities *near* the cores result in resonant scattering to completely dominate the observed velocity profiles. In contrast, the similarity between the [O II] and Ly $\alpha$  profiles at PA = 81° suggests that *outside* the central regions Ly $\alpha$  *can* be used as a tracer of the kinematics of the gas.

### 4.3 Kinematics

#### 4.3.1 General kinematic structures

The general characteristics of the spectra presented in this paper are similar to what has been reported on previous observations of emission line regions around radio galaxies in the literature (e.g., van Ojik et al. 1996; Dey 1999; Villar-Martín et al. 2003). They show clear evidence for a distinction between disturbed and more quiescent regions. The inner regions have high surface brightnesses, are characterized by large velocity dispersions (FWHM  $\sim 1500 \text{ km s}^{-1}$ ) which are likely the result of shocks at the edge of the expanding radio source, and seem to be embedded in low surface brightness regions with FWHMs of order  $\sim 500 \text{ km s}^{-1}$ .

Except for the high velocity tails originating close to the nucleus the oxygen lines have typical FWHMs  $\sim 600 \text{ km s}^{-1}$ , which is narrower than seen in the Ly $\alpha$  lines. This is probably because the oxygen lines better reflect the real motions of the gas, whereas the Ly $\alpha$  lines may have been broadened by resonant scattering.

In addition to evidence for interactions with the radio sources there is evidence for velocity shears in the extended regions of both 4C 41.17 and 4C 60.07. Moreover, Fig. 6 shows that for 4C 41.17 the velocity structure along PA  $\sim 20^\circ$  (at an angle of  $\sim 55^\circ$  to the radio axis) has a symmetric distribution, as expected for rotation.

For B2 0902+34 none of the emission lines show strong indications for rotation or any ordered motion.

#### 4.3.2 Outflows

Evidence was found also for large scale outflows. Below we discuss the findings for each galaxy in detail.

#### 4C 41.17

The velocity structure of the bulk of the emission line gas appears predominantly redward shifted in the O, H $\beta$ , and Ly $\alpha$  lines. A similar velocity structure but shifted bluewards in its entirety is seen in the extended CO J=4–3 emission (De Breuck et al. 2004), suggesting that the AGN may be offset from the systemic redshift of the galaxy. The central CO component is situated at a relative velocity of  $-125 \text{ km s}^{-1}$ . This is similar to the relative velocity ( $-135 \pm 45 \text{ km s}^{-1}$ ) of the absorption seen in the low ionization species of [S II], C II, and [O I] (Dey et al. 1997).

The off-center CO component coincides with the position of the Ly $\alpha$  gap between the ‘cloud’ and the galaxy as discussed in Paper I, suggesting that it is absorbing

the Ly $\alpha$  emission at this location. Interestingly, it has a velocity of  $-550 \text{ km s}^{-1}$  relative to systemic, surprisingly close to the measured velocity offset (approximately  $-600 \text{ km s}^{-1}$ ) of both the Ly $\alpha$  and the [O II] emission along the Western filament.

#### 4C 60.07

The most striking feature of the emission line nebula associated with 4C 60.07 is the extended Ly $\alpha$  filament. Imaging showed this filament to have approximately constant surface brightness, to be sharply bounded on the NE side, and more “fluffy” on the SW side. As was discussed in Paper I the overall morphology is suggestive of a cone/superwind like structure. The galaxy at the tip of the filament would then be a chance superposition. If, however, the galaxy at the tip of the filament is at a redshift comparable to 4C 60.07, another explanation may be more likely. In this case the filament is best explained with a tidal tail. The galaxy may have passed through the gaseous halo of 4C 60.07 and due to ram pressure is being stripped of its gas. Such tails are seen also in cosmological simulations by for example Springel & Hernquist (2003) and could explain the lack of emission lines since only little fuel for star formation and AGN activity would remain. This would also explain naturally why the velocity offset between the filament and 4C 60.07 is largest near the galaxy. This is where the infalling galaxy reached its largest relative velocity, and it has been decelerating since and is likely to reach its turn-around point soon. For an average relative speed of  $\sim 250 \text{ km s}^{-1}$  the encounter must have happened approximately 300 Myr ago. This is comparable to the typical timescales of starbursts, but much longer than the radiative timescale ( $\sim 10^5 \text{ yr}$ ; Osterbrock 1989) of Ly $\alpha$  emission for conditions typical of the ISM. This implies that the gas in the filament must have been recently ionized. What can be the source of the ionization? One possibility is that stars which may have formed in this tidal tail, similar to what is seen in the UV observations with GALEX (Martin et al. 2003) of the Antennae, provide the ionizing radiation. Another possibility is that the galaxy is moving through a dense inter cluster medium, which is gravitationally focussed by the passage of the galaxy and is then cooling in its wake. This latter scenario was proposed by Fabian et al. (2001) to explain an 80 kpc filament seen in Abell 1795.

#### B2 0902+34

The velocity structure of the Ly $\alpha$  emission around B2 0902+34 seems to consist of two components. One component being the typical triangular shape resulting from spatially extended absorption that is blue-shifted relative to the systemic velocity (e.g., Dey 1999). The other component is the Ly $\alpha$  emission near the position of the radio core, but at a relative velocity of  $-500 \text{ km s}^{-1}$ . One explanation for this blue-shifted component is that the H I density in this region is lower than elsewhere, such that the Ly $\alpha$  is not completely absorbed. While it is certainly likely that the gas on the Eastern side of the galaxy is denser, as this is where imaging showed it to be brightest (stronger interaction with the radio source), this may form only part of the explanation.

The fact that only the blue-shifted component appears to have associated C IV  $\lambda 1549$  emission is surprising and argues against a simple density effect. A more interesting possibility is that this is a sign of a metal rich outflow from the central region, the result of a direct interaction between the peculiar radio source (see Carilli 1995, for details)



with the emission line gas, or possibly a sign of a merger between a metal-poor and metal-rich component (c.f. Overzier et al. 2001). A merger of two gaseous halos is also a viable option to explain the global structure of the emission line nebula which shows two bright areas. One of these areas did not show associated continuum emission, possibly because the stars in merging systems experience less drag than the gas and are moving faster towards the center of mass. However, it would be difficult for this latter scenario to explain how the smaller component could be in a more advanced evolutionary state. The most likely explanation therefore is that the blue-shifted Ly $\alpha$  and C IV emission is related to a metal enriched outflow, possibly driven by the passage of the radio jet.

#### 4.4 A comparison with CO observations

It is interesting to relate the ionized gaseous halos of 4C 41.17 and 4C 60.07 to recently discovered molecular gas associated with these objects.

For 4C 60.07, observations with mm-interferometers of the redshifted CO J=4–3 transition have resulted in the discovery of two kinematically and spatially separate gaseous reservoirs (Papadopoulos et al. 2000). Recently this result has been confirmed by VLA observations of the CO J=1–0 transition (Greve et al. 2004). After many unsuccessful attempts CO has now been detected also in 4C 41.17. Similar to what was found for 4C 60.07, De Breuck et al. (2004) report that the CO is distributed in two massive ( $> 5 \times 10^{11} M_{\odot}$ ) components. For both galaxies the CO components have been indicated on the 2-D spectra in Figures 4 and 7.

The presence of two separate molecular reservoirs near both galaxies suggests that mergers play a fundamental role in the triggering of AGN and starburst activity in HzRGs. Interestingly, similar velocity centroids are observed for the molecular and emission line gas of the filaments of 4C 41.17 and 4C 60.07. This may indicate a connection between the filaments and the gas, and is consistent with a superwind scenario.

#### 4.5 Metallicity

The discovery of both extended oxygen and CO lines throughout the emission line nebulae prompts an important question: Is the extended gas enriched or is it pristine primordial material? This is particularly important in considering whether enriched material from the nuclear regions can escape from the deep potential wells via large scale outflows and enrich the IGM.

For distant H II regions two methods are commonly used to determine the metallicity. One is based on the abundance of nitrogen, and the other on the abundance of oxygen.

For HzRGs N V is often used as a reliable tracer of the abundances, because it is rather insensitive to shock ionization, density fluctuations, ionization parameter, and has a quadratic dependence on the metallicity (Villar-Martín et al. 1999). Vernet et al. (2001) presented a metallicity sequence for HzRGs that is similar to the one for quasars (Hamann & Ferland 1993). 4C 41.17 was included in their study and a metallicity of  $Z \sim 1.3 Z_{\odot}$  was inferred for the central region (aperture of  $2'' \times 1''$  Dey et al. 1997).

The oxygen based indicator Pagel et al. ( $R_{23}$ ; 1979) does not place strong constraints for sources hosting luminous AGN. Still, the extent and luminosity of the oxygen lines confirm not only that there must have been at least one significant generation of massive stars, but also that this must have happened early in the formation of 4C 41.17 for the oxygen to have spread throughout the halo.

#### 4.6 Mass estimates

One of the outstanding questions in galaxy formation is how the bulk of galaxy mass assembles. In scenarios of monolithic collapse this is expected to be more or less instantaneous, whereas in models of hierarchical structure formation the mass is envisaged to grow gradually over long time scales. Determining accurate masses for distant objects can help differentiate between the two scenarios.

##### 4.6.1 Luminosity based masses

Typically, the  $K$ -band magnitudes of HzRGs suggest that they are already massive systems (e.g., De Breuck et al. 2002; Rocca-Volmerange et al. 2004). For example, Graham et al. (1994) inferred for 4C 41.17 a stellar mass of order  $20 L_*$ .

Assuming an absence of absorption by dust, a mass limit for the nebula can be obtained also from photoionization modelling of the total  $\text{Ly}\alpha$  flux. In Paper I we thus inferred gas masses of the order  $0.3 - 1.3 \times 10^{10} \times f_{v,-5}^{1/2} M_\odot$ , where  $f_{v,-5}$  is the volume filling factor of the extended  $\text{Ly}\alpha$  emitting gas relative to  $f_v = 10^{-5}$ . For  $f_v \sim 1$  this amount is substantial and comparable to that of fully formed, massive elliptical galaxies in the local Universe. Similarly, assuming a filling factor of  $f_v = 10^{-5}$ , Villar-Martín et al. (2003) inferred masses  $10^9 - 10^{10} M_\odot$  with densities in the range  $\sim 17 - 150 \text{ cm}^{-3}$  for 9 extended emission line halos associated with radio galaxies at  $z \sim 2.5$ .

##### 4.6.2 Dynamical mass estimates

van Ojik et al. (1997) and Villar-Martín et al. (2003) have presented dynamical mass estimates for the more quiescent parts of the emission line regions in their studies. There are two methods of estimating the dynamical masses. First, one can assume that the halos consist of gas that has settled in rotating disks. Secondly, the halos can be envisaged as consisting of virialized clumps, which have velocity dispersions that balance the gravitational forces.

##### *Rotating disks*

In the case of rotating disks, the mass can be estimated by measuring the velocity shear across the halo and using:  $M_{\text{dyn}}^{\text{rot}} = \frac{RV^2}{G \sin^2 i}$  with  $R$  the radius of the disk,  $V$  half the amplitude of the rotation curve, and  $i$  the inclination of the disk with respect to the plane of sky. Villar-Martín et al. (2003) found evidence for rotation in 5 out of 9 halo velocity fields and inferred masses of order  $M_{\text{dyn}}^{\text{rot}} \times \sin^2 i \sim 0.3 - 3 \times 10^{12} M_\odot$ .

For 4C 41.17 the measured relative velocity distributions beyond the radio lobes show a velocity shear of  $\sim 300 \text{ km s}^{-1}$  ( $+100 \text{ km s}^{-1}$  to  $-200 \text{ km s}^{-1}$ ) at  $\text{PA} = 76^\circ$ , over a distance of  $R = 20''/2 = 77 \text{ kpc}$ . From this we infer a dynamical mass of about  $M_{\text{dyn}}^{\text{rot}} \times$

$\sin^2 i \sim 4 \times 10^{11} M_{\odot}$ . The velocity profiles at position angles PA = 19°, and 21° show no signs of a shear, consistent with their approximate alignment along an axis of rotation. Similarly, for 4C 60.07 a velocity shear of  $\sim 400 \text{ km s}^{-1}$  (+200  $\text{km s}^{-1}$  to  $-200 \text{ km s}^{-1}$ ) at PA = 81° over a distance of  $R = 7''/2 = 25 \text{ kpc}$  yields an inferred dynamical mass of  $M_{\text{dyn}}^{\text{rot}} \times \sin^2 i \sim 3 \times 10^{11} M_{\odot}$ .

For comparison, CO observations by De Breuck et al. (2004) and Papadopoulos et al. (2000) yield dynamical mass estimates  $M_{\text{dyn}}^{\text{CO}} \times \sin^2 i > 5 \times 10^{11} M_{\odot}$  and  $M_{\text{dyn}}^{\text{CO}} \times \sin^2 i > 8 \times 10^{11} M_{\odot}$  for 4C 41.17 and 4C 60.07 respectively.

#### *Pressure supported clouds*

In contrast to the extended emission line halos of 4C 41.17 and 4C 60.07, the velocity field for B2 0902+34 does not show evidence for rotation. We therefore also estimate masses for the halos if they would be supported against gravitation by velocity dispersions of the cloudlets in the halo. For this scenario the dynamical mass is given by:  $M_{\text{dyn}}^{\text{vir}} = 5RV_R^2/G$ , with  $V_R$  the radial velocity dispersion of the clouds (Carroll & Ostlie 1999). With this dynamical masses for the outer regions of  $M_{\text{dyn}}^{\text{vir}} = 5 - 10 \times 10^{12} M_{\odot}$  are inferred. For the inner regions, where signal-to-noise is better, we find lower masses of  $M_{\text{dyn}}^{\text{vir}} \sim 2 \times 10^{12} M_{\odot}$ .

### 4.7 Cosmological Implications

Absorbing gas associated with low velocity outflows has now been observed in several HzRGs (van Ojik et al. 1997; Jarvis et al. 2003). Almost all of these show asymmetric Ly $\alpha$  profiles suggesting the presence of blue-shifted absorbing gas which appears to be spatially extended over the entire emission line region (see e.g., Dey 1999). Spectroscopic evidence for outflows at high redshifts exists also for other, presumably less massive ( $\lesssim L_*$ ), and less metal enriched ( $Z \sim 0.3 Z_{\odot}$ ) galaxies (Pettini et al. 2001; Dawson et al. 2002; Shapley et al. 2003).

There is an ongoing debate whether massive ( $> L_*$ ) galaxies or less massive ( $< L_*$ ) galaxies enrich the ICM. Martin (1999) and Heckman et al. (2000) found that outflow speeds are largely independent of galaxy mass. This would imply that smaller galaxies are more efficient at ejecting enriched material to large radii. Specifically, Heckman (2002) claim that for massive galaxies the metals will not escape the deep potential wells. However, recent modelling suggests that this needs to be true only for the most massive halos ( $v_{\text{esc}} > 600 \text{ km s}^{-1}$ ) before discrepancies with the mass/metallicity relation become significant, and that the bulk of the metals in clusters are produced by  $L_*$  and brighter galaxies (e.g., Nagashima et al. 2004). Sensitive spectroscopic observations of ultra luminous infrared galaxies, now also find that more luminous galaxies drive faster stellar winds (Martin 2004), and that the terminal outflow velocities always approach the galactic escape velocity.

For all three HzRGs we have found features that can be interpreted as signs of outflows. The extended optical filament of 4C 60.07 is reminiscent of an outflow in the plane of sky. The blue-shifted carbon-rich component of B2 0902+34 could be the result of an outflow of enriched material with an outflow velocity of up to  $1000 \text{ km s}^{-1}$ . The near-infrared [OII] spectroscopy (Figs. 4, 5, 13), and earlier optical Ly $\alpha$  spectroscopy

of 4C 41.17 (Fig. 4; Dey et al. 1997), show that both emission lines exhibit large blue-shifted velocities  $\sim 600 - 900 \text{ km s}^{-1}$  (in projection) along the radio axis. In particular, the gas is very disturbed along the south-west filament, with  $\text{Ly}\alpha$  velocity widths ranging up to  $\sim 900 - 1600 \text{ km s}^{-1}$ . Beyond the radio hotspot, the velocity and velocity widths decrease abruptly. The kinematics, the radial filamentary structure, and chemical enrichment of the gas all indicate a process of entrainment of material away from the central regions by the radio jet. In this scenario, the optical filament represents the shocked radiative cocoon of the radio source.

The multiple component, asymmetric, and twisted radio structure of 4C 41.17 suggests that the central SMBH has experienced multiple periods of radio source activity and precession, presumably triggered by the interaction with one of the many clumpy components which make up the complex galaxy structure (van Breugel et al. 1999; Steinbring et al. 2002). The precessing radio source excavates the central region of the galaxy, exposing surrounding material to a strong radiation field and mass outflow from the active nucleus.

For a galaxy mass of  $1 \times 10^{12} M_{\odot}$ , which seems typical for HzRGs, the escape velocity is approximately  $v_{\text{esc}} \sim 400 \text{ km s}^{-1}$ . The velocity gradients found from the spectroscopic observations are a factor 1.5–2.5 larger. While it may still be true that purely starburst powered super galactic winds may not be sufficiently energetic for significant amounts of enriched nuclear material to escape from the galactic potentials, the additional driving forces of the central AGN and the path cleared by the radio source seem able to overcome this easily. Therefore, entrainment of nuclear material seems a viable scheme of enriching the ICM.

The time scales for star formation and radio source activity in 4C 41.17 are very similar (Chambers et al. 1990; Bicknell et al. 2000) and comparable to that for transporting the  $[\text{O II}]$  gas along the filament out to the vicinity of the south-west hotspot ( $\sim 7 \times 10^7$  yrs at  $\sim 900 \text{ km s}^{-1}$ ). It suggests an overall picture where the growth of the galaxy through merging, the triggering of SMBH and starburst activity, and the enrichment of its environment through outflows are all closely coupled processes.

## 5 Conclusion

One of our most important new results is the discovery of very extended  $[\text{O II}]$  and  $[\text{O III}]$  emission associated with the gaseous halos of HzRGs. In particular, for 4C 41.17  $[\text{O II}]$  emission has been detected as far as  $\sim 60 \text{ kpc}$  from the nucleus, providing evidence that the  $\text{Ly}\alpha$  nebula, at least in this direction, is not only the result of scattering but must be locally ionized. Furthermore, the presence of the oxygen emission lines shows that the extended halo gas is not chemically pristine gas falling into the galaxy, but is instead derived from regions of active star formation, and possibly transported outward from regions located closer to the nucleus.

The evidence presented here could help cast observational light on the amazingly good correlation found in galaxies between the stellar velocity dispersion and the black hole mass (Gebhardt et al. 2000; Ferrarese & Merritt 2000). Silk & Rees (1998) and Sazonov et al. (2004) have speculated that this results from outflows which are driven by the radiation pressure provided by the black hole. These serve to limit the ratio of

the black hole mass to bulge mass by ejecting the excess gas when such outflows can overcome the galactic potential. In the case of 4C 41.17 we have good evidence that the radio lobes are driving this outflow, assisted by radiation pressure and starburst winds. Precession of the axis of ejection is likely to gradually clear out the gas in the halo over a time period comparable with the dynamical timescale of the halo. Thus, for 4C 41.17 we may be observing the moment where galaxy collapse gives way to mass ejection. These processes may help shape the high-mass end of the galaxy luminosity function.

## Acknowledgements

It is a pleasure to thank Carlos De Breuck and Andrew Zirm for stimulating discussions. We thank all staff at the W.M. Keck Observatory for their excellent support. The authors wish to recognize and acknowledge the very significant cultural role and reverence that the summit of Mauna Kea has always had within the indigenous Hawaiian community. We are most grateful to have the opportunity to conduct observations from this mountain. M.R. thanks Mario Livio for generous hospitality at the Space Telescope Science Institute. The work by M.R., W.v.B., W.d.V., and S.A.S. was performed under the auspices of the U.S. Department of Energy, National Nuclear Security Administration by the University of California, Lawrence Livermore National Laboratory under contract No. W-7405-Eng-48. The work of D.S. was carried out at Jet Propulsion Laboratory, California Institute of Technology under a contract with NASA. M.D. acknowledges the support of the ANU and the Australian Research Council (ARC) for his ARC Australian Federation Fellowship, and also under the ARC Discovery project DP0208445. This work was supported by the European Community Research and Training Network "The Physics of the Intergalactic Medium".

## References

- Aguirre, A., Hernquist, L., Schaye, J., et al. 2001, *ApJ*, 561, 521  
Ahn, S. 2004, *ApJ*, 601, L25  
Allen, M. G., Dopita, M. A., & Tsvetanov, Z. I. 1998, *ApJ*, 493, 571  
Athreya, R. M., Kapahi, V. K., McCarthy, P. J., & van Breugel, W. 1998, *A&A*, 329, 809  
Benson, A. J., Bower, R. G., Frenk, C. S., et al. 2003, *ArXiv Astrophysics e-prints*  
Best, P. N., Röttgering, H. J. A., & Longair, M. S. 2000, *MNRAS*, 311, 23  
Bicknell, G. V., Sutherland, R. S., van Breugel, W. J. M., et al. 2000, *ApJ*, 540, 678  
Bower, R., Morris, S. L., Bacon, R., et al. 2004, *MNRAS*, in press  
Briggs, F. H., Sorar, E., & Taramopoulos, A. 1993, *ApJ*, 415, L99+  
Carilli, C. L. 1995, *A&A*, 298, 77  
Carilli, C. L., Owen, F. N., & Harris, D. E. 1994, *AJ*, 107, 480  
Carilli, C. L., Röttgering, H. J. A., van Ojik, R., Miley, G. K., & van Breugel, W. J. M. 1997, *ApJ*, 109, 1  
Carroll, B. & Ostlie, D. 1999, *An Introduction to Modern Astrophysics* (Addison Wesley)  
Carson, J. E., Larkin, J. E., McLean, I. S., et al. 2001, *ApJ*, 563, 63  
Chambers, K. C., Miley, G. K., & van Breugel, W. J. M. 1990, *ApJ*, 363, 21  
Chambers, K. C., Miley, G. K., van Breugel, W. J. M., et al. 1996, *ApJ*, 106, 247  
Chapman, S. C., Lewis, G. F., Scott, D., et al. 2001, *ApJ*, 548, L17  
Cody, A. M. & Braun, R. 2003, *A&A*, 400, 871  
Dawson, S., Spinrad, H., Stern, D., et al. 2002, *ApJ*, 570, 92  
De Breuck, C., Neri, R., Downes, D., et al. 2004, *A&A*, submitted

| Object     | Line          | $\lambda_{\text{rest}}$<br>Å | $\lambda_{\text{obs}}$<br>Å | z                   | FWHM<br>Å      | FWHM<br>km s <sup>-1</sup> | Observed flux<br>$\times 10^{-17}$ erg s <sup>-1</sup> cm <sup>-2</sup> | EW <sub>obs</sub><br>Å |
|------------|---------------|------------------------------|-----------------------------|---------------------|----------------|----------------------------|---|------------------------|
| B2 0902+34 | Ly $\alpha$   | 1216                         | 5334.69 $\pm$ 0.09          | 3.3883 $\pm$ 0.0001 | 21.9 $\pm$ 0.2 | 1233 $\pm$ 13              | 49.4 $\pm$ 0.5  | 431 $\pm$ 12           |
|            | C IV(doublet) | 1549                         | 6795.00 $\pm$ 0.62          | 3.3867 $\pm$ 0.0004 | 22.7 $\pm$ 1.5 | 1003 $\pm$ 65              | 11.2 $\pm$ 0.4  | 109 $\pm$ 5            |
|            | He II         | 1641                         | 7199.37 $\pm$ 0.37          | 3.3886 $\pm$ 0.0002 | 17.2 $\pm$ 0.9 | 718 $\pm$ 37               | 8.9 $\pm$ 0.3   | 127 $\pm$ 7            |
|            | [O III]       | 3727                         | 1637.67 $\pm$ 0.14          | 3.3941 $\pm$ 0.0004 | 42.0 $\pm$ 3.0 | 778 $\pm$ 62               | 71.2 $\pm$ 7.5  | 310 $\pm$ 370          |
|            | Ly $\alpha$   | 1216                         | 5826.52 $\pm$ 0.07          | 3.7928 $\pm$ 0.0001 | 47.1 $\pm$ 0.2 | 2425 $\pm$ 12              | 41.1 $\pm$ 0.2  | 4976 $\pm$ 497         |
| 4C 60.07   | C IV(doublet) | 1549                         | 7420.75 $\pm$ 1.34          | 3.7907 $\pm$ 0.0009 | 36.5 $\pm$ 3.3 | 1475 $\pm$ 132             | 5.0 $\pm$ 0.3   | 597 $\pm$ 179          |
|            | He II         | 1641                         | 7855.7 $\pm$ 1.07           | 3.7887 $\pm$ 0.0007 | 73.9 $\pm$ 2.7 | 2820 $\pm$ 104             | 9.5 $\pm$ 0.3   | 788 $\pm$ 68           |
|            | C III]        | 1909                         | 9141.88 $\pm$ 1.82          | 3.7896 $\pm$ 0.0010 | 59.9 $\pm$ 4.7 | 1963 $\pm$ 156             | 0.2 $\pm$ 0.8   | 14 $\pm$ 63            |
|            | [O III]       | 3727                         | 17851. $\pm$ 10             | 3.790. $\pm$ 0.0030 | 82. $\pm$ 30   | 1361. $\pm$ 500            | 267. $\pm$ 100  | 190. $\pm$ 80          |
|            | [O III]       | 3727                         | 17904. $\pm$ 20             | 3.803. $\pm$ 0.0060 | 45. $\pm$ 20   | 754. $\pm$ 335             | 75. $\pm$ 40  | 400. $\pm$ 200         |
| 4C 41.17   | H $\beta$     | 4861                         | 23356 $\pm$ 8               | 3.8047 $\pm$ 0.0017 | 54.6 $\pm$ 15  | 701 $\pm$ 271              | 34.8 $\pm$ 11.6   | 112 $\pm$ 54           |
|            | [O III]       | 4959                         | 23811 $\pm$ 3               | 3.8015 $\pm$ 0.0006 | 50.8 $\pm$ 7.8 | 640 $\pm$ 98               | 129.4 $\pm$ 20.5  | 259 $\pm$ 85           |
|            | [O III]       | 5007                         | 24042 $\pm$ 1               | 3.8017 $\pm$ 0.0002 | 58.4 $\pm$ 3.0 | 728 $\pm$ 37               | 484.7 $\pm$ 22.6  | 1031 $\pm$ 352         |

Table 3 — Summary of Emission-Line Measurements of the galaxies in this program

- De Breuck, C., Röttgering, H., Miley, G., van Breugel, W., & Best, P. 2000, *A&A*, 362, 519
- De Breuck, C., van Breugel, W., Stanford, S. A., et al. 2002, *AJ*, 123, 637
- Dey, A. 1999, in *The Most Distant Radio Galaxies*, 19–+
- Dey, A., van Breugel, W., Vacca, W. D., & Antonucci, R. 1997, *ApJ*, 490, 698
- Dunlop, J. S., Hughes, D. H., Rawlings, S., Eales, S. A., & Ward, M. J. 1994, *Nature*, 370, 347
- Eales, S. A. & Rawlings, S. 1993, *ApJ*, 411, 67
- Eisenhardt, P. & Dickinson, M. 1992, *ApJ*, 399, L47
- Fabian, A. C., Sanders, J. S., Ettori, S., et al. 2001, *MNRAS*, 321, L33
- Ferrarese, L. & Merritt, D. 2000, *ApJ*, 539, L9
- Gebhardt, K., Bender, R., Bower, G., et al. 2000, *ApJ*, 539, L13
- Graham, J. R., Matthews, K., Soifer, B. T., et al. 1994, *ApJ*, 420, L5
- Greve, T. R., Ivison, R. J., & Papadopoulos, P. P. 2004, *A&A*, in press
- Hamann, F. & Ferland, G. 1993, *ApJ*, 418, 11
- Heckman, T. M. 2002, in *ASP Conf. Ser. 254: Extragalactic Gas at Low Redshift*, 292–+
- Heckman, T. M., Lehnert, M. D., Strickland, D. K., & Armus, L. 2000, *ApJ*, 129, 493
- Hippelein, H. & Meisenheimer, K. 1993, *Nature*, 362, 224
- Inskip, K. J., Best, P. N., Rawlings, S., et al. 2002, *MNRAS*, 337, 1381
- Iwamuro, F., Motohara, K., Maihara, T., et al. 2003, *ApJ*, 598, 178
- Jarvis, M. J., Wilman, R. J., Röttgering, H. J. A., & Binette, L. 2003, *MNRAS*, 338, 263
- Kauffmann, G. & Haehnelt, M. 2000, *MNRAS*, 311, 576
- King, A. 2003, *ApJ*, 596, L27
- Lilly, S. J. 1988, *ApJ*, 333, 161
- Loeb, A. 1993, *ApJ*, 403, 542
- Magorrian, J., Tremaine, S., Richstone, D., et al. 1998, *AJ*, 115, 2285
- Martin, C., Barlow, T., Barnhart, W., et al. 2003, in *Future EUV/UV and Visible Space Astrophysics Missions and Instrumentation*. Edited by J. Chris Blades, Oswald H. W. Siegmund. Proceedings of the SPIE, Volume 4854, pp. 336–350 (2003)., 336–350
- Martin, C. L. 1999, *ApJ*, 513, 156
- Martin, C. L. 2004, *ApJ*, submitted
- Martin-Mirones, J. M., Martinez-Gonzalez, E., Gonzalez-Serrano, J. I., & Sanz, J. L. 1995, *ApJ*, 440, 191
- Massey, P., Strobel, K., Barnes, J. V., & Anderson, E. 1988, *ApJ*, 328, 315
- Maxfield, L., Spinrad, H., Stern, D., Dey, A., & Dickinson, M. 2002, *AJ*, 123, 2321
- McCarthy, P. J. 1993, *ARA&A*, 31, 639
- McLean, I. S., Becklin, E. E., Bendiksen, O., et al. 1998, in *Proc. SPIE Vol. 3354, p. 566–578, Infrared Astronomical Instrumentation*, Albert M. Fowler; Ed., 566–578
- Meinköhn, E. & Richling, S. 2002, *A&A*, 392, 827
- Nagashima, M., Lacey, C. G., Baugh, C. M., Frenk, C. S., & Cole, S. 2004, *ArXiv Astrophysics e-prints*
- Neufeld, D. A. 1990, *ApJ*, 350, 216
- Oke, J. B., Cohen, J. G., Carr, M., et al. 1995, *PASP*, 107, 375
- Osterbrock, D. E. 1989, *Astrophysics of gaseous nebulae and active galactic nuclei* (Research supported by the University of California, John Simon Guggenheim Memorial Foundation, University of Minnesota, et al. Mill Valley, CA, University Science Books, 1989, 422 p.)
- Overzier, R. A., Röttgering, H. J. A., Kurk, J. D., & De Breuck, C. 2001, *A&A*, 367, L5
- Pagel, B. E. J., Edmunds, M. G., Blackwell, D. E., Chun, M. S., & Smith, G. 1979, *MNRAS*, 189, 95
- Papadopoulos, P. P., Röttgering, H. J. A., van der Werf, P. P., et al. 2000, *ApJ*, 528, 626
- Pentericci, L., Van Reeve, W., Carilli, C. L., Röttgering, H. J. A., & Miley, G. K. 2000, *A&AS*, 145, 121
- Pettini, M., Shapley, A. E., Steidel, C. C., et al. 2001, *ApJ*, 554, 981
- Rauch, M., Sargent, W. L. W., & Barlow, T. A. 2001, *ApJ*, 554, 823
- Reuland, M., van Breugel, W., Röttgering, H., et al. 2003, *ApJ*, 592, 755
- Rocca-Volmerange, B., Le Borgne, D., De Breuck, C., Fioc, M., & Moy, E. 2004, *A&A*, 415, 931
- Röttgering, H. J. A., van Ojik, R., Miley, G. K., et al. 1997, *A&A*, 326, 505
- Sazonov, S. Y., Ostriker, J. P., Ciotti, L., & Sunyaev, R. A. 2004, *ArXiv Astrophysics e-prints*
- Scharf, C., Smail, I., Ivison, R., et al. 2003, *ApJ*, 596, 105
- Shapley, A. E., Steidel, C. C., Pettini, M., & Adelberger, K. L. 2003, *ApJ*, 588, 65

- Sheinis, A. I., Miller, J. S., Bolte, M., & Sutin, B. M. 2000, in Proc. SPIE Vol. 4008, p. 522-533, Optical and IR Telescope Instrumentation and Detectors, Masanori Iye; Alan F. Moorwood; Eds., 522–533
- Silk, J. & Rees, M. J. 1998, *A&A*, 331, L1
- Springel, V. & Hernquist, L. 2003, in IAU Symposium, 273–+
- Steinbring, E., Crampton, D., & Hutchings, J. B. 2002, *ApJ*, 569, 611
- Stevens, J. A., Ivison, R. J., Dunlop, J. S., et al. 2003, *Nature*, 425, 264
- Tody, D. 1993, in ASP Conf. Ser. 52: Astronomical Data Analysis Software and Systems II, 173–+
- Uson, J. M., Bagri, D. S., & Cornwell, T. J. 1991, *Physical Review Letters*, 67, 3328
- van Breugel, W., Stanford, A., Dey, A., et al. 1999, in *The Most Distant Radio Galaxies*, 49–+
- van Ojik, R., Röttgering, H. J. A., Carilli, C. L., et al. 1996, *A&A*, 313, 25
- van Ojik, R., Röttgering, H. J. A., Miley, G. K., & Hunstead, R. W. 1997, *A&A*, 317, 358
- Vernet, J., Fosbury, R. A. E., Villar-Martín, M., et al. 2001, *A&A*, 366, 7
- Villar-Martín, M., Fosbury, R. A. E., Binette, L., Tadhunter, C. N., & Rocca-Volmerange, B. 1999, *A&A*, 351, 47
- Villar-Martín, M., Vernet, J., di Serego Alighieri, S., et al. 2003, *MNRAS*, 346, 273
- Wilman, R. J., Jarvis, M. J., Röttgering, H. J. A., & Binette, L. 2004, *MNRAS*, 351, 1109



# Nederlandse samenvatting

## Introductie

DE doelstellingen die astronomen zichzelf stellen zijn ambitieus: het begijpen van de vorming en de evolutie van het Heelal. In de sterrenkunde is het in het algemeen niet mogelijk om de objecten onder studie aan te raken. Ook is het meestal niet mogelijk om hun omgeving te veranderen en te zien wat voor invloed dat heeft op hun gedrag. Dit is in tegenstelling tot vele andere wetenschappen, en stelt astronomen voor een extra uitdaging<sup>3</sup>.

Gelukkig helpt de natuur ons een handje. Het feit dat de lichtsnelheid eindig is, impliceert dat licht van verre objecten lang onderweg is geweest wanneer wij het waarnemen<sup>4</sup>. Dit licht bevat daarom informatie over de toestand van objecten zoals ze lang geleden waren. Hoewel veel grootschalige processen in het Heelal slechts veranderen over tijdschalen veel langer dan een mensenleven, is het hierdoor mogelijk hun evolutie te bestuderen. De truc is om objecten te vinden die intrinsiek hetzelfde zijn maar op verschillende afstanden tot ons staan.

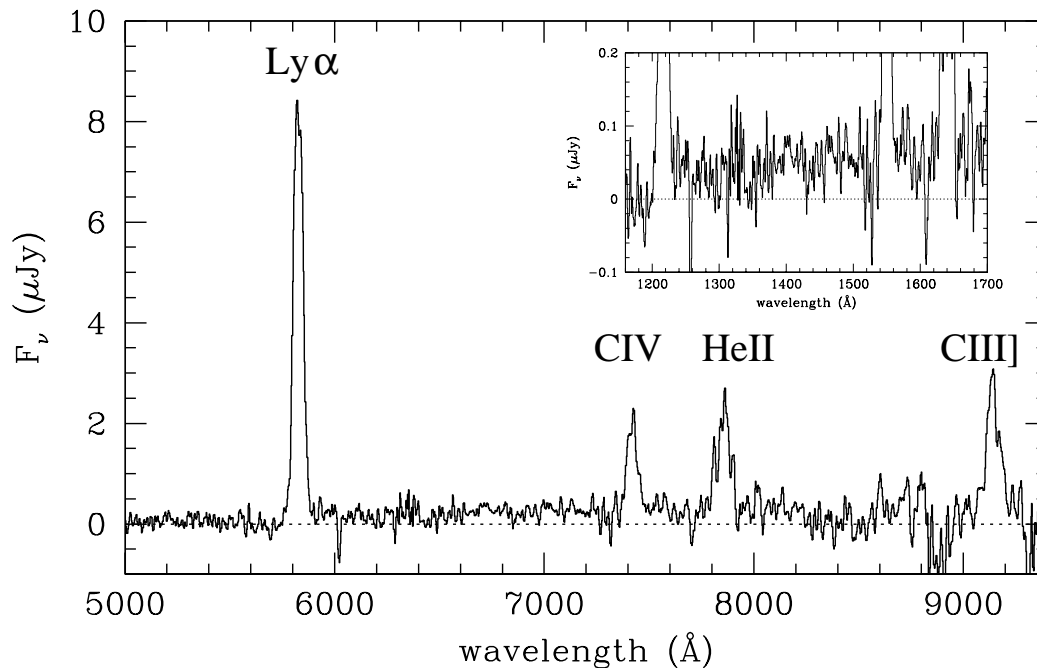
Het bepalen van grote afstanden in de sterrenkunde maakt gebruik van de uitdijning van het heelal<sup>5</sup>. Deze expansie werd voor het eerst ontdekt door Edwin Hubble. Verre gelegen stelsels bewegen zich sneller van ons af dan dichterbij gelegen stelsels. Dit leidt tot een fenomeen vergelijkbaar met het Doppler effect, waarvan de verandering in toonhoogte van een passerende brommer of een sirene van een ambulance bekende voorbeelden zijn (de toon is lager als het object zich van ons afbeweegt dan wanneer het nadert). Licht wordt op de zelfde manier “uitgerekt” en korte golflengtes worden langer (roder). In formule vorm:  $\lambda_{\text{waargenomen}} = \lambda_{\text{uitgezonden}} \times (1 + z)$ . De grootte  $z$  noemt men de roodverschuiving. In de kosmologie wordt de roodverschuiving zoveel gebruikt, dat men deze vaak zelf als maat van afstand gebruikt. Het licht van objecten met een roodverschuiving  $z = 1$  werd uitgezonden toen het Heelal de helft van zijn huidige leeftijd had (volgens huidige schattingen leven wij nu 13.7 miljard jaar na de oerknal). In dit proefschrift worden objecten bekeken met roodverschuivingen  $z = 3-5$ . Het Heelal was toen nog maar 1-2 miljard jaar oud.

---

<sup>3</sup>Hoewel in een vak als neurowetenschappen experimenteren mogelijk is kent het vergelijkbare problemen: ontleed een brein om de werking te bestuderen, en het houdt op te werken.

<sup>4</sup>Reizend met een snelheid van een snelle sportwagen, zeg 200 km/h, duurt het 85 jaar om de Zon te bereiken, 23 miljoen jaar om de dichtstbijzijnde ster Proxima Centauri te bereiken, en langer dan 100 miljard jaar om ons eigen Melkwegstelsel te verlaten in het vlak van rotatie. Daarom drukken astronomen afstanden uit in zogeheten parsecs (pc; en vaak zelfs kilo pc en Mega pc). De parsec is gedefinieerd als de afstand waarop de straal van de baan van de Aarde om de Zon een boogseconde beslaat. De auto uit ons voorbeeld zou er 17.6 miljoen jaar over doen om een parsec af te leggen. Licht reist veel sneller (ongeveer 300.000 km/s), maar heeft er nog altijd 3.26 jaar voor nodig.

<sup>5</sup>Voor kleine tot middellange afstanden wordt een verscheidenheid aan methodes gebruikt, die onafhankelijke schattingen voor afstanden geven. De grote afstanden in de sterrenkunde zijn gekalibreerd aan deze zogeheten afstandsladder



**Figuur 14** — Optisch 1-D spectrum van het radiostelsel 4C 60.07, besproken in Hoofdstuk 7. De prominente emissielijnen  $\text{Ly}\alpha$ , C IV, He II, en C III] zijn aangegeven. Gebaseerd op de He II  $\lambda 1640$  lijn wordt de roodverschuiving bepaald op  $z = 3.7887 \pm 0.0007$ . De inzet is een vergroting van het UV gebied van het spectrum, getransformeerd naar de rust golflengtes zoals het spectrum in het stelsel werd uitgezonden.

Het bepalen van roodverschuivingen gaat het eenvoudigste door het meten van de golflengte van verschoven emissielijnen (licht) met een bekende rustgolflengte. Emissielijnen zijn geassocieerd met specifieke atomen. Elektronen bevinden zich in banen om de kern van het atoom. Als een atoom geëxciteerd wordt (bijvoorbeeld door botsingen of bestraling) kan een elektron losspringen, of tijdelijk verschuiven naar een grotere baan met meer energie. Als na verloop van tijd het atoom weer terugvalt naar zijn grondtoestand komt de opgenomen energie weer vrij. Doordat, op grond van de quantumfysica, slechts bepaalde banen zijn toegestaan, komen er bij het verspringen van de ene naar de andere baan discrete hoeveelheden energie vrij met elk hun eigen golflengte. Als nu de rustgolflengte bekend is, kan men uit het geobserveerde spectrum (vgl. een prisma dat zonlicht omzet in een regenboog) van een stelsel de roodverschuiving bepalen. Figuur 14 is een weergave van zo'n spectrum voor een (radio) sterrenstelsel. Dit figuur laat een relatief zwak continuum zien met daarbovenop de emissielijnen van verschillende elementen. Het continuum komt grotendeels van sterren en de emissielijnen van gas dat door straling van de sterren (en door de straling geassocieerd met een zwart gat) geëxciteerd wordt. Als een spectrum maar één lijn bevat is identificatie daarvan lastig. Gelukkig zijn er in dit spectrum vier lijnen duidelijk waarneembaar, en omdat ze alle vier dezelfde roodverschuiving moeten geven is er maar één oplossing mogelijk: de roodverschuiving is  $z = 3.8$ . Het licht is dus 11.5 miljard jaar onderweg geweest voordat het door onze telescoop werd opgevangen.

Zoals Figuur 14 ook aangeeft, zenden atomen bij sommige golflengtes meer straling uit dan bij andere. De helderste lijn, Lyman alpha ( $Ly\alpha$ ), is geassocieerd met geïoniseerd waterstof. Waterstof komt erg veel voor in het Heelal, ongeveer 73% van massa van de elementen (25% is helium en de overige 2% is de rest, waaronder wij). Uit deze mix van waterstof en helium ontstaan de meeste sterren en melkwegstelsels. Door kernfusie in sterren worden deze elementen langzaam omgezet in “afvalproducten” zoals koolstof, zuurstof, ijzer etc. Zware sterren leven kort maar krachtig gedurende een paar miljoen jaar. Tegen het einde van het leven van een zware ster, worden deze afvalproducten in een grote supernova explosie de ruimte ingeslingerd. Relatief kleine sterren dragen nauwelijks bij aan de verspreiding van de elementen, omdat ze veel langzamer branden. Onze zon bijvoorbeeld is al 5 miljard jaar oud en zal nog zo’n 5 miljard jaar meegaan.

Als er genoeg afvalproducten bijelkaar komen, vormen ze grote stofwolken die tot wel 1 miljoen zonsmassa’s<sup>6</sup> kunnen bevatten. Omdat dit stof de binnengelegen gebieden afschermt tegen straling van buitenaf, kunnen deze gebieden afkoelen. Daardoor kunnen ze zich samentrekken en uiteindelijk weer nieuwe sterren vormen. Vier dingen zijn hier belangrijk. Ten eerste: stof is een product van stervorming. Ten tweede: stof faciliteert verdere stervorming. Ten derde: de meeste stervormings gebieden zijn volledig aan het oog onttrokken door de gas en stofwolken waarin ze zich bevinden. Het laatste belangrijke punt is dat nieuwe sterren het stof opwarmen, waardoor dit in het verre infrarood gaat stralen. Wij zullen de intensiteit van de straling afkomstig van dit stof in Hoofdstuk 2, 3, 4, en 5 gebruiken als maat voor de snelheid waarmee nieuwe sterren zich vormen.

## Dit proefschrift

Sterrenstelsels worden geclassificeerd in twee verschillende hoofdsoorten. Er zijn majestueuze spiraalstelsels die er schijfvorming uitzien en er zijn meer rugbybalachtige elliptische stelsels. Verder zijn er nog tussenvormen en onregelmatige stelsels. Sterrenstelsels bestaan uit vaak wel 100 miljard sterren en verder grote hoeveelheden gas en stof, en materiaal dat we niet kunnen zien (de zogeheten donkere materie).

Het doel van dit proefschrift is het bestuderen van de vorming en evolutie van specifiek de grote en zware melkwegstelsels door gebruik te maken van waarnemingen van radiostelsels. We zullen verderop aangeven waarom juist radiostelsels hierover unieke informatie kunnen geven. Eerst volgt nu een kort overzicht van twee populaire theoriën van de vorming van melkwegstelsels.

De algemeen aanvaarde theorie met betrekking tot het ontstaan van het Heelal is de zogeheten Oerknal theorie. Deze stelt dat het Heelal in het begin infinitesimaal klein en heel heet was en hierna als gevolg van een soort explosie bezig is uit te dijen en langzaam afkoelt. De gloed van deze explosie is nog steeds waarneembaar, de kosmische achtergrond straling. De straling heeft een gladde verdeling, de afwijkingen zijn van de orde 1:100.000. Dit geeft aan dat het Heelal in het begin en vlak na de oerknal heel glad geweest moet zijn, vaak genoemd de oersoep. Als we echter naar het lokale Heelal kijken, zien we dat dit bestaat uit sterren en sterrenstelsels met enorme

<sup>6</sup>1 zonsmassa komt overeen met  $2 \times 10^{30}$  kg.

hoeveelheden "lege" ruimte er tussenin. Het Heelal om ons heen is dus klonterig. Een van de grote vragen in de sterrenkunde is: hoe en wanneer zijn sterrenstelsels ontstaan uit deze initiële afwijkingen in de dichtheidsverdeling en hoe zijn ze verder geëvolueerd?

Er zijn twee populaire scenarios: het scenario waarin melkwegstelsels zich vormen uit een enkele grote afkoelende gaswolk, en het scenario van hiërarchische structuurvorming. In dit laatste scenario vormen grote structuren pas laat, door het botsen en samengaan van jongere kleinere objecten. In beide scenarios zijn pas geboren objecten gasrijk. Het tweede scenario stelt dat botsingen een belangrijke manier zijn om het gas zodanig samen te persen dat zwaartekracht de overhand krijgt en ze nog verder samen doet trekken en er sterren ontstaan.

Een recente ontdekking is dat waarschijnlijk (bijna) alle sterrenstelsels centrale zwarte gaten bevatten van een paar miljoen tot een miljard zonsmassa's. Het blijkt dat de massa's van sterrenstelsels en hun centrale zwarte gaten met elkaar gecorreleerd zijn. Dit is iets dat een theorie van de vorming van melkwegstelsels zou moeten kunnen verklaren.

Hedendaagse theoriën van de vorming van melkwegstelsels doen goede voorspellingen voor het aantal stelsels dat een bepaalde massa heeft. Toch zijn er nog grote verschillen tussen theorie en waarnemingen. Een van de discrepanties is dat men op grond van deze theoriën een veel hoger aantal *zware* melkwegstelsels verwacht dan wordt waargenomen. Hier is nog geen goede verklaring voor, behalve dat er waarschijnlijk een beperkend proces moet plaatsvinden dat relatief meer invloed heeft op het groeiproces van zware stelsels. De preciese vorm hiervan is nog onbekend. Een mogelijkheid is dat galactische winden, aangedreven door energie van stervorming en zwarte gaten, het overtollig materiaal uit de stelsels blazen. Dit zou daarmee ook een verklaring kunnen vormen voor het feit dat er ook "afvalstoffen" worden waargenomen in de "lege" ruimte, waar slechts weinig of geen sterren worden waargenomen.

### Radiostelsels

Verweg gelegen radiobronnen komen over het algemeen voor in de meest zware, uitgestrekte en heldere stelsels. Er wordt aangenomen dat de radiostraling veroorzaakt wordt door de accretie van materiaal op ronddraaiende superzwarte (1 miljard zonsmassa's) zwarte gaten.

Omdat radiostelsels zo helder zijn, kunnen ze tot op grote afstand en dus tot vroeg in het Heelal worden waargenomen. Het zijn daarom goede kosmologische bakens. Bovendien is het feit dat ze zo uitgestrekt zijn erg handig om de melkwegstelsels zelf te bestuderen. Omdat ze *en* massieve zwarte gaten bevatten *en* heel erg zwaar zijn, zijn ze bij uitstek geschikt om de relatie tussen zwarte gaten en stervorming in het formatieproces van zware melkwegstelsels te bestuderen.

Een paar reeds bekende resultaten voor radiostelsels volgen hieronder:

Waarnemingen met de *Hubble* ruimtetelescoop hebben laten zien dat radiostelsels met een hoge roodverschuiving uit vele kleine klontjes bestaan. Berekeningen tonen aan, dat het waarschijnlijk is dat deze op tijdschalen van 100 miljoen jaar zullen bot-

sen en versmelten tot een groter object. Dit is consistent met het scenario van hiërarchische structuurvorming. Een andere voorspelling van het hiërarchisch model die door radiostelsels bevestigd lijkt te worden, is dat zware radiostelsels gebruikt kunnen worden om de voorlopers van de grootste structuren in het Heelal, clusters van sterrenstelsels, te vinden op hoge roodverschuiving.

In sommige verweggelegen radiostelsels is bewijs gevonden voor hoge stervormingssnelheden. Dit was voornamelijk gebaseerd op optische waarnemingen, en dus onzeker door de mogelijke verduistering door stof. Recent is ook bewijs gevonden dat dit niet slechts in kleine gebiedjes gebeurt maar door de hele stelsels. Het lijkt erop dat deze stelsels op dat moment het grootste gedeelte van hun totale sterpopulatie aan het vormen zijn. In hoofdstuk 2, 3, 4 en 5 hebben wij hier meer onderzoek naar gedaan.

Van verweggelegen radio stelsels is ook bekend dat ze zich bevinden in grote gasvormige halo's. Het zou kunnen dat ze zich hieruit aan het vormen zijn. Een andere mogelijke verklaring is dat dit gas is, dat naar buiten geblazen is vanuit de meer centrale gebieden. De precieze rol van de halo's is nog niet bekend. Hoofdstuk 6 en 7 beschrijven de resultaten van onderzoek naar deze gaswolken.

Specifieke vragen die in dit proefschrift aan de orde komen zijn:

Wanneer vormen radio stelsels zich?

Wat is de rol van stof in dit vormingsproces?

Wat is de betekenis van de gashalo's waarin ze zich bevinden?

Wat kunnen we van ze leren over de connectie tussen de groei van zwarte gaten en stervorming?

## Hoofdstuk 2

In Hoofdstuk 2 bestuderen we de stof emissie van een groot aantal verweggelegen radiostelsels. Zoals we eerder hebben besproken wordt dit stof geproduceerd en verhit door sterren, zodat er ver-infrarode straling ontstaat. De sterren zelf zijn door dit stof grotendeels aan het oog onttrokken. Door nu de intensiteit van dit ver-infrarode licht te meten op verschillende roodverschuivingen kan men hopen de geschiedenis van de stervorming te bepalen. In dit hoofdstuk hebben wij een analyse gemaakt voor de aldus afgeschatte stervorming in radiostelsels tijdens zeer verschillende periodes in het Heelal. Het resultaat van deze analyse is dat de stervorming veel hoger was toen het Heelal pas 1–2 miljard jaar oud was dan toen het 7 miljard jaar oud was. Een ander resultaat is dat de stervormingssnelheid erg hoog is: er worden tot een paar duizend zonsmassa's per jaar aan nieuwe sterren gevormd. Dit is veel meer dan in ons eigen Melkwegstelsel, dat slechts een stervormingssnelheid van ongeveer 3 zonsmassa's per jaar kent. Het belang van deze vinding is dat stelsels in staat lijken in 100 miljoen jaar ongeveer 100 miljard sterren te vormen. Dit is vergelijkbaar met de massa van een volledig melkwegstelsel. Het lijkt er dus op dat radiostelsels zich redelijk snel in een groot kosmisch vuurwerk vormen, waarna ze een wat rustiger leven leiden.

### Hoofdstuk 3 & 4

In deze twee hoofdstukken bestuderen we stelsels waarin de radiobron pas net is gaan werken. Het blijkt dat deze stelsels nog meer verduisterd zijn door stof dan de stelsels besproken in Hoofdstuk 2, en vergelijkbare of zelfs hogere stervormingssnelheden hebben. Hieruit concluderen wij dat het ontstaan van radiojets en een erg hoge snelheid van stervorming waarschijnlijk aan elkaar gerelateerd zijn.

### Hoofdstuk 5

Een complicatie bij de interpretatie van heldere ver-infrarode straling is dat stof niet alleen door sterren maar ook door straling geassocieerd met zwarte gaten verhit kan worden. In dit hoofdstuk hebben wij daarom de bijdragen van deze twee componenten gemodelleerd en vergeleken met waarnemingen. Uit deze vergelijking blijkt dat de emissie geassocieerd met zwarte gaten tot wel 60% van de ver-infrarode lichtkracht kan veroorzaken. Deze fractie neemt niet toe met toenemende lichtsterkte. Wel lijkt het zo te zijn dat krachtigere bronnen hogere stof temperaturen hebben. Omdat een object efficiënter straalt als het heter wordt, en er een *niet*-stervormingsgerelateerde component is, kunnen de stervormingssnelheden voor heel heldere objecten in het vroege Heelal met een factor 2–3 naar beneden bijgesteld worden.

### Hoofdstuk 6 & 7

In deze laatste twee hoofdstukken bestuderen wij de gaswolken waarin verre radiostelsels zich bevinden. Stelsels ontstaan uit afkoelende gaswolken. Deze gaswolken kunnen bijvoorbeeld stralen omdat ze gravitationele energie moeten kwijtraken voordat ze verder kunnen samentrekken, of omdat ze verlicht worden door centrale stervormingsgebieden en straling van actieve zwarte gaten. Omdat de gaswolken voornamelijk uit waterstof bestaan is de dominante straling de eerder beschreven Lyman alpha emissie. Het is mogelijk om filters te maken die precies het golflengtegebiedje van de roodverschoven  $Ly\alpha$  omvatten. Deze filters hebben daardoor weinig last van andere storende straling en zijn dus heel gevoelig. Wij hebben zo'n filter geïnstalleerd op een van de grootste optische telescopen ter wereld (de Keck Telescoop met een 10-m spiegel), en hiermee drie radiostelsels, waaronder die van Figuur 14, geobserveerd. Een van deze waarnemingen is de meest gevoelige in zijn soort ooit gedaan.

De resulterende plaatjes zijn beschreven in Hoofdstuk 6 en laten enorme en spectaculaire gaswolken zien met een grootte tot 200 kpc. De gaswolken vertoonden nooit eerder geziene langgerekte filamenten en het was ook niet eerder bekend dat ze zo uitgebreid waren. Een verklaring voor de uitgebreidheid van deze wolken is dat dit gas is dat vanuit grote afstand naar binnen valt en waaruit deze stelsels bezig zijn zich te vormen. Een mogelijke verklaring voor de filamenten is dat ze een teken zijn van grootschalige stromen die weggeblazen worden vanuit het centrum. Dit zou interessant zijn, omdat, zoals eerder gezegd, er een correlatie is tussen de massa van stelsels en hun centrale zwarte gaten. Het is mogelijk dat door deze uitstromingen de groei van het zwarte gat en stervorming op een zodanig zelfgereguleerde manier plaatsvinden dat het tot de waargenomen correlatie leidt.

Hoofdstuk 7 gaat hierop verder, door de kinematica en de samenstelling van het gas te bepalen. Er werd gevonden dat het gas erg hoge snelheden heeft op de locatie van de radiobron. Bovendien werd gevonden dat het gas niet puur uit waterstof en helium bestaat, maar dat er ook sterke sporen van zuurstof zijn met een vergelijkbaar snel-

heidsprofiel. Dit geeft aan dat het gas secundair materiaal is dat al eens onderdeel van een ster is geweest. Een mogelijkheid is dat dit inderdaad verrijkt materiaal is dat door de krachtige radiobron en sterrewinden vanuit de centrale stervormingsgedeelten van het stelsel naar buiten wordt geblazen. Omdat je gas nodig hebt om sterren te vormen, zouden zulke processen de groei van zware stelsels kunnen beperken. Deze waarnemingen zouden kunnen helpen om de theoretische en waargenomen massaverdelingen van stelsels met elkaar in overeenstemming te brengen.





## Publications not included in this thesis

- De Breuck, C., Downes, D., Neri, R., van Breugel, W., Reuland, M., Omont, A. & Ivison, R., 2005, *A&A*, in press, "Detection of Two Massive CO Systems in 4C 41.17 at  $z=3.8$ "
- Dopita, M., Groves, B., Fischera, F., Sutherland, R., Tuffs, R., Popescu, C., Kewley, L., Reuland, M. & Leitherer, C., 2005, *ApJ*, in press, "Modelling the pan-spectral energy distribution of starburst galaxies: I, The role of ISM pressure & the molecular cloud dissipation timescale"
- De Breuck, C., Bertoldi, F., Carilli, C., Omont, A., Venemans, B., Röttgering, H., Overzier, R., Reuland, M., Miley, G., Ivison, R. & van Breugel, W., 2004, *A&A*, 424, 1, "A multi-wavelength study of the proto-cluster surrounding the  $z=4.1$  radio galaxy TN J1338-1942"
- Scharf, C., Smail, I., Ivison, R., Bower, R., van Breugel, W. & Reuland, M., 2003, *ApJ*, 596, 105, "Extended X-Ray Emission around 4C 41.17 at  $z = 3.8$ "
- Reuland, M., Röttgering, H. & van Breugel, W. 2003, *New Astronomy Review*, 47, 303, "SCUBA observations of high redshift radio galaxies"
- Stevens, J. A., Ivison, R. J., Dunlop, J. S., Smail, Ian R., Percival, W. J., Hughes, D. H., Röttgering, H. J. A., van Breugel, W. J. M. & Reuland, M., 2003, *Nature*, 425, 264, "The formation of cluster elliptical galaxies as revealed by extensive star formation"
- De Breuck, C., Neri, R., Morganti, R., Omont, A., Rocca-Volmerange, B., Stern, D., Reuland, M., van Breugel, W., Röttgering, H., Stanford, S. A. et al. , 2003, *A&A*, 401, 911, "CO emission and associated HI absorption from a massive gas reservoir surrounding the  $z = 3$  radio galaxy B3 J2330+3927"
- Dawson, S., Spinrad, H., Stern, D., Dey, A., van Breugel, W., de Vries, W. & Reuland, M., 2002, *ApJ*, 570, 92, "A Galactic Wind at  $z=5.190$ "



# Curriculum vitae

OP 21 juni 1972 werd ik geboren in Groningen. Het grootste gedeelte van mijn jeugd bracht ik door in Roden. Mijn middelbare school opleiding volgde ik aan het Willem Lodewijk Gymnasium te Groningen alwaar ik in juni 1990 mijn diploma behaalde in tien vakken.

In datzelfde jaar begon ik met mijn studie Sterrenkunde aan de Universiteit Leiden, waar ik in 1991 mijn propedeutisch examen haalde. Onder leiding van dr. J.H.J. de Bruijne, dr. R. Hoogerwerf en prof. dr. P.T. de Zeeuw heb ik tijdens de doctoraalfase met behulp van computersimulaties onderzoek gedaan naar de kinematica en evolutie van OB associaties. Dit onderzoek had als doel de specificaties van een toekomstige astrometrische satelliet te helpen bepalen. In augustus 1999 behaalde ik mijn doctoraal diploma. Tijdens mijn studie voerde ik van 1995 tot en met 1999 een eenmanszaak gespecialiseerd in aanleg en beheer van computer netwerken.

Op 1 oktober 1999 begon ik met mijn promotieonderzoek dat beschreven is in dit proefschrift. Dit onderzoek vond plaats in het kader van een samenwerkingsproject tussen Leiden en Lawrence Livermore National Laboratories. Aan de Sterrewacht Leiden stond dit onderzoek onder leiding van prof.dr. G.K. Miley en dr. H.J.A. Röttgering. Prof.dr. W.J.M. van Breugel had de leiding over het werk dat ik gedurende drie jaar in de Verenigde Staten heb verricht. Daar was ik verbonden aan het Institute of Geophysics and Planetary Physics van het Lawrence Livermore National Laboratory te Livermore, Californië en aan de University of California at Davis. Tijdens dit onderzoek ben ik vele malen op waarneemreis geweest naar telescopen op Hawaii (Keck, JCMT), Spanje (IRAM) en Californië (Lick). Ook heb ik gebruik gemaakt van data verkregen met de *Hubble* Space Telescope en het *Chandra* X-ray Observatory. Verder legde ik werkbezoeken af aan de Landessternwarte Heidelberg (Duitsland), de Research School of Astronomy & Astrophysics van de Australian National University (Australië) en bezocht ik een winterschool op La Palma (Spanje), een herfstschool in Dwinglo en conferenties in Groningen, Leiden en Ile d'Oleron (Frankrijk).

Daarnaast heb ik tijdens mijn verblijf in Californië verscheidene Big Walls beklommen (El Capitan, Half Dome, Leaning Tower, Washington Column).



## Nawoord / Acknowledgments

ALS eerste wil ik iedereen bedanken die, bewust of onbewust, en elk op zijn/haar eigen manier heeft bijgedragen aan de totstandkoming van dit proefschrift.

This project would not have been possible without the ideal scientific environments that the IGPP/LLNL and the Sterrewacht have provided. In these times research depends heavily on the smooth workings of computer networks. I would like to thank the respective computer groups for ensuring that the systems were always operating at their finest.

Op een beslissend moment in mijn leven hebben Jos, Ronnie en hun begeleider mij als eerste laten zien waar het in de wetenschap nu echt om gaat. Hiervoor ben ik hen erg dankbaar. Ik had de uitdaging en spanning van de echte sterrenkunde die uiteindelijk geresulteerd heeft in dit proefschrift niet willen missen.

During and outside working hours, the LLNL cosmology group: Wim, Jerry & Jenn, Brad, Mark Lacy, and Steve provided much needed fun, discussion and relaxation. Dan Stern, and Steve Dawson showed me the finer bits of Berkeley style astronomy.

De (ex-)bewoners van Vliet 11 en team "Bus 1+1" hebben er voor gezorgd dat ik me soms ook bewust was van een wereld buiten de sterrenkunde. Speciale dank gaat natuurlijk uit naar Lodewijk, die mij niet alleen de Vliet heeft binnengeloodst, maar ook in Livermore een prima huisgenoot was. Lysbeth wil ik bedanken voor de gezellige discussies. We hebben veel van elkaar geleerd.

The Sunrise Crew: Ed, Gary, Steve, Annie, Brent, Chad, Christina, Deke, Dan, Danny, Darlene, Dustin, Ed, Eric, Kendra, Kristine, Kyle, Jill, Jimmy, Jonathan, Luke, Little D., Matt, Mike, Nick, Paul, Rob, Russ, Scott, Sunny, Tom, Tony. All of you made my stay in California unforgettable. Special thanks to those people who were crazy enough to go out on multi-day climbs of ridiculously steep walls with a guy from a land that has no mountains and where most of the population lives below sea level. Paul, Luke, Brent and Tom, you have made my dreams come true! I am sure many more great adventures are in store.

Op de Sterrewacht gaat mijn dank uit naar allen, maar in het bijzonder naar Andrew, Roderik, Bram, Leonie, en Mariska. Voor mij was terugkomen in Nederland veel moeilijker dan weggaan. Jullie hebben er voor gezorgd dat ik mij langzamerhand weer thuis voelde.

Dan zijn er nog de mensen die mij al vanaf kinds af aan kennen, en richting hebben gegeven aan mijn leven. Mevrouw Roede, ik kan u niet genoeg bedanken voor de warme omgeving waarin ik ben opgegroeid. Bart, in de loop der jaren hebben we teveel samen meegemaakt om op te noemen. Ik hoop dat dit alleen maar meer wordt.

Natuurlijk ben ik ook mijn familie veel verschuldigd. Ascelijn, Marike, Merijn, en mijn ouders hebben me altijd in alles gesteund en met veel liefde omringd. Dit proefschrift is voor jullie allemaal.

Joke, jouw praktische insteek en eigen ervaring met het promoveren op afstand heeft me geholpen dit project tot een succesvol einde te brengen. Zonder jou had ik geen halve marathon gelopen, geen onbeklimbare bergen beklommen, en gewoon niet zoveel lol gehad. We maakten van bergen hobbeltjes en van puinhopen een feest. Soms andersom, maar aan het einde telt dat we er toch samen zijn geweest.

*Als je onzeker bent, schiet dan gewoon zo hard mogelijk. Als jij niet weet waar de bal heengaat, weet de keeper het ook niet.*

Johan Neeskens